AXONAL INJURY FOLLOWING FOCAL CEREBRAL ISCHAEMIA

Philippa S. Yam BSc BVM&S CertSAM MRCVS

Thesis submitted for the degree of Doctor of Philosophy,

to the Faculty of Medicine, University of Glasgow.

Wellcome Surgical Institute & Hugh

Fraser Neuroscience Laboratories,

Garscube Estate

Bearsden road

Glasgow

G61 1QH

ProQuest LLC.
789 East Eisenhower Parkway
P.O. Box 1346
Ann Arbor, MI 48106 – 1346

ABSTRACT

Myelinated axons are essential for the normal functioning of the brain. Since myelinated axons, like grey matter, are dependent on a continuous supply of energy, it is likely that ischaemic injury compromises axonal function as well as that of the neuronal cell bodies. Axonal injury following cerebral ischaemia has attracted less attention than damage in grey matter. However, it is becoming increasingly recognised that axons are highly vulnerable to focal ischaemia. Since white matter does not contain neuronal cell bodies or synapses it is likely that the mechanisms of injury and strategies for its protection are different from those in grey matter.

To define markers of axonal injury appropriate for use in the assessment of axonal pathology consequent to focal cerebral ischaemia, immunocytochemical methods were employed. Antibodies to a synaptosomal associated protein of 25 kDa (SNAP25), which is transported by fast anterograde transport; the 68-kDa neurofilament subunit (NF68kD) and microtubule-associated protein 5 (MAP5), were investigated on sections from rats subjected to 30 minutes, 1, 2, and 4 h of ischaemia induced by permanent middle cerebral artery (MCA) occlusion. After 4 h of occlusion, there was increased SNAP25 immunoreactivity which was bulbous in appearance, reminiscent of axonal swellings which occur following blunt head injury. Increased SNAP25 immunoreactivity was present in circumscribed zones in the subcortical white matter and in the axonal tracts at the border of infarction, a pattern similar to that previously described for amyloid precursor protein. Although less marked, similar changes in immunoreactivity in axons were evident following 2 h of ischaemia. MAP5 and NF68kD had striking changes in immunoreactivity in axonal tracts permeating the caudate nucleus within the MCA territory at 4 h. The appearance was roughened and

disorganised compared to the smooth regular staining in axons within the non-ischaemic areas. Profiles reminiscent of axonal bulbs were evident in MAP5 stained sections. The changes seen with NF68kD and MAP5 were also evident at 2 h but were more subtle at 1 h. There were no changes in axonal immunoreactivity with SNAP25 or NF68kD at 30 minutes post MCA occlusion. Altered immunoreactivity following ischaemia using SNAP25, MAP5 and NF68kD provide further evidence for the progressive breakdown of the axonal cytoskeleton following an ischaemic insult. NF68kD and MAP5 appear to be sensitive markers of the structural disruption of the cytoskeleton, which precedes the subsequent accumulation of SNAP25 within the damaged axons. Axonal cytoskeletal breakdown and disruption of fast axonal transport, which are well recognised features of traumatic brain injury, are also sequelae of an ischaemic insult.

To allow future assessments of protection of white matter by therapeutic interventions, a method by which axonal injury can be quantified is required. For this purpose, immunocytochemical methods using amyloid precursor protein (APP) were investigated following permanent MCA occlusion in the rat. APP is transported by fast anterograde axonal transport and has been shown to accumulate following a variety of insults to axons, indicative of dysfunction of axonal transport. The topographical relationship between APP accumulation and region of infarction was mapped using immunocytochemistry and image analysis techniques. Additionally, using a semi-quantitative scoring system in the rat, a relationship was demonstrated between the amount of APP accumulation and the volume of infarction following middle cerebral artery occlusion.

A number of studies have shown certain drugs to be neuroprotective following focal cerebral ischaemia in the rat and cat. However, the effect of neuroprotection has often been assessed by a reduction in neuronal necrosis volume; the effect on axons

being largely ignored. Since APP has been shown to be a good marker of axonal injury, and a method of semi-quantitative analysis was developed, the method was utilised to determine whether BW619C89 or MK-801 protects axons following focal cerebral ischaemia in the rat. Both drugs failed to significantly reduce the APP score. However, in the rat brain the volume of white matter is relatively small compared to the volume of grey matter. Therefore the possibility that neuroprotective drugs such as MK-801 are saving white matter but that this protection is unable to be detected in the rat, was addressed.

The cat brain offers several advantages over the rat for the purpose of assessment of axonal injury. Conceivably, a shift in the boundary and a change in the quantity of APP accumulation could be more readily appreciated following neuroprotection in the cat. The study undertaken in the cat demonstrated that increased APP immunoreactivity is a consistent outcome in white matter after focal cerebral ischaemia. Secondly, using two different scoring systems for APP, which were developed to overcome the limitations encountered in the rat tissue, it was found that the larger the volume of the ischaemic lesion, the greater the extent of APP immunoreactivity. Once these two facts had been established, it was possible to assess whether MK-801 protects axons following focal cerebral ischaemia. MK-801 failed to reduce the APP score in the cat following MCA occlusion. Further analysis suggested that following MK-801 administration, the axonal injury:neuronal necrosis ratio was higher than in vehicle treated animals. That is, MK-801 failed to protect axons. The potential implications for drug development are huge. The failure of many recent drug trials and the findings of the present study, suggest that the success of future strategies may be dependant on the protection of the brain as a whole.

LIST OF CONTENTS

LIST OF FIGURES

CHAPTER 1

CHAPTER 2

CHAPTER 3

CHAPTER 4

CHAPTER 5

CHAPTER 6

LIST OF TABLES

CHAPTER 1

CHAPTER 2

CHAPTER 3

CHAPTER 4

CHAPTER 5

CHAPTER 6

CHAPTER 7

APPENDIX 4

LIST OF ABBREVIATIONS

APP	Amyloid precursor protein
BOLD	Blood oxygen level dependant
CAP	Compound action potential
CNS	Central nervous system
DAI	Diffuse axonal injury
EM	Electron microscopy
FAM	Formaldehyde, acetic acid, methanol
MABP	Mean arterial blood pressure
MAP5	Microtubule associated protein 5
MCA	Middle cerebral artery
MCID	Microcomputer Imaging Device
MRI	Magnetic resonance imaging
MT	Microtubules
NMDA	N-methyl-D-aspartate
NF	Neurofilaments
NF68kD	Neurofilament subunit of 68-kDa
PAM	Paraformaldehyde
PBS	Phosphate buffered saline
PKC	Protein kinase C
SHRSP	Spontaneously Hypertensive Rat, Stroke Prone
SNAP25	Synaptosomal associated protein of 25 kDa
TBI	Traumatic brain injury

ACKNOWLEDGEMENT

During the last three years I have had the pleasure of working with a number of distinguished people. These include Tei Takasago, Laurence Dunn, Rammanjit Gill, Jim Patterson, David Maxwell and Leonard Miller. Some of the highlights of my PhD have included the chance to meet people from other departments; a special mention must go to Professor David Graham and Dr. Will Maxwell with whom I have had the opportunity on several occasions to 'talk science' and seek advice. I must also thank the staff at the Wellcome for their technical support, in particular Joan Stewart and Eileen Harrop; and the excellent and forthcoming help from animal nurses, Christine Stirton and Julie Summerhill. Most of all, my thanks must go to Professor Jim McCulloch. I could never have anticipated what an all round education I was to get at the Wellcome. His enthusiasm for Neuroscience goes without saying; it was other subjects ranging from American history, geometry and Greek philosophy that took me by surprise. When I first started my PhD I attended a course on supervisor-student relations. One exercise entailed describing the ideal attributes of a supervisor. Apart from myself, I wonder how many other students who attended that course can reflect on their good fortune to have had a supervisor who fulfilled so many of those attributes? Jim's enthusiasm, insight, humour and availability to discuss matters, together with his ability to calm my anxiety, will not be forgotten.

PREFACE AND DECLARATION

This thesis presents results from investigations conducted within 4 broadly defined areas.

1. To define markers of axonal injury appropriate for use in the assessment of axonal pathology consequent to focal cerebral ischaemia
2. To develop quantitative techniques for the assessment of axonal injury
3. To apply a suitable marker of axonal injury and a method of quantification of axonal injury in the rat following focal cerebral ischaemia
4. To explore the utility of techniques of quantification of axonal injury in species where there is a larger volume of white matter compared to that in the rat brain.

The thesis comprises my own original work and has not been presented previously as a thesis in any form. Mr. L. Dunn performed the middle cerebral artery occlusions in the cats and Dr. T. Takasago performed the middle cerebral artery occlusions in the rat study described in Chapter 4.

For Mum and Dad

CHAPTER 1

INTRODUCTION

1.1 GENERAL INTRODUCTION

A number of prevalent clinical conditions, including stroke, expose the central nervous system (CNS) to anoxic/ischaemic damage. Neurons of the brain and spinal cord rely on axonal connections for signal transmission. Both cell bodies and axons are therefore critical for normal operation of the CNS, and understanding the basic mechanisms of injury in both grey and white matter is essential for the rational design of therapeutic intervention for optimal protection of the brain. Many neurological diseases result in damage to the myelinated, subcortical fibre tracts, ranging from demyelination as seen with multiple sclerosis to ischaemic injury occurring with strokes. There is a large body of work dealing with anoxic/ischaemic injury of grey matter (Haddad and Jiang, 1993; Choi, 1990; Siesjo, 1986), but until recently, virtually no information was available on the mechanisms of anoxic/ischaemic damage in central white matter tracts. Given the drastically different structure of grey and white matter regions of the mammalian CNS, it is reasonable to expect that these mechanisms might be different. During the last few years experimental investigation of white matter following ischaemia/anoxia has revealed that it is vulnerable to this type of injury (Follis et al. 1993; Pantoni et al. 1996) (Table 1.1) and in vitro studies have started to unravel the fundamental cellular mechanisms involved. The recognition of white matter injury following ischaemic insults, and an understanding of the pathological mechanisms involved, is crucial for the efficient and logical designs of therapeutic interventions in diseases in which white matter is a prominent target.

Table 1.1 Clinical conditions resulting in axonal injury

Condition	Description
Central	
Stroke	Both white and grey matter injury in artery territory infarcts, or more selective white matter damage in lacunar stroke syndromes
Spinal cord injury	A significant portion of axonal damage may occur on a vascular basis
Ischaemic optic neuropathy	Arteritic or nonarteritic
Traumatic optic neuropathy	Secondary ischaemic injury from vasospasm and optic nerve swelling
Radiation-induced white matter necrosis	Evidence for selective ischaemic injury to white matter
Vascular dementia	Chronic anoxia/ischaemia of subcortical white matter
Neonatal leukomalacia	Preferential injury to white matter in neonates as a result of hypotension and ischaemia
Peripheral	
Diabetic neuropathy	Pathogenesis may be partly due to decreased blood flow and endoneurial hypoxia
Vasculitis	May result in multiple mononeuropathy, or symmetric or asymmetric polyneuropathy
Compression	Combination of mechanical deformation and ischaemia from damaged intraneural blood vessels

Examples of conditions in which anoxia/ischaemia is implicated as an important or major mechanism of axonal dysfunction and injury. (Adapted from Stys et al., 1995).

1.2 ACUTE BRAIN INJURY

1.2.1 Stroke

Stroke is the third major cause of death and an important cause of hospital admission and long term disability in most industrialised populations. In Scotland, about 7% of all hospital bed days are accounted for by stroke patients; this bed usage is greater than all other conditions with the exception of 'mental disorders' and 'mental handicap'. In financial terms, stroke absorbs 6% of hospital running costs and 4.6% of all National Health Service costs and these figures have remained much the same for a decade (Isard and Forbes, 1992). The World Health Organisation definition of stroke is, 'rapidly developing clinical signs of focal (or global) disturbance of cerebral function, with symptoms lasting 24 hours or longer leading to death, with no apparent cause other than of vascular origin', although this definition is probably no longer adequate. Stroke accounts for 10-12% of all deaths in industrialised countries; about 88% of the deaths attributed to stroke are among people over 65 years (Bonita, 1992). About 20% of strokes result from intracerebral and subarachnoid haemorrhage and about 80% are due to blood vessel occlusion by a blood clot originating from the heart or atherosclerotic plaque. Multiple risk factors are associated with ischaemic stroke in man. These include age, diabetes mellitus, cigarette smoking, diet and alcohol, obesity and hypertension (Marmot and Poulter, 1992). Strokes restricted to white matter have also been identified as a major class of neurological injury, comprising approximately 1/4 of strokes seen clinically (Bamford et al. 1987; Fisher, 1982). These so called lacunar syndromes are defined clinically and are highly predictive of small deep lesions affecting the motor and sensory pathways i.e. in the corona radiata, internal capsule, thalamus, cerebral peduncle and pons (For review see Warlow, 1993).

1.2.2 Traumatic brain injury

The problems posed by head injuries are vast, varied and vext (Teasdale, 1995). Head injury accounts for 1% of all deaths but for 15-20% between the ages of 5 and 35 years. In the UK, one million patients per annum attend hospital after sustaining a head injury. Males outnumber females by more than two to one and almost half of the cases are children less than 15 years old.

Brain damage after head injury can be classified by pattern and by time course. The patterns are essentially separated into focal and diffuse varieties. In time course, the differentiation is between primary damage (such as free radical formation, calcium flux and inflammation), developing at the moment of impact, and secondary damage due to subsequent complications (including ischaemia, raised intracranial pressure, seizures or infection). The eventual outcome is dependent on the overall effect of all these described parameters (Graham, 1996).

In the context of this thesis, traumatic brain injury is of interest since diffuse axonal injury (DAI) is the single most important lesion to result (Adams et al. 1989). DAI can be defined as the occurrence of diffuse damage to axons in the cerebral hemispheres, corpus callosum, brain stem and sometimes also in the cerebellum resulting from head injury (Adams et al. 1989). This is of importance since it has been suggested that in both man (Adams et al. 1980; 1982; 1983; 1977) and a non-human primate model (Gennarelli et al. 1982) that there is a direct link between the extent of DAI and the extent of ensuing patient morbidity. DAI consists of scattered damage of axons throughout the white matter of the brain. Injury to individual axons can be recognised only by microscopy on fatal cases; silver stains show 'retraction balls' which represent swollen blobs of axoplasm. More recently, a variety of other markers have been investigated in order to define the responses of axons to injury including amyloid

precursor protein (APP) (Sherriff et al. 1994a; Gentleman et al. 1993; Gentleman et al. 1995), neurofilament subunits (Ng et al. 1994; Christman et al. 1994; Grady et al. 1993) and ubiquitin (Gultekin and Smith, 1994).

1.3 FUNCTIONAL ANATOMY OF CEREBRAL WHITE MATTER

White matter occupies nearly one half the volume of the adult cerebral hemispheres in man, and myelinated tracts connect grey matter structures throughout the brain. In the cerebrum, three groups of white matter pathways are recognised: projection fibres convey sensory and motor information to and from the cortex; commissural fibres, primarily via the corpus callosum, mediate interhemispheric communication; and association fibres connect various cortical areas. Short association fibres, also known as U or arcuate fibres connect remote intrahemispheric zones. The blood supply of the hemispheric white matter comes primarily from long penetrating arteries arising from large vessels at the base of the brain. Prominent among these are the lenticulostriate arteries that originate from the middle cerebral artery. Additional blood supply comes from the recurrent artery of Heubner (medial striate artery) and the anterior choroidal artery (Filley, 1998).

1.4 MYELINATED AXONS - STRUCTURE AND FUNCTION

In the CNS, the myelinated axon originates from the neuronal perikaryon. It may extend for a considerable distance but has a characteristic constant diameter throughout its length. Most axons do not branch or form synaptic contacts before their termination. Almost all axons with diameters above 0.2μm in the CNS are myelinated and the

segments of myelin are separated by nodes of Ranvier along the length of the axon. The myelin is composed of layers of protein and lipid. In myelinated axons, the excitable axonal membrane is exposed to the extracellular space only at the nodes of Ranvier; this is the location of sodium channels (section 1.5.3) and impulse propagation jumps from node to node. The internode length is generally proportional to the axon diameter. In the CNS it is the oligodendroglial cells which form the myelin, and each glial cell can myelinate many separate axons. The axon contains fewer organelles as compared to the soma, because it does not have Golgi apparatus or rough endoplasmic reticulum. It is surrounded by the axolemma which is about 8 nm thick and appears morphologically similar to the plasma membrane of the neuronal soma. The axoplasm itself is specialised to maintain its tube-like shape and considerable length. The cytoskeleton is a highly dynamic character, involved in many essential cellular processes including cell movement, process elongation and intracellular transport. The cytoskeleton, which imparts structure to the axon cylinder and serves to maintain the required distribution of channels (Salzer, 1997), is unique to eukaryotic cells and consists of three major classes of cytoskeletal fibres: neurofilaments (NF's), microtubules (MT's) and microfilaments (Ludin and Matus, 1993) (Fig.1.1).

Figure 1.1 The components of the cytoskeleton

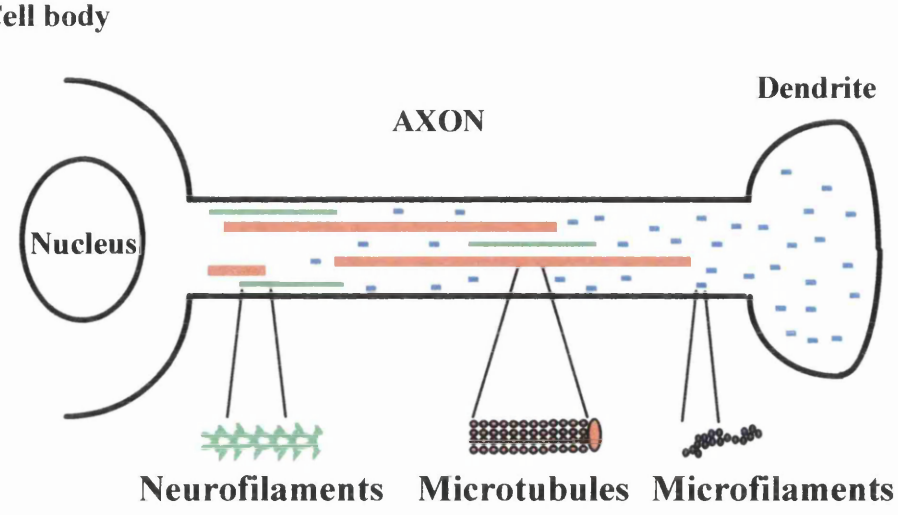

1.4.1 Neurofilaments

Neurofilaments are members of the intermediate filament family, whose name derives from the characteristic diameter of 8-10 nm, which is intermediate between actin filaments (6 nm) and microtubules (24 nm). NF's are long, unbranched filaments that in large myelinated axons accumulate as the most abundant structures (Lee and Cleveland, 1996). NF's are composed from three subunit polypeptides, the so-called 'neurofilament triplet' (Hoffman and Lasek, 1975). In mammals these distinct polypeptides are NFH (180-200 kDa), NFM (130-170 kDa) and NFL (60-70 kDa) with each being encoded by a separate gene. The size difference between the NF proteins occurs mainly in the length of the carboxy-terminal tail sequences. NF-M and NF-H are phosphorylated at many sites, mostly in the carboxy-terminal tail region of the molecule with a few other sites in the amino-terminal head region. Biochemically purified NF's from various sources have

in general been found to contain NFL, NFM, and NFH in a ratio of about 5:2:1. In neurons, it is primarily the NFH, and to a lesser degree NFM polypeptides, which participate in a cross linking function between filaments (Hirokawa et al. 1984).

NF's are moved into and through axons via slow axonal transport although the mechanism remains unsettled. Despite the traditional view that NF's are static, evidence suggests that they can be highly dynamic structures (Okabe et al. 1993). Both the level and phosphorylation state of NFH have been proposed to regulate the rate of NF transport and axonal calibre. Phosphorylation may slow NFH transport by the formation of cross bridges between NFH's (Hirokawa et al. 1984) or by causing dissociation of NF's from the axonal transport machinery (Hisanaga et al. 1990). After arriving at the nerve terminal, it is believed that NF's are degraded.

NF accumulation, although detectable during neurite elongation, becomes robust only after synapse formation and is concomitant with myelination (Lee and Cleveland, 1996). Therefore, NF's are suggested to play a critical role in determining axonal calibre (Hoffman et al. 1984). Earlier evidence had shown a linear relationship between NF number and cross-sectional area throughout radial growth and regrowth following axonal injury (Hoffman et al. 1985; Friede and Samorajski, 1970). This increase in axonal diameter is important for normal nerve function because calibre is a principal determinant of the speed at which nerve impulses are propagated along the axon (Gillespi and Stein, 1983).

1.4.2 Microtubules

Microtubules provide a structural framework for axons and dendrites, tracks for organelle traffic and have a role during neuronal growth and development. They are 24 nm in diameter, cylindrical structures with walls made up of 12-14 protofilaments (for

review see Hammerschlag et al. 1994). Microtubules are arranged haphazardly in the perikaryon but longitudinally in axons and dendrites and may reach lengths of 100μm. Distinct domains exist within microtubules that vary in composition and degrees of stability. The primary polypeptides of microtubules are α and β tubulins. These are subject to a variety of post-translational modifications which may relate to microtubule stability although this is uncertain. Microtubules in vivo include a members of heterogeneous set of polypeptides known as microtubule associated proteins (MAP's). MAP's interact with microtubules maintaining a constant stoichiometry with the tubulin through cycles of assembly and disassembly. MAP's may stimulate microtubule formation and stabilise existing microtubules in vivo (Pedrotti et al. 1996). Despite the crosslinks formed by MAP's, microtubules can slide relative to one another.

1.4.3 Microfilaments

Microfilaments comprise of actin subunits arranged like two strings of pearls intertwined to form fibrils 4-6 nm in diameter. Actin microfilaments can be found throughout neurons and glia but are concentrated in presynaptic terminals, dendritic spines, growth cones and subplasmalemmal cortex. In the axon, microfilaments are most apparent in the vicinity of microtubules and near the plasma membrane. Microfilaments and associated proteins e.g. spectrin, a protein which binds actin filaments and links them to the plasma membrane (Bennett, 1985), form the membrane cytoskeleton which is important for cell shape, cell to cell interactions and distribution of membrane proteins. At the leading edge of the elongating process is the growth cone which, through controlled polymerisation and rearrangement of the actin fibres, is responsible for process extension.

1.4.4 Axonal transport

In mature neurons, the extreme asymmetry of the neuron with its small cell body relative to the long lengths of its axons and dendrites and the restriction of the non-mitochondrial protein synthetic machinery to the cell body has led to the development of a specialised form of bi-directional intracellular transport. This process is termed axonal transport and is responsible for maintaining the integrity of the axon and its nerve terminal. Fast anterograde transport is a collective term for the two fastest rate components, with the faster carrying membranous organelles at approximately 400 mm/day and the slower carrying mitochondria at approximately 50 mm/day (Lewen et al. 1996). Organelles are transported down the axon utilising axonal microtubules as 'tracks'. Movement in the anterograde direction is mediated by the molecular motor, kinesin while the force necessary to move retrograde organelles is generated by dynein (Fig. 1.2). The slow component of axonal transport is responsible for the anterograde movement of the cytoskeleton and enzymes of intermediary metabolism (Ochs, 1972). Retrograde axonal transport carries axonal constituents from the periphery to the cell body at approximately half the rate of fast anterograde transport (Ochs, 1972). Thus, anterograde axonal transport is responsible for the movement of neurotransmitters, proteins and mitochondria from the cell body to the nerve terminals whereas retrograde axonal transport carries lysosomes, trophic factors, and tracer molecules from the nerve terminal to the cell body. Without normal axonal transport processes occurring within the axon, the integrity of the axon is compromised. Intact axonal transport systems are vital to the survival of all neurons.

Figure 1.2 Illustration of movement of membrane-associated material in fast axonal transport

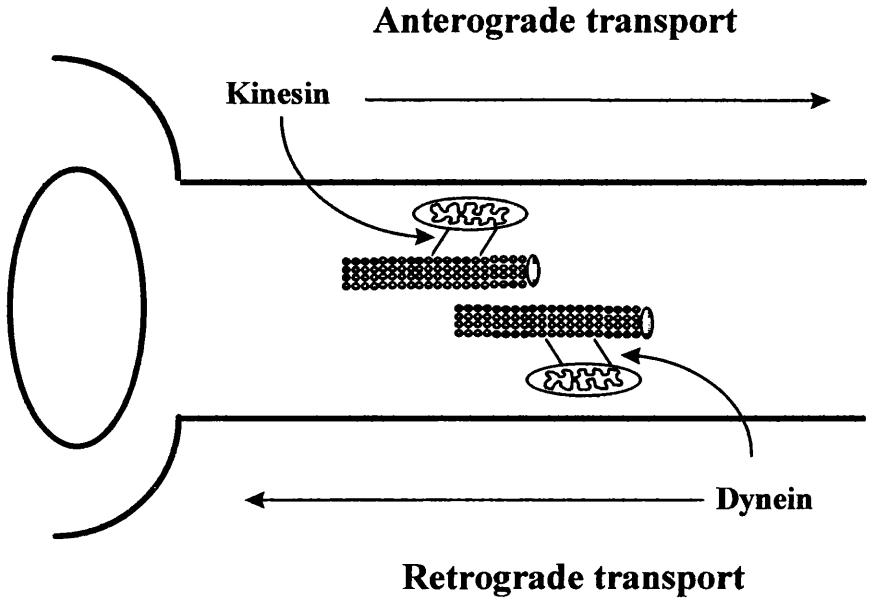

1.4.5 Axonal ion channels

Myelinated axons have a unique architecture allowing them to transmit action potentials reliably and in an energy efficient manner (Waxman and Ritchie, 1993; Salzer, 1997). There is a highly segregated distribution of ion channels and transporters on the axon membrane that are designed to carry ionic currents required for action potential generation and propagation. Internodal K^+ channels are thought to contribute largely to the maintenance of a hyperpolarised resting membrane potential of about -80mV (Stys et al. 1997; Bostock and Grafe, 1985; Chiu and Ritchie, 1984; Chiu and Ritchie, 1982). The Na^+-K^+-ATPase is the main active ion transporter designed to maintain adequate

transmembrane gradients of Na^+ and K^+, pumping Na^+ out of the cell and K^+ into the cell.

Voltage gated sodium ion channels are responsible for initiation and conduction of the neuronal action potential and, therefore play a fundamental role in the normal function of the nervous system. In cell bodies and axon initial segments, sodium ion channels determine the threshold for action potential generation and effect the duration and frequency of repetitive neuronal firing. There is a very high density of voltage-gated, rapidly activating and rapidly inactivating, sodium channels at the nodes of Ranvier (approx. 1,000-2,000 channels/μm^2) (Waxman, 1995). A non-inactivating sodium conductance has also been demonstrated in the optic nerve (See section 1.5.3) (Stys et al. 1992a).Whether this non-inactivating sodium conductance represents a homogeneous population of sodium channels, a fraction of which fails to inactivate completely, or represents a distinct subpopulation of sodium channels, or even a uniform population which switches between gating modes, remains unclear. In synapses, repetitive sodium influx through voltage-gated sodium channels initiate glutamate release by propagating a depolarising stimulus to the sites of vesicular release. Presynaptic voltage-activated calcium channels at the release sites are opened in response to this depolarisation. The resultant elevation of cytoplasmic calcium levels in the nerve terminal initiates the process of exocytosis of glutamate.

The Na^+-Ca^{2+} transporter couples transmembrane fluxes of Na^+ to opposite fluxes of Ca^{2+}. Under normal conditions the energy stored in the electrochemical Na^+ gradient is used to export Ca^{2+} from the cytoplasm, thus contributing to cellular Ca^{2+} homeostasis (Steffensen and Stys, 1996). A number of other transport mechanisms also contribute to overall ionic homeostasis (Section 1.5.3). Together with electrically tight paranodal myelin seals, axonal ion channels generate transmembrane currents that are

conducted from node to node in a saltatory fashion, thus allowing very rapid and efficient signal transduction.

1.5 MECHANISMS OF NERVE INJURY

1.5.1 Introduction

The CNS is divided into regions containing grey matter (cell bodies, dendrites and synapses) and white matter (nerve fibres and associated glia). Although historically there has been more interest in grey matter injury, both white and grey matter are dependent on an adequate blood supply, and any interruption of the CNS vasculature can compromise function in both types of tissue. Following the interruption of blood supply, while there are a number of common steps to both grey and white matter injury, there are also many events that are unique to white matter injury. Disruption of ion transporters, the cytoskeleton or glia, including the overlying myelin sheath, may result in impairment or complete failure of impulse transmission.

1.5.2 Glutamate-receptor-mediated neuronal cell body damage

Certain amino acids play important transmitter and modulatory roles in the brain, controlling functions such as learning, memory, and emotions. Glutamate and aspartate act as fast excitatory signal transmitters. Work by Lucas and Newhouse in 1957 showed that retinal neurons were damaged following prolonged exposure to glutamate. Since then it has become widely accepted that high extracellular concentrations of glutamate are neurotoxic (Rothman and Olney, 1986). Glutamate has been hypothesised to have a pivotal role in the pathogenesis of neuronal cell death due to acute focal or global ischaemia of the CNS (Muir and Lees, 1995). A 40-fold increase in extracellular

glutamate in the striatum after middle cerebral artery occlusion in the rat has been demonstrated (Butcher et al. 1990).

Glutamate receptors can be differentiated into two main classes, i.e., ionotropic and metabotropic receptors. The ionotropic receptors contain integral, cation-specific ion channels, whereas the metabotropic receptors are coupled to G proteins and modulate the production of intracellular messengers (Fig. 1.3). The utilisation of recombinant DNA techniques has greatly advanced the understanding of the structure, properties and expression of the glutamate receptors. The metabotropic glutamate receptors are currently classified into three different groups according to their sequence identity, transduction mechanisms and agonist pharmacology (for review see Conn and Pin, 1997). Group I metabotropic receptors are coupled to the stimulation of phosphoinositide hydrolysis whereas group II and III are negatively coupled to cAMP formation. Several studies have suggested that agonists of group II and III metabotropic receptors can be neuroprotective whereas agonists of group I are without effect or may potentiate excitotoxicity. Interestingly, a recent study using a highly selective group II metabotropic glutamate receptor agonist resulted in no significant reduction in infarct volume in a rat model of focal cerebral ischaemia (Lam et al. 1998).

Ionotropic receptors are ligand gated ion channels, and they include N-methyl-D-aspartate (NMDA) and α-amino-3-hydroxy-5-methyl-4-isoxazole propionic acid (AMPA)/kainate receptors. NMDA receptors are composed of homo- or heteromeric complexes of NMDAR-1 subunit and at least one of four NMDAR-2 subunits (NMDAR-2A, -2B, -2C, -2D) (Nakanishi, 1992). The NMDA receptor ion complex appears to be confined to the central nervous system, with a particularly high density in the hippocampus and the cerebral cortex. This complex possesses a number of modulatory sites in addition to that at which glutamate binds (Fig. 1.4). Under normal

circumstances, NMDA receptor-mediated calcium fluxes couple receptor activation to intracellular responses such as protein phosphorylation, enzyme activation, and changes in gene expression. However, when cerebral blood flow is significantly reduced, nerve cells and glia are deprived of oxygen and nutrients such that their ability to generate high-energy phosphates to fuel the membrane-bound pumps is depressed. As a result, K^+ leaks out and glutamate is not pumped into presynaptic nerve cells and glia, thus accumulating in the synaptic cleft. Electrical depolarisation of the presynaptic neuronal membrane causes calcium entry through voltage-gated calcium channels. Increased intracellular calcium leads to exocytotic release of glutamate into the extracellular milieu, further increasing its concentration in the synaptic cleft leading to an *overload* phenomenon and excitotoxicity (Olney, 1978). Glutamate binds to the NMDA, AMPA/kainate and metabotropic receptors on the postsynaptic membrane. Depolarisation also activates postsynaptic NMDA receptors by removing the magnesium plug in their ion channels. The pattern of glucose hypermetabolism in the peri-ischaemic zone corresponds both topographically and temporally with the uptake of both ^{3}H-MK-801 and ^{123}I-MK-801 after MCA occlusion (Wallace et al. 1992). ^{3}H-MK-801 is a specific ligand for the agonist gated NMDA ion channel, therefore the in vivo binding is indicative of glutamate-induced ion channel activation. Activation of the ionotropic receptors allows for the entry of calcium and sodium through NMDA ion channels and sodium through AMPA/kainate ion channels in the postsynaptic membrane into neurons. In addition, metabotropic receptor stimulation leads to the generation of inositol-1,4,5-triphosphate (IP_3) and diacylglycerol (DAG), which liberates calcium from internal stores (e.g., mitochondria and endoplasmic reticulum). Neuronal calcium concentration increases and activates a number of intracellular enzymes (e.g., kinases, calpains, xanthine oxidase, phospholipase A_2, nitric oxide

synthetase) which damage the nerve cell (Holt, 1997). Additionally, the stimulation of the enzyme nitric oxide synthetase leads to the accumulation of large amounts of nitric oxide. This in turn, can generate oxygen-derived free radicals that can damage cells and have effects on the redox site at the NMDA receptor to promote further calcium entry. Since the excitotoxic cascade has been developed, many other cascades, as alluded to above, have also been proposed to be involved in the pathophysiological response to cerebral ischaemia. Although these are not considered within this thesis, the challenge in the first instance being excitotoxicity, reviews and papers include, Viossat et al. 1993; Sharkey et al., in press; Hallenbeck, 1996; Arvin et al. 1996. Glutamate mediated neuronal damage is summarised in Fig. 1.3.

Figure 1.3 Glutamate mediated neuronal damage

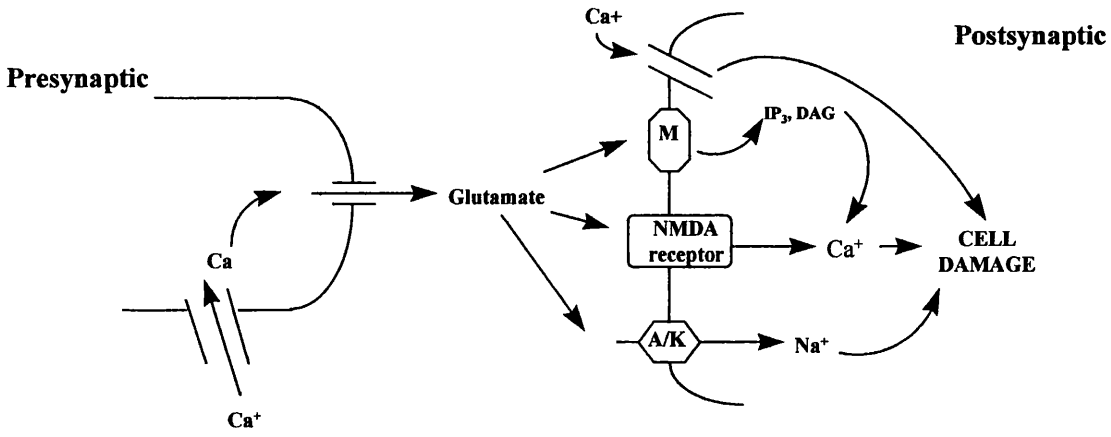

A/K AMPA/kainate

M metabotropic

IP_3 inositol triphosphate

DAG diacylglycerol

Electrical depolarisation of the presynaptic neuronal membrane causes calcium entry through voltage-gated calcium channels. Increased intracellular calcium leads to exocytotic release of glutamate into the extracellular milieu. The binding of glutamate activates NMDA, AMPA/kainate and metabotropic receptors on the postsynaptic membrane. Depolarisation also activates postsynaptic NMDA receptors by removing the magnesium plug in their ion channels. Activation of ionotropic receptors allows for entry of calcium and sodium through NMDA ion channels and sodium through AMPA/kainate channels in the postsynaptic membrane into neurons. Metabotropic stimulation results in liberation of calcium from internal stores. Neuronal calcium increases and activates a number of intracellular enzymes (Holt, 1997).

Figure 1.4 The NMDA receptor-ion channel complex

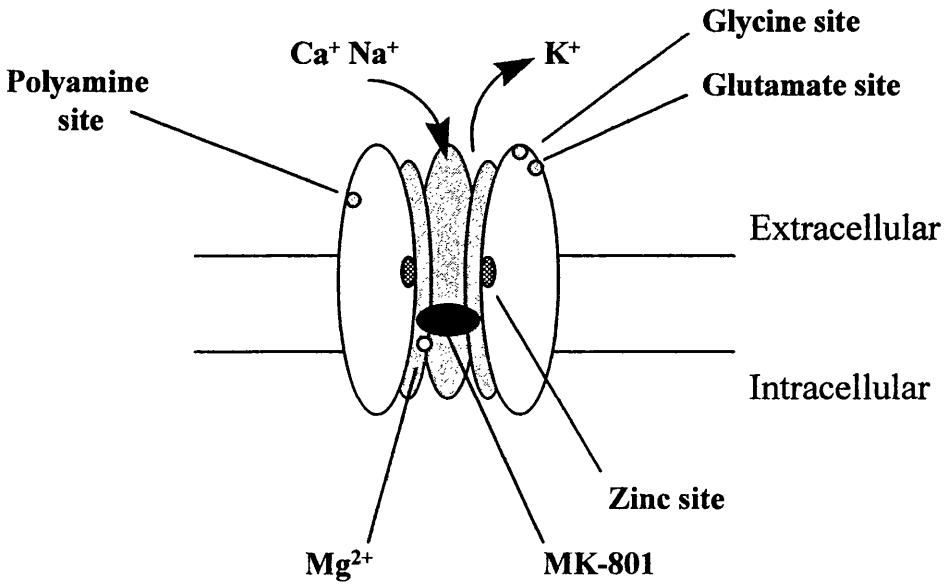

Binding of glutamate to the glutamate binding site and electrical depolarisation activate the NMDA receptor-ion channel complex. This promotes the extrusion of the magnesium plug from the ion channel and allows for the entry of sodium and calcium and the exit of potassium. The NMDA ion channel can be blocked at a variety of different sites including the glycine, glutamate, polyamine and zinc sites. MK-801 binds in a non-competitive manner within the ion channel pore at a site distinct from the magnesium binding site. (Modified from Holt, 1997).

1.5.3 White matter injury

Despite a large body of work dealing with the pathophysiology of grey matter, much less is known about that of anoxic/ischaemic injury to CNS myelinated axons. In vitro studies using an isolated optic nerve preparation have helped to elucidate the fundamental mechanisms involved in anoxic/ischaemic injury in white matter tracts. This is an ideal preparation to study the mechanisms involved in white matter injury since, unlike whole-animal studies, the preparation is devoid of synaptic connections, is composed exclusively of myelinated axons, oligodendrocytes and astrocytes and it is amenable to pharmacologic manipulations (Waxman et al. 1991). Function of excised rat optic nerves are studied in an interface chamber with suction electrodes which record the compound action potential (CAP) following supramaximal orthodromic stimulation. The area under the CAP provides an estimate of the number of fibres that are capable of conducting action potentials, a measure of the overall functional integrity of the optic nerve bundle.

Optic nerve function rapidly fails when it is exposed to anoxia (Stys et al. 1995). It is now well established that irreversible nerve injury is critically dependent on the molar concentration of extracellular calcium. Maintaining the tissue in calcium free solution throughout the anoxic period results in 100% CAP recovery, whereas increasing the perfusion of calcium during anoxia from zero to 4mM results in progressively less recovery. As the introduction of calcium free solution is progressively delayed with respect to onset of anoxia, a graded decrease in recovery of function is observed, suggesting that in white matter the deleterious effects of calcium accumulate slowly during anoxia (Stys et al. 1990). Supportive ultrastructural studies following anoxic injury indicate dissolution of the axonal cytoskeleton, swollen mitochondria and retraction of paranodal myelin (Waxman et al. 1992). In contrast, when calcium is

removed from the bathing medium, the axons retain normal ultrastructural appearing microtubules and neurofilaments (Waxman et al. 1993).

Although the increase in intracellular calcium may arise partially from intracellular stores, most of the increase is due to influx across the axolemma. Identification of the precise routes of abnormal transmembrane ion flux is of paramount importance for the rational design of therapeutic intervention. A number of routes by which calcium crosses the axonal membrane during anoxia have been proposed; namely, (1) voltage-activated calcium channels such as NMDA receptors, (2) ligand-gated calcium channels, (3) leakage of calcium through channels imperfectly selective for another ionic species, such as sodium or potassium channels, (4) reverse operation of the sodium-calcium exchanger, a countertransporter that normally exports calcium across cell membranes, and (5) non-specific flux across the axolemma, possibly rendered leaky by early hypoxic injury (Stys et al. 1995).

Ketamine, a dissociative anaesthetic known to block NMDA receptors, was shown to protect the optic nerve following anoxia. However, NMDA agonists including glutamate (at concentrations which would cause severe injury to neurons), have no toxic effect on the optic nerve making it unlikely that ketamine's protective effect was caused by NMDA receptor blockade (Ransom et al. 1990b). It is more likely that the high concentrations of ketamine resulted in blockade of the voltage-gated sodium channels. Initial observations indicated that calcium influx in white matter did not occur through conventional voltage- or ligand- gated calcium channels as it does in grey matter models of anoxia/ischaemia. However, it was observed that substantial improvement in CAP recovery occurred when voltage-gated sodium channels were blocked during anoxia with sodium channel blockers such as tetrodotoxin or saxitoxin (Stys et al. 1991b, 1992b). Furthermore, increasing sodium channel permeability with veratridine during

anoxia resulted in greater injury (Stys et al. 1992b) and removal of sodium prior to anoxia also protected the axons to some degree. These results indicate that influx of sodium ions through sodium channels is a necessary step in the anoxic cascade. The route for *sustained* entry of sodium into white matter during anoxia posed an interesting question since the classical voltage-gated sodium channels, which initiate the rapid upstroke of the axonal action potential, also contribute to its termination by fast and complete inactivation, implying that these channels should rapidly close during anoxic depolarisation. Further investigations suggested that it is a non-inactivating sodium channel responsible for the continued influx of sodium ions during anoxia (Stys et al. 1993). Like the classical sodium channel, this conductance rapidly activates with depolarisation but inactivates either very slowly or incompletely even with prolonged depolarisation. More recent evidence suggests that a small component of sodium also enters through a cesium sensitive mixed Na^+ and K^+ permeable inward rectifier (Stys et al. 1998).

As already intimated, calcium influx across the membrane occurs secondary to a rise in the intra-axonal sodium. The calcium influx occurs mainly, although not exclusively, due to the reverse operation of the sodium-calcium exchanger following the large sodium influx from the extracellular space (Stys et al. 1991a). The Na^+-Ca^+ exchanger membrane protein functions under normoxic conditions to maintain calcium homeostasis by extruding calcium from the cytoplasm in exchange for sodium influx, using the energy stored in the transmembrane sodium gradient. Blockers of the sodium-calcium exchanger (bepradil, benzamil, dichlorobenzamil), significantly protect the optic nerve from anoxic injury (Stys et al. 1991b; Stys et al. 1992b). A small proportion of Ca^+ also enters directly through Na^+ channels. The possibility that the damaging influx of calcium is via voltage-sensitive calcium channels was originally investigated

using inorganic calcium blockers (Co^{2+}, Mn^{2+} or La^{3+}) and organic blockers (nifedipine and nimodipine). Although no statistical improvement in recovery of the CAP with either group of drugs was reported (Ransom et al. 1990a), subsequent work suggests that L-type, and to a lesser degree, N-type calcium channels *are* involved in the development of anoxic injury in CNS white matter (Fern et al. 1995a). Clearly, the contribution of voltage-gated calcium channels still requires some clarification (Stys, 1998).

In summary, a number of steps are involved in anoxic/ischaemic white matter injury (Fig. 1.5). An impairment of glucose and/or oxygen delivery causes ATP levels to decrease, resulting in the failure of several key ATP-dependant ion pumps such as the axolemmal Na^+-K^+-ATPase, thus causing accumulation of Na^+ within and loss of K^+ from the axoplasm, and endoplasmic reticulum Ca^{2+}-ATPase failure allowing Ca^{2+} to escape from the internal stores. A rise in intracellular Na^+ and depolarisation due to K^+ loss promotes reverse operation of the Na^+-Ca^{2+} exchanger admitting large quantities of Ca^{2+} into the fibre.

Figure 1.5 Anoxia-induced calcium accumulation in myelinated CNS axons

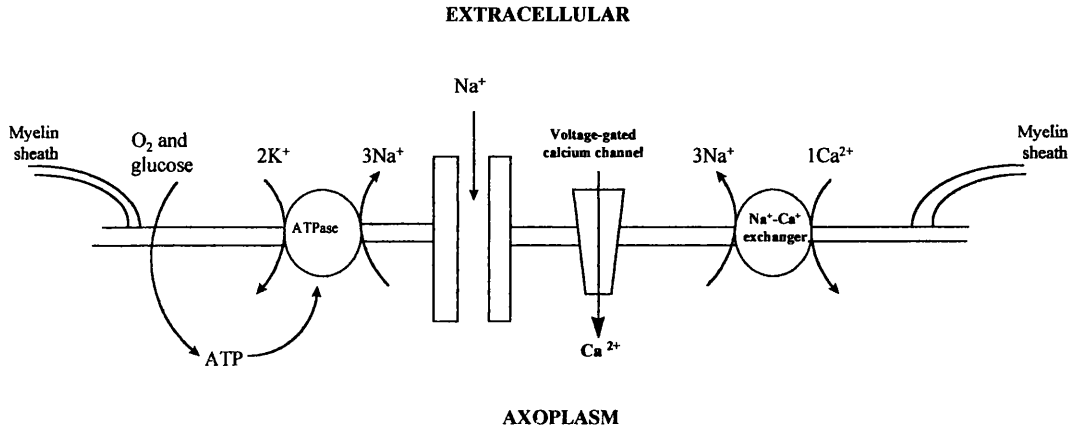

Hypothetical sequence of events leading to anoxia-induced calcium accumulation in myelinated CNS axons. Under conditions of anoxia/ischaemia, reserves of ATP are depleted rapidly, leading to failure of the Na,K-ATPase and subsequent collapse of ionic gradients. Sodium ions enter the axoplasmic space through persistently open sodium channels. This influx of sodium ions leads to a rise in intracellular sodium concentration, which may be exaggerated by restricted diffusion of ions under the nodal membrane. Both membrane depolarisation and an increase in intracellular sodium concentration cause reverse operation of the Na^+-Ca^+ exchanger, which admits damaging quantities of calcium into the cell. Voltage-gated calcium channels may provide a parallel route for calcium entry. (Modified from Stys, P.K., 1998).

Recently, the anoxic cascade has been shown to be subject to modulation via an autoprotective mechanism that involves both GABA, acting on the $GABA_B$ receptors, and adenosine, acting via adenosine receptors (Fig 1.6) (Fern et al. 1995b). Maximal recovery from anoxia was obtained with GABA concentration of 1μM, with less effective protection at higher concentrations perhaps indicative of receptor desensitisation. Adenosine produced a protective effect similar to that found with GABA (Fern et al. 1994). Furthermore, GABA and adenosine act synergistically through different receptors, to produce a protective action at the low concentrations found in anoxic white matter. It is thought that the two receptors are linked to a common effector mechanism via a G protein linked to the intracellular second messenger protein kinase C (PKC). The exact mechanism by which PKC translates into axonal protection is unclear. It has been suggested that activation of PKC results in down regulation of the Na^+/Ca^+ exchange thus reducing calcium influx during anoxia. Alternatively, PKC may result in down regulation of the Na^+ channels which mediate the Na^+ influx for driving the Na^+/Ca^+ exchanger in reverse mode during anoxia (Fern et al. 1996a). Nifedepine is a potent inhibitor of the release of adenosine and also blocks the actions of adenosine at the adenosine receptors. Therefore the observation that higher concentrations of nifedipine failed to protect white matter from anoxic injury is fully consistent with the earlier work of Stys (Stys et al. 1992b). The lack of effect of polyvalent cations has been reconciled with the fact that they irreversibly reduce the CAP when applied for 100 min and it is this apparent toxicity, rather than a lack of effect on calcium channel blockade, that accounts for this lack of effect on the development on anoxic injury. The potential for manipulating the autoprotective mechanisms provide exciting therapeutic potential (Fern et al. 1996b).

Figure 1.6 Anoxia induced GABA release

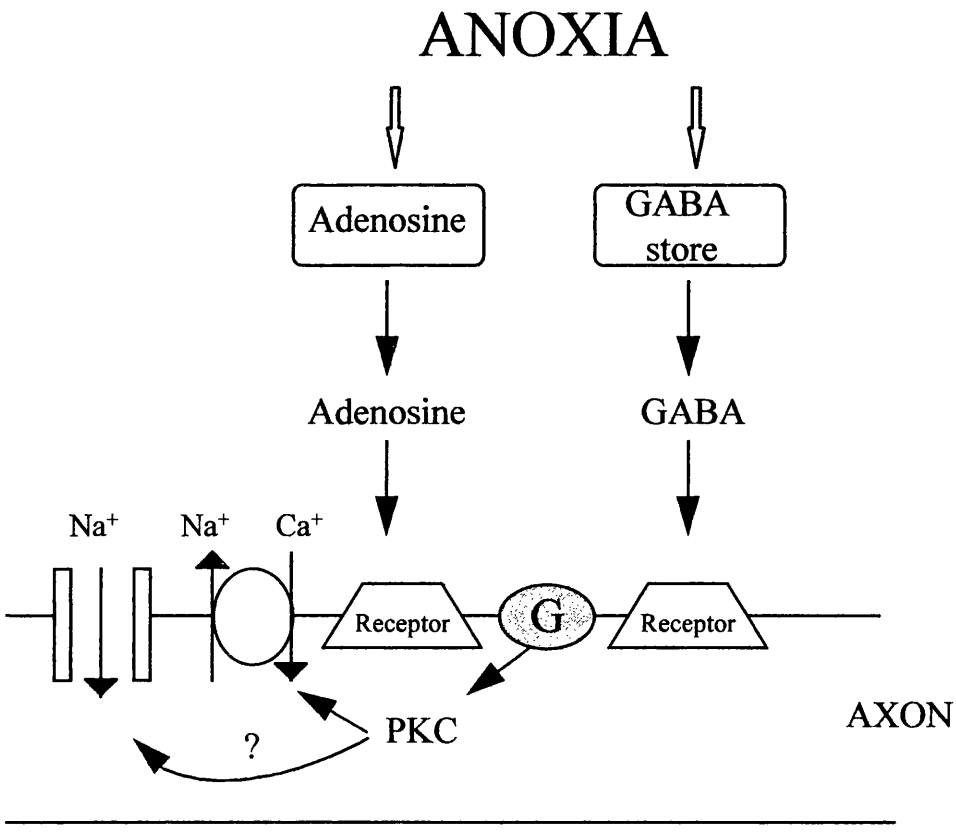

Anoxia induces release of GABA and adenosine from sites endogenous to the nerve. The resulting increase in the extracellular concentration of GABA and adenosine triggers the activation of adenosine and $GABA_B$ receptors, initiating an intracellular pathway involving a G-protein/PKC cascade. Optic nerve axons are made more resistant to anoxia as a result. The target of PKC phosphorylation is unknown, but could be the Na^+/Ca^+ exchanger, whose phosphorylation, and subsequent down regulation would limit Ca^+ influx or the Na^+ channel. (Modified from Fern et al. 1996a).

1.5.4 Action of calcium

Cellular calcium overload is generally thought to represent a key and fundamental step in the pathogenesis of axonal damage following grey and white matter injury (Fig. 1.7) (For review see Orrenius et al. 1996). As described in section 1.5.3, irreversible anoxic injury depends on energy failure and the presence of extracellular Ca^{2+}. Electron probe X-ray microanalysis has confirmed the gradual and continuous accumulation of axoplasmic Ca^{2+}, which increases from a baseline of 0.8 mM total Ca (free and bound) to 3.5 mM at the end of 60 min of anoxia (Stys, 1996). Recent work has begun to implicate proteolysis of cytoskeletal proteins as an important component in the neurodegeneration cascade following cerebral trauma, cerebral ischaemia and spinal cord injury (Kampfl et al. 1997) (see section 7.2.3). High intracellular concentrations of calcium may cause irreversible injury through mitochondrial injury and overactivation of various calcium dependent systems such as lipases, calpains and protein kinase C. Indeed, calcium alone is capable of disassembly of certain types of microtubules (for review see Maxwell et al. 1997a). Mitochondrial injury following ischaemia occurs due to degradation of mitochondrial phospholipids (Nakahara et al. 1991), collapse of mitochondrial membrane potential and subsequent failure of respiratory chain-linked oxidative phosphorylation and ATP synthesis (Orrenius et al. 1996; Sciamanna et al. 1992).

In moderate to severe blunt head injury, the change in axolemmal permeability (Povlishock et al. 1997; Pettus and Povlishock, 1996; Pettus et al. 1994) could allow normally excluded ions, including calcium, to enter the intra-axonal compartment, and result in microtubular disruption and NF sidearm loss by calcium activated proteases (calpains) (Povlishock and Christman, 1995; Hall and Lee, 1995; Maxwell, 1995). Horse-radish peroxidase was used in the above studies to demonstrate altered

axolemmal permeability, and it has been suggested that it is not an appropriate marker of damage to the axolemma at an ionic level (Maxwell et al. 1998). Recently, cytochemical evidence has demonstrated an increased content of intra-axonal calcium following optic nerve stretch injury with subsequent loss of an organised axonal cytoskeleton (Maxwell et al. 1995). A similarly close relationship of calcium mediated damage following head injury exists between influx of calcium ions and ischaemic damage (Waxman et al. 1992, 1993, 1994).

Although the relative contributions of various calcium regulated processes to neuronal cytoskeleton damage are as yet unknown, the properties and localisation of the calcium-activated neutral proteases, calpains, in the CNS have supported their proposed roles in cytoskeletal proteolysis, neuronal cell damage, cell death, and impaired neurobehavioral function following experimental brain injuries in vivo (Kampfl et al. 1997). Several lines of evidence suggest that overactivation of calpains may play a major role in cerebral ischaemia in vivo. Activation of calpains caused by an influx of calcium ions, is an attractive explanation for rapid disassembly of microtubules and further breakdown of their structural components following traumatic and ischaemic insults (for review see Kampfl et al. 1997). Calpains are calcium-activated, neutral, cysteine proteases. Two major isoforms of calpains exist, differing primarily in the concentration of calcium required for activation with one form requiring μM levels of calcium for activation, and the other form requiring mM levels (Bartus, 1997). Calpains are located throughout the neuron in somatodendritic regions and in axons (Hamakubo et al. 1986) and also may be a constituent of myelin (Li and Banik, 1995). Calpain substrates are numerous and diverse and include microtubules, microfilaments and neurofilament polypeptides, and in particular, the high molecular weight microtubule associated protein (MAP2), NFH, NFM and spectrin (see section 1.3) (Siman et al.

1996). Because uncontrolled simultaneous proteolysis of these multiple substrates would be neurotoxic, unregulated calpain proteolysis potentially represents a final common neuropathogenic pathway and could have profound effects on neuronal cell body and axonal structure and function.

Pathobiological calpain activation is believed to occur when intracellular free calcium levels surpass a certain threshold. Indirect evidence that calpain is activated in neurons following experimental injury has been shown by the use of antibodies that react specifically to calpain mediated breakdown products of cytoskeletal proteins such as spectrin. Spectrin is believed to provide shape and structural integrity to the cell while contributing to regulation of motility and function of various transmembrane proteins. The role of calpains in axonal injury following ischaemia is still under investigation but increased immunoreactivity for calpain-degraded α-spectrin has been shown in animal models following cerebral ischaemia in vivo (Roberts-Lewis et al. 1994). Some reports provide evidence that calpain activation can contribute to axonal damage following TBI (Saatman et al. 1996a), although others disagree (Yaghmai and Povlishock, 1992; Pettus et al. 1994). While the reason for these discrepancies is not entirely clear it may be that calpain-mediated proteolysis in axons involves the most severe end of the injury spectrum (Povlishock et al. 1997).

Inhibition of calpain mediated proteolysis might be a potential therapeutic strategy for reducing injury induced cellular damage and neurobehavioural deficits following acute CNS injury. In recent years considerable interest has been directed to the potential value of calpain inhibitors as postischaemia treatment of stroke (Bartus, 1997). Protease inhibitors that block calpain activation have proven to be neuroprotective following cerebral ischaemia and traumatic brain injury providing support for the calpain hypothesis (Saatman et al. 1996b; Posmantur et al. 1997; Hong et

al. 1994; Bartus et al. 1997). Although no specific reference to axonal salvation was suggested, the calpain inhibitor (AK295) administration has proven to significantly reduce infarct volume in an animal model of cerebral ischaemia (Bartus et al. 1994).

Figure 1.7 Mechanisms of grey and white matter injury compared

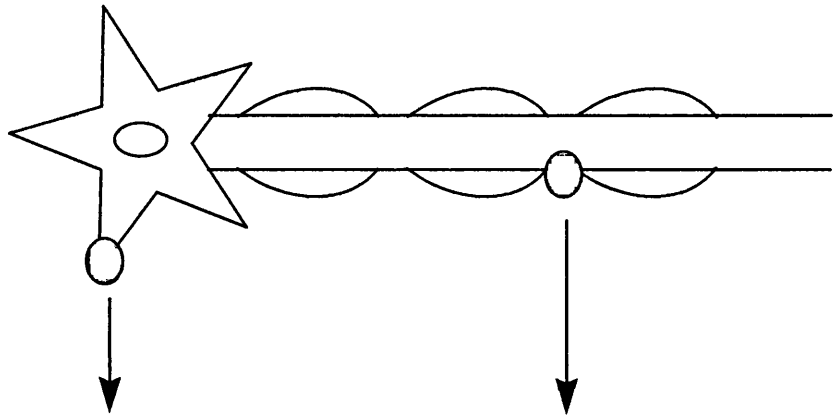

Energy failure, impaired ion pumping

•Glutamate excitotoxicity
•Na^+ influx via Na^+ channels
•Membrane depolarisation

•Activation of VSCC's
•Reverse sodium-glutamate transport
•Release of calcium from stores

•Na^+ influx via sodium channels and inward rectifiers
•Membrane depolarisation

•Reverse Na^+-Ca^+ exchange
•Release of calcium from internal stores?
•Reverse Na^+-glutamate transport?

•Ca^{2+} overload
•Ca^{2+} activated enzymes
•Free radical injury
•Mitochondrial damage

Cell death

VSCC's: voltage-sensitive calcium channels

Modified from Stys, P. K., 1998

1.6 NEUROPROTECTION WITH GLUTAMATE ANTAGONISTS

1.6.1 Introduction

Since glutamate is implicated in the pathophysiology of brain damage, prevention of its release or blockade of its postsynaptic action to protect central mammalian neurons from hypoxic-ischaemic injury has been extensively examined. Many neuroprotective studies have been performed with a variety of NMDA and non-NMDA glutamate antagonists, and glutamate release inhibitors, the majority of which have shown neuroprotective efficacy in animal models (Gill et al. 1991; Park et al. 1988a; Park et al. 1988b; Ozyurt et al. 1988). Although many different glutamate antagonists have been produced by the pharmaceutical industry, the investigations described in this thesis concentrate on two; namely, MK-801 and BW19C89. A brief description of the mode of action of these two drugs is discussed below.

1.6.2 Blockade of postsynaptic action of glutamate

NMDA-mediated elevation of intracellular free calcium appears to be pivotal in the initiation of irreversible cell death. The NMDA ion channel can be blocked at a variety of different sites. The effects of NMDA receptor antagonists in experimental models of focal ischaemia effect a marked reduction in the amount of irreversible ischaemic damage irrespective of the species, the model of cerebral ischaemia, when the animals are sacrificed after the ischaemic episode, whether ischaemia is permanent or temporary and followed by reperfusion, and irrespective of the particular site within the NMDA receptor at which the drug acts (McCulloch, 1992). Dizoclipine/MK-801 (Merck Sharp and Dohme) binds in a non-competitive manner at a binding site within the ion channel pore (Fig. 1.4) and is a use dependent, open channel blocker which binds more

effectively when NMDA receptors are activated by elevated levels of extracellular glutamate. In 1987 MK-801 was shown to prevent NMDA-induced cell death in the chicken retina (Olney et al. 1987). Since then, the non-competitive antagonist, MK-801 (Kemp et al. 1987; Wong et al. 1986) has been demonstrated to significantly reduce the volume of ischaemic damage in the cerebral hemisphere when administered pre or post occlusion of the middle cerebral artery in cat and rat models (Gill et al. 1991; Park et al. 1988a; Park et al. 1988b; Ozyurt et al. 1988) (Fig. 1.8).

The NMDA receptor-ion channel complex appears to be confined to the central nervous system, with a particularly high density in the hippocampus and cerebral cortex. Although there is a plethora of evidence to support the neuroprotective effects of NMDA receptor antagonists, there is little evidence to support the protective effect of such drugs on white matter following ischaemia. Negligible NMDA receptors have been demonstrated in myelinated axonal tracts (Jones and Baughman, 1991) and NMDA agonists do not damage the rat optic nerve *in vitro* (Ransom et al. 1990a). Clearly, the pathophysiological mechanisms involved in grey matter injury described above, and the consequent rationale for the use of NMDA antagonists in grey matter protection, cannot be so readily applied to white matter.

Figure 1.8

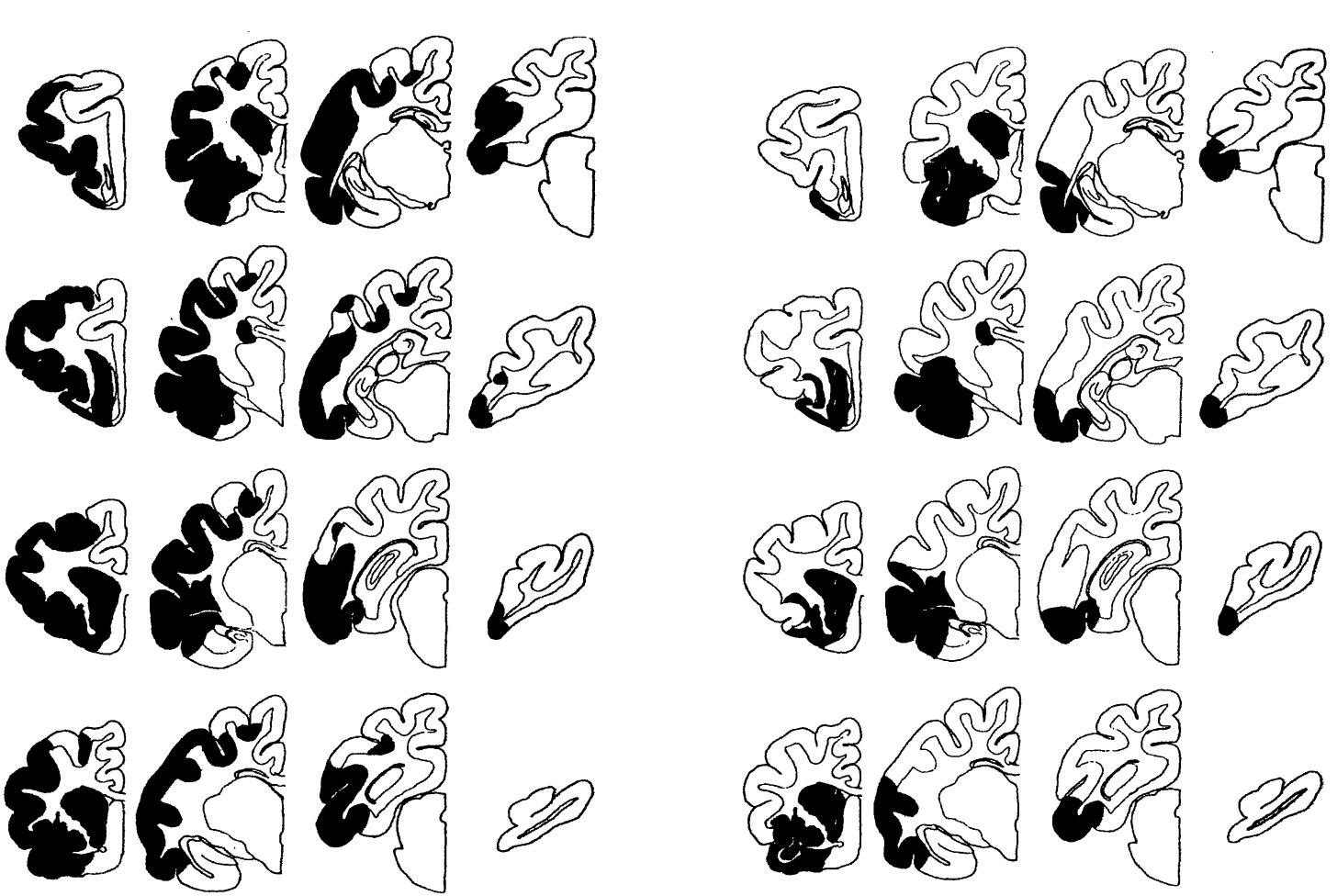

Cerebral hemisphere infarction = 3,280mm^3 **Cerebral hemisphere infarction = 1,428 mm^3**

Diagrammatic representation of the 16 coronal levels showing the areas of infarction (represented in black) for the median animals from a vehicle treated group and MK-801 treated group. MK-801 significantly reduced the area of ischaemic damage in each coronal plane when administered prior to MCA occlusion. Modified from Ozyurt et al, 1988.

1.6.3 Prevention of glutamate release

A fresh approach to ameliorating ischaemic brain infarction has been investigated through blocking the presynaptic release of glutamate (Leach et al. 1993). Presynaptic blockade of glutamate release is advantageous in that it prevents the activation of both the NMDA and non-NMDA receptor sites. The contribution of sodium ion channels to the mechanisms leading to anoxic white matter injury have been well characterised by Waxman and co-workers in the optic nerve (see section 1.5.3).

BW619C89 is an inhibitor of neuronal sodium ion channels and blocks ischaemia induced presynaptic glutamate release. It is 'use dependent', meaning that it blocks glutamate release with greater efficacy under conditions of persistent or repetitive depolarisation, as would be encountered under pathological circumstances, than under normal physiological circumstances (Goldin et al. 1995). It has been shown to decrease the release of glutamate in vitro, decrease the release of ischaemia induced glutamate in vivo, and decrease infarction following permanent and temporary MCA occlusion in rats (Kawaguchi and Graham, 1997; Leach et al. 1993; Smith et al. 1993). Unlike NMDA antagonists it does not produce the cytopathological and behavioural side effects that are produced by MK-801 (Graham et al. 1994). In addition, the reduction in brain damage by BW619C89 correlates with significant long-term functional improvement in rats (Smith et al. 1997). BW619C89 also inhibits glutamate release in the caudate nucleus, even though they do not prevent infarction in this region. Given the demonstrated benefit of sodium channel blockade in the anoxic rat optic nerve, it is interesting to posit that sodium channel blockers, such as BW619C89 administered in vivo will be effective axonal protectors following ischaemic injury. It is also of interest to note that BW619C89, as well as inhibiting sodium channels, has recently been demonstrated to inhibit human N-type voltage-gated Ca^{2+} channels

(McNaughton et al. 1997). These Ca^{2+} channels have also been indicated to be involved in the development of anoxic injury in CNS white matter (Fern et al. 1995a) (section 1.5.3). The assessment of axonal protection following administration of BW619C89 will be of interest, particularly as it acts at two channel sites, both of which are integral to the pathogenesis of axonal injury following ischaemia.

1.7 ASSESSMENT OF WHITE MATTER INJURY IN VIVO

1.7.1 Introduction

With increasing awareness of the importance of white matter injury following both traumatic and ischaemic insults, attention has turned to methods by which white matter injury can be assessed. The levels of resolution of methods used to investigate white matter injury are diverse, ranging from the investigation of structural components of the axonal cytoskeleton using immunocytochemistry, to the assessment of white matter tract abnormalities using magnetic resonance imaging (MRI). There does not appear to be a 'gold standard' by which white matter structure and function can be assessed; by concentrating solely on one aspect of white matter function, such as measurement of an action potential, only a partial view is obtained. Perhaps a combination of techniques will always be required to fully assess axonal structure and function. In the following section, a few of the techniques that are currently used to advance our knowledge of white matter injury are discussed.

1.7.2 Immunohistochemistry

Unlike grey matter, where standard histological techniques such as haematoxylin and eosin staining allow a neuropathologist to delineate neuronal death, more complex

protocols are required for the assessment of axonal injury. For many years a standard histological silver impregnation technique was used which allowed the visualisation of axonal retraction balls following head injury. The availability of a whole spectrum of antibodies targeted towards axonally transported proteins, components of microtubules, microtubule associated proteins and neurofilament proteins, has revolutionised investigations of axonal structure and function following both traumatic and ischaemic insults. Results obtained using immunocytochemical markers of axonal injury indicated that the frequency of axonal injury had previously been vastly underestimated using conventional silver techniques (Gentleman et al. 1995).

Amyloid precursor protein (APP) and synaptosomal associated protein of 25kDa (SNAP25) are two examples of proteins which move by anterograde axoplasmic transport and accumulate in detectable levels following cytoskeletal disruption due to inhibition of axoplasmic flow (Sherriff et al. 1994a; Koo et al. 1990). The discovery that antibodies against these proteins could be used to study axonal injury following ischaemia was serendipitous. Original interest in APP was in relation to Alzheimer's disease since the main component of the amyloid plaques, a pathologic hallmark of Alzheimer's disease, is βA4, a 39-43 amino acid peptide cleaved from APP (Coria et al. 1992; Glenner and Wong, 1984). The localisation of APP in rat brain has recently been studied with a cytoplasmic domain-specific antibody and found to be present, in varying degrees, in most neurons (Card et al. 1988; Ouimet et al. 1994). This suggests that this protein plays a role common to all neurons, perhaps with a more specific role in the functions of certain classes of neurones. APP may function in cell-cell adhesion or contact, stabilisation of synaptic contacts, neuritic outgrowth, serine protease inhibition, growth regulation, or it may be a receptor for an unidentified ligand involved in some signal transduction process (Ouimet et al. 1994). It has been speculated that interference

of axonal transport is an integral step in the subsequent tangle and dystrophic neurite formation and in β-amyloid protein deposition in Alzheimer's disease. Blockade of axoplasmic flow could cause an accumulation of APP resulting in amyloidogenesis. Several studies of APP in relation to Alzheimer's research has given insight into the use of APP as a marker of axonal damage in other conditions including ischaemic damage.

Similarly, original interest in SNAP25 had not been as a marker of axonal injury but its role in the synaptic function of specific neuronal systems (Oyler et al. 1989; Oyler et al. 1992). In development, the expression of SNAP25 mRNA and protein corresponds with the onset of synaptogenesis and recent evidence has shown that in addition to being involved in neurotransmitter release, it is involved with the fusion between synaptic vesicles and the presynaptic membrane, and many other membrane fusion processes within axons (Duc and Catsicas, 1995; Sollner et al. 1993). The fact that SNAP25 is incidentally transported by fast anterograde transport along axons lends it as another possible candidate as a marker of axonal injury (to be discussed in more detail in subsequent chapters).

Despite there being a plethora of axonally transported proteins, and the availability of antibodies targeted towards them, quantification of axonal injury has posed a perplexing problem. The awareness of the need to quantify axonal injury has been highlighted by the absence, or at best a scant presence, of suitable methods described in the literature. In man, grading of diffuse axonal injury has been useful for diagnostic purposes but does not provide the detailed information about the anatomical distribution of axonal injury. In grade1 diffuse axonal injury there is only microscopic evidence of axonal injury, in grade 2 there is also a focal lesion in the corpus callosum and in grade 3 there is an additional focal lesion in the dorsolateral quadrant of the brainstem (Adams et al. 1989). Similarly, many scientific papers assess the presence of

APP only by semi-quantitative means such as allocating a score based on the amount of APP as small, moderate and extensive (Graham et al. 1995), negative, sparse, moderate, dense (Roberts et al. 1991) or present and absent (Gentleman et al. 1993) (Fig. 1.9). More recently a sector scoring method has been described where the presence of axonal injury from head injury, is defined by APP positive immunoreactive axonal swellings recorded on a series of line diagrams of standard whole brain divided into 116 sectors to provide an Axonal Injury Sector Score ranging from 0-116. The advantage of this technique is that by identifying those sectors in which there is evidence of axonal damage, an overview of the pattern of axonal injury in a particular brain is seen readily and by counting the number of sectors in which axonal injury is present, an axonal injury sector score is also obtained (Blumbergs et al. 1995). The disadvantage of this method is that a positive score is given irrespective of whether there is mild or extensive APP immunoreactivity so at best, this method gives only an indirect measure of the amount of axonal injury in a given brain. Nevertheless, in general, the higher scores correlate with the Glasgow Coma Scale allocated to patients. A modified sector scoring method has also been used in an experimental setting to investigate axonal injury in sheep following head impact (Lewis et al. 1996). Again, there is a good correlation between the sector score and index of physiological response to injury. Although the sector scoring method gives some information about topographical distribution of increased immunoreactivity, it still is only semi-quantitative assessment of APP immunoreactivity.

In order to evaluate the success of putative therapies on axonal injury, a more quantitative approach may be required. Quantitative analysis of immunocytochemical staining of βAPP in the entorhinal cortex has been developed using a computerised cell counting programme. This was found to be both accurate and efficient compared to

manual cell counting (McKenzie et al. 1995). Sections were examined microscopically and images captured using a video camera, a sensitivity threshold selected such that APP positive cells were distinguished from background staining on the basis of the contrast in colour, and the cell number then automatically counted. A similar method using modern image analysis techniques has also been reported to quantify prion protein deposition in Creutzfeldt-Jacob disease (Sutherland et al. 1996). The deposits are recognised by the computer in terms of image intensity and a value for the overall amount of prion protein deposition can then be produced. In the latter example, the area of prion deposits were calculated, rather than the number of positive cells as described for the βAPP quantification. The quantification of axonal injury using APP as a marker forms a substantial part of the work described in more detail in subsequent chapters of this thesis.

Figure 1.9

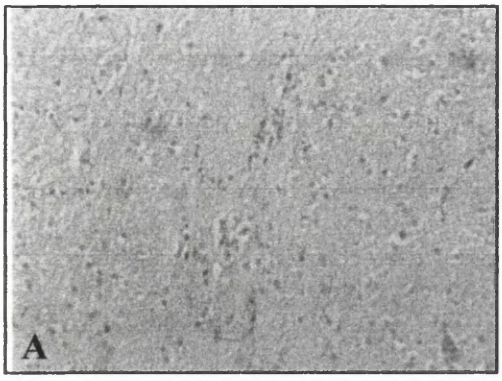

Score rating 1, (3 hours survival)

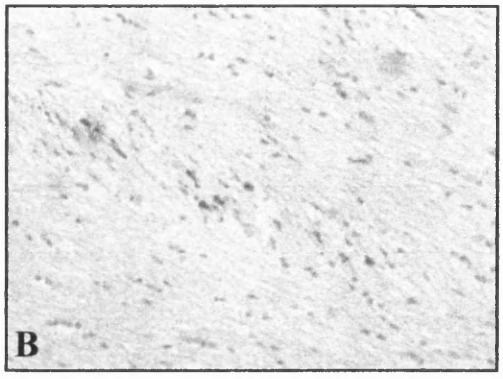

Score rating 2, (6 hours survival)

Score rating 3, (12 hours survival)

Score rating 3 with prominent bulb formation (24 hours survival)

Figures A, B, C and D illustrate semi-quantitative grading system used to quantify APP immunoreactivity following head injury in man. (Courtesy of D. I. Graham)

1.7.3 Evoked potentials

Evoked potentials are electrical waves that can be recorded from the brain after stimulation of the sense organs. The contribution of fibre tract ischaemia to functional impairment of the cortex has been deduced indirectly from abolition of evoked potentials in normally perfused cortical areas (Graf et al. 1990a). Graf and colleagues performed some very elegant experiments recording regional cerebral blood flow, somatosensory evoked potentials, and auditory evoked potentials in the thalamic relay nuclei and in the somatosensory and auditory cortices during and after 1 h of transient MCA occlusion (Graf et al. 1990b). Regional cerebral blood flow was also measured in the thalamocortical tracts. Regional cerebral blood flow was severely reduced during MCA occlusion in the left primary auditory cortex and in white matter pathways. In contrast, regional cerebral blood flow did not change significantly in the somatosensory cortex or in either thalamic nucleus. However, evoked potentials were abolished in both cortical areas. Cortical somatosensory evoked potentials disappeared later than auditory evoked potentials suggesting that ischaemic tolerance is higher in the white matter tracts than in the grey matter. In addition, following recirculation, there was a rapid and almost complete recovery of somatosensory evoked potentials, but little recovery of the auditory evoked potentials. Again, this suggests that the white matter tracts have a better recovery than grey matter once blood flow is restored. Since cortical somatosensory blood flow was unchanged following MCA occlusion, the loss of somatosensory evoked potentials following MCA occlusion must have been due to ischaemia of the white matter tracts and not due to ischaemia of the grey matter. Much information can be gleaned about the function of white matter tracts following ischaemic insults using electrophysiological techniques. The knowledge of functional circuitry combined with

the technique of evoked potentials exemplifies the type of research that could allow the evaluation of putative therapies on axonal function following ischaemic insults.

1.7.4 MRI

The advent of computed tomography (CT) and magnetic resonance imaging (MRI) has resulted in a dramatic change in the evaluation of patients with suspected intracranial abnormalities. MRI is more sensitive than CT particularly for white matter (Baird and Warach, 1998) and has become the method of choice for the clinical evaluation of the brain in normal and pathological conditions (Makris et al. 1997). MRI depends on the physical phenomenon of spinning subatomic particles of nuclei called nucleons. When in a magnetic field, the spinning nucleons are either in parallel or antiparallel to the direction of the field, and nuclei with an even number of nucleons do not exhibit significant magnetic properties since the nucleons tend to cancel one another out. Unpaired atomic nuclei act like small spinning bar magnets when placed in a strong magnetic field. The most commonly utilised nucleus is hydrogen due to its relatively strong MRI signal and its natural abundance in biological tissue. Tissues placed in a strong magnetic field result in a tendency for these protons to orientate in a direction along the magnetic field. When a radiofrequency wave is introduced, it adds energy to the protons. It is introduced at an energy level or frequency specific for both the magnetic field strength and the particular proton. The introduction of the radiofrequency pulse causes protons to move out of alignment with the magnetic field direction. When the radiofrequency excitation is stopped, the proton is free to return to the orientation of the magnetic field direction. This return to the original direction occurs over time. The process of a proton returning to the orientation of the magnetic field is called relaxation. During relaxation, the proton gives off the radiofrequency energy on signal acquired

during radiofrequency pulsation. This signal can be detected by a sensitive antenna or coil, is then amplified and processed by a computer. The specific area of tissue emitting a signal can be identified through a system known as magnetic field gradients. Image intensity varies with proton relaxation properties and depends on their chemical composition and binding. Because MRI depends on the detection of weak radiofrequency signals emitted by protons that are situated in a strong magnetic field, the image is dependent on the difference in detected signals in varying tissue types. Unlike most other imaging modalities, MRI allows a variety of manipulations to obtain a diagnostic image and vary the contrast on the images. In particular, the independent tissue variables that provide contrast on diagnostic examinations include the proton density, the T_1 and T_2, and flow. The T_1 relaxation time is the time required for the nucleons to return to their original alignment within the strong static magnetic field. The T_2 component is a measurement of the decreasing transverse activity. The type of tissue contrast obtained depends on the type of imaging sequence. In general T_1 weighted sequence is used to obtain anatomic detail. The T_1-weighted image places an emphasis on fat tissue; the fat in images appears white. A T_2-weighted image has the emphasis on increased tissue water or liquid structures, and these structures appear white. In general, an area of increased intensity (white) on an MRI image is designated as having a short T_1 (T_1 weighted imaging). If it is dark it has a long T_1 (T_1 weighted imaging). An area of increased signal intensity on a T_2 weighted image is referred to as having a long T_2; and if the signal is decreased on T_2 weighted imaging it is referred to as having a short T_2 (Orrison, 1989).

The contrast between white and grey matter is largely due to the myelination of the white matter tracts. Myelin is composed of a bilayer of lipids, cholesterol, and large proteins. There are differences in the relaxation time between white matter and grey

matter. In white matter, the myelin lipids themselves contain few mobile protons visible to routine MRI, but they are hydrophobic, and therefore, as myelination progresses, there is a loss of brain water and a decrease in T_2 signal. Cholesterol tends to have a short T_1, and the increased protein also decreases the T_1 of water. This results in white matter having a reduced intensity on T_2-weighted images and increased intensity on T_1-weighted images compared with unmyelinated fibres or grey matter. MRI is very sensitive to white matter abnormalities but not specific. Following a critical reduction in blood flow to a particular region, normally myelinated white matter is destroyed.

Advances in MRI include diffusion imaging, which gains an understanding of microscopic water shifts as the different types of oedema develop, and perfusion imaging, which can assess microvasculature perfusion at a high resolution. The overall principle of diffusion measurement is that the spatial location of each water molecule is tagged such that any movement of a water molecule over the time of observation results in a signal loss or darkening of the images. Thus on diffusion weighted images, regions of relatively fast rates of diffusion (e.g., cerebrospinal fluid) will appear darker than regions of normal brain, which appear darker than regions of hyperacute ischaemic injury, which have slower than normal diffusion (for review see Baird and Warach, 1998). Diffusivity is anisotropic in orientated tissue such as fibre tracts and the latest techniques in diffusion -weighted MRI have resulted in the definition of white matter lesions following stroke (Warach et al. 1995) and the capability to map (in terms of orientation, location and size) the 'stem' (compact portion) of the principal association, projection, and commissural white matter pathways of the human brain in vivo. In addition, following stroke, differences in the relative size of major association pathways have been illustrated in the living human (Makris et al. 1997). In the clinical domain,

this method will have a potential impact on the understanding of the diseases that involve white matter such as stroke.

The different techniques of MR perfusion imaging typically deal with blood volume, transit times, and blood flow as relative measures, although absolute quantification may also be possible. Two types of MR perfusion imaging have found applicability to clinical conditions and scientific studies- (1) susceptibility-based techniques that use either paramagnetic contrast agents, most commonly those containing gadolinium (contrast agent block tracking), or endogenous changes in deoxyhaemoglobin, which is an intrinsic paramagnetic molecule (blood oxygen level dependant [BOLD]); and (2) arterial spin labelling techniques (Baird and Warach, 1998). In the first method, gadolinium is injected intravenously and the scan may be performed every 1-2 seconds for 1-2 minutes. The amount of signal loss is proportional to the concentration of the contrast agent and is directly proportional to the blood volume of healthy brain tissue. BOLD imaging detects changes in the concentration of deoxyhaemoglobin that may occur under conditions of altered blood flow. When a region of neural tissue becomes active, its oxygen consumption increases. Blood flow to the region also increases, but so much that it overfulfills tissue oxygen requirements, so that deoxyhaemoglobin concentration actually falls resulting in an increased BOLD signal intensity (Prichard and Cummings, 1997). In ischaemia there is a decrease in the BOLD signal intensity reflecting decreased tissue oxygenation. The major limitations to the routine clinical and experimental use of perfusion MRI are the availability, practicality and the time intensive nature of the processing of perfusion data. The great attraction of diffusion weighted imaging and perfusion imaging in the investigation of ischaemic stroke pathophysiology is that diffusion weighted imaging provides an early marker of cellular injury in developing ischaemic lesions and serial, high resolution

studies can be performed to provide temporal information. Other techniques such as magnetic resonance spectroscopy allows the measurement of specific brain metabolites, e.g. lactate which appears in ischaemic tissue, allow even greater insight into the pathophysiology of ischaemic brain conditions. These techniques can be successfully applied to animal models of stroke and may provide insights of major relevance to human stroke about the pathophysiology and mechanisms of ischaemic lesion evolution.

1.8 AIMS OF THESIS

A large body of work exists dealing with the pathophysiology of grey matter. In contrast, much less is known about the fundamental mechanisms of anoxic/ischaemic injury to CNS myelinated axons, despite the fact that white matter has been shown to be very vulnerable to this type of injury (Pantoni et al. 1996; Follis et al. 1993). These observations emphasise that differences in the pathophysiology of grey and white matter anoxic injury are likely to necessitate multiple strategies for optimal CNS protection.

Myelinated axons are essential for the normal functioning of the brain. Since myelinated axons, like grey matter, are dependent on a continuous supply of energy, it is likely that strokes compromise axonal function as well as that of the neuronal cell bodies. Although many drugs have been targeted towards cell body protection, it has not yet been established whether this approach also protects axons. In order to establish this, the tools required include a suitable marker of axonal injury, a method by which the marker can be quantified and an animal model in which to test the hypothesis. The aims of the work described in this thesis were fourfold:

- To define markers of axonal injury appropriate for use in the assessment of axonal pathology consequent to focal cerebral ischaemia
- To develop quantitative techniques for the assessment of axonal injury
- To apply a suitable marker of axonal injury and a method of quantification of axonal injury in the rat following focal cerebral ischaemia
- To explore the utility of techniques of quantification of axonal injury in species where there is a larger volume of white matter compared to that in the rat brain.

CHAPTER 2

MATERIALS AND METHODS

The following chapter describes the materials and methods frequently used in the work relating to this thesis. The first section describes the general methods used in animal experimentation and this is followed by the description of light and electron immunocytochemistry used to assess axonal injury. The sources of commonly used materials are listed in Appendix 1 and the composition of routinely used stock solutions and buffers in Appendix 2. Additional materials and chemicals not listed are specified elsewhere in the text. The specific details for individual studies are described in subsequent chapters.

2.1 FOCAL CEREBRAL ISCHAEMIA IN THE RAT

2.1.1 Source and Strain

The studies employed adult, male Fischer 344 rats weighing approximately 300g. The Fischer rats were supplied by Harlan Olac Ltd., Bicester, Oxon, U.K.. On arrival the rats were allowed to acclimatise for five days before any surgical procedures were performed. The rats were maintained under controlled lighting and thermal environment and were allowed free access to food and water. The Fischer 344 rat was used throughout the studies described in this thesis. This decision was based on evidence suggesting that the Fischer 334 strain is the normotensive strain of choice for MCA occlusion studies. The influence of rat strain on the quantification of cerebral infarction was investigated by Duverger and MacKenzie who found that following MCA occlusion the lesion in the Fischer rat was sizeable and similar to that observed in the Sprague-

Dawley rat, yet the co-efficient of variation was considerably less significant than the latter (Duverger and MacKenzie, 1988). This was supported by a later study investigating the strain-dependent drug effects following MCA occlusion in the rat. Quantitative differences in infarction volume between strains existed, not only when there was no drug intervention, but also following the administration of three different drug classes (including MK-801). However, the largest effects with all three drug classes was attained in the Fischer 344 rats, and this strain showed the biggest volume of infarction with the least variance among the normotensive strains of rats (Sauter and Rudin, 1995) (Fig. 2.1). The above described attributes of the Fischer rats were considered to offer advantages in the study of the pathophysiology and therapy of focal cerebral ischaemia.

2.1.2 Anaesthesia

Anaesthesia was induced by placing the rats in a perspex chamber into which 70% nitrous oxide, 30% oxygen and 5% halothane was flowing. For acute experiments, a tracheostomy was performed. A femoral artery and vein were cannulated using polyethylene catheters (Portex:external diameter 0.96 mm; internal diameter 0.58 mm) to allow the continuous monitoring of mean arterial blood pressure (P231D Gould Stratham, Model 2202), the repeated sampling of blood and the administration of fluids when appropriate. Animals were maintained normocapnic, normoxic and normothermic throughout the experimental period by adjusting the volumes of gases delivered to the animal. Rectal temperature was measured and the rats were maintained normothermic ($37 \pm 0.5°C$) by heating lamp.

The protocol for survival animals is as described above except that, instead of performing a tracheostomy, rats were intubated per os using a 45 mm, 16 gauge catheter.

In addition, arterial and venous lines were exteriorised at the dorsal surface at the neck to allow continuous monitoring of blood pressure and drug/fluid administration once the animals had recovered from anaesthesia. Following middle cerebral artery occlusion, anaesthesia was discontinued and the animals allowed to regain consciousness under strict observation. Saline was injected subcutaneously (2.5 ml) to minimise dehydration post-operatively. The animals were housed individually and had access to softened food and water.

Figure 2.1

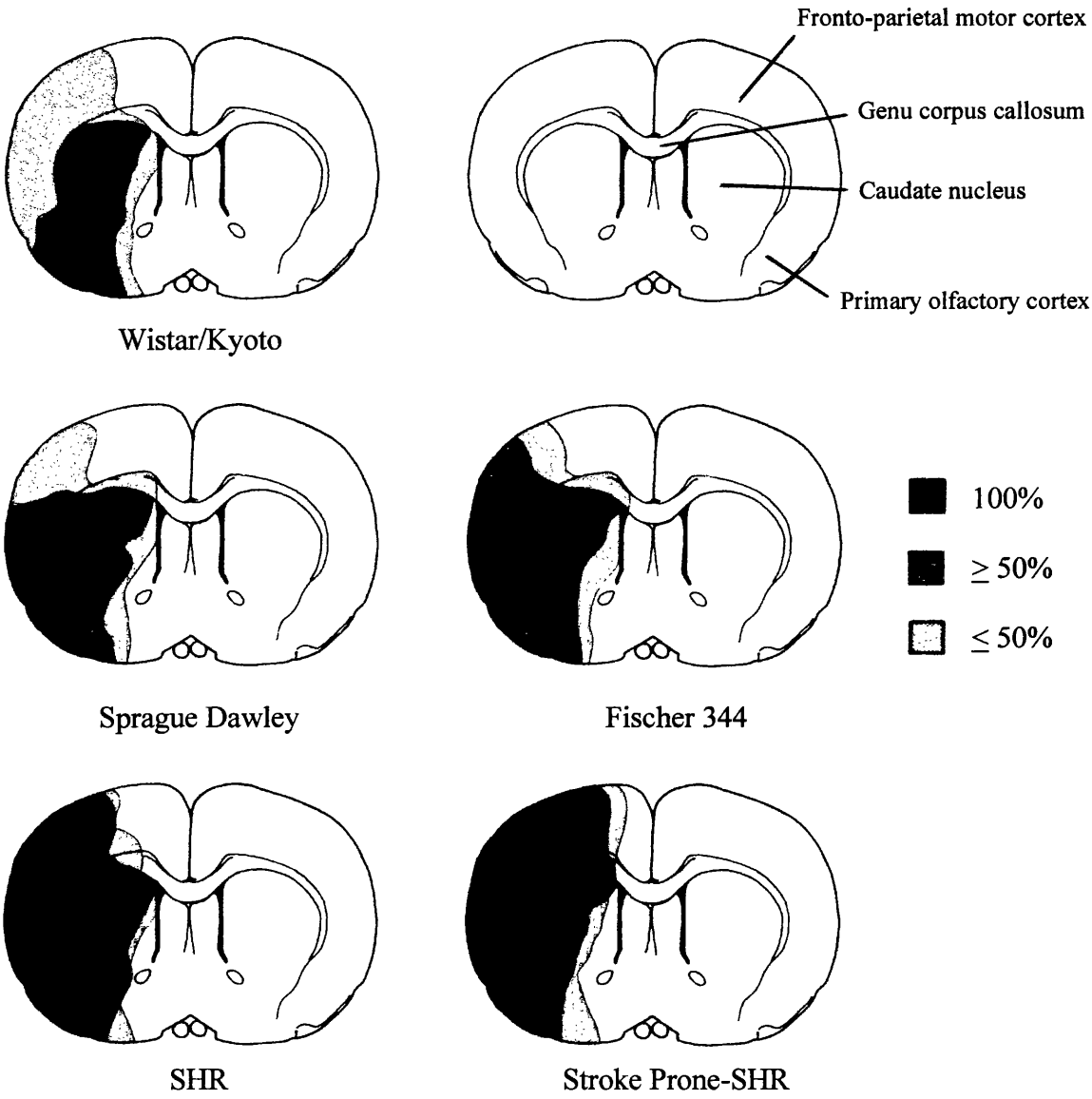

Incidence and topography of the infarction at the level of the caudate nucleus in five rat strains. Adapted from Duverger and MacKenzie, 1988.

2.1.3 Middle cerebral artery occlusion

The middle cerebral artery (MCA) occlusion model are used extensively in stroke research and have been suggested to be of particular importance to the drug discovery process because of their clinical relevance. This is because the most common sites for obstruction in man are points of bifurcation of blood vessels, especially in the territory of the MCA. Experimental stroke models generally involve MCA occlusion either by electrocoagulation (Tamura et al. 1981) or by blockade with a luminal filament thread (Zea Longa et al. 1989) (for review of focal models of stroke see McAuley, 1995). All studies within this thesis involved MCA occlusion by electrocoagulation (Fig. 2.2).

The left MCA was exposed using a subtemporal approach (Tamura et al. 1981), leaving the zygomatic arch intact (Shigeno et al. 1985). The animals were placed in lateral recumbency and a 1 cm vertical skin incision made between the left orbit and the external auditory canal. The underlying fascia was removed and the exposed temporalis muscle bluntly dissected and retracted to expose the inferior part of the temporal fossa. A small craniectomy was made using a dental drill at the junction between the medial wall and the roof of the temporal fossa, approximately 1 mm dorsal to the foramen ovale. The dura was opened using a 30 gauge dental needle and then removed using a fine hook to reveal the MCA. The main trunk of the artery was exposed proximal to the olfactory tract to where it crosses the inferior cerebral vein. The exposed artery was occluded by micropolar coagulation from its origin to the point where it crosses the inferior cerebral vein and then severed to prevent recanalisation. The craniectomy was covered by Gelfilm® (Upjohn). The muscle and skin were sutured using 2/0 braided silk.

The survival periods and protocol for drug administration for each study are described in the following chapters.

Figure 2.2

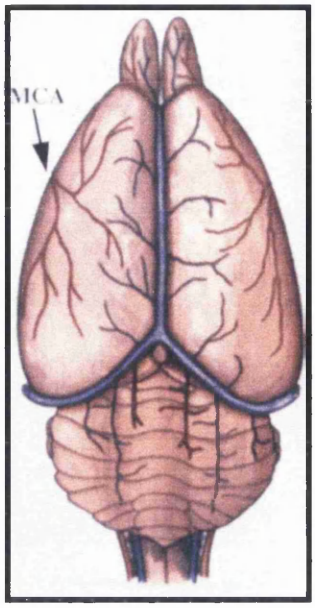

Dorsal view of rat brain showing middle cerebral artery

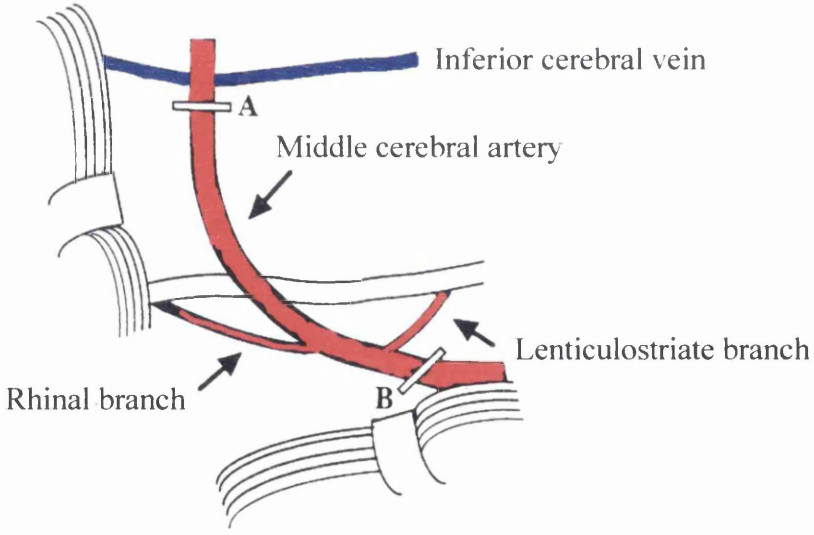

Schematic diagram of middle cerebral artery. Occlusion was performed between sites A and B. (Modified from M. A. McAuley, 1995.)

2.1.4 Transcardiac perfusion and subsequent tissue processing

At the end of the procedure the halothane anaesthesia was deepened and the animal placed supine. A thoracotomy was performed and a cannula inserted into the ascending aorta via the left ventricle, the right atrium was incised, and 200 ml of heparinised saline infused at the animals mean arterial blood pressure, followed by 200 ml of fixative. Different fixatives were used in the studies described in this thesis, the choice being dependent on the subsequent work to be performed on the tissue. Tissue processing varied for each fixative used and is described below.

Formaldehyde (4%) fixation

The fixative used was 40% formaldehyde, glacial acetic acid, absolute methanol in the ratio 1:1:8, v/v. Following transcardiac perfusion, the animal was decapitated and the head stored in fixative for at least 24 hours at 4°C before being removed and transferred to a 70% solution of methanol. After detaching the hindbrain, the forebrain was cut into four equally spaced coronal blocks, embedded in paraffin wax, and sectioned (nominally 10 μm thick) at multiple levels.

Paraformaldehyde (4%) fixation

The fixative composed of 4% paraformaldehyde in 50 mM phosphate buffered saline was used for immunocytochemical studies at the light microscope level. Following transcardiac perfusion, the animal was decapitated and the brain removed, post-fixed for 48 h and cryoprotected in 30% sucrose in phosphate buffered saline at 4°C. Following this the brain was frozen in isopentane at -42°C for two minutes. Coronal sections of 30

μm were cut in a cryostat and stored in cryprotectant solution (30% glycerol/ 30% ethylene glycol in sodium phosphate buffer) at -20°C.

Gluteraldehyde (0.5%) and paraformaldehyde (4%) processing

Brain material to be used for electron microscope studies was fixed using a mixture of gluteraldehyde and paraformaldehyde since this combination gives a better preservation of tissue than using either aldehyde alone. Formaldehyde penetrates tissues much more rapidly than gluteraldehyde and it is thought that the formaldehyde temporarily stabilises structures which are subsequently fixed more permanently by the gluteraldehyde (Karnovsky, 1965). The fixative was buffered with phosphate rather than cacodylate since the latter contains arsenic which is toxic. Since fixation is more rapid and effective the higher the temperature of the perfusate, the perfusion fluids (saline and fixative) were transfused at 37°C. Careful consideration was given to the duration of the prewash with saline since the organs and vasculature would be deprived of oxygen during this wash. Saline was therefore perfused for a period until blood was removed from the circulation and was followed immediately by the fixative for at least 10 minutes at a pressure equal to or greater than the systolic blood pressure. The brain was removed and left in the fixative overnight at 4°C. The fixed brain was cut using a vibrating microtome into 50μm sections and collected into cell wells containing phosphate buffer. Adjacent sections were collected for light microscopy and electron microscopy.

2.2 FOCAL CEREBRAL ISCHAEMIA IN THE CAT

2.2.1 Source

The studies employed adult, male and female cats weighing 3-4 kg. On arrival the cats were allowed to acclimatise for five days before any surgical procedures were performed. The cats were housed outdoors and fed twice daily.

2.2.2 Anaesthesia

The cats were anaesthetised initially with Saffan (Alphaxalone/Alphadolone) (9mg/kg i.v.), intubated, and connected to a positive pressure ventilator delivering nitrous oxide and oxygen in an open circuit. Polyethylene catheters were inserted into both femoral veins and one femoral artery for the administration of drugs and the continuous monitoring of arterial blood pressure, and blood gases and glucose. Anaesthesia was maintained throughout the course of the investigation with chloralose (60 mg/kg i.v.), supplemented as necessary to prevent the return of the corneal reflex. Throughout the experimental period, the animals were maintained normotensive (mean arterial blood pressure (MABP) greater than 80 mm Hg); normocapnic (P_aCO_2 close to 32 mm Hg) by adjusting the stroke volume of the respirator. Metabolic acidosis was corrected by administration of sodium bicarbonate (8.4%). Samples of arterial blood were taken frequently for the determination of the respiratory status using a direct reading electrode system and for the measurement of plasma glucose levels (automated assay based on the glucose oxidase reaction). The cats were maintained normothermic (rectal temperature 37°C) by means of a heating blanket with feedback control via a rectal thermometer.

2.2.3 Middle cerebral artery occlusion

The left MCA was occluded via a transorbital approach. The head of the cat was placed in a stereotactic frame. With microsurgical techniques, the left orbit was exenterated and the optic foramen and optic fissure were enlarged with a dental drill to expose the dura mater overlying the MCA close to its origin. Under the operating microscope the dura was incised and the MCA exposed. The trunk of the MCA and all visible branches of the lenticulostriate arteries were coagulated with a bipolar diathermy and divided with microscissors.

Six hours after the occlusion of the middle cerebral artery, the cat was killed by transcardiac perfusion fixation with FAM (see 2.1.4). Briefly, the cat was placed in a supine position and heparinised. A thoracotomy was performed and a cannula was introduced into the ascending aorta via the left ventricle. Physiological saline was infused at a pressure equivalent to mean arterial pressure until blood was removed from the body. This was followed immediately by 1.5 l of FAM fixative at the same pressure. After perfusion, the cats were decapitated and the head stored in fixative at 4° C for at least 12 h; the brain was then removed and left in FAM for a further 24 h before transfer to 70% methanol. After marking the left-hand side of the forebrain with Indian ink, the hindbrain was detached by a cut through the midbrain and the cerebral hemispheres were cut into five equally spaced coronal blocks. These blocks were embedded in paraffin wax and 6 sections 10 μm thick were cut at 200 μm intervals throughout the specimens.

2.3 LIGHT MICROSCOPE IMMUNOHISTOCHEMISTRY

2.3.1 FAM fixed material

Sections were mounted on 3-aminopropyltriethoxy-saline (APES) or poly-L-lysine coated slides and dried at 37°C overnight. In order to remove the wax, the sections were placed in xylene. The sections were dehydrated by placing them in absolute alcohol for two minutes and rinsed in methanol. They were left in methanol and hydrogen peroxide solution (0.5%) for 30 minutes. Tissue pretreatments, if required, took place at this stage (see 2.3.4). The sections were then rinsed in tap water and finally phosphate buffered saline (PBS) for 2 minutes. Bovine serum albumin (5%) and normal horse serum (10%) in PBS, was applied for 1 hour to block non-specific binding sites. The excess blocker was wiped off and optimally diluted primary antibody, which had been made up in the bovine serum albumin and normal horse serum in PBS, was applied and was left overnight at 4°C. As controls, the primary antibody was eliminated. No positive staining was seen in any of the control sections (Fig. 2.3). The sections were washed in PBS for 3 x 10 minutes. Diluted biotinylated antibody solution was applied for 1 h and sections washed again in PBS for 3 x 10 minutes. The avidin/biotinylated horseradish peroxidase solution (Vectastain Elite ABC Kit or Vectastain Standard ABC kit, Vector Labs) which had been prepared 30 minutes prior to use, was applied for 1 h. The washing procedure with PBS was repeated and then the sections allowed to develop in 3,3'-diaminobenzidine solution (Sigma) for 8-10 minutes. Finally, the sections were rinsed with water, dehydrated, cleared and mounted in DPX mountant.

Figure 2.3 Negative control

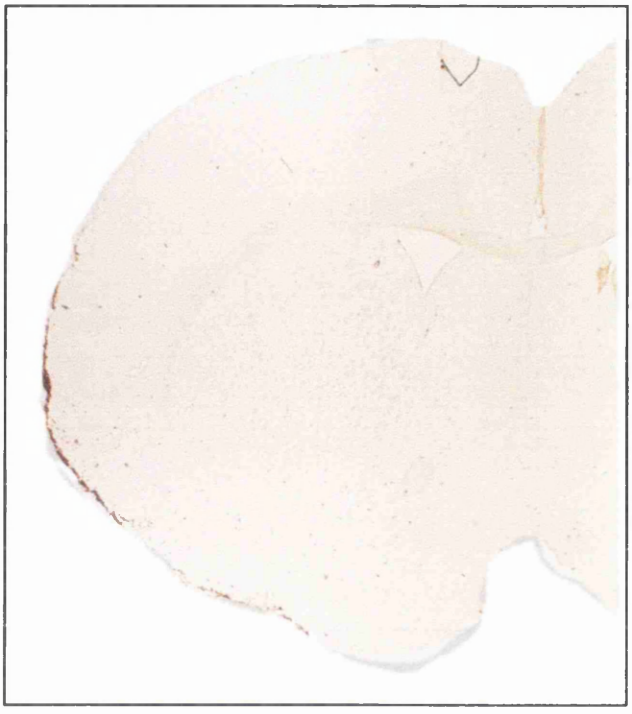

A typical example of a negative control section used in immunohistochemistry using DAB as the chromagen. Negative controls in which the primary antibody was omitted, were carried out for each immunohistochemistry run. Non-specific immunoreactivity was not detected in these tissue sections.

2.3.2 PAM fixed sections

Free-floating sections were rinsed in PBS, incubated for 30 min in 0.2% Triton X-100 followed by 20 min in 3% H_2O_2 and then for 1 h in 10% normal horse serum and 2% bovine serum albumin in PBS to block non-specific binding sites. Incubations with primary antibodies diluted in blocking buffer were overnight at 4°C. As controls, the primary antibody was eliminated. No positive staining was seen in any of the control sections. Primary antibody binding was detected using a biotinylated secondary antibody (rat adsorbed horse anti-mouse IgG (H+L), 1:100, Vector Labs) diluted in blocking buffer and an avidin-biotin complex kit (Standard and Elite Vectastain, Vector Labs) with 3,3'-diaminobenzidine (DAB Substrate Kit, Sigma) as the chromagen. Finally, the sections were washed in tap water before being dehydrated, cleared and mounted in DPX mountant.

2.3.3 Tissue pretreatments

A large proportion of the material used for immunohistochemistry in this thesis was FAM fixed and paraffin embedded. Fixation is known to cause partial or complete masking of the ß-amyloid precursor protein epitopes (ßAPP). The demonstration of the ßAPP antigen could be significantly improved by treatment with the proteolytic enzyme, trypsin. Antigen demonstration is improved due to the enzyme breaking the protein cross links formed by the FAM fixation and thereby exposing the hidden antigenic sites (Jackson and Blythe, 1993). Optimal immunolabelling occurred when the sections were pretreated with trypsin (0.1%) with calcium chloride (0.1%) at 37 °C for 15 minutes.

The microwave oven was also used to enhance antigenicity as this method has previously been demonstrated to improve ßAPP immunoreactivity (greater contrast with low background staining) following axonal injury (Sherriff et al. 1994b). Sections were

brought to the boil in citrate buffer (pH 6) in the microwave oven for 5 minutes, checked to ensure that they were still covered with buffer, reboiled for a further 5 minutes and then allowed to cool for 20 minutes before continuing with the immunohistochemistry protocol. Although the exact reason for the success of the microwave is uncertain, it is suggested that the procedure breaks some of the weak intramolecular cross-linkages that are formed during fixation.

2.3.4 Antibody concentrations

Dilution curves were carried out to determine the optimum dilution for each antibody i.e. that which produced the best signal to background ratio. Tables 2.1, 2.2 and 2.3 show the optimum concentration of antibodies and pretreatments for material fixed by both FAM and PAM.

Table 2.1 Concentration curves for immunocytochemistry on FAM fixed rat material

Concentration of APP	ABC kit Standard/Elite	Microwave	Trypsin	Quality of immunostaining
1:60	Elite	No	Yes	+++
1:120	Elite	No	Yes	+++
1:300	Standard	No	Yes	+
1:300	Elite	No	Yes	+
1:3,000	Elite	Yes	No	++

Table 2.2 Concentration curves for immunocytochemistry on PAM fixed rat material

Antibody	Concentration	ABC kit Standard/Elite	Quality of immunostaining
SNAP25	1:60,000	Standard	++
	1:120,000	Standard	+++
	1:240,000	Standard	+
MAP5	1:250	Standard	+
	1:500	Standard	++
	1:1,000	Standard	+++
NF68kD	1:10	Standard	+++
	1:50	Standard	+
	1:100	Standard	+
	1:200	Standard	+
	1:400	Standard	+
	1:800	Standard	+
	1:10	Elite	+++
	1:100	Elite	+++
	1:1,000	Elite	++
APP	1:10	Standard	+++
	1:20	Standard	+++
	1:300	Standard	+
	1:600	Standard	+
	1:300	Elite	+
β-tubulin	1:5,000	Standard	++
	1:10,000	Standard	+++

Table 2.3 Cat tissue concentration curves for amyloid precursor protein

Antibody concentration	Trypsin	Microwave	ABC kit Standard/Elite	Quality of staining
1:500	No	Yes	Elite	++++
1:1000	No	Yes	Elite	++
1:3000	No	Yes	Elite	+
1:50	No	No	Elite	++
1:100	No	No	Elite	+
1:300	No	No	Elite	+
1:500	No	No	Elite	+
1:50	Yes	No	Elite	++
1:100	Yes	No	Elite	+
1:300	Yes	No	Elite	+
1:500	Yes	No	Elite	+
1:50	No	Yes	Standard	++++
1:100	No	Yes	Standard	+++
1:300	No	Yes	Standard	+

2.4 HISTOLOGICAL PROCEDURES

Sections were stained with haematoxylin & eosin and a method that combines luxol fast blue and cresyl violet (Appendix 3). This combination allows the identification of early ischaemic brain damage where the cell body and nucleus are shrunken and become triangular in shape and the cytoplasm stains intensely with eosin and bright blue to dark mauve with the Luxol fast blue/cresyl violet technique (Graham, 1977).

2.5 MEASUREMENT OF VOLUME OF INFARCTION

2.5.1 Determination in the rat

The sections stained by haematoxylin and eosin and Luxol fast blue and cresyl violet were examined by conventional light microscopy by an investigator 'blinded' to the immunocytochemistry results. Areas of infarction (Brierley and Graham, 1984) were delineated on paraffin sections at the eight preselected stereotactically determined coronal levels and transcribed onto scale diagrams (x 4 actual size) of forebrain drawn from the atlas of Konig and Klippel (Osborne et al. 1987; Konig and Klippel, 1963) (Fig. 2.4 and Fig. 2.5). An approximation to total volume of ischaemic damage was achieved by integration of area with the distance between each level.

2.5.2 Determination in the cat

The sections were stained by haematoxylin and eosin and cresyl violet and Luxol fast blue. Those sections that corresponded most closely to 16 stereotactically predetermined coronal planes of cat brain from the atlas of Reinoso-Suarez, (1961) were examined by conventional light microscopy without prior knowledge of the animal's history. Any abnormalities were charted on the diagrams drawn to scale and formed the basis of

quantitative assessment of ischaemic brain damage in manner analogous to that previously described for the rat (Osborne et al. 1987) (Fig. 2.6). The area of ischaemic necrosis in the cerebral hemisphere, cerebral cortex and caudate nucleus was determined from the diagrams at each of the 16 coronal planes. The volumes of ischaemic necrosis were calculated from the areas of damage at the different coronal planes and their anterior-posterior co-ordinates.

Figure 2.4

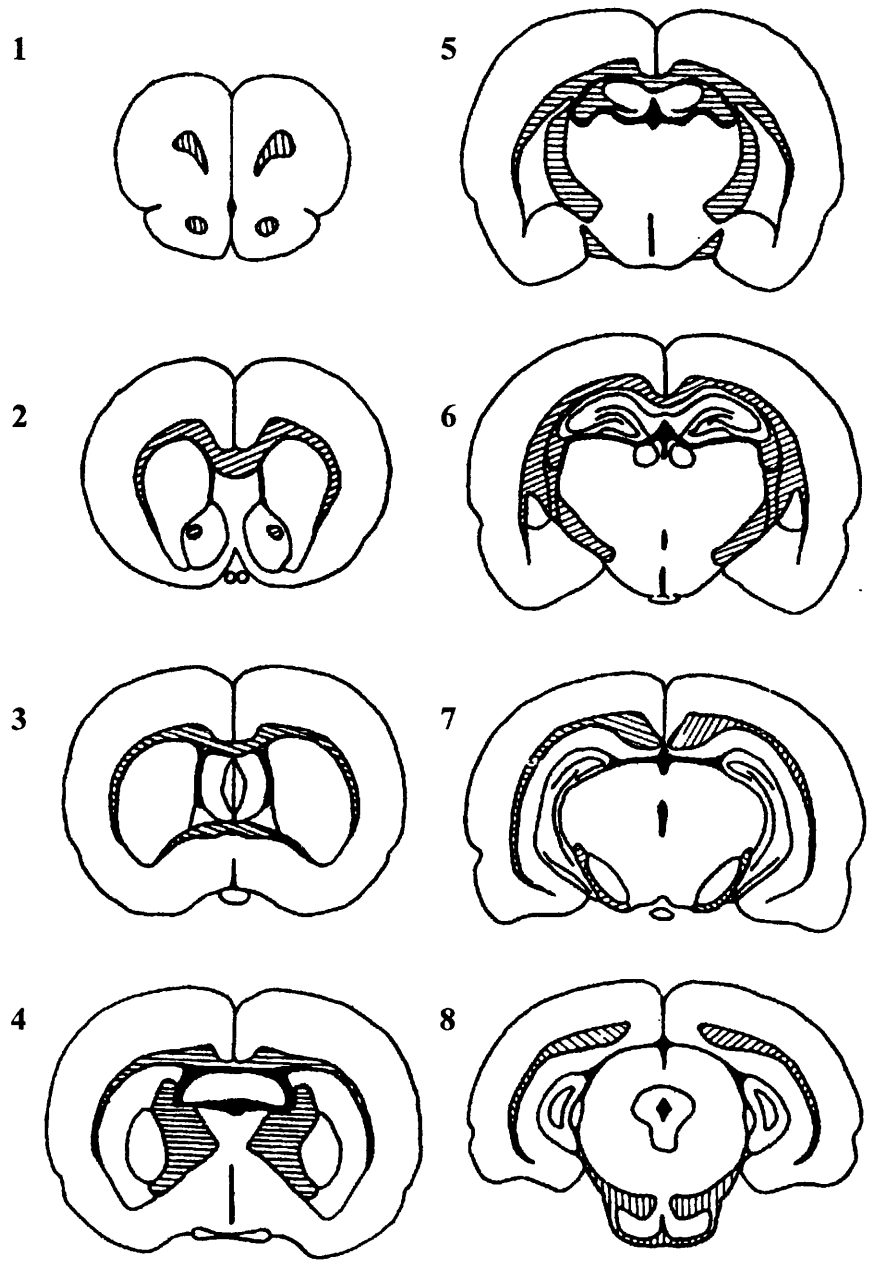

The eight coronal levels in the rat brain selected from the atlas of Konig and Klippel for quantification of infarction following MCA occlusion. Co-ordinates for the levels one to eight are 10.5 mm, 8.92 mm, 7.19 mm, 6.06 mm, 5.15 mm, 3.75 mm, 2.18 mm and 1.02 mm respectively.

Figure 2.5

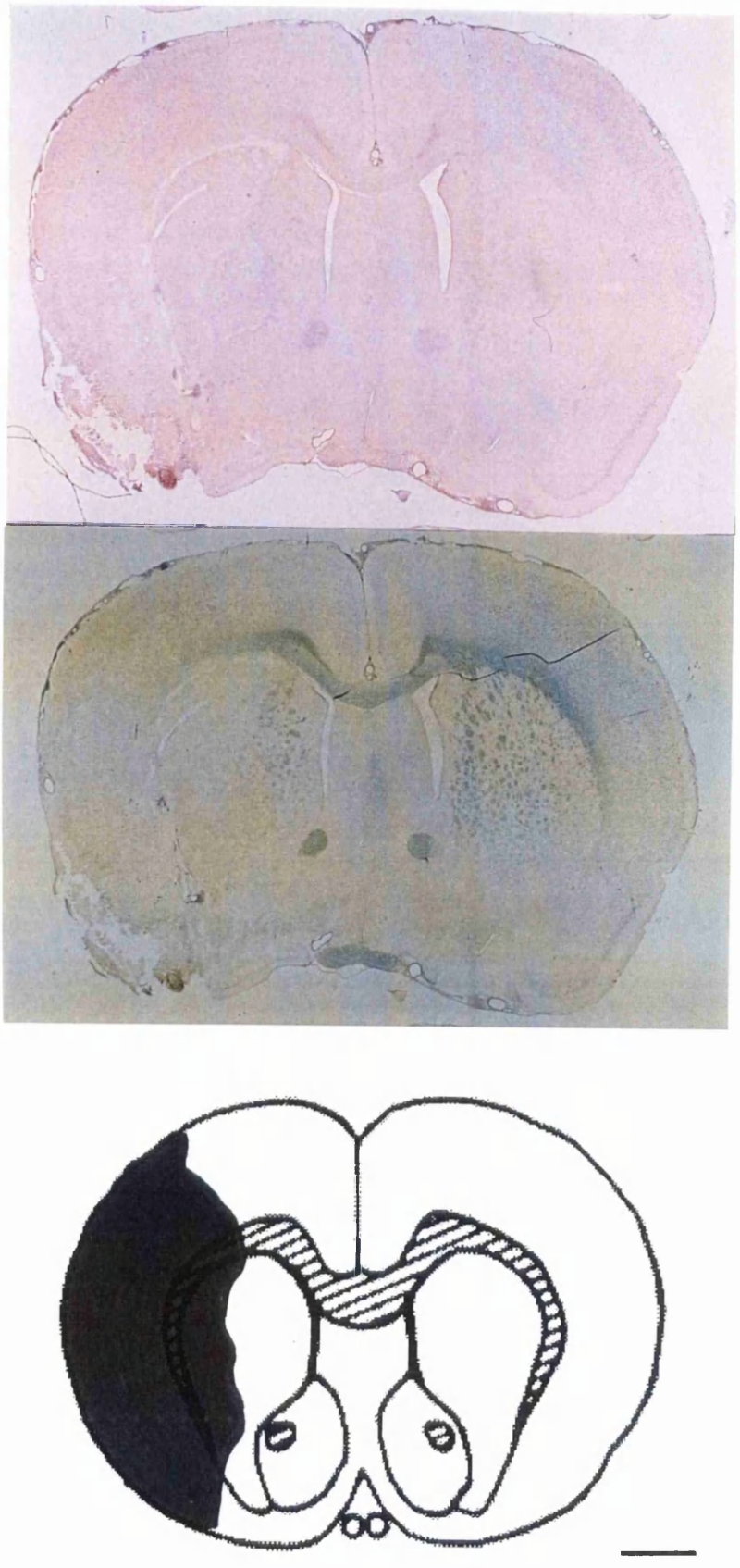

Representative sections from coronal level 2 (anterior co-ordinate 8.92 mm) from a single animal to show transcription of area of infarction onto a line diagram, as assessed by viewing adjacent sections with haematoxylin and eosin, and luxol fast blue. Scale bar is approximately 1.1 mm.

Figure 2.6

Sixteen coronal levels in the cat brain selected from the atlas of Reinoso-Suarez for quantification of infarction following MCA occlusion.

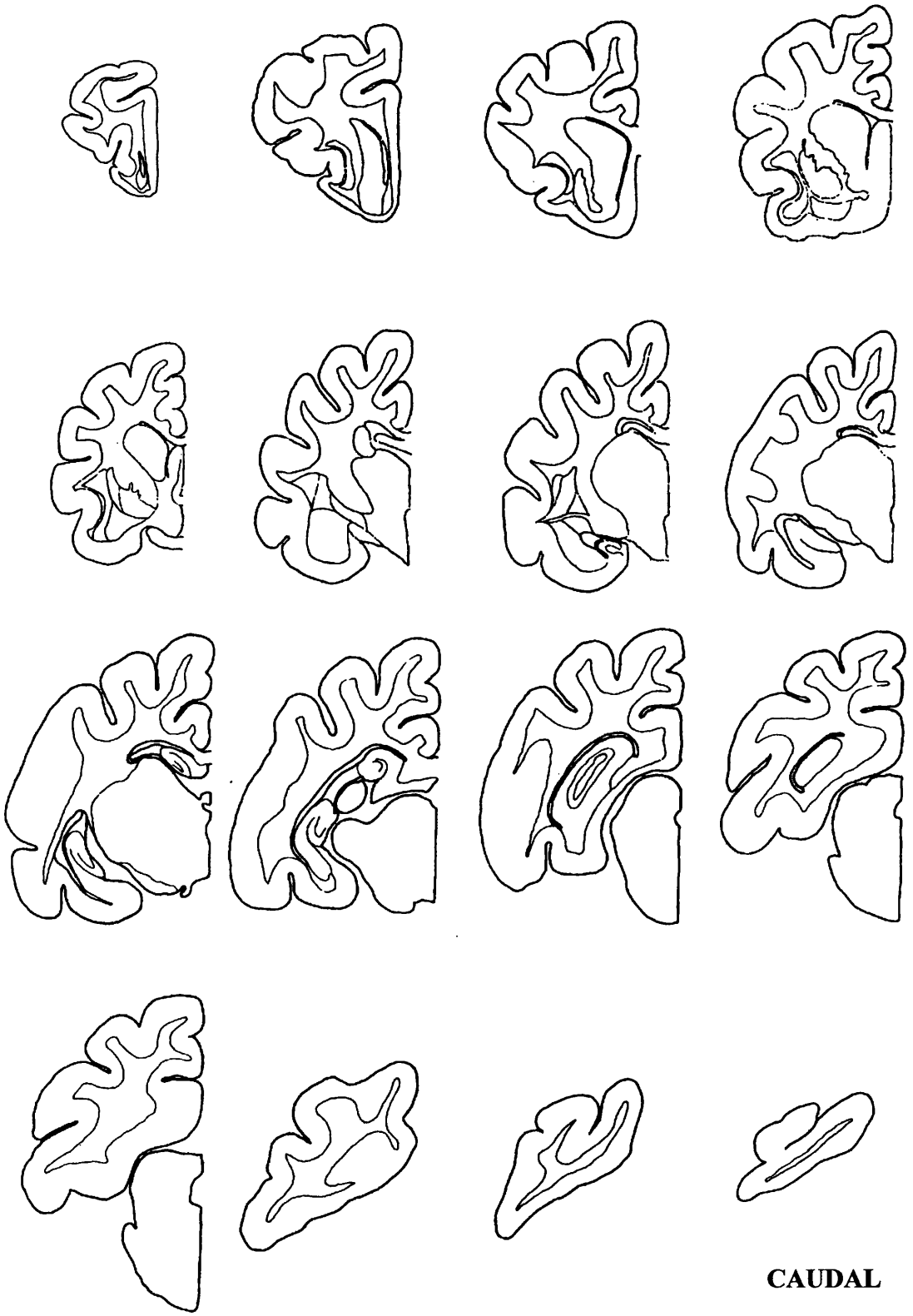

2.6 ELECTRON MICROSCOPE IMMUNOHISTOCHEMISTRY

2.6.1 Correlated light and electron microscopy

Following sectioning of the tissue (see 2.1.4), the 50μm brain slices were placed in 50% ethanol for 30 minutes. Endogenous peroxidase activity was inhibited by placing the sections into a solution of 10% methanol and 3% hydrogen peroxide in PBS for a period of about 5 minutes. Sections were washed with PBS several times until bubbles ceased to rise. The immunocytochemistry was performed as described (see 2.3.1). On completion of the immunostaining the sections that were for light microscopy were picked up on slides, dehydrated, cleared and mounted with cover slips. The remaining sections were processed so that they could be visualised by electron microscopy.

Sections were washed with 0.1 M phosphate buffer (pH 7.4) in glass vials and then 1-2 ml of 1% osmium tetroxide solution was applied using a glass pipette and the vials covered. This was performed in a fume hood. The sections were post-fixed for approximately 20-25 minutes before pipetting off the osmium which was placed in waste osmium bottles. The brain sections were washed at least three times for 15 minutes each in phosphate buffer. Prior to resin embedding, water was removed by sequentially placing the tissue into 70%, 95%, and 2 x 100% ethanol solutions for 10 minutes each. Once all the water was removed the tissue was gradually transferred to pure resin (Appendix 2) by passing it through a 3:1 ethanol:resin, 1:1 ethanol:resin, 1:3 ethanol:resin mixture for 30 minutes each. Finally the sections were placed into two changes of pure resin with at least one change overnight. The sections were then embedded between two acetate sheets. A weight was placed on top so that the sections were flat, and left at 60°C overnight to allow the resin to polymerise. Sections that had been stained for light microscopy were examined and the areas of interest were then

identified in the adjacent sections that had been processed for electron microscopy (correlated light and electron microscopy) (Fig. 2.7).

The top acetate sheet was peeled away and, having identified the region of interest using the light microscope, guidecuts were made in the resin with a pointed scalpel blade. The resin was softened by placing the section on a hot plate and the area of interest (which was still adherent to the bottom acetate sheet) cut and removed with fine forceps. The piece of tissue was placed into a truncated embedding capsule which was then filled with resin and labelled. The resin was polymerised at 60°C for 48 h. Once the resin had hardened the capsule was removed using a razor blade.

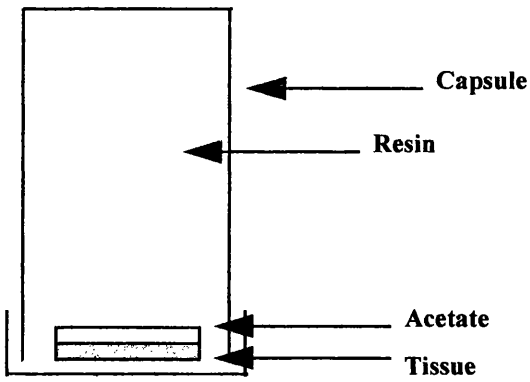

Thick sections (2μm) were cut using a pyramitome and, in some instances, stained with 1% toluidine blue in borax. These were viewed by light microscopy and the region of interest isolated by further trimming with the pyramitome. Fine sections were cut using an Ultratome II and placed on copper grids. The thickness of the sections was monitored by their interference colours, in this case in the silver-gold band. The sections were stained with uranyl acetate and lead citrate (Appendix 2). Electron microscopy was performed using Jem 100cxII. The effects of tissue preparation for transmission electron

microscopy may introduce artefacts (Maxwell et al. 1997); this may be especially pertinent for ischaemic tissue in which the main blood vessel supplying the region has been occluded thus compromising fixation.

2.6.2 Antibody concentrations

Dilution curves were carried out to determine the optimum dilution for each antibody (Table 2.4).

Table 2.4 Concentration curves for immunocytochemistry on material for electron microscopy

Antibody	Concentration	ABC kit Standard/Elite	Quality of immunostaining
NF68kD	1:100	Elite	++
	1:1000	Elite	+++
APP	1:10	Elite	+++
	1:100	Elite	++

Figure 2.7 Correlated light and electron microscopy

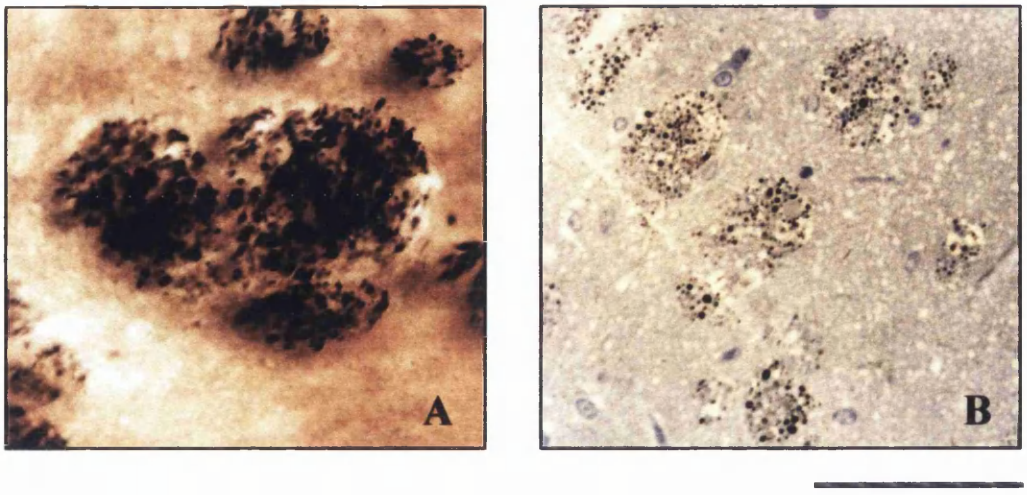

Sections that were stained for light microscopy were examined. A) Light microscope appearance of immunostaining for NK68kD in the MCA territory in the caudate nucleus following 4 h MCA occlusion (50μm). Once the areas of interest had been identified by light microscopy, adjacent sections were processed for electron microscopy. B) A thick section (2μm) showing NF68kD immunostaining in the caudate nucleus.
Scale bar = 20μm

CHAPTER 3

MARKERS OF AXONAL INJURY

3.1 INTRODUCTION

White matter injury may be a major determinant of clinical outcome. The study of traumatic brain injury in both man and in a non-human primate model of experimental injury, suggests a direct link between the extent of diffuse axonal injury and the ensuing patient morbidity (Gennarelli et al. 1982; Adams et al. 1989). Axonal injury following cerebral ischaemia has attracted less attention than damage in grey matter. However, there is now increasing evidence that damage to axons does occur following an ischaemic insult (Pantoni et al. 1996; Dewar and Dawson, 1997; Yam et al. 1997). In order to define the responses of axons to injury a variety of markers have been investigated. Amyloid precursor protein (APP) (Sherriff et al. 1994a; Gentleman et al. 1993; Gentleman et al. 1995), neurofilament subunits (Ng et al. 1994; Christman et al. 1994; Grady et al. 1993) and ubiquitin (Gultekin and Smith, 1994) have been used to investigate axonal injury after head injury and these immunocytochemical labels suggest that axonal injury is more widespread than originally indicated by traditional silver stains (Gentleman et al. 1995). Furthermore, local neurofilament changes following blunt head injury in human postmortem and experimental studies have been described using antibodies targeted against the 68kD subunit (NFL subunit as described in Chapter 1). Alterations in the staining of these antibodies are sensitive in detecting early changes in the axon which correlate with the genesis of impaired axoplasmic transport (Yaghmai and Povlishock, 1992; Grady et al. 1993; Erb and Povlishock, 1988; Povlishock et al. 1983).

Prior to writing this thesis, little work had been done to investigate the axonal changes following focal cerebral ischaemia in the rat. Therefore, a study was undertaken to determine the time course of changes induced by focal cerebral ischaemia in axonal transport and proteins associated with the microtubular and neurofilament components of the cytoskeleton. Alterations in immunoreactivity of antibodies directed at an axonally transported protein, microtubule associated and neurofilament proteins were investigated at different time points following permanent MCA occlusion in rats. SNAP25 which plays a role in synaptic exocytosis and like APP, undergoes fast anterograde transport (Sollner et al. 1993; Oyler et al. 1989); the NF68kD subunit of neurofilament protein, which has been extensively studied in diffuse axonal injury after traumatic brain injury (Yaghmai and Povlishock, 1992; Grady et al. 1993; Erb and Povlishock, 1988; Povlishock et al. 1983), and MAP5 which is a component of the microtubular system (Ochs, 1972) and has been shown to be sensitive to cerebral ischaemia (Dewar and Dawson, 1997), were all examined. In addition to the light microscope studies, electron microscopic studies were performed at one time point to further investigate the immunolabelling in the axon using antibodies specific for APP and NF68kD following MCA occlusion.

3.2 LIGHT MICROSCOPIC STUDIES

3.2.1 Animal preparation

Investigations were performed in 24 adult male Fischer rats (263-360 g). Anaesthesia, cannulation of blood vessels, MCA occlusion was performed as described in section 2.1.2 and 2.1.3. Following MCA occlusion, anaesthesia was maintained for periods of 30 minutes (n = 4), 1 h (n = 4), 2 h (n = 4) or 4 h (n = 4). Sham-operated animals (n = 2

at each time point) underwent the same experimental procedure except that the MCA was not occluded. The animals were killed by transcardiac perfusion with saline followed 4% paraformaldehyde (section 2.1.4). and subsequent processing as previously described (section 2.1.4). Immunostaining was performed on free-floating sections (section 2.3.2). The following mouse monoclonal antibodies were used: MAP5 (Sigma, clone AA6, 1:1000), NF68kD (Sigma, clone NR4 1:1000), SNAP25 (Sternberger, clone SMI 81, 1:120,000), βAPP (Boehringer Mannheim, clone 22C11, 1:20) and MAP2 (Sigma, clone HM-2, 1: 750).

3.2.2 Analysis of material

Equivalent coronal sections from each animal were viewed by conventional light microscopy and the pattern and intensity of the immunostaining of antibodies targeted to SNAP25, MAP5 and NF68kD in the subcortical white matter and myelinated fibre tracts, were assessed. A semi-quantitative rating was given for alterations in immunoreactivity at each time point for each antibody, viz., 0 for no change in immunoreactivity from sham operated animals, + for a mild alteration in pattern or intensity of immunoreactivity, + + for a moderate and + + + for a marked alteration in pattern or intensity of immunoreactivity.

3.2.3 Results

The results are summarised in Table 3.1

Table 3.1 Immunoreactivity of SNAP25, NF68kD and MAP5 at different time points following MCA occlusion in the rat

	SHAM	30 min	1 h	2 h	4 h
SNAP25	-	-	+	++	+++
NF68kD	-	-	-	++	+++
MAP5	-	+	+	++	+++

The relative changes of SNAP25, NF68kD and MAP5 immunoreactivity following 30 min, 1, 2 and 4 h of MCA occlusion. Immunostaining in sham operated animals, -. Altered immunoreactivity from mild to marked: + to + + +.

MAP2 immunostaining

MAP2 has been shown to be a sensitive marker of ischaemic damage at short survival times following MCA occlusion (Dawson and Hallenbeck, 1996; Yanagihara et al. 1990; Kitagawa et al. 1989). Since traditional histologic stains such as haematoxylin and eosin do not permit definitive conclusions to be drawn concerning neuronal viability at short survival times, the anatomical extent of ischaemic damage in this study was detected using MAP2 immunostaining. Figure 3.1 shows equivalent sections stained for MAP2, H&E and LFB. In sham operated controls ipsilateral to the MCA and in the contralateral hemispheres of MCA occluded animals, there was no reduction in MAP2 immunostaining. However, at 30 min, 1, 2 and 4 h after MCA occlusion, MAP2 immunostaining was decreased in the caudate nucleus ipsilateral to the occluded MCA in all animals (Fig. 3.2). The reduction of immunostaining was most marked at 4 h. In addition, areas of decreased immunoreactivity were detected in the cerebral cortex ipsilateral to the MCA, although the reduction was patchy in its distribution. Figure 3.3 shows the relationship between ischaemic damage, as assessed by MAP2 immunostaining, and the topography of axonal changes seen with SNAP25, NF68kD and MAP5 immunostaining.

SNAP25 immunostaining

In sham operated controls ipsilateral to the exposed MCA and in the contralateral hemispheres of MCA occluded animals, axons in subcortical white matter and white matter tracts permeating the striatum were lightly stained with SNAP25 (Fig. 3.4 and Fig. 3.5).

Following 4 h of MCA occlusion there was a marked increase in SNAP25 immunoreactivity which was bulbous in appearance in axons in subcortical white matter

and in the myelinated tracts permeating the striatum in the ipsilateral hemisphere at the border of ischaemic damage (Fig. 3.4 and 3.5). At 2 h following MCA occlusion, the immunoreactivity was less marked than that at 4 h. Following 1 h of MCA occlusion, there was only a slight increase in SNAP25 immunoreactivity. This was less noticeable at 30 min following MCA occlusion. Axonal immunostaining with APP was similar in both time course and distribution (not shown). However, superior immunostaining was obtained with SNAP25 despite the concentration of antibody being 1:120,000 compared to that used for APP of 1:20. APP pattern of APP immunostaining was more easily assessed in FAM fixed material and is described in greater detail in Chapter 4. The pattern of SNAP25 immunoreactivity was similar in all animals at a given time point.

NF68kD immunostaining

In sham operated controls and in the contralateral hemisphere of MCA-occluded animals, NF68kD immunostaining had a smooth regular appearance in the subcortical white matter and in the myelinated fibre tracts within the caudate nucleus (Fig. 3.6 and Fig. 3.7).

Following 4 h of MCA occlusion the pattern of NF68kD staining had a rough, disorganised and tortuous appearance in the ipsilateral hemisphere within MCA territory. This was particularly prominent in the axons permeating the caudate compared to the subcortical white matter (Fig. 3.7). Changes in the pattern of immunostaining were confined to the ipsilateral MCA territory. Changes in immunoreactivity within axons were also evident following 2 h of MCA occlusion, although it was less marked at this time point. At 1 h post occlusion, there were only subtle changes evident in axons in subcortical white matter and those permeating the caudate nucleus, and the pattern of immunostaining was more regular and smooth in appearance, resembling that of sham

operated animals. No changes in NF68kD immunostaining were evident following 30 min of MCA occlusion.

MAP5 immunostaining

In sham-operated controls and in the contralateral hemisphere of MCA-occluded animals, MAP5 antibody only lightly stained axons in subcortical white matter and white matter tracts permeating the caudate (Fig. 3.8). The pattern seen was smooth, regular and organised.

In similarity to the immunostaining obtained with NF68kD, the changes seen with MAP5 immunostaining were progressive over time following MCA occlusion. These changes were particularly marked at 4 h following MCA occlusion when there was a bulb-like immunoreactivity in the axons permeating the caudate nucleus and in the subcortical white matter. (Fig. 3.8). At 2 h post occlusion, there was both increased immunoreactivity and a rougher, globular, punctate pattern of staining compared to sham operated animals. At 1 h post occlusion, there was a slight increase in immunoreactivity and subtle changes in the orientation of the pattern of staining in axons within MCA territory. Following 30 min of MCA occlusion there was a subtle increase in MAP5 immunoreactivity but not orientation of the staining in the axons permeating the caudate nucleus. The changes described were present in all the animals in each group within the ischaemic white matter.

Figure 3.1

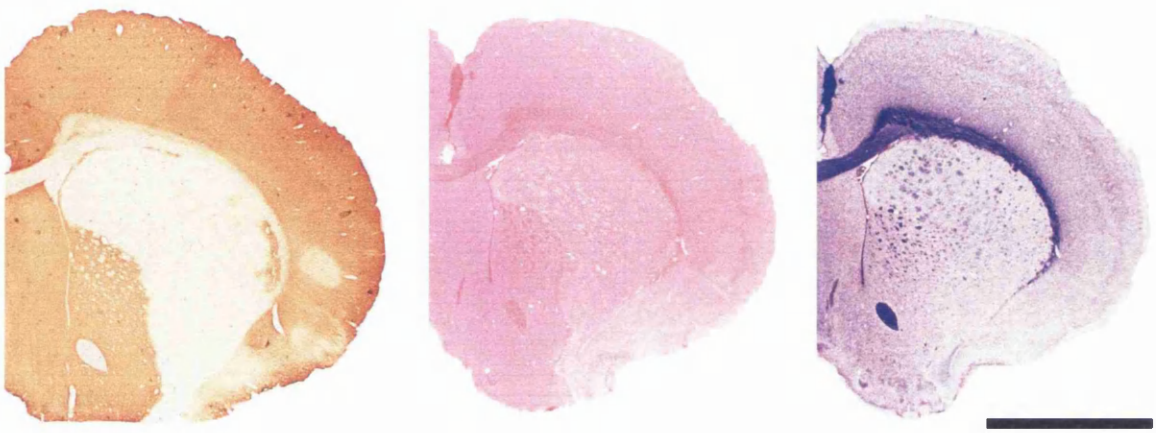

MAP2 H&E LFB

Equivalent coronal section stained for MAP2, H&E and LFB following 4h MCA occlusion. Scale bar is approximately 2.5 mm.

Figure 3.2

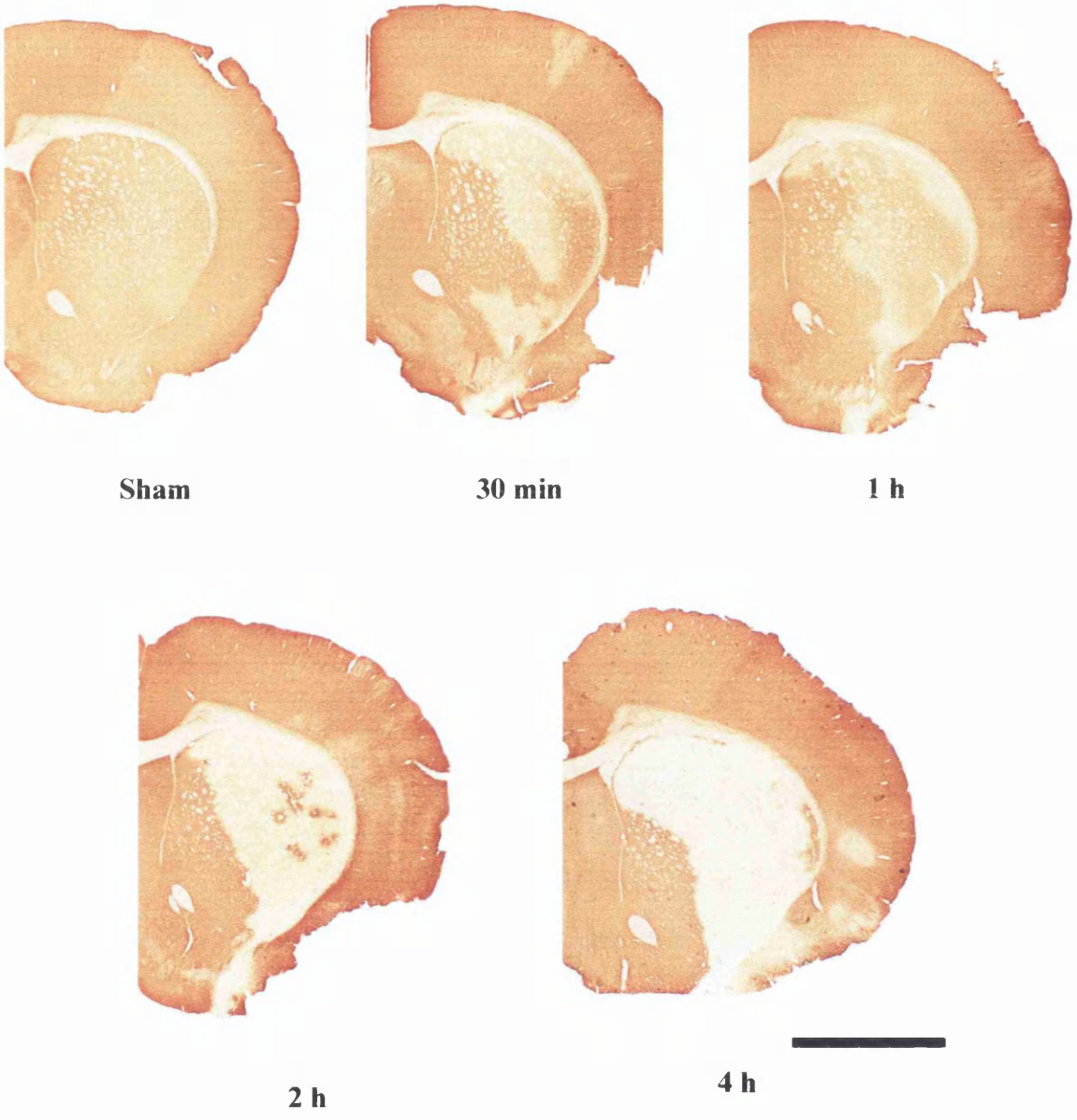

Photomicrgraphs showing the pattern of MAP2 immunoreactivity following a sham, 30 min, 1h, 2h and 4h MCA occlusion in the rat. Scale bar is approximately 2.5 mm.

Figure 3.3

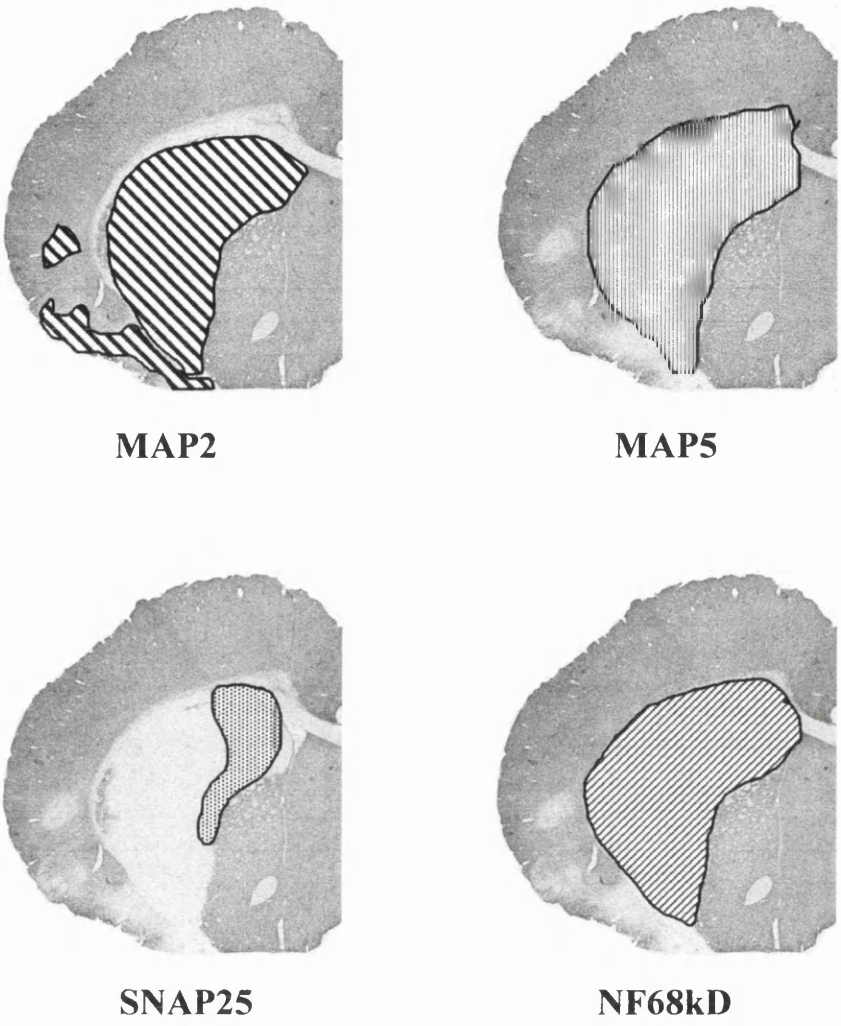

Representative section stained for MAP2 following 4 h MCA occlusion. Shaded areas represent regions of altered immunoreactivity for each antibody, namely, MAP5 (top right), SNAP25 (bottom left) and NF68kD (bottom right) in relation to the topography of decreased MAP2 immunoreactivity (top left).

Figure 3.4

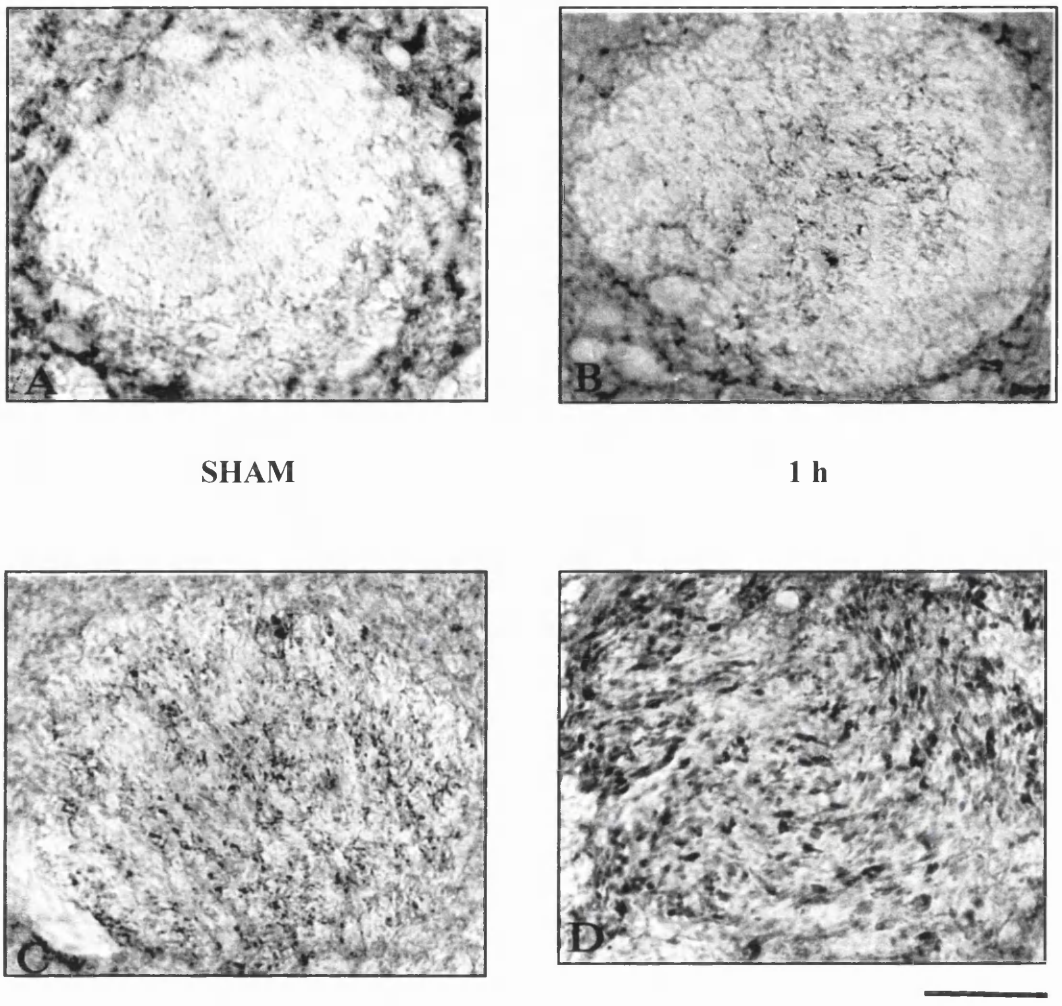

Immunostaining of SNAP25 in myelinated fibre tracts in the caudate nucleus in a sham operated rat and at 1, 2 and 4 h after middle cerebral artery (MCA) occlusion. The changes in immunoreactivity were progressive from 1 h to 4 h following MCA occlusion. By 4 h following occlusion the increase in immunoreactivity was most dramatic and was bulbous in appearance (scale bar = 5 μm).

Figure 3.5

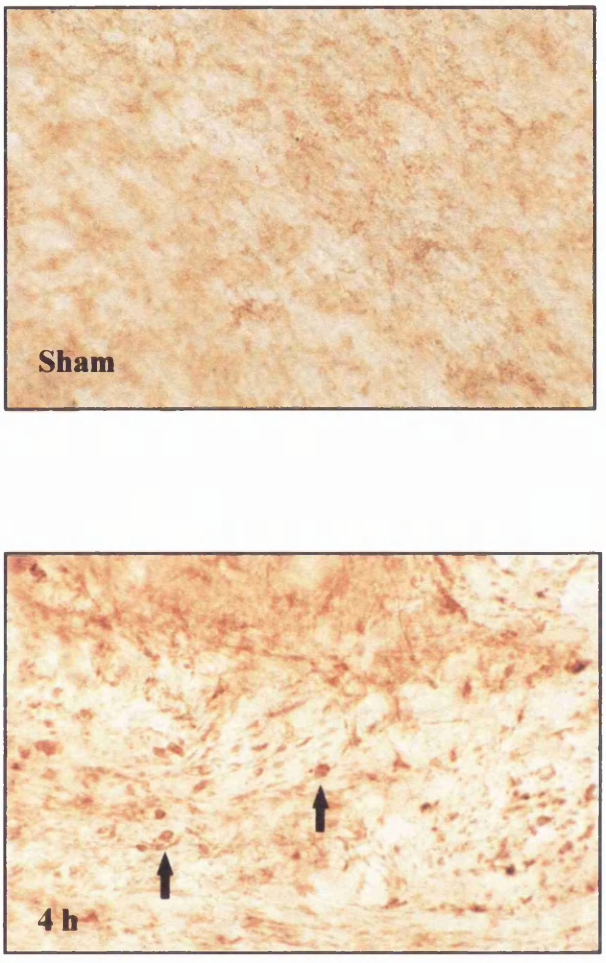

Immunostaining of SNAP25 in myelinated fibre tracts in the subcortical white matter in a sham operated animal and at 4 h after MCA occlusion. In the sham operated animal the white matter was lightly stained with SNAP25 immunoreactivity. However, following 4 h of occlusion increased SNAP25 immunoreactivity could be seen which was bulbous in appearance (arrows). Magnification x 750.

Figure 3.6

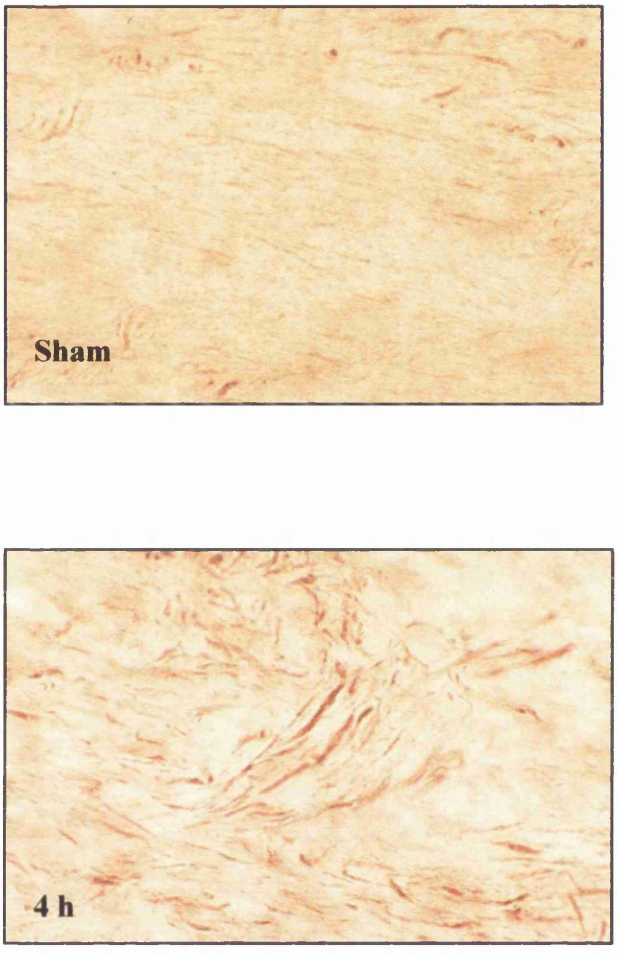

Immunostaining of NF68kD in myelinated fibre tracts in the subcortical white matter in a sham operated rat and 4 h after MCA occlusion. Progressive changes in the pattern of staining were observed. This was most obvious at 4 h post occlusion but was more subtle than that observed in the myelinated fibre tracts permeating the striatum (x 750 magnification.)

Figure 3.7

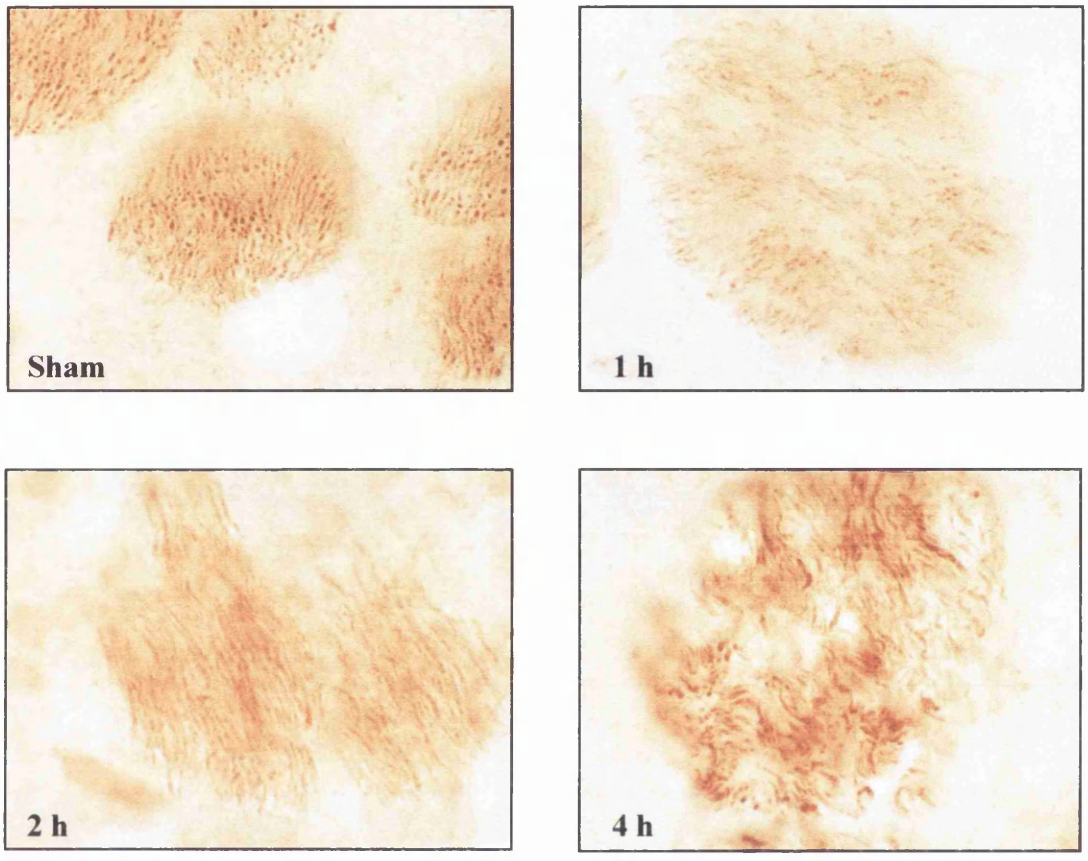

Immunostaining of NF68kD in myelinated fibre tracts in the caudate nucleus in a shamoperated rat and at 1, 2, and 4 h after MCA occlusion. The changes in immunoreactivity were progressive from 1 h to 4 h following MCA occlusion. By 4 h, the pattern of NF68kD staining had a rough, disorganised and tortuous appearance in the ipsilateral hemisphere within the MCA territory. Changes in axons at 1 and 2 h were also present although less marked (x 750 magnification).

Figure 3.8

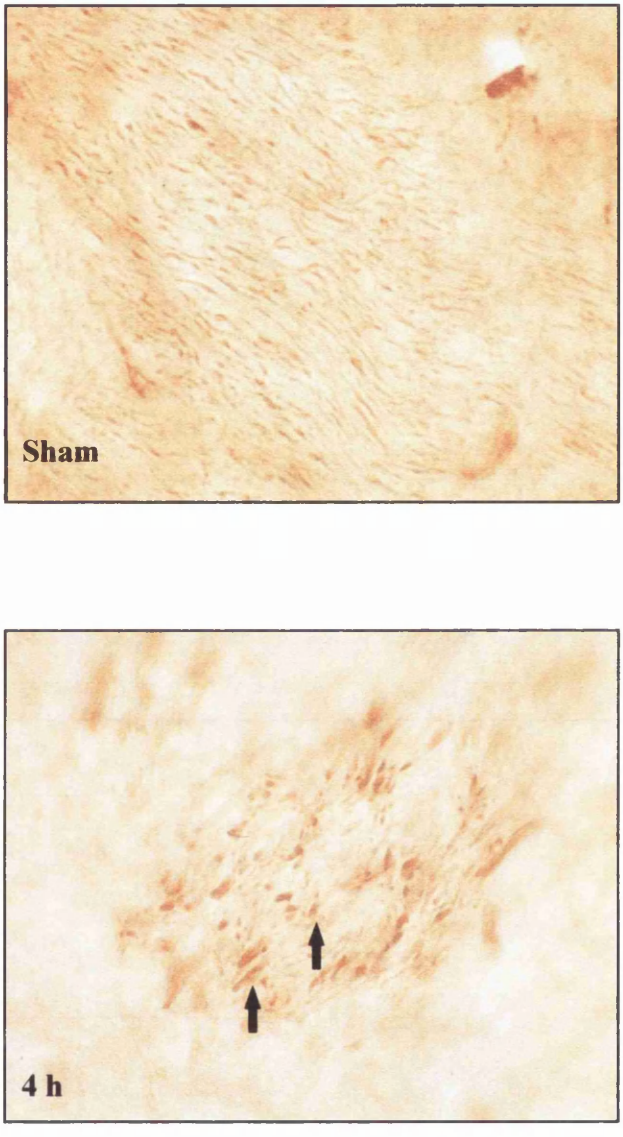

Immunostaining of MAP5 in myelinated fibre tracts in the caudate nucleus in a sham operated rat and at 4 h after MCA occlusion. As with NF68kD staining, progressive changes with immunostaining were observed following MCA occlusion. These changes were most dramatic at 4 h when there was a disorganised pattern and bulb like immunoreactivity (arrows) (x 750 magnification).

3.3 ELECTRON MICROSCOPE STUDIES

3.3.1 Animal Preparation

Investigations were performed in 3 adult male Fischer rats. Anaesthesia, cannulation of blood vessels and MCA occlusion was performed as described in section 2.1.2 and 2.1.3. Following MCA occlusion, anaesthesia was maintained for 4 h. The animals were killed by transcardiac perfusion with saline followed by gluteraldehyde (0.5%) and paraformaldehyde (4%) (section 2.1.4). and subsequent processing as previously described. Immunostaining was performed on free-floating sections (section 2.3.2). The following mouse monoclonal antibodies were used: NF68kD (Sigma, clone NR4 1:1000) and βAPP (Boehringer Mannheim, clone 22C11, 1:10). The material was then processed for correlated light and electron microscopy (see section 2.6.1). Equivalent coronal sections were viewed from each animal using the electron microscope. Since the fixation was optimised for immunocytochemistry, resulting in poorer tissue fixation, analysis of the material was qualitative rather than quantitative. Areas of interest included the corpus callosum and caudate in both the ipsilateral and contralateral hemispheres.

3.3.2 Results

NF68kD

Within the caudate nucleus in the contralateral hemisphere immunoreactivity to NF68kD was evident mainly in the larger myelinated fibres (Fig. 3.9). In the contralateral hemisphere following 4h MCA occlusion, the immunostaining was smooth and regular in the caudate nucleus. However, following 4h of MCA occlusion the pattern of NF68kD in the ipsilateral hemisphere within the MCA territory was more

disorganised and disrupted compared to the contralateral hemisphere. At higher magnifications, there appeared to be increased spacing in NF68kD immunostaining in the ipsilateral hemisphere compared to the contralateral hemisphere (Fig. 3.10). This is consistent with light microscopic findings (Fig. 3.7).

APP

Within the caudate nucleus and subcortical white matter in the contralateral hemisphere there was no evidence of increased immunoreactivity at 4h following MCA occlusion. However, following 4h of MCA occlusion in the ipsilateral hemisphere, increased APP immunoreactivity was present within some of the myelinated tracts in both the subcortical white matter and caudate nucleus adjacent to the core of infarction, denoting the sites of injury and impaired axoplasmic transport (Fig. 3.11). Within the corpus callosum there were axons that appeared to be in stages of axotomy (Fig. 3.12). This is supported by further findings of axonal bulb formation with the accumulation of large amounts of APP seen longitudinal section (Fig. 3.13A), and accumulation of many mitochondria (also transported by fast axonal transport) and APP in a transverse fibre tract in the caudate nucleus (Fig. 3.13B).

Figure 3.9

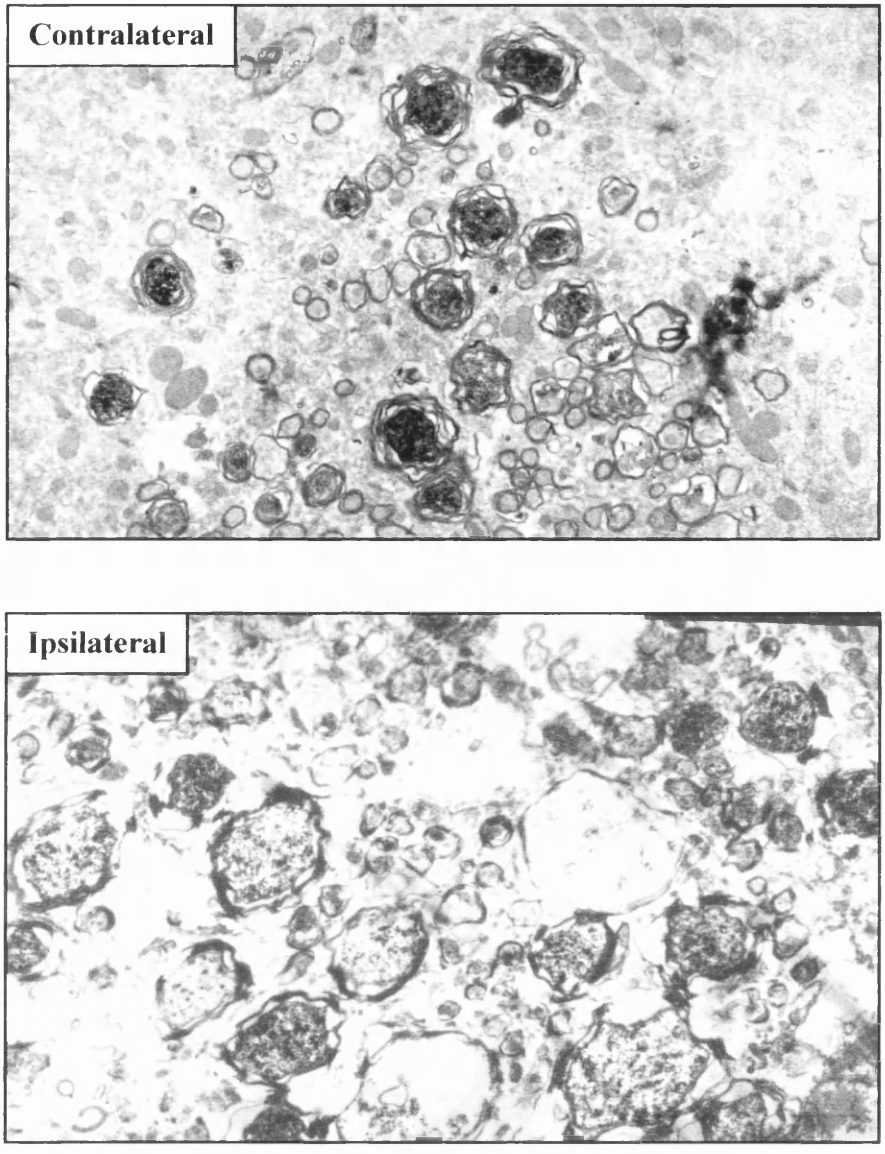

Immunostaining of NF68kD in myelinated fibre tracts in the caudate nucleus in the contralateral hemisphere and ipsilateral hemisphere following 4 hours of MCA occlusion in the rat. The NF68kD immunoreactivity was more obvious in the larger myelinated fibre tracts in both the ipsilateral and contralateral hemispheres. The pattern of NF68kD staining within the infarcted territory in the ipsilateral hemisphere was dispersed and more disorganised compared to the contralateral hemisphere. Original magnification x 4,000.

Figure 3.10

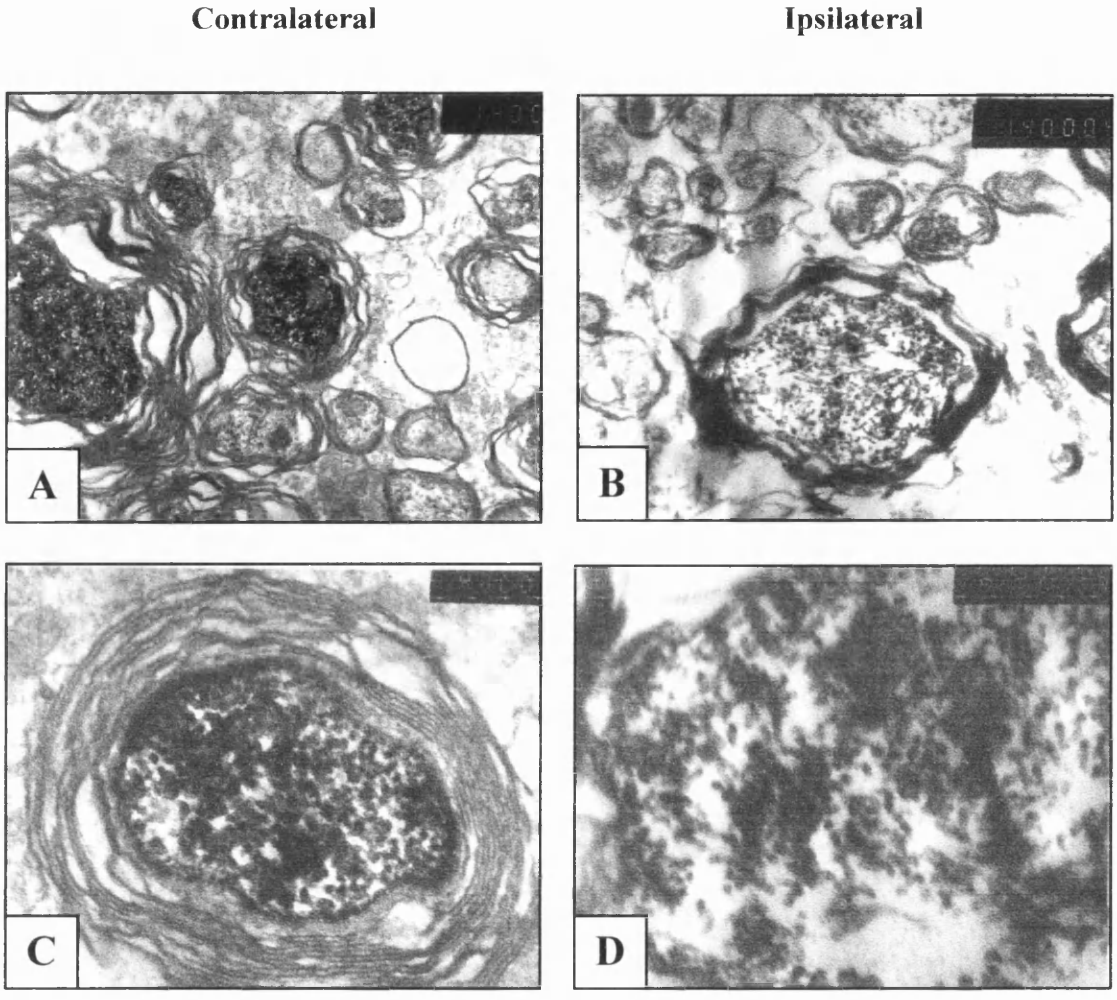

Immunostaining of NF68kD in contralateral (A and C) and ipsilateral (B and D) caudate nucleus following 4 h MCA occlusion. Original magnification x14,000 (A and B) and x 40,000 (C and D). In the contralateral sections the immunostaining of NF68kD within the myelinated axons is dense. However, in the ipsilateral sections, the NF68kD immunostaining is more dispersed.

Figure 3.11

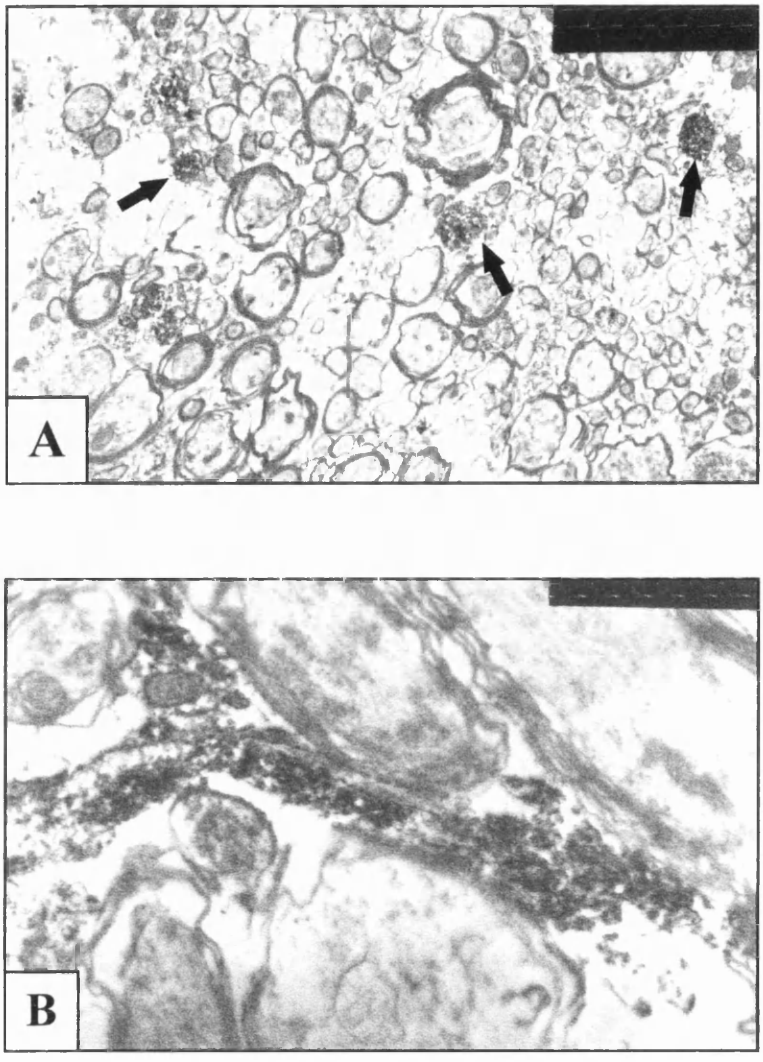

A) Transverse section of fibre tracts in the caudate nucleus from a rat 4 h after MCA occlusion. Increased APP accumulation is evident within some of the fibres (arrows). Original magnification x 4,000. B) Longitudinal section of an axon showing accumulation of APP. Original magnification x 14,000. The APP accumulation in A and B is indicative of axonal transport dysfunction.

Figure 3.12

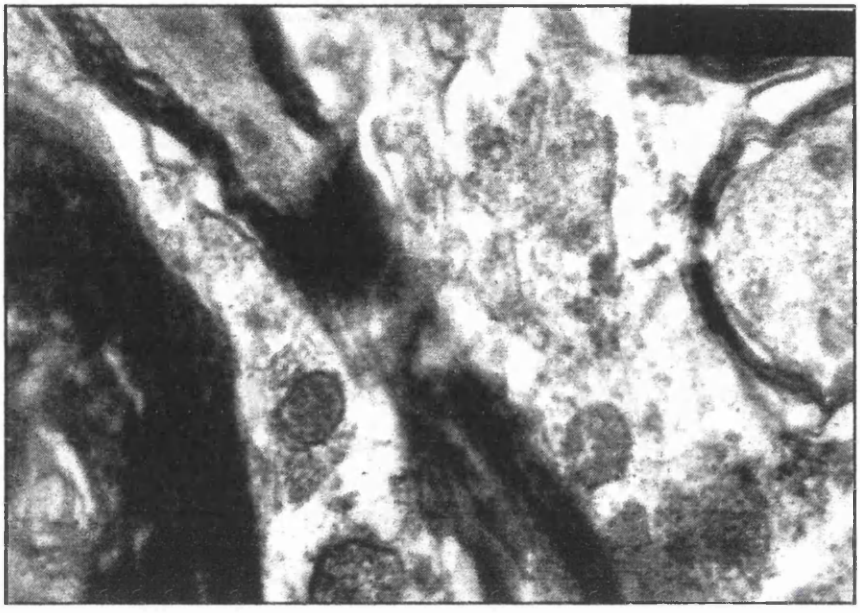

Longitudinal section from the corpus callosum following 4h MCA occlusion in the rat. There is evidence of impending axotomy. Original magnification x 20,000.

Figure 3.13

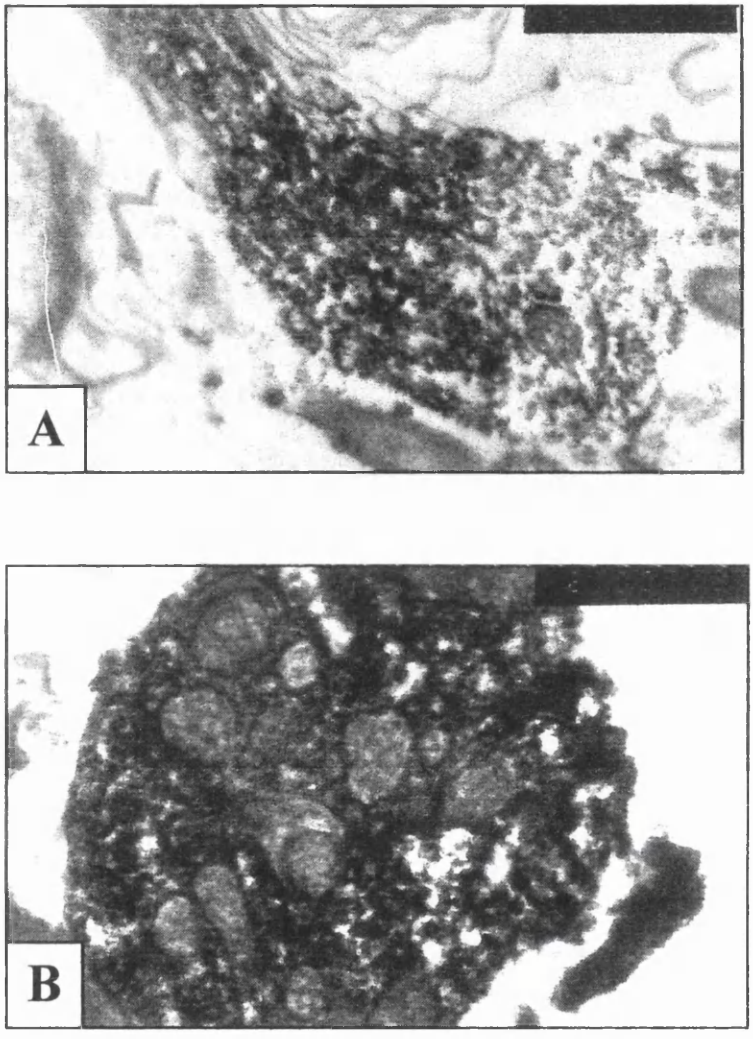

A) A longitudinal thin section of an axon in the corpus callosum in the ipsilateral hemisphere adjacent to area of infarction in a rat following 4h of MCA occlusion. The APP immunolabelling has accumulated in an axonal bulb. This finding is consistent with axotomy. Original magnification x 20,000. B) A transverse section of a fibre tract in the caudate nucleus from a rat 4h after MCA occlusion. There is accumulation of organelles and a marked increase in APP immunoreactivity. Original magnification x 27,000.

3.4 DISCUSSION

The studies described in this chapter are the first to assess the time course of changes to NF's, proteins that undergo fast axonal transport and a structural component of the microtubular system following 30 minutes of focal cerebral ischaemia in the rat. In addition, immunocytochemistry has been visualised at the electron microscope level revealing novel changes in NF structure and extends observations previously noted of axonal bulb formation following both trauma and ischaemia.

Neurofilaments, and their three dimensional relationships to other NF's, MT's, and the microtrabecular matrix including the cytoskeleton of the axolemma and actin filaments, govern the integrity and calibre of the axon (section 1.4.1) (for review see Hirano and Llena, 1995). The finding in this study of NF68kD immunoreactivity in the larger myelinated axons is consistent with reports of highest NF expression in neurons with large-calibre myelinated axons (Cleveland et al. 1991). Following traumatic brain injury and experiments using the anoxic optic nerve model, disruption of the axonal cytoskeleton has been suggested by local NF changes, most frequently involving the large calibre axons (Waxman et al. 1992; Yaghmai and Povlishock, 1992). As a result of moderate or severe traumatic brain injury induced by fluid percussion, antibodies targeting the NF68kD subunit revealed intense immunoreactivity associated with the progression of axonal change, and the NF's were tightly packed and aligned in a random fashion in relation to the long axis of the cylinder (Povlishock et al. 1997). This contrasts with the changes seen in a small proportion of axons following optic nerve stretch-injury in the guinea-pig (Jafari et al. 1998), and those observed following focal ischaemia described above, where the NF's seemed more sparse or 'dispersed', and unlike in traumatic brain injury, were not localised centrally within the axon. The

reasons underlying the difference in NF disruption following these different types of insults are uncertain. One could posit that there may be different mechanisms involved in initial axonal damage following traumatic and ischaemic brain injury or that the axons are being viewed at different stages of the injury cascade. There certainly appears to be a time course in damage to the NF as evidenced by light microscopy (Fig. 3.7).

The cause of cytoskeletal changes following ischaemia and trauma is thought to be related to excessive calcium influx and altered calcium homeostasis (section 1.5.4). Influx of calcium has been suggested following stretch injury of the guinea-pig optic nerve (Maxwell, 1996; Maxwell et al. 1995) and a central role for calcium in anoxic injury to the rat optic nerve has been demonstrated using electrophysiological techniques (Stys et al. 1990). More recent quantitative data suggestive of increased intracellular calcium content following anoxic injury, supports the hypothesis that influx of calcium is a pivotal event in the pathogenesis of axonal damage (Brown et al. 1998). The exact route(s) of intracellular calcium influx is still under investigation. An alteration in axolemmal permeability is well established following traumatic brain injury as demonstrated by a change in extracellularly confined horse-radish peroxidase (Povlishock and Pettus, 1996; Pettus and Povlishock, 1996; Pettus et al. 1994). However, because of its relative size, horse-radish peroxidase is possibly not an appropriate marker of damage to the axolemma at an ionic level (Maxwell et al. 1998). Physiological studies in the anoxic rat optic nerve, and recent studies using freeze-fracture and cytochemical techniques in the adult guinea-pig optic nerve subjected to stretch-injury, have provided evidence for changes in membrane structure (Maxwell et al. 1998) and the activity of membrane pumps (Stys et al. 1995; Maxwell et al. 1998). Perhaps altered membrane pump activity and cytoskeletal changes are the sequelae of mitochondrial failure. In this regard, controlled cortical impact injury (Xiong et al.

1997) and ischaemia (Orrenius et al. 1996; Sciamanna et al. 1992; Nakahara et al. 1991) in rats induces sustained perturbation of cellular Ca^{2+} homeostasis with ultimate mitochondrial Ca^{2+} overload and inhibition of mitochondrial chain-linked functions.

Loss of normal ionic gradients may provide a mechanism for influx of calcium which could then result in subsequent cytoskeletal disruption by the action of calpain mediated proteolysis (Hall and Lee, 1995), activation of kinases (Maxwell et al. 1997) or activation of calcium-independent proteases (Goldstein et al. 1987). Because there is evidence of 'increased' NF subunit following traumatic brain injury, it has been suggested that the axonal degeneration is not calpain mediated (Povlishock et al. 1997; Yaghmai and Povlishock, 1992), although this is still under debate. However, the finding of decreased NF68kD immunoreactivity and increased NF spacing following focal cerebral ischaemia is consistent with the calpain hypothesis (section 1.5.4). It is also interesting to note from the light microscope findings that the changes in NF68kD immunostaining are progressive from 1 h to 4 h following MCA occlusion, a finding consistent with calcium-mediated damage (Povlishock, 1992).

Ultimately, the repertoire of axonal change to various injuries is limited. It is likely, that despite the possibility of different initiating mechanisms of cytoskeletal disruption following traumatic and ischaemic injury, both insults result in impaired axoplasmic transport due to perturbation of the cytoskeleton. In this regard, NF misalignment (Fig. 3.10) (Yaghmai and Povlishock, 1992) and other cytoskeletal changes, as evidenced by light microscopic studies using antibodies targeted towards MAP5 (Fig. 3.8) and the demonstration of MT loss following optic nerve stretch (Maxwell and Graham, 1997) and anoxia (Waxman et al. 1992), would support this view. Although MT's were not assessed directly following ischaemia the alteration in the MAP5 immunostaining would be highly suggestive of disrupted MT's. Perhaps

more convincing of MT disruption is the increased immunoreactivity of proteins normally transported along the MT's. Local swelling and expansion of the axonal cylinder was apparent due to accumulation of organelles and proteins, the latter being detected with antibodies to APP by electron microscopy (Fig. 3.13) and SNAP25 by light microscopy (Fig. 3.4 and 3.5). The changes in MAP5 immunoreactivity was an early event, preceding that of increased SNAP25 immunoreactivity. Finally, there was evidence of lobulation of the focal axonal swelling and eventual disconnection, so-called 'secondary axotomy' (Fig. 3.12).

Each antibody makes its own contribution to the understanding of the events occurring following ischaemic injury. In this study, antibodies have been used that target relatively stationary cytoskeletal elements and those that undergo rapid axonal transport. The findings and implications of the light and electron microscope studies described in this chapter are discussed further in Chapter 7.

CHAPTER 4

QUANTITATIVE ANALYSIS OF AXONAL INJURY IN THE RAT

4.1 INTRODUCTION

To allow future assessments of protection of white matter by therapeutic interventions, a method by which axonal injury can be visualised and quantified is required. One such candidate marker of axonal injury is amyloid precursor protein (APP). This is a transmembrane glycoprotein from which β-amyloid protein, the main component of amyloid plaques in Alzheimer's disease, is derived (Coria et al. 1992; Glenner and Wong, 1984). APP is ubiquitously expressed in the nervous system from early embryogenesis throughout adulthood (Allinquant et al. 1994). It is associated with the cytoskeleton (Refolo et al. 1991) and undergoes fast anterograde axonal transport in the peripheral nervous system (Koo et al. 1990). The interruption of axonal transport, whether it be due to traumatic (Otsuka et al. 1991), ischaemic (Kalaria et al. 1993; Stephenson et al. 1992) or chemical insults (Nakamura et al. 1992; Kawarabayashi et al. 1991), or colchicine injection (Shigematsu and McGeer, 1992), has been shown to result in the accumulation of APP. These observations are of considerable interest as they provide compelling evidence that APP accumulates after disruption of axonal transport and, since axonal transport is an integral component of axonal function, APP may be a good marker of axonal injury.

The following study was undertaken to investigate APP as a suitable marker of white matter injury in response to MCA occlusion in the rat. Only once this has been

established, can APP be used as a marker to assess the effect of therapeutic intervention on the salvage of axons. The aims of the study were threefold: (1) to determine whether increased APP immunoreactivity is a consistent observation after focal ischaemia, (2) to determine the topography of increased APP immunoreactivity in relation to the boundary of ischaemic lesions following MCA occlusion and (3) to determine whether there is a quantitative relationship between increased APP immunoreactivity and volume of the focal ischaemic lesion.

4.2 METHOD

4.2.1 Anaesthesia and MCA occlusion

Anaesthesia was induced in 14 rats and MCA occlusion performed as previously described (section 2.1.3). MCA occlusion was performed by Dr. Tei Takasago. Following MCA occlusion, anaesthesia was discontinued and, under strict observation, the animals allowed to regain consciousness. Twenty-four hours after MCA occlusion, the rats were re-anaesthetised and maintained with 3% halothane by face mask. The animals were killed by transcardiac perfusion with 200ml of heparinised saline followed by 200 ml of FAM (section 2.1.4).

Physiological parameters were monitored over the 24h period. There were minimal interanimal variability in measured physiological parameters which may influence the extent of infarction (Table 4.1). Blood pressure was lower in the operative period than in the post-operative period reflecting the halothane anaesthesia. P_aO_2 was higher at this time, reflecting the higher level of oxygen in the inspired gas mixture than air.

Table 4.1 Physiological variables prior to and following middle cerebral artery occlusion

	MABP (mmHg)	pH	$PaCO_2$ (mmHg)	PaO_2 (mmHg)	Glucose (mM)	Rectal Temp (°C)
pre-MCAO*	87.6 ± 3.9	7.42 ± 0.01	38.7 ± 0.7	159 ± 6	8.0 ± 0.3	37.2 ± 0.0
MCAO*	90.6 ± 3.3	7.39 ± 0.01	42.3 ± 0.9	147 ± 6	7.7 ± 0.3	37.0 ± 0.1
1 h	116.1 ± 3.1	7.41 ± 0.00	40.2 ± 0.9	76 ± 2	6.4 ± 0.3	37.5 ± 0.1
24 h	120.2 ± 1.8	7.49 ± 0.01	34.7 ± 0.6	97 ± 2	6.1 ± 0.3	38.1 ± 0.1

MABP: Mean arterial blood pressure, Rectal Temp: Rectal temperature. Data are presented as mean ± SEM. n=14. * Animals were anaesthetised for surgical occlusion of the MCA. At 1 h and 24 h the animals were conscious.

4.2.2 Mapping areas of infarction

After detaching the hindbrain, the forebrain was cut into four equally spaced coronal blocks, embedded in paraffin wax, and sectioned (nominally 10 μm thick) at multiple levels. The sections were stained by haematoxylin and eosin and a method that combines Luxol fast blue and cresyl violet, and were examined by conventional light microscopy (section 2.4). Areas of infarction were delineated on paraffin sections at eight preselected stereotactically determined coronal levels (Fig. 2.4), previously shown to be the minimum number of levels at which the assessment can be made without loss of accuracy (Osborne et al. 1987), and transcribed onto anatomical scale diagrams (x 4 actual size) of forebrain drawn from the atlas of Konig and Klippel (Fig. 2.5). The areas of ischaemic damage in the cerebral hemisphere, were determined from the diagrams, at each of the eight coronal planes using a computer based image analysis system (MCID). Following calibration, the area of infarction was measured at each coronal level. An approximation to total volume of ischaemic damage for each animal was achieved by integration of area with the distance between each level (Table 4.2).

In order to obtain a diagram showing total area of ischaemia for the 14 animals, for each rat, the areas of ischaemia shown on the 8 anatomical diagrams were transposed to a manually drawn diagram. This was carried out on a light box to allow accurate placement of the ischaemic areas in relation to the anatomical diagrams. Fiducial marker points at the four corners of the template were also copied to each diagram to allow for co-registration of all the completed diagrams. The diagrams were then digitally scanned using a UMAX Powerlook flatbed scanner and imported into the NIH program on the Apple computer. The diagrams were aligned to an identical orientation using the Alignment software and guided by the fiducial markers. The image for each diagram was converted to a binary form with the area of ischaemia being allocated the value of 1.

The set of 14 aligned images were added using the Image Math facility on NIH Image. In this way an area of consistent ischaemia, seen at the same position in all rats, had a value of 14 and areas with less consistent ischaemia had lower values on the 1-14 scale. The final combined image was overlaid onto a scanned image of the 8 section template to show the anatomical positions of the combined ischaemic areas. The final image was displayed using a 15 colour look-up table image (Fig. 4.1).

4.2.3 Immunocytochemistry

Sections adjacent to those used for mapping areas of infarction were prepared for immunocytochemistry so that the topography of increased APP immunoreactivity could be compared to that of infarction. Immunocytochemistry was performed as previously described (see 2.3.1). In this case the APP antibody (clone 22C11, Boehringer Mannheim) was at a concentration of 1:500. As there were over 100 sections, they were immunostained in batches on different days.

4.2.4 Topography of increased APP immunoreactivity

Since diaminobenzidine was used as a chromagen in the immunocytochemistry, the increase in APP immunoreactivity within the white matter was brown. Equivalent coronal sections from each animal, at defined coronal planes (Osborne et al. 1987), were placed on a light box and the image captured via an 8 bit standard CCD video camera and transferred to a MCID-M4 image analyser. The complete coronal section could then be viewed on a monitor at x10 magnification, digitised and image printed using an HP laser printer. The images produced showed the increased APP immunoreactivity. The sections were also viewed using a conventional light microscope (Leitz DMRB) at x 50 magnification to check that all the increased APP immunoreactivity was visible on the

printed images. This procedure was repeated for each animal at each coronal level. Therefore, an accurate determination of the overall topography of increased APP immunoreactivity for the 14 animals could be established by tracing and superimposing the increased APP immunoreactivity at each coronal level for the 14 animals onto a single line diagram which was drawn on an acetate sheet (Fig. 4.2). The superimposition of increased APP immunoreactivity for the 14 animals was repeated at each of the 8 coronal levels (Fig. 4.1).

4.2.5 Quantitative analysis of APP immunoreactivity

In order to investigate a quantitative assessment of the relationship between increased APP immunoreactivity and infarction, a method was developed using the MCID to measure the area of increased APP immunoreactivity. Although different approaches for densitometric analysis were explored, the methods were flawed and considered unsuitable for further use within this thesis. The methods, results and discussion relating to the densitometric analysis of APP can be found in full in Appendix 4.

A semi-quantitative method of APP analysis, which had several advantages over the densitometric method (appendix4), was developed in order to assess the relationship of APP immunoreactivity and volume of ischaemia. Each coronal section was analysed for APP by light microscopy and a semi-quantitative rating given viz. 0 for no APP, 1 for some APP , 2 for a moderate amount of APP and 3 for large amounts of APP (Table 4.3 and Fig. 4.3). The total APP immunoreactivity score for each animal, out of a maximum of 24, was the sum of the scores for the eight coronal levels (Table 4.2). To determine the reproducibility of this semi-quantitative scoring system, the APP score was determined for five animals on two separate occasions (Fig 4.4).

Table 4.2 Hemispheric infarction and APP accumulation score

Animal No.	1	2	3	4	5	6	7	8	9	10	11	12	13	14
Hemisphere infarction (mm^3)	70.5	87.5	145.2	110.0	109.4	105.7	143.3	160.0	153.8	158.2	108.0	169.1	190.3	195.7
Total APP accumulation score	2	6	6	7	8+	9	10	10	11	11	14	16	16	17

Based on the scoring system described, the total APP accumulation score for each animal was calculated. With increasing size of infarction volume, there was a general increase in APP accumulation score. (No appropriate sections were available for analysis at coronal level 1 or 2 for animal number 5, therefore the total accumulation score allocated was 8+).

Table 4.3 APP score for each coronal level

Coronal level	1	2	3	4	5	6	7	8
Anatomical Landmark	Olfactory tract	Nucleus accumbens	Septal nuclei	Globus pallidus	Anterior hypothalamus	Lateral habenula	Medial geniculate	Aqueduct
Co-ordinate (mm)	10.50	8.92	7.19	6.06	5.15	3.75	2.18	1.02
Animal No.								
1	+	+	–	–	–	–	–	–
2	–	+	+	++	–	++	–	–
3	++	++	–	–	+	+	–	–
4	–	++	+++	+	+	–	–	–
5	ns	ns	+++	+++	++	–	–	–
6	+	+++	+++	++	–	–	–	–
7	+	+	++	++	++	++	–	–
8	++	+	++	++	+	++	–	–
9	+	++	+	+	+++	+++	–	–
10	+	++	+++	++	++	+	–	–
11	++	+++	+++	+++	+++	–	–	–
12	+	+++	+++	+++	+++	+++	–	–
13	+	+++	+++	+++	+++	+++	–	–
14	++	+++	+++	+++	+++	+++	–	–

Semi-quantitative scale showing allocated APP score at each coronal level for the 14 animals. -, no APP; +, some APP; + +, moderate amount of APP; + + +, lots of APP. In subsequent analysis, a score of 0 for -, 1 for +, 2 for + + and 3 for + + +, was given. Rat brain co-ordinates taken from the Atlas of Konig and Klippel. ns, no appropriate section available.

Figure 4.1

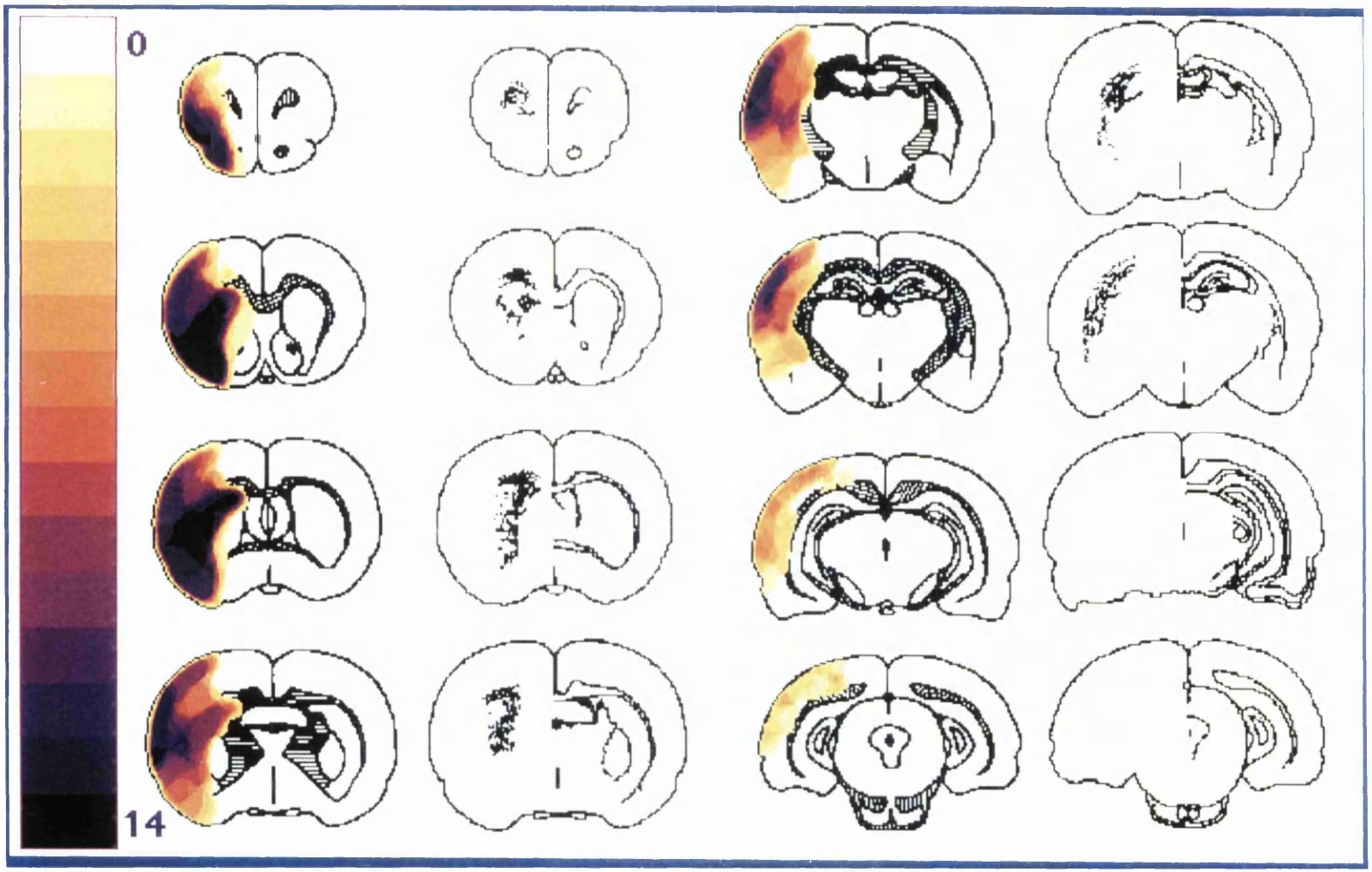

Incidence and topography of the ischaemic lesion and APP immunoreactivity for the eight preselected coronal levels in 14 rats after MCA occlusion. To gain an impression of the topography and incidence of ischaemic damage, the area of the ischaemic lesion of individual coronal slices, at given co-ordinates, was superimposed using NIH Image. Colour scale bar represents number of animals with ischaemic damage. To gain an overall impression of distribution and relationship to area of the ischaemic lesion, increased APP immunoreactivity for the 14 animals was mapped onto line diagrams which were subsequently superimposed (represented as dots on ipsilateral hemisphere).

Figure 4.2

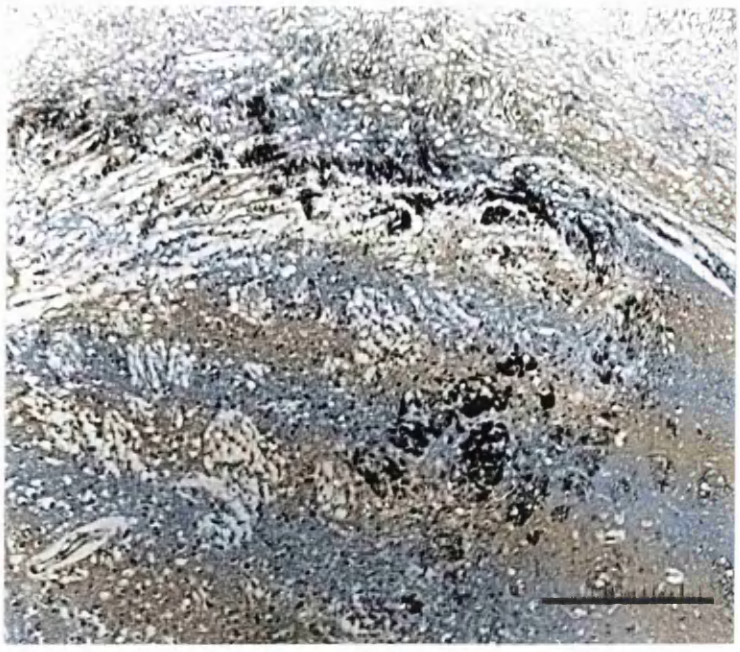

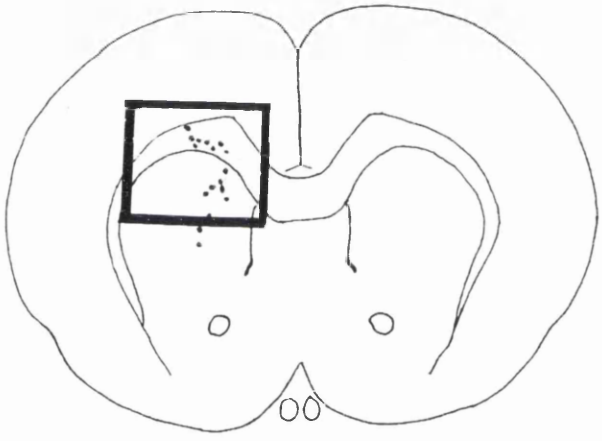

Photomicrograph showing increased APP immunoreactivity in subcortical white matter and along myelinated fibre tracts permeating the striatum (Bar = 400μm). Below is a representative example of a line diagram showing increased APP immunoreactivity transcribed from the section shown in the photomicrograph.

Figure 4.3

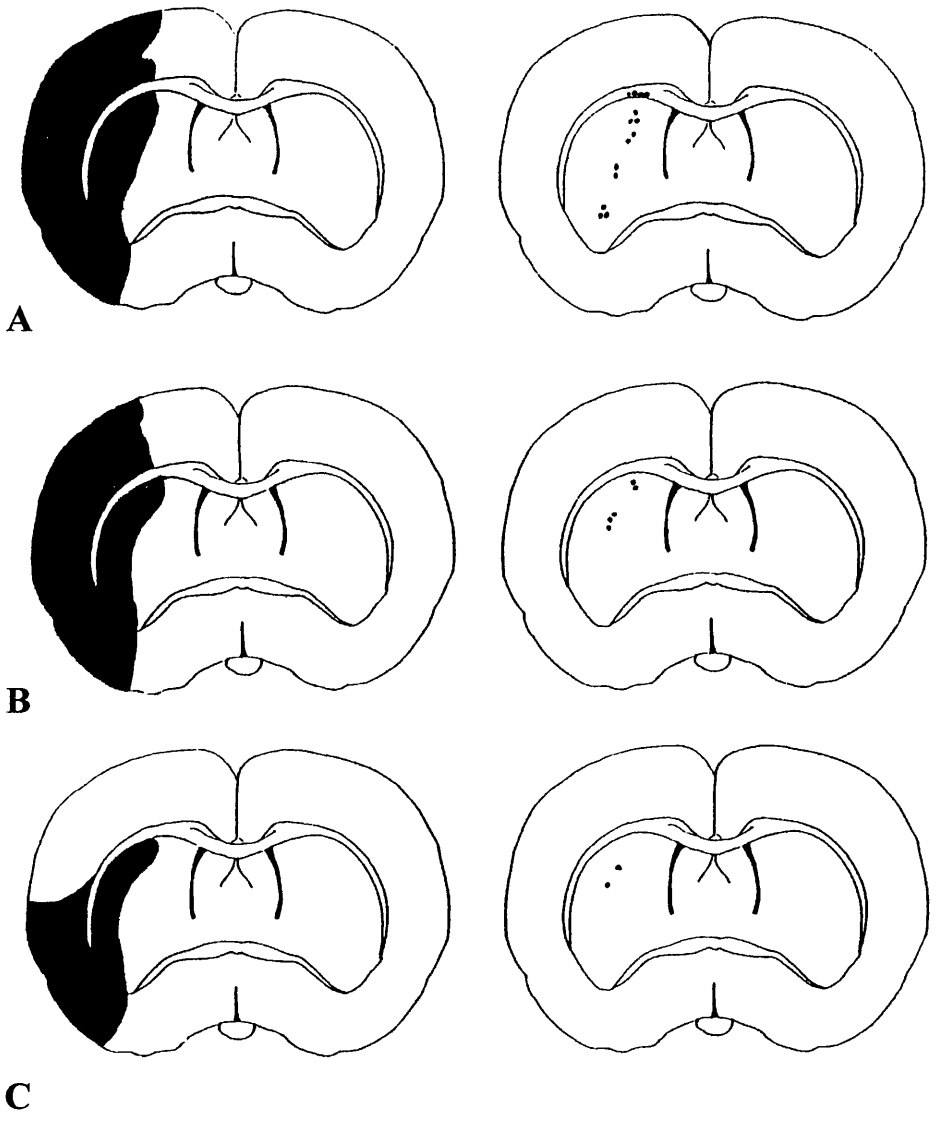

Representative line diagrams from three animals showing areas of neuronal necrosis (A, B and C) and the location of increased APP immunoreactivity. The APP score for these animals was 3, 2 and 1 respectively.

4.3 RESULTS

4.3.1 APP immunocytochemistry after middle cerebral artery occlusion

In the non-ischaemic contralateral hemisphere, in all animals, APP immunoreactivity was faint. In contrast, in the ipsilateral ischaemic hemisphere, all animals had anatomically circumscribed zones of increased APP immunoreactivity in the subcortical white matter and in the myelinated fibre tracts permeating the striatum. The increased axonal immunoreactivity was 'bulbous' in appearance (Fig. 4.5), reminiscent of axonal swellings which occur following traumatic brain injury and which have been suggested as an early indicator of axotomy (Povlishock, 1992) (discussed further in section 7.2). Increased APP immunoreactivity was present in both the medial caudate and dorsal subcortical white matter and was confined to a zone immediately adjacent to the boundary of ischaemia. This could be readily seen when zones of ischaemic damage and points of APP immunoreactivity were visualised either at a single level within an animal (Fig. 4.3) or in the composite diagram for the 14 animals (Fig. 4.1). Increased APP immunoreactivity was detected in cell bodies in the ischaemic side as has been reported in previous studies (Stephenson et al. 1992). Increased APP immunoreactivity was not detected in the subcortical white matter or in myelinated fibre tracts in the lateral caudate deep within the areas of ischaemia (Fig. 4.6).

4.3.2 Reproducibility of semi-quantitative analysis

To determine the reproducibility of the semi-quantitative scoring system, the APP score was determined for five animals on two separate occasions (Fig 4.4). On 57.5% of occasions the score allocated was the same, and on 95% of occasions the score allocated was the same or just one point different. The non parametric Spearman correlation, r =

0.75. The reproducibility at the individual coronal levels was reasonable and the errors random. Since the total APP score for each rat was the summation of the APP scores for each of the eight coronal levels, the reproducibility was enhanced.

4.3.3 Relationship between ischaemia and APP accumulation

Zones of ischaemic damage (Brierley and Graham, 1984), were restricted to those areas of the brain normally supplied by the middle cerebral artery (Yamori et al. 1976). There was ischaemia in all the animals at level 2 (anterior co-ordinate of 8.92 mm). Levels 1 and 3 (anterior co-ordinates of 10.50 and 7.19 mm respectively (Konig and Klippel, 1963)) were affected in the majority of animals and fewer animals had evidence of ischaemia in the more caudal coronal sections (anterior co-ordinates of 2.18 and 1.02 mm). Ischaemia was not seen in the contralateral hemisphere in any case. The volume of ischaemia in the cerebral hemisphere was 136 ± 10 mm^3 (mean $\pm$ standard error, n = 14). The volume of cortical necrosis was 105 ± 9 mm^3 and the volume of striatal necrosis was 24 ± 1 mm^3. There was an association between the volume of ischaemic damage and the amount of increased APP immunoreactivity as assessed by semi-quantitative analysis (Fig. 4.7), the increase in APP immunoreactivity being greatest in rats with the largest volumes of neuronal necrosis. A similar association could be discerned between the area of ischaemic damage and the extent of increased APP immunoreactivity at individual coronal planes (Fig. 4.8).

Figure 4.4 Reproducibility of semi-quantitative APP analysis

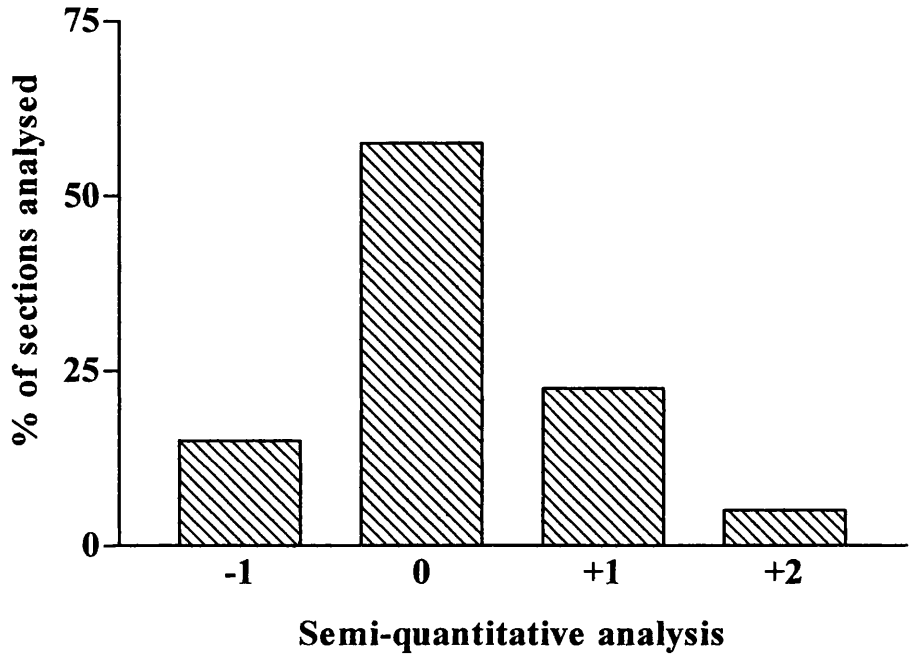

Forty rat sections were analysed on two separate occasions to assess scoring reproducibility. An APP score of 0, 1, 2 or 3 was given on each occasion as previously described. The value allocated on the second occasion was deducted from that on the first occasion to give a final result ranging from -1 to +2. Therefore, where a section was given the same score on both occasions the value allocated was 0.

Figure 4.5

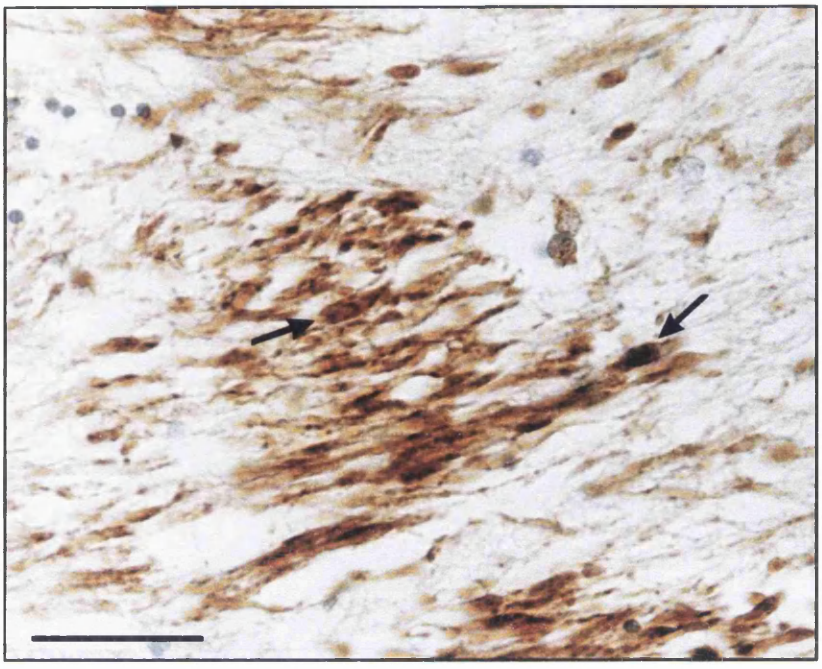

Increased APP immunoreactivity in the caudate nucleus following 24 h MCA occlusion in the rat. The immunoreactivity was 'bulbous' in appearance (arrows). Bar = 50 μm.

Figure 4.6 Location of increased APP immunoreactivity

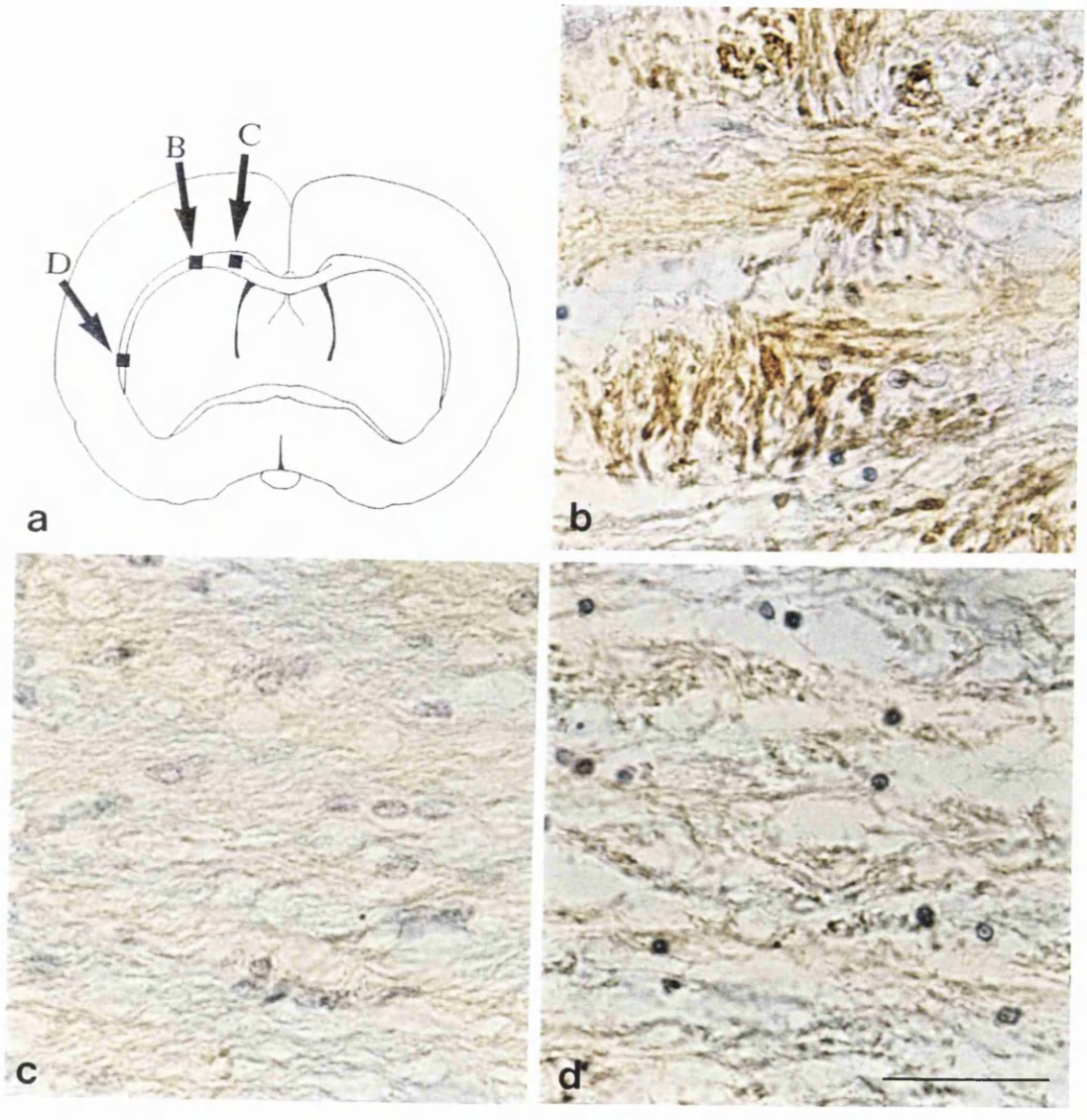

(a) Line diagram of coronal level 3 showing the location of the following photomicrographs. (b) Increase in APP immunoreactivity in corpus callosum immediately adjacent to the ischaemic lesion, (c) no increase in APP immunoreactivity evident in the non-ischaemic corpus callosum and (d) no increase in APP immunoreactivity evident in the densely ischaemic corpus callosum. (Bar = 50 μm for b, c and d).

Figure 4.7

Relationship of APP accumulation to volume of infarction

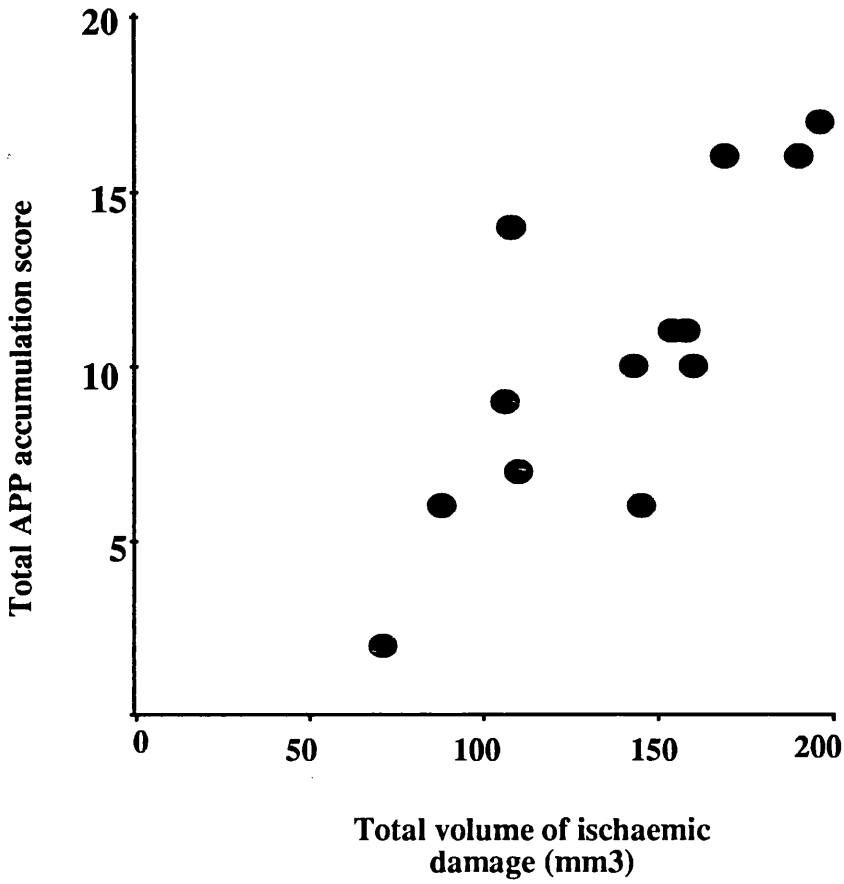

The volume of ischaemic damage was compared to total accumulation of APP for each animal. The total APP accumulation was the score sum for the eight coronal levels. Total APP accumulation score increased with increasing volume of infarction. Each point represents data from a single animal

Figure 4.8

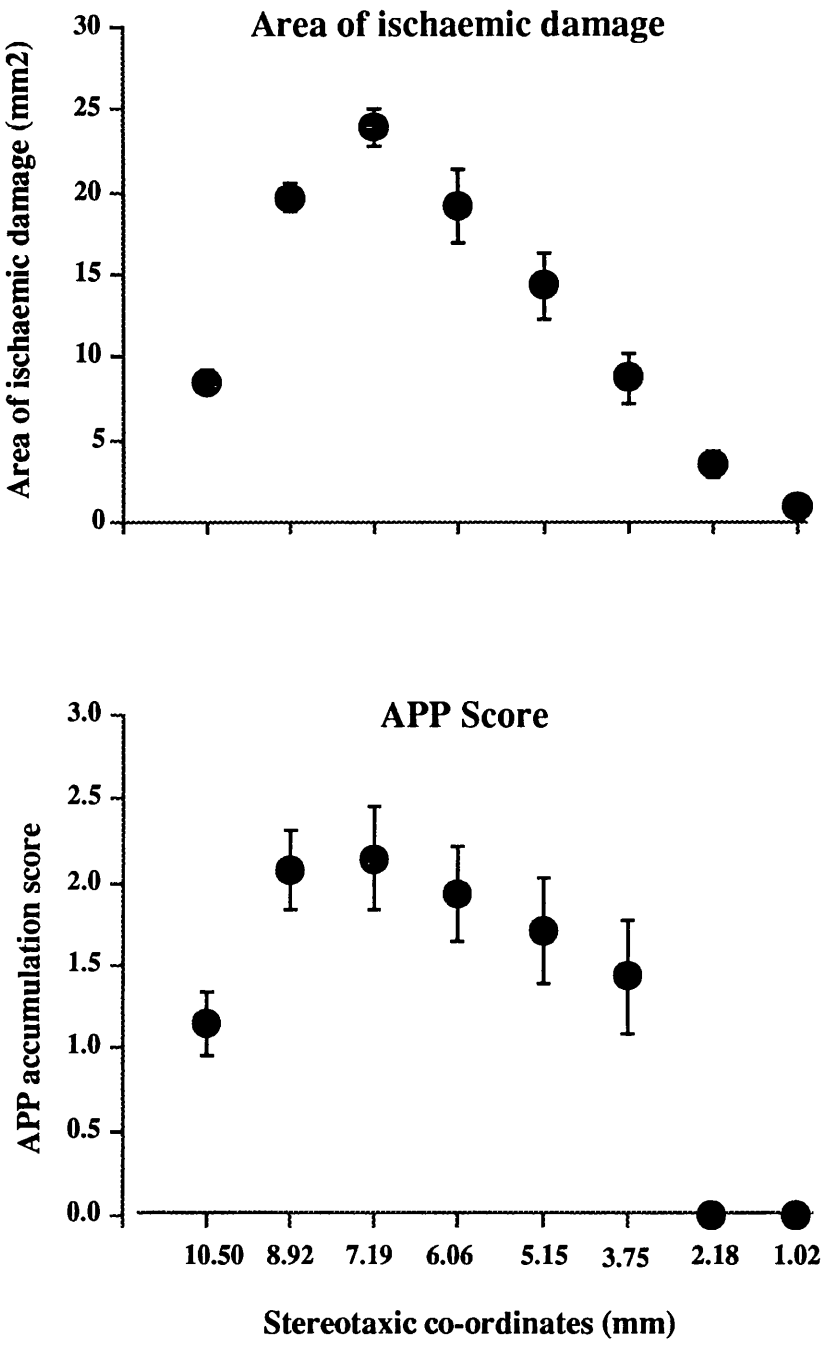

Mean APP accumulation score and mean area of the ischaemic lesion for the 14 animals at each coronal level were calculated. Mean APP accumulation score was highest in the coronal levels with the largest area of ischaemic damage (anterior co-ordinates 7.19 and 8.92 mm). data are presented as mean ± SEM (n=14).

4.4 DISCUSSION

This study demonstrated that increased APP immunoreactivity is a consistent outcome in white matter after focal cerebral ischaemia. APP undergoes fast anterograde axonal transport (Koo et al. 1990) and the interruption of this transport is likely to reflect APP accumulation (Shigematsu and McGeer, 1992). In order to use APP as a quantitative marker of axonal injury, and to assess the potential beneficial effects of therapeutic intervention, a reliable method of quantifying the increased APP immunoreactivity is required. Although, it is generally accepted that quantification of immunocytochemistry is complex, a semi-quantitative method of APP quantification was developed. This is the first study where an attempt has been made to map and quantify the accumulation of APP and relate this to the region and extent of ischaemic damage.

Semi-quantitative analysis was relatively straight forward and quick to perform. All eight coronal levels could be scored in one day, an important requisite for consistent scoring using this method. The sensitivity of this method was limited and methods by which it could be improved are discussed and utilised in subsequent chapters of this thesis (Chapter 6 and 7). Nevertheless, the amount of APP accumulation was shown to be related to lesion size. Because of the ease with which semi-quantitative analysis could be performed, and the fact that it has shown that APP accumulation is determined by lesion size, this method was chosen for the quantification of APP following therapeutic intervention in the rat (Chapter 5).

CHAPTER 5

QUANTITATIVE ANALYSIS OF APP FOLLOWING DRUG INTERVENTION IN THE RAT

5.1 INTRODUCTION

Extracellular glutamate level elevation is one of the major events contributing to the spread of secondary damage following CNS injury of grey matter (for review see Holt, 1997). Consequently a variety of drugs have been developed by the pharmaceutical industry to reduce the extent of glutamate-mediated pathologies either by inhibiting the release of glutamate or by inhibiting the activation of postsynaptic receptors by glutamate. Voltage-activated sodium channels in axons and nerve terminals affect glutamate release by propagating a depolarising stimulus to sites of vesicular release . Presynaptic voltage-activated Ca^{2+} channels at the release sites are opened in response to this depolarisation. The elevation of cytoplasmic Ca^{2+} levels in the nerve terminal initiates the process of exocytosis of glutamate (Goldin et al. 1995). Neuronal sodium channel antagonists include the compound BW619C89; this compound apparently also has calcium channel blocking properties (McNaughton et al. 1997) (see section 1.6.3). Presynaptic blockade of glutamate release is advantageous in that it prevents the activation of both the NMDA and non-NMDA receptor sites.

In order for glutamate to exert its biological effect it must bind to specific sites on the target tissues. Glutamate receptors are reviewed in section 1.5.2. The NMDA receptor is recognised to be involved in the mediation of glutamate toxicity. Accordingly, research aimed at reducing secondary damage after injury has been

directed toward pharmacological blocking of NMDA receptors. Many of the studies on neuroprotection have involved the use of the non-competitive NMDA antagonist, MK-801 (Wong et al. 1986) (see section 1.6.2). In injuries involving grey matter, the mechanism of protection by MK-801 involves blockage of the NMDA receptors which are permeable not only to monovalent cations but also to calcium, and which are known to be opened during ischaemia due to excessive release (and impaired uptake) of glutamate.

A number of studies using BW619C89 and MK-801 have shown them to be neuroprotective following focal cerebral ischaemia in the rat (Gill et al. 1991; Park et al. 1988b; Graham et al. 1994; Kawaguchi and Graham, 1997; Leach et al. 1993). However, in all of these studies, 'neuroprotection' was assessed by a reduction in infarct volume; the effect on axons being largely ignored. In Chapter 4, APP was shown to be a suitable marker of axonal injury and a method has been developed for its quantification. The studies described in this chapter use APP as the marker of axonal injury to assess whether either BW619C89 or MK-801 protect axons following focal cerebral ischaemia in the rat.

5.2 METHOD

5.2.1 MK-801 treated animals

The investigation was carried out in 26 adult male Fischer rats. Anaesthesia and MCA occlusion was performed as previously described (2.1.2 and 2.1.3). The animals were divided into two groups: MCA occlusion vehicle group (n = 13) and MCA occlusion drug treatment group (n = 13). In the drug treatment group, 0.12 mg/kg of MK-801 was given as an i.v. bolus immediately after completion of MCA occlusion and 1.8

μg/kg/min as an infusion, a regime previously shown to maintain a steady state plasma level of MK-801 throughout the ischaemic period and shown to give a highly significant reduction in volume of ischaemic brain damage in the cerebral cortex and hemisphere (Gill et al. 1991). The control group received a 1ml/kg i.v. bolus of saline followed by an infusion of saline at a rate of 0.0079 ml/min. For both groups, initial dosing was started immediately following MCA occlusion, the bolus dose being administered over a 30 s period and the infusion continued for the duration of the experiment which was 4 h.

5.2.2 BW619C89 treated animals

The investigation was carried out in 21 adult male Fischer rats. Anaesthesia and MCA occlusion was performed as previously described (2.1.2 and 2.1.3) by Dr. Ramanjit Gill. The animals were divided into two groups: MCA occlusion vehicle group (n = 10) and MCA occlusion drug treatment group (n = 11). In the drug treatment group, 10mg/kg of BW619C89 was given as an i.v. bolus over a period of 10 minutes, 5 minutes after completion of MCA occlusion. The drug was kindly supplied by Hoffman-La Roche Ltd. The control group received a 1ml/kg i.v. bolus of saline over 10 minutes, 5 minutes after MCA occlusion. Following MCA occlusion the animals, anaesthesia was discontinued and the animals allowed to regain consciousness. The animals were killed 24 h following MCA occlusion.

5.2.3 Tissue processing and APP analysis

The animals were killed by transcardiac perfusion, the fixative being FAM (see 2.1.4). The brain was cut into 10μm sections at the eight preselected coronal levels and histology performed using haematoxylin and eosin and Luxol fast blue and cresyl violet (see section 2.4). Sections adjacent to those used for mapping areas of infarction were

prepared for immunocytochemistry (see 2.3.1) so that the topography of increased APP immunoreactivity could be compared to that of infarction.

The method of semi-quantitative analysis of APP accumulation as described in Chapter 4, was applied. Equivalent coronal sections from each animal, at defined coronal planes (Konig and Klippel, 1963) were viewed by conventional light microscopy and the distribution of increased APP immunoreactivity mapped onto line diagrams by an observer 'blind' to the topography of the ischaemic lesion in grey matter. To determine the topography of APP accumulation for the animals, the line diagrams on which the increased APP immunoreactivity was mapped, at predetermined co-ordinates, were superimposed for the two groups.

In order to assess the APP immunoreactivity further, each coronal section was analysed for APP by light microscopy and a semi-quantitative rating given viz. 0 for no APP, 1 for some APP, 2 for a moderate amount of APP and 3 for large amounts of APP. The total APP immunoreactivity score for each animal, out of a maximum of 24, was the sum of the scores for the eight coronal levels. The distribution and quantity of APP accumulation in relation to volume of infarction for the drug treated (MK-801 and BW619C89) and vehicle treated animals were compared.

5.3 RESULTS OF MK-801 STUDY

5.3.1 Physiology

There was minimal interanimal variability in measured physiological parameters which may influence the extent of infarction (Table 5.1). After MK-801 administration the rats showed a fall in blood pressure as has been previously reported (Park et al. 1988b). Since this might be expected to increase brain damage, blood pressure was normalised to 80 mmHg by decreasing halothane administration.

5.3.2 APP immunocytochemistry after MCA occlusion

In the non-ischaemic contralateral hemisphere, in all animals, APP immunoreactivity was faint. In contrast, in the ipsilateral hemisphere, in both the drug and vehicle groups, all animals had anatomically circumscribed zones of increased APP immunoreactivity in the subcortical white matter and in the myelinated fibre tracts permeating the striatum. In both groups, the increased APP immunoreactivity was confined to a zone immediately adjacent to the boundary of ischaemia. This can be readily visualised in the composite diagrams for each of the two groups (Fig 5.1).

5.3.3 Effect of MK-801 on ischaemic damage

Ischaemic damage was observed only within the territory of the occluded MCA, that is, in the dorsolateral cortex and in the caudate nucleus. The standard deviation of lesion size for the two groups was small; 25% for the vehicle group and 31% for the MK-801 treated group. The histological appearance of the ischaemic brain tissue in rats treated with MK-801 was similar to that in the untreated group. The administration of MK-801 reduced the volume of ischaemic damage in the cerebral hemisphere by 15.0%

compared to untreated rats and by 15.1% in the cerebral cortex compared to untreated rats following MCA occlusion (see Table 5.2 and Table 5.3 and Fig. 5.2A). The areas of ischaemic damage in the hemisphere in the animals treated with MK-801 were smaller than those in the untreated control group at each stereotactic coronal plane examined (Fig. 5.3A).

5.3.4 Effect of MK-801 on APP accumulation

In the MK-801 treated rats, with increasing volume of ischaemic damage there was a general increase in APP accumulation as assessed by semi-quantitative analysis (Fig. 5.4). The primary hypothesis being tested was that if MK-801 protects axons, the APP score should be reduced. However,

The mean total APP score for the vehicle treated group was 11.3 $\pm$ 0.7 and the mean total APP score for the MK-801 treated group was 10.6 $\pm$ 0.9 (Table 5.4). In addition to looking at the total APP score, the relationship of the APP score and area of ischaemia at different coronal planes (Fig. 5.3B) and subgroup analysis was performed to assess if there were any trends in the data. Subgroup analysis was performed whereby the drug treated group was separated into those with infarction greater than 100mm^3 and those with infarction less than 100mm^3 and APP score compared to vehicle treated animals. Even in the latter group, in which there was an overall reduction in volume of infarction of 30% compared to the vehicle group, there was not a statistically significant reduction in mean APP accumulation score in this subset compared to the vehicle group (ANOVA, $F = 1.183$, $P = 0.32$) (Fig. 5.5). The data provided no evidence to suggest that MK-801 reduces the APP score.

Table 5.1 Physiological variables prior to and following MCA occlusion in MK-801 study

	MABP (mmHg)	pH	$PaCO_2$ (mmHg)	PaO_2 (mmHg)	Rectal Temp. (°C)
Vehicle					
pre-MCAO	73.3 ± 2.2	7.40 ± 0.02	41.9 ± 1.0	184 ± 12	37.1 ± 0.2
MCAO	77.7 ± 1.7	7.41 ± 0.01	40.2 ± 0.5	189 ± 10	37.1 ± 0.2
1 h	76.7 ± 2.0	7.42 ± 0.01	41.4 ± 0.6	202 ± 11	37.1 ± 0.1
2 h	77.2 ±1.6	7.42 ± 0.01	39.7 ± 0.8	192 ± 9	37.2 ± 0.2
3 h	73.9 ± 2.0	7.43 ± 0.01	38.0 ± 0.6	191 ± 8	36.8 ± 0.1
4 h	75.2 ±1.5	7.43 ± 0.01	39.1 ± 0.6	193 ± 9	36.7 ± 0.2
MK-801					
pre-MCAO	76.9 ±1.9	7.44 ± 0.01	39.4 ± 0.8	189 ± 4	37.1 ± 0.2
MCAO	76.9 ± 1.2	7.43 ± 0.01	38.6 ± 0.8	195 ± 4	37.0 ± 0.2
1 h	79.9 ±1.1	7.43 ± 0.01	40.6 ± 0.8	197 ± 5	37.0 ± 0.1
2 h	78.9 ±1.1	7.42 ± 0.01	39.0 ± 1.2	197 ± 5	37.0 ± 0.1
3 h	77.7 ± 1.0	7.42 ± 0.01	38.8± 1.1	184 ± 10	37.1 ± 0.2
4 h	78.4 ± 1.0	7.43 ± 0.01	40.4 ± 1.4	189 ± 4	36.9 ± 0.1

Figure 5.1

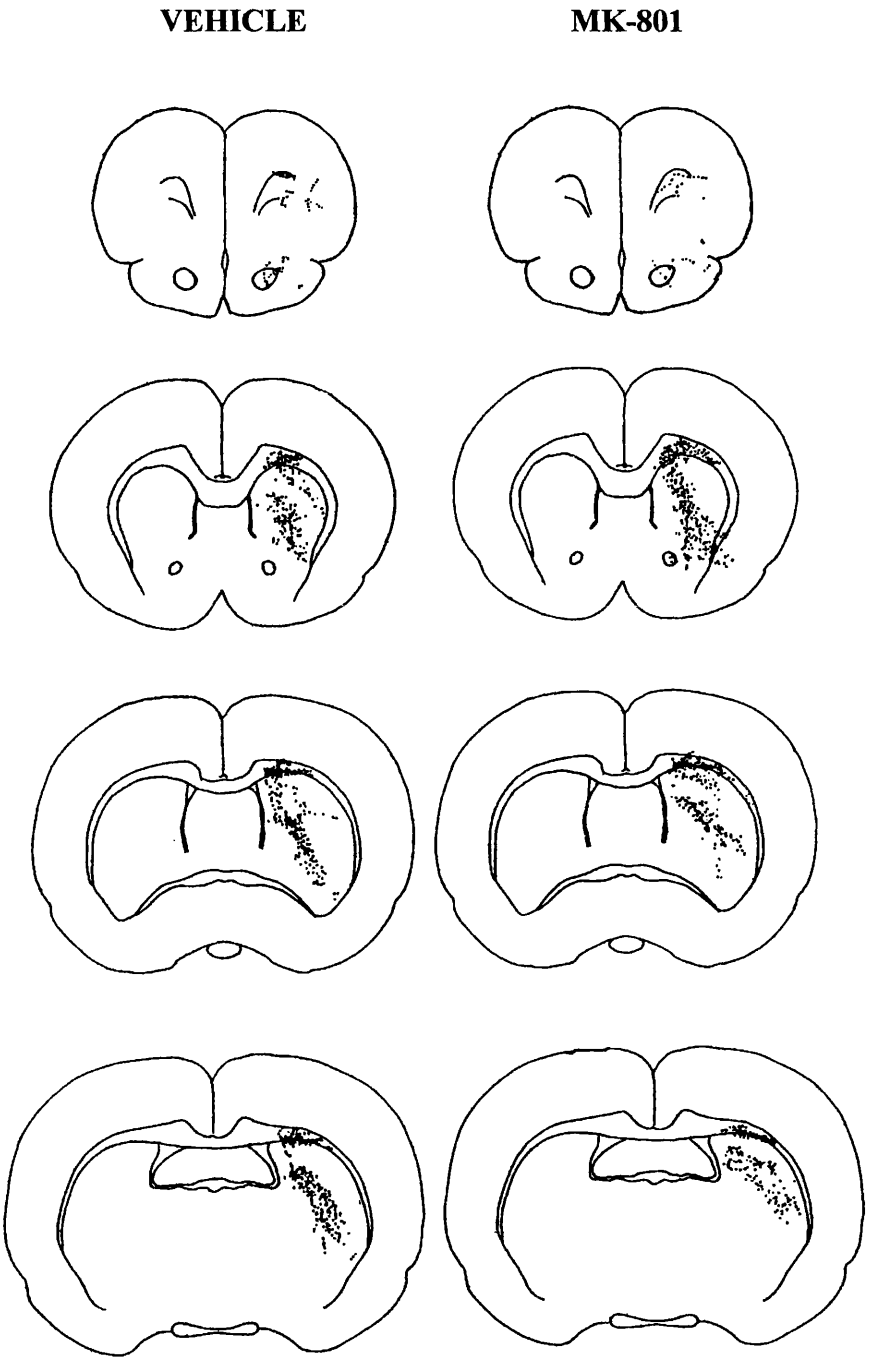

To gain an overall impression of distribution of increased APP immunoreactivity for the vehicle and drug treated animals, the increased APP immunoreactivity for the two groups was mapped onto line diagrams which were subsequently superimposed (represented as dots on ipsilateral hemisphere).

Figure 5.1 cont...

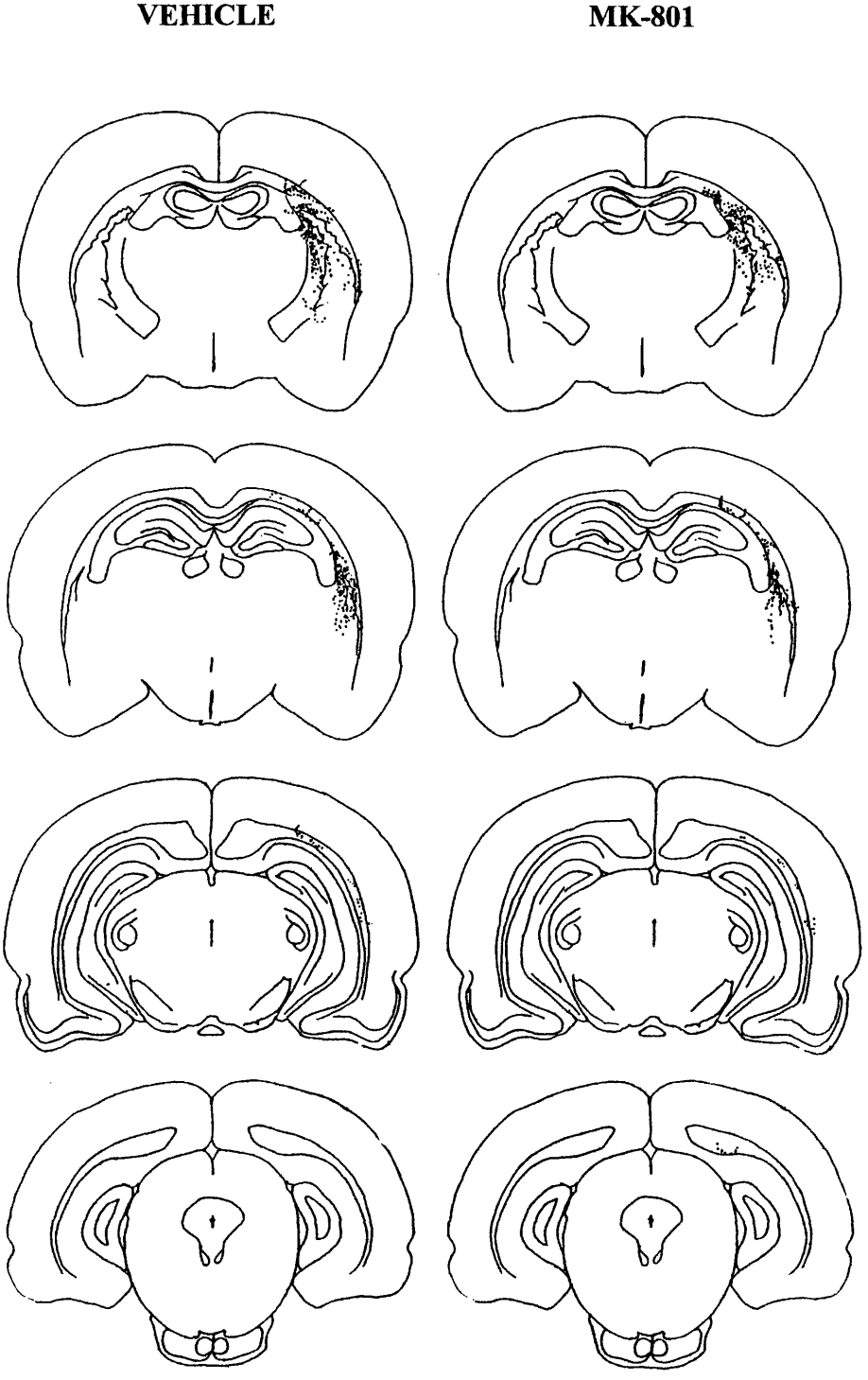

Table 5.2 Ischaemic damage following MCA occlusion: vehicle group

Hemisphere	Level 1	Level 2	Level 3	Level 4	Level 5	Level 6	Level 7	Level 8	Total (mm3)
1	6.3	12.3	15	16	13.8	7.1	5.5	1	103.9
2	7.5	13.7	21.6	16.3	11.6	11.1	2.6	4.4	121.6
3	5	12.7	19.6	24	22.7	7.3	5.5	0	126.4
4	4.2	17.1	20.2	19.9	17.9	3.7	1.5	0.7	113.4
5	4.8	11.3	11.9	9.7	8.7	3.9	2.8	1.2	74.7
6	3.5	11.2	12.2	15.8	7.9	3.5	2.1	1	76.5
7	4.4	18.7	19.4	23	22.9	10	7.6	1	142.3
8	2.9	15	20.8	18.3	16.4	8.9	7.1	4.3	125.6
9	4.8	16.2	14.9	14.8	13	1.6	0	0	88.6
10	3.1	13.2	14.8	12.1	9.5	1.5	0	0	73.6
11	4.9	16.9	20.4	20.4	14.4	11.2	1.5	2.2	124.2
12	6	15.4	18.9	23.4	18.7	12	7.6	3.2	140.2
13	1.9	7.9	13.1	14.9	6.5	4.4	1.4	1.7	68.3
Mean	4.6	14.0	17.1	17.6	14.2	6.6	3.5	1.6	106.1
Std Dev	1.5	3.0	3.5	4.4	5.4	3.8	2.8	1.5	26.7
SEM	0.4	0.8	1.0	1.2	1.5	1.0	0.8	0.4	7.4
Cortex									
1	6.3	8.6	11.5	11.8	9.5	7.1	5.5	1	83.4
2	7.5	8.6	14.9	9.8	8.7	9.4	2.6	4.4	91.3
3	5	8.2	11.8	16.1	17.3	7.3	5.5	0	93.4
4	4.2	11.3	12.4	10.6	11.7	2.7	1.5	0.7	74.6
5	4.8	7.5	6.2	5.4	4.4	3.9	2.5	1.2	50.7
6	3.5	6.9	6.2	9.6	3.5	2.7	2.1	1	48.1
7	4.4	13.2	13.2	15.5	16.5	10	7.6	1	109.5
8	2.9	10.3	13	12.3	11.9	7.4	7.1	4.3	93.2
9	4.8	10.6	7.7	8.3	8.1	0.5	0	0	55
10	3.1	7.8	8	6.2	4.9	1.5	0	0	43.7
11	4.9	11.3	13.1	12.5	10.1	9.1	1.5	2.2	88.3
12	6	10.1	11.5	14.8	12.8	10.4	7.6	3.2	103
13	1.9	3.5	6.8	7.4	2.7	3.6	1.4	1.7	38.7
Mean	4.6	9.1	10.5	10.8	9.4	5.8	3.5	1.6	74.8
Std Dev	1.5	2.5	3.1	3.5	4.7	3.5	2.8	1.5	24.4
SEM	0.4	0.7	0.8	1.0	1.3	1.0	0.8	0.4	6.8
Caudate									
1		2.2	2.4	2.6	1.6	0			10.6
2		3.3	5	4.7	1.7	0.9			18.8
3		3.7	6.4	6.2	3.7	0			24.5
4		3.1	5.2	6.7	4.1	0.8			23.6
5		2.1	3.8	3.3	2.8	0			14.7
6		2.3	5	5.2	4.2	0.8			20.9
7		3.6	4.8	5.7	4.1	0			21.9
8		3.2	6.2	4.4	2.7	0.6			21
9		4.2	6.2	5.8	4.1	0.8			25.4
10		4.5	6.2	5.2	4.2	0			24.7
11		4.2	5.7	6.7	3.4	0.6			24.8
12		4.2	6.2	7	4.1	0.8			26.5
13		4.4	5.9	6.8	3.9	0.7			26
Mean		3.5	5.3	5.4	3.4	0.5			21.8
Std Dev		0.9	1.2	1.4	0.9	0.4			4.7
SEM		0.3	0.4	0.4	0.3	0.1			1.5

Table 5.2 Ischaemic damage following MCA occlusion: MK-801 group

Hemisphere	Level 1	Level 2	Level 3	Level 4	Level 5	Level 6	Level 7	Level 8	Total (mm3)
1	6.2	18.2	20.3	23.3	23.2	11.4	3.9	1.6	144.4
2	5.1	14.6	12.9	6	5.2	0.8	1.5	0	66.2
3	4.6	13.5	15.7	16.4	5	1.9	1.8	0.4	80.6
4	0	10	16.2	17.6	3.6	3.9	3.4	0	72.2
5	4.1	14.1	11.2	11.5	12.3	8	3.3	1.3	90.3
6	1.3	14.3	7.1	3.9	1.3	1.2	0.8	0	44.3
7	3.3	13.3	10.6	7.3	3.2	2.7	0.6	0	58.4
8	0	9.7	13.8	16.9	10.7	2.9	8.2	2.6	84.3
9	4.4	15.7	16	18.9	19	8.9	0	0	110.4
10	2.4	18.2	17.9	21.2	19.4	10.7	4.2	4.6	131.3
11	6.6	11.6	19.9	16.2	8.6	2.9	0.6	0	89.9
12	4.5	12.7	16.2	12	13.7	5.7	0.4	0	88.6
13	4.7	16	17.1	16.5	18.7	4.8	3.4	1.8	111.3
Mean	3.6	14.0	15.0	14.4	11.1	5.1	2.5	0.9	90.2
Std Dev	2.1	2.7	3.8	5.9	7.3	3.6	2.3	1.4	28.3
SEM	0.6	0.7	1.0	1.6	2.0	1.0	0.6	0.4	7.8
Cortex									
1	6.2	13.8	13.2	16.3	17.7	10.7	3.9	1.6	112.4
2	5.1	10.2	8.3	4.6	2.7	0.8	1.5	0	48.1
3	4.6	9.6	9.5	9.8	1.9	1.9	1.8	0.4	55
4	0	6.1	8.7	10.4	1.1	3.9	3.4	0	44.7
5	4.1	10.9	8.8	9.5	7.3	5.9	3.3	1.3	70.8
6	1.3	8.7	7.1	3.9	1.3	1.2	0.8	0	35
7	3.3	8.9	6	2.2	1.2	1.8	0.6	0	35.7
8	0	4.8	7.3	9.6	7.2	1.7	8.2	2.6	53.8
9	4.4	10.3	9.7	13	12.2	5.5	0	0	73.5
10	2.4	12.1	11.5	14.7	14.1	10.7	4.2	4.6	99.4
11	6.6	8.1	11.2	8.7	5.5	2.3	0.6	0	59.5
12	4.5	8.1	9	6.1	9.8	4.5	0.4	0	58.4
13	4.7	10.1	9.8	10.5	13.3	4.8	3.4	1.8	78.7
Mean	3.6	9.4	9.2	9.2	7.3	4.3	2.5	0.9	63.5
Std Dev	2.1	2.4	1.9	4.2	5.7	3.3	2.3	1.4	23.2
SEM	0.6	0.7	0.5	1.2	1.6	0.9	0.6	0.4	6.4
Caudate									
1		2.6	5.2	5.4	3.1	0.7			20.5
2		3.1	3.7	0.8	2.1	0			12.2
3		2.7	5.2	6	2.7	0			20.1
4		3.5	5.4	4.8	2.6	0			20
5		1.9	1.3	0.9	4.1	0.9			10.7
6		3.7	0	0	0	0			4.6
7		3.4	3.3	4	2	0.9			16.1
8		3.9	4.8	5.1	2.4	0.9			20.6
9		4.1	5	5	4	0.7			22.7
10		3.7	4.6	4.3	2.9	0			19
11		2.5	7	6.3	2.5	0.6			23
12		3.6	6.1	5.3	3	0.7			22.7
13		4.6	6.1	4.7	3.9	0			23.8
Mean		3.3	4.4	4.0	2.7	0.4			18.2
Std Dev		0.7	1.9	2.0	1.0	0.4			5.5
SEM		0.2	0.5	0.6	0.3	0.1			1.5

Table 5.3 Influence of MK-801 upon the volume of ischaemic damage and APP score after MCA occlusion

	Volume of infarction (mm^3)	
	Vehicle	MK-801
Cerebral hemisphere	106.1 ± 7.4	90.2 ± 7.8
Cerebral cortex	74.8 ± 6.8	63.5 ± 6.4
Caudate nucleus	21.8 ± 1.5	18.2 ± 1.5
APP score	11.3 ± 0.7	10.6 ± 0.9

Data are presented as means ± SEM. Vehicle (n = 13); MK-801 (n = 13).

Table 5.4 APP score for each coronal level in vehicle and MK-801 treated animals

Coronal level	1	2	3	4	5	6	7	8	Total
Vehicle									
1	0	0	1	1	2	2	0	0	6
2	2	2	1	1	1	1	1	0	9
3	0	3	3	3	2	2	1	0	14
4	1	1	2	2	2	1	1	0	10
5	1	2	2	1	2	1	2	0	11
6	0	1	2	2	1	2	1	0	9
7	3	2	2	2	2	1	0	0	12
8	1	2	3	1	2	2	1	0	12
9	1	1	2	1	2	2	0	0	9
10	2	3	3	1	2	2	0	0	13
11	1	2	3	3	2	2	1	1	15
12	1	2	3	2	2	2	2	0	14
13	1	2	2	3	2	2	1	0	13
Average	1.2	1.8	2.2	1.8	1.8	1.7	0.8	0.1	11.3
Std dev	0.8	0.8	0.7	0.8	0.4	0.5	0.7	0.3	2.6
SEM	0.2	0.2	0.2	0.2	0.1	0.1	0.2	0.1	0.7
Drug									
1	2	3	2	1	1	1	0	0	10
2	3	3	1	1	1	1	0	0	10
3	2	3	2	1	1	0	1	0	10
4	0	3	2	1	2	1	1	0	10
5	2	1	1	2	2	2	0	0	10
6	0	2	1	0	0	0	0	0	3
7	2	2	2	1	2	1	0	0	10
8	1	2	3	3	2	2		1	14
9	1	2	1	2	2	1	0	0	9
10	1	3	3	2	2	2	2	0	15
11	1	1	3	2	2	1	0	0	10
12	1	2	2	2	2	2	1	0	12
13	2	2	3	3	1	1	2	1	15
Average	1.4	2.2	2.0	1.6	1.5	1.2	0.6	0.2	10.6
Std dev	0.9	0.7	0.8	0.9	0.7	0.7	0.8	0.4	3.1
SEM	0.2	0.2	0.2	0.2	0.2	0.2	0.2	0.1	0.9

Semi-quantitative score allocated for amount of APP at each coronal level for the 26 animals. 0, no APP; 1, some APP; 2, moderate amount of APP; 3, lots of APP.

Figure 5.2 Effect of MK-801 on total volume of ischaemic damage and total APP score following MCA occlusion

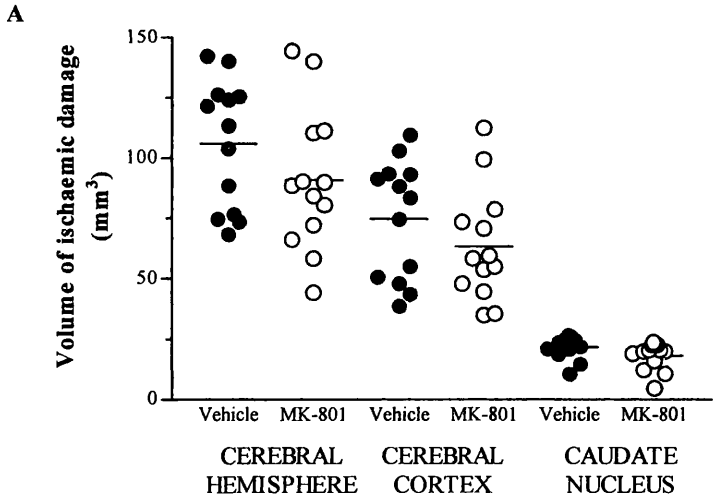

Volume of ischaemic brain damage in the cerebral hemisphere, cerebral cortex and caudate nucleus in vehicle treated control rats and in rats treated with MK-801. Each point represents data from a single animal. The mean value for the group is indicated by a solid horizontal line.

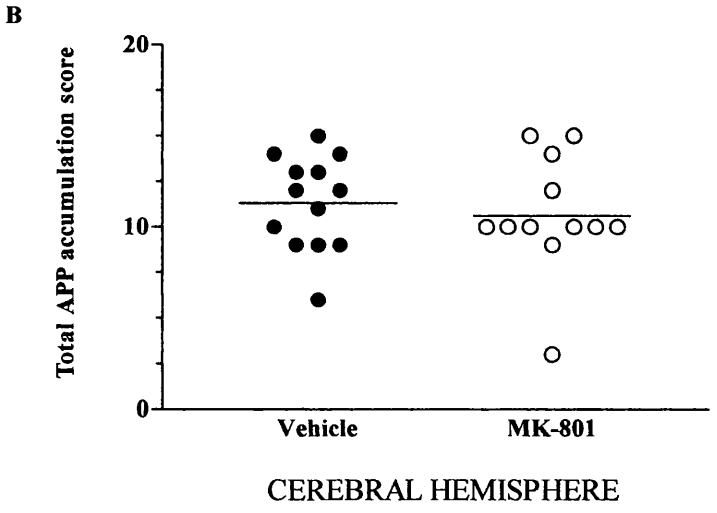

Total APP accumulation score in the cerebral hemisphere in vehicle treated control rats and in rats treated with MK-801 after MCA occlusion. Each point represents data from a single animal. The mean value for the group is indicated by a solid horizontal line.

Figure 5.3 Effect of MK-801 on area of ischaemic damage and mean APP score at eight defined coronal levels following MCA occlusion

A

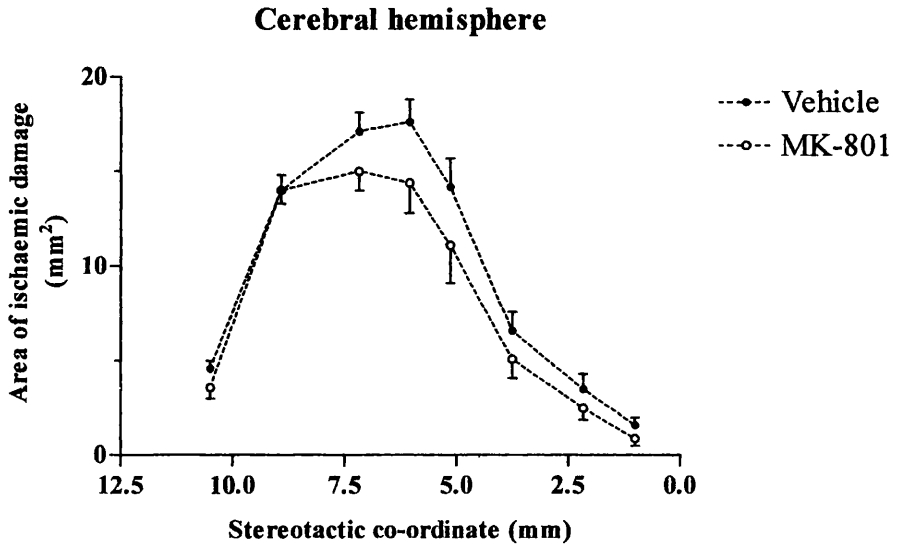

The effect of MK-801 upon the area of ischaemic damage in the cerebral hemisphere at 8 defined coronal planes. Data are presented as mean ± SEM. Vehicle (n = 13); MK-801 (n = 13).

B

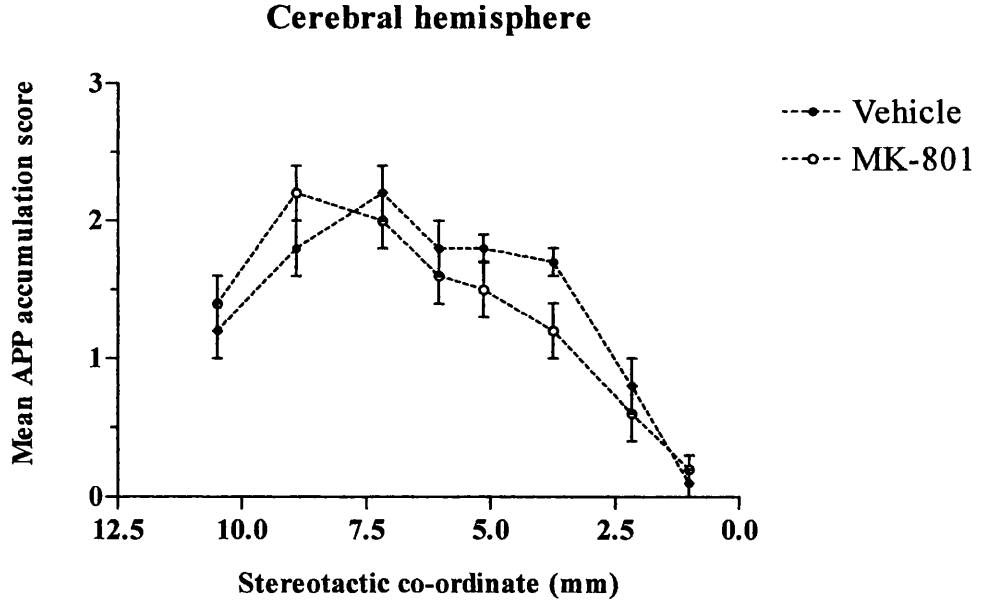

The effect of MK-801 upon the mean APP score in the cerebral hemisphere at 8 defined coronal planes. Data are presented as mean ± SEM. Vehicle (n = 13); MK-801 (n = 13).

Figure 5.4 Relationship of volume of ischaemic damage and APP accumulation score: effect of MK-801

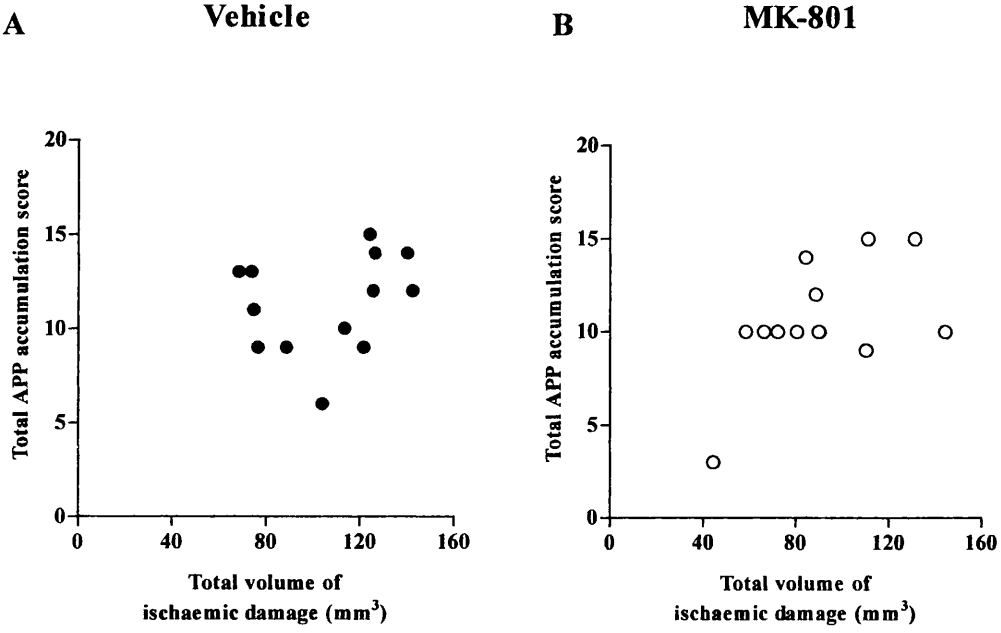

The volume of ischaemic damage was compared to total accumulation of APP for each animal in A) Vehicle treated animals and B) MK-801 treated animals. The total APP accumulation was the score sum for the 8 coronal levels. Total APP accumulation score increased with increasing volume of infarction. Each point represents data from a single animal.

Figure 5.5 APP accumulation score in MK-801 treated animals: subgroup analysis

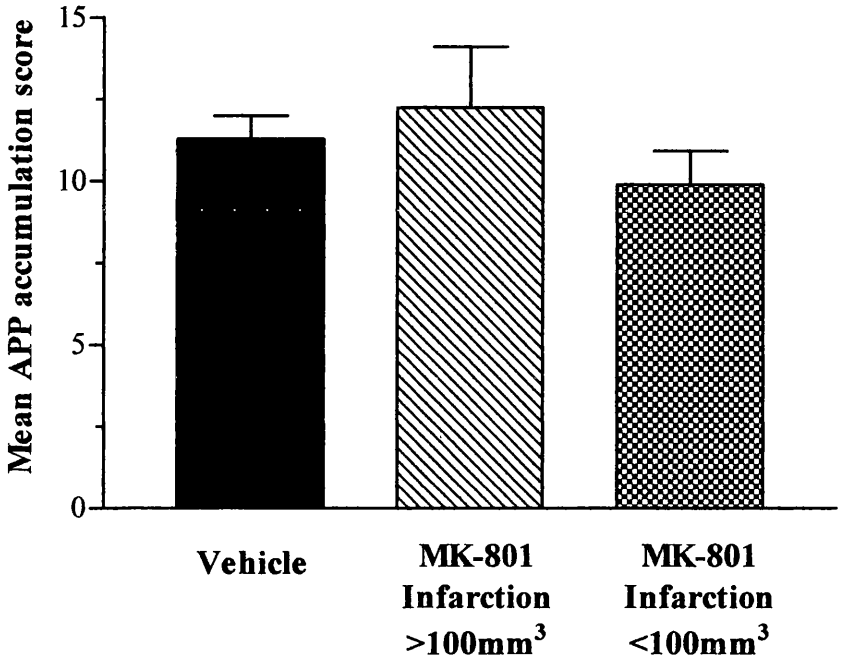

The mean APP score for the vehicle treated group and for the MK-801 treated animals was compared. The drug treated group was further broken down into those animals that had hemispheric infarction greater than $100mm^3$ and those with less than $100mm^3$. The drug treated animals with the smallest volumes of infarction did not have a significant decrease in mean APP accumulation score. Data are presented as mean $\pm$ SEM. Vehicle (n = 13); MK-801 with infarction > $100mm^3$ (n = 4) and MK-801 with hemispheric infarction < $100mm^3$ (n = 9).

5.4 RESULTS OF BW619C89 STUDY

5.4.1 APP immunocytochemistry after MCA occlusion

The APP immunoreactivity in the drug treated and vehicle animals had a similar distribution to that described for the MK-801 study (section 5.3.2). In both groups, the increased APP immunoreactivity was confined to a zone immediately adjacent to the boundary of ischaemia. In general, the APP immunoreactivity in both the vehicle and drug treated groups was not as intense as that seen in the rat material from the MK-801 study. The topography of APP accumulation for the two groups of animals is illustrated in Fig. 5.6. The distribution of APP in the two groups is similar.

5.4.2 Effect of BW619C89 on ischaemic damage

The administration of BW619C89 reduced the volume of ischaemic damage in the cerebral hemisphere by 16.1% compared to untreated rats and by 20.6% in the cerebral cortex compared to untreated rats following MCA occlusion (Table 5.5 and Table 5.6 and Fig. 5.7A). The volume of ischaemic damage in the caudate nucleus was minimally effected by treatment with BW619C89. In the cerebral hemisphere and cortex, BW619C89 reduced the area of ischaemic damage in every coronal plane studied (Fig. 5.8A).

5.4.3 Effect of BW619C89 on APP accumulation

In the non-ischaemic contralateral hemisphere, in all animals, APP immunoreactivity was faint. In contrast, in the ipsilateral ischaemic hemisphere, all animals had anatomically circumscribed zones of increased APP immunoreactivity in the subcortical white matter and in the myelinated fibre tracts permeating the striatum. However,

despite there being a reduction in the volume of infarction in the BW619C89 treated animals, BW619C89 failed to significantly reduce the APP score (Table 5.7 and Fig. 5.7B). The mean total APP score for the vehicle treated group was 12.2 $\pm$ 1.3 and the mean total APP score for the BW619C89 treated group was 11.3 $\pm$ 1.2 (Table 5.6).

The relationship of APP score and volume of infarction for the two groups of animals is illustrated in Fig. 5.9. In the vehicle animals there was not a clear linear relationship between APP accumulation score and volume of ischaemic damage as has been previously reported (Yam et al. 1997). BW619C89 showed no evidence of reducing the APP score. In addition to looking at the total APP score, the mean APP score was assessed at each of the eight coronal levels for the drug treated and vehicle groups. Again, there was no evidence of a reduction of APP score in the drug treated group. Subgroup analysis was performed whereby the drug treated group was separated into those with infarction greater than $100mm^3$ and those with infarction less than $100mm^3$ and APP score compared to vehicle treated animals. Even in the latter group, in which there was an overall reduction in volume of infarction of 32% compared to the vehicle group, there was not a statistically significant reduction in mean APP accumulation score in this subset compared to the vehicle group (Fig. 5.10). The data provided no evidence to suggest that BW619C89 reduces the APP score.

Figure 5.6

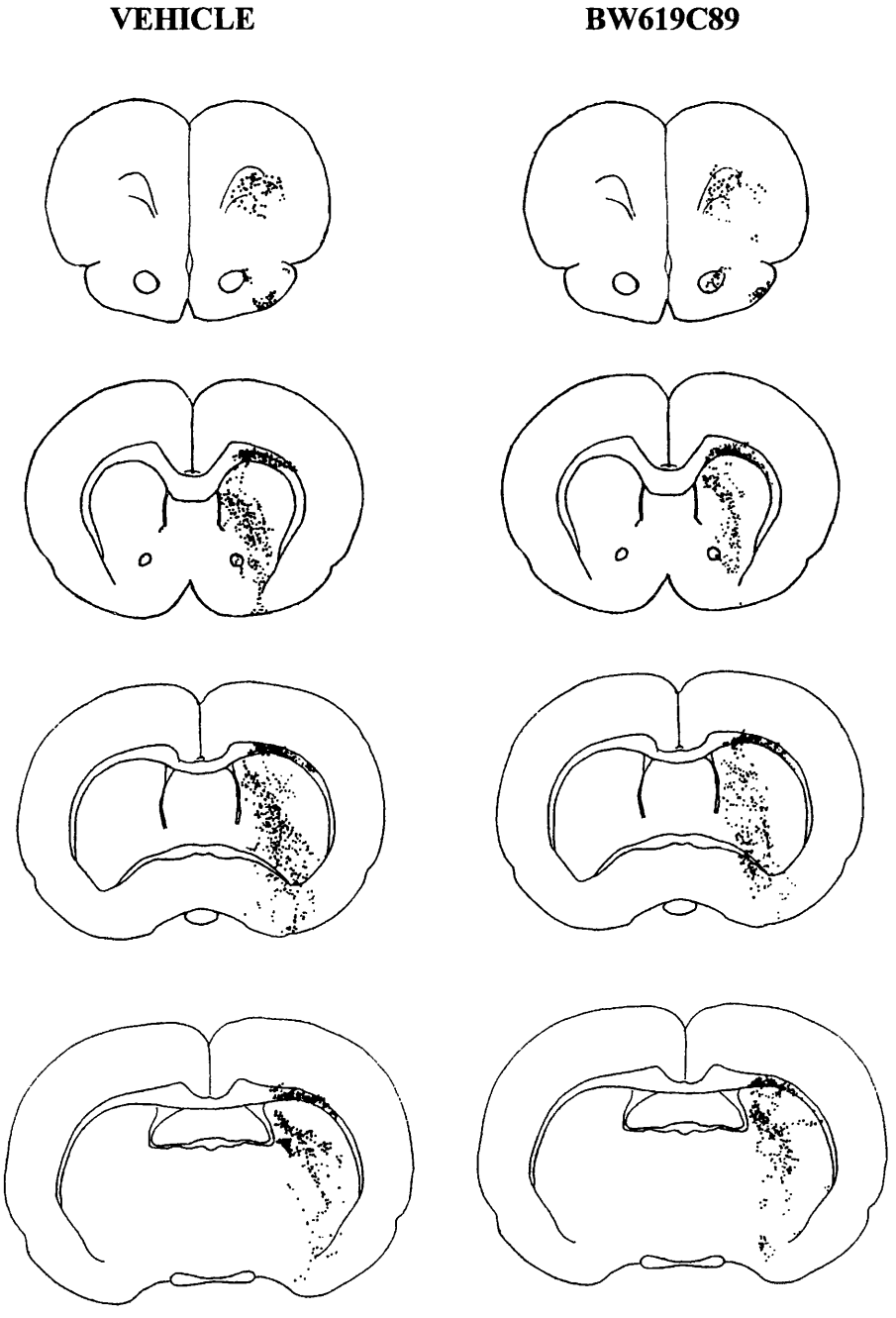

To gain an overall impression of distribution of increased APP immunoreactivity for the vehicle and drug treated animals, the increased APP immunoreactivity for the two groups was mapped onto line diagrams which were subsequently superimposed (represented as dots on ipsilateral hemisphere).

Figure 5.6 cont...

VEHICLE **BW619C89**

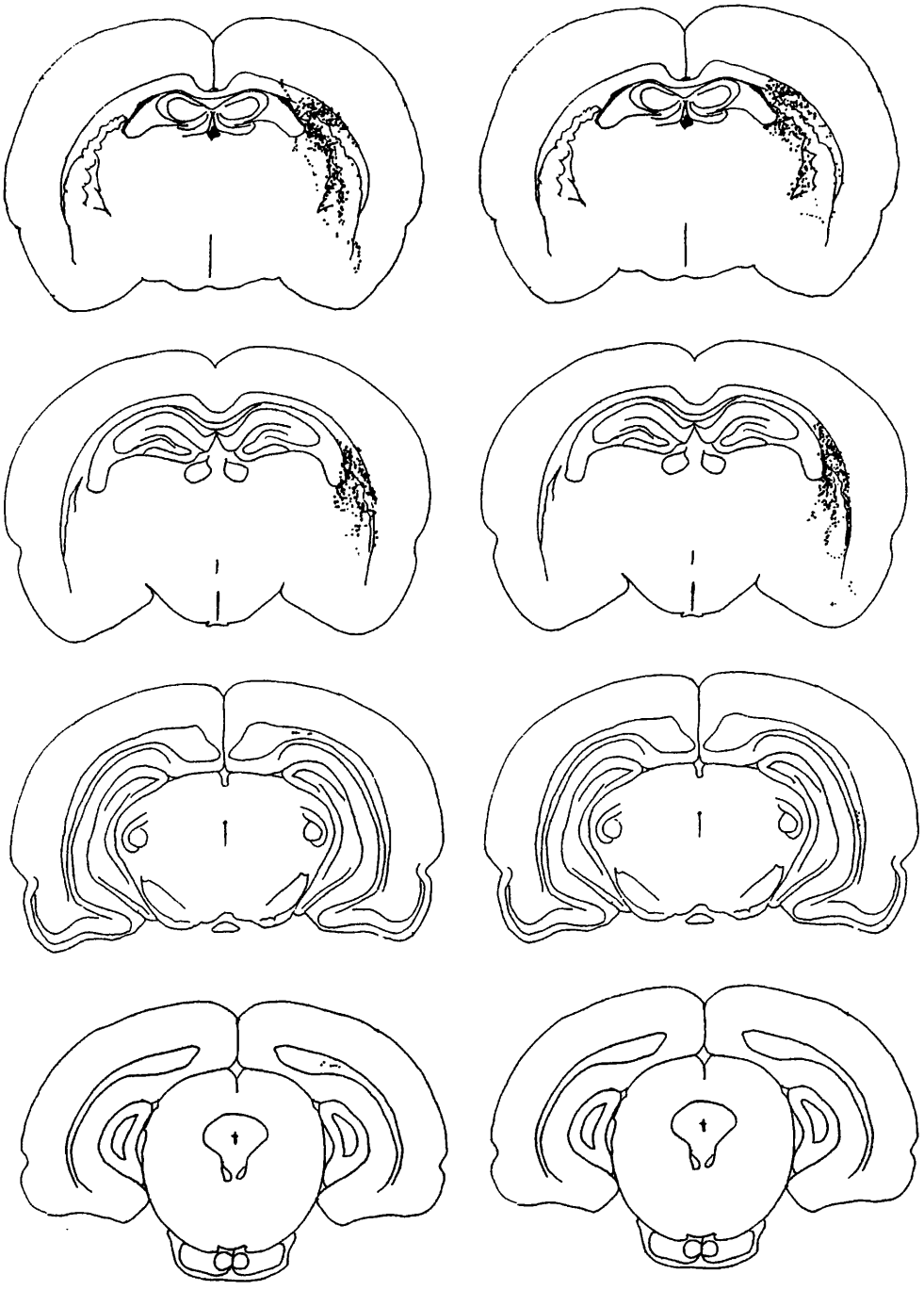

Table 5.5 Ischaemic damage following MCA occlusion: vehicle group

Hemisphere	level 1	level 2	level 3	level 4	level 5	level 6	level 7	level 8	Total (mm3)
1	4.2	14.8	19.4	22.2	21.5	15.9	3.4	0.7	135.8
2	4.6	16.6	19.2	19.5	18.5	8.9	1.8	1	120.7
3	5	16.7	17.7	20.4	21	11.8	2.2	2.2	129.6
4	5.2	18.8	23.8	16.7	15.8	7	1.5	0	121.5
5	6.2	17.8	16.8	18.6	18.2	6.2	1.2	0	114.5
6	8.1	19.1	21.3	19.7	21.3	9.8	8.6	3.8	151.5
7	4.6	11	16.5	14	10.7	3.9	0.9	0	82.9
8	6.8	18.2	23.1	22.3	18.5	15.2	7.2	5.2	158
9	7.1	15.5	15.5	17.8	18.4	3.9	2.3	0	107.8
10	9.1	16.6	17.7	17.4	20.3	5.2	2.6	1.1	121.6
Average	6.1	16.5	19.1	18.9	18.4	8.8	3.2	1.4	123.8
Std Dev	1.7	2.4	2.8	2.5	3.2	4.4	2.6	1.8	22.7
SEM	0.5	0.8	0.9	0.8	1.0	1.4	0.8	0.6	7.2
Cortex									
1	4.2	10.4	12.3	14.1	15.5	13.9	3.4	0.7	100.3
2	4.6	10.8	12.4	11.4	12.9	7.7	1.8	1	84.8
3	5	8.8	10.5	12.3	15.1	10.9	2.2	2.2	89.9
4	5.2	9.9	12.7	10.4	11.2	6	1.5	0	77.7
5	6.2	9	9.9	11.2	13	5	1.2	0	74.8
6	8.1	12.9	12.1	12.5	15.6	9	8.6	3.8	112.9
7	4.6	7.1	9.1	7.4	6.7	3.2	0.9	0	53.4
8	6.8	11.8	14.2	14.7	12.9	13.9	7.2	5.2	118.6
9	7.1	9.7	9.2	10	13.2	3.3	2.3	0	74.3
10	9.1	8.5	8.9	9.7	14.4	4.4	2.6	1.1	79.8
Average	6.1	9.9	11.1	11.4	13.1	7.7	3.2	1.4	86.7
Std Dev	1.7	1.7	1.8	2.2	2.6	4.1	2.6	1.8	19.5
SEM	0.5	0.5	0.6	0.7	0.8	1.3	0.8	0.6	6.2
Caudate									
1		3.4	5.8	6.9	3.7	1			20.8
2		4.2	5.5	7	3.6	0.8			21.1
3		6.7	6.3	6.8	3.8	0.7			24.3
4		7.8	9.9	5.4	3.5	0.7			27.3
5		7.6	6.2	6.6	4.1	0.8			25.3
6		4.3	8	6.2	3.7	0.7			22.9
7		3.3	6.8	6.6	3.8	0.7			21.2
8		4.3	7.6	6.1	3.7	0.9			22.6
9		4.7	5.6	6.8	4	0.6			21.7
10		7.5	8.4	6.7	4	0.8			27.4
Average		5.4	7.0	6.5	3.8	0.8			23.46
Std Dev		1.8	1.4	0.5	0.2	0.1			4.0
SEM		0.6	0.5	0.2	0.1	0.0			1.3

Table 5.5 cont... Ischaemic damage following MCA occlusion:

BW619C89 group

Hemisphere	level 1	level 2	level 3	level 4	level 5	level 6	level 7	level 8	Total (mm3)
1	3.1	11.1	18.3	16.4	6.1	1.4	0.5	0	76.2
2	5.5	17.3	16.5	15.6	11.7	2.1	0	0	93.9
3	2.7	14.7	17.7	20.5	16.7	11.7	2.5	0.8	116
4	2.6	10.6	14.5	16.7	16.3	2.9	0	0	82.5
5	4.1	17.6	21.6	19.8	20.5	14.1	2.6	0	135.1
6	2.9	13.3	12.3	14.6	13.4	7.9	1	0	87.8
7	6	21.1	21.6	20	19.9	12.6	8.9	4.6	156
8	4.5	12.6	18.1	17.3	17.5	10.4	1.9	2.3	113.1
9	5.5	13.7	18.1	19.9	18.7	9.4	3.2	0	117.7
10	3	11	16	15.9	10.8	2.4	2.4	1.9	84
11	0.6	13.5	14.2	14.9	13.2	3.5	1.2	0	80.7
Average	3.7	14.2	17.2	17.4	15.0	7.1	2.2	0.9	103.9
Std Dev	1.6	3.3	2.9	2.2	4.4	4.8	2.5	1.5	25.7
SEM	0.5	1.0	0.9	0.7	1.3	1.4	0.7	0.5	7.8
Cortex									
1	3.1	6.5	6.7	8.8	1.8	0.5	0.5	0	37.8
2	5.5	8.5	8.6	8.1	7.4	1.3	0	0	54.1
3	2.7	9.4	10.3	12.5	11.8	10.5	2.5	0.8	81.2
4	2.6	7.9	8.4	8.9	10.9	1.8	0	0	53.8
5	4.1	11	13.2	11.7	15.2	13	2.6	0	96.2
6	2.9	6.9	4.9	7.6	8.7	6.7	1	0	52.3
7	6	12.2	11.5	12.6	14.7	11.1	8.9	4.6	111.1
8	4.5	8.8	11.3	10	12.4	9.2	1.9	2.3	81.9
9	5.5	8.9	10.2	11.8	12.7	8.3	3.2	0	81.7
10	3	7	9.4	8.8	7.2	2.4	2.4	1.9	56.7
11	0.6	8.5	8	7.8	8.6	2.8	1.2	0	50
Average	3.7	8.7	9.3	9.9	10.1	6.1	2.2	0.9	68.8
Std Dev	1.6	1.7	2.3	1.9	3.9	4.5	2.5	1.5	22.8
SEM	0.5	0.5	0.7	0.6	1.2	1.4	0.7	0.5	6.9
Caudate									
1		4.1	11	6.8	3.7	0.8			26.4
2		7.2	7.2	7	3.7	0.7			25.8
3		3.9	5.4	6.6	3.4	0.7			20
4		2	5	6.6	3.6	0.7			17.9
5		4.7	7.3	6.8	3.3	0.7			22.8
6		5.4	6.9	6.6	3.9	0.7			23.5
7		7	9.1	6	3.6	0.8			26.5
8		3.3	6	6.5	3.9	0.8			20.5
9		3.7	7	6.7	4	0.7			22.1
10		3.6	5.8	6.5	3.4	0			19.3
11		4.3	5.8	6.8	3.8	0.6			21.3
Average		4.5	7.0	6.6	3.7	0.7			22.4
Std Dev		1.6	1.8	0.3	0.2	0.2			2.9
SEM		0.5	0.5	0.1	0.1	0.1			0.9

Table 5.6 Influence of BW619C89 upon the volume of ischaemic damage and APP score after MCA occlusion

	Volume of ischaemic damage (mm^3)	
	Vehicle	BW619C89
Cerebral hemisphere	123.8 ± 7.2	103.9 ± 7.8
Cerebral cortex	86.7 ± 6.2	68.8 ± 6.9
Caudate nucleus	23.5 ± 1.3	22.4 ± 0.9
APP score	12.2 ± 1.3	11.3 ± 1.2

Data are presented as means ± SEM. Vehicle group (n = 10); BW619C89 treated group (n = 11).

Table 5.7 APP score for each coronal level in vehicle and BW6119C89 treated animals

Coronal level	1	2	3	4	5	6	7	8	Total
Vehicle									
1	2	1	2	2	1	2	0	2	12
2	0	2	2	2	2	2	0	0	10
3	2	1	1	1	0	0	1	0	6
4	1	2	2	1	1	1	0	0	8
5	1	3	3	3	3	2	0	0	15
6	1	1	1	1	1	1	2	1	9
7	2	3	2	2	3	2	0	1	15
8	3	3	3	3	2	3	1	1	19
9	3	3	2	3	2	1	0	0	14
10	1	2	3	2	2	2	1	1	14
Average	1.6	2.1	2.1	2	1.7	1.6	0.5	0.6	12.2
Std dev	1.0	0.9	0.7	0.8	0.9	0.8	0.7	0.7	3.9
SEM	0.3	0.3	0.2	0.3	0.3	0.3	0.2	0.2	1.3
BW619C89									
1	1	1	2	3	1	1	1	0	10
2	3	1	1	2	1	1	0	0	9
3	2	1	1	0	0	0	0	0	4
4	1	1	2	2	1	2	0	0	9
5	1	2	2	2	2	2	0	0	11
6	1	2	2	2	2	1	0	0	10
7	2	1	1	3	2	1	2	1	13
8	2	2	3	2	2	1	0	0	12
9	1	2	2	2	2	2	0	0	11
10	2	3	2	3	3	3	1	1	18
11	1	3	3	3	3	3	1	0	17
Average	1.5	1.7	1.9	2.2	1.7	1.5	0.5	0.2	11.3
Std dev	0.7	0.8	0.7	0.9	0.9	0.9	0.7	0.4	3.8
SEM	0.2	0.2	0.2	0.3	0.3	0.3	0.2	0.1	1.2

Semi-quantitative score allocated for amount of APP at each coronal level for the 26 animals. 0, no APP; 1, some APP; 2, moderate amount of APP; 3, lots of APP.

Figure 5.7 Effect of BW619C89 on total volume of ischaemic damage and total APP score following MCA occlusion

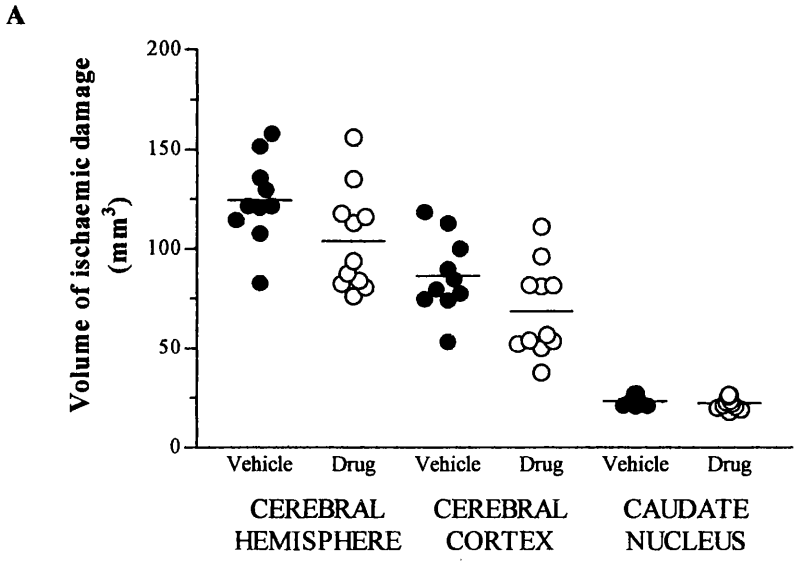

Volume of ischaemic brain damage in the cerebral hemisphere, cerebral cortex and caudate nucleus in vehicle treated control rats and in rats treated with BW619C89. Each point represents data from a single animal. The mean value for the group is indicated by a solid horizontal line.

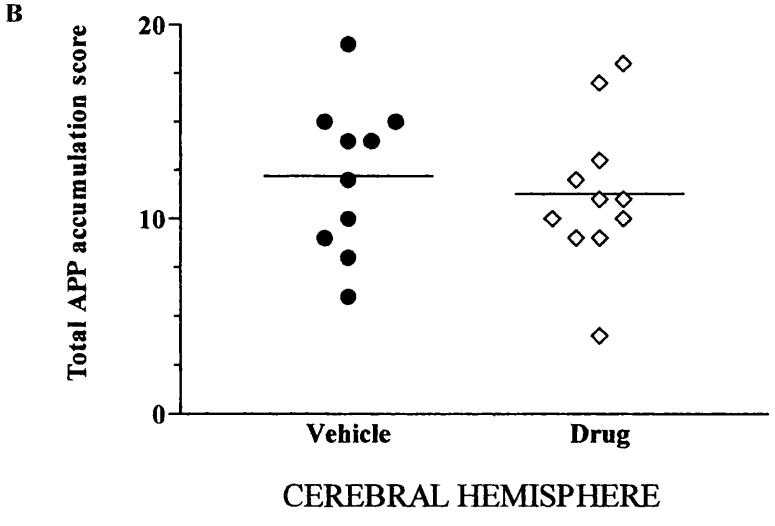

Total APP accumulation score in the cerebral hemisphere in vehicle treated control rats and in rats treated with MK-801 after MCA occlusion. Each point represents data from a single animal. The mean value for the group is indicated by a solid horizontal line.

Figure 5.8 Effect of BW619C89 on area of ischaemic damage and mean APP score at eight defined coronal levels following MCA occlusion

A

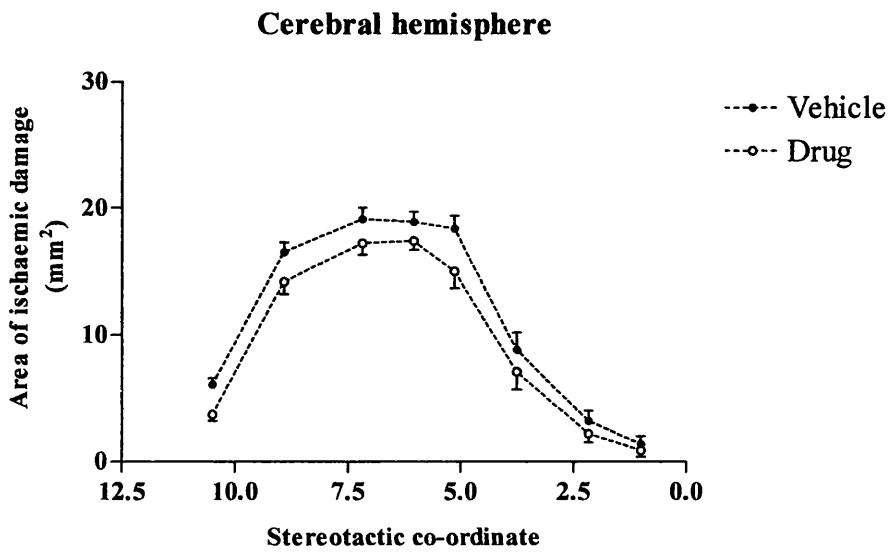

The effect of BW619C89, administered following MCA occlusion, upon the area of ischaemic damage in the cerebral hemisphere at 8 defined coronal planes. Data are presented as mean ± SEM. Vehicle (n = 10); BW619C89 (n = 11).

B

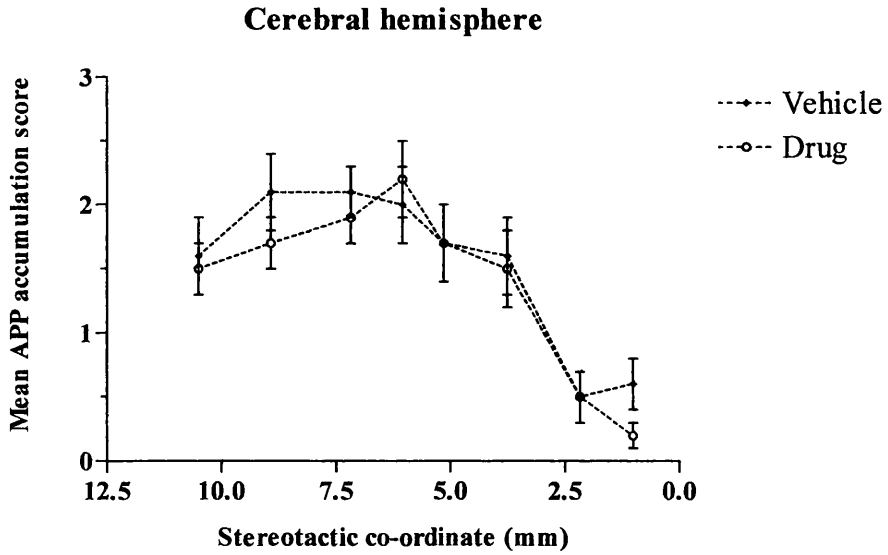

The effect of BW619C89 upon the mean APP score in the cerebral hemisphere at 8 defined coronal planes. Data are presented as mean ± SEM. Vehicle (n = 10); BW619C89 (n = 11).

Figure 5.9 Volume of ischaemic damage and APP accumulation score: BW619C89

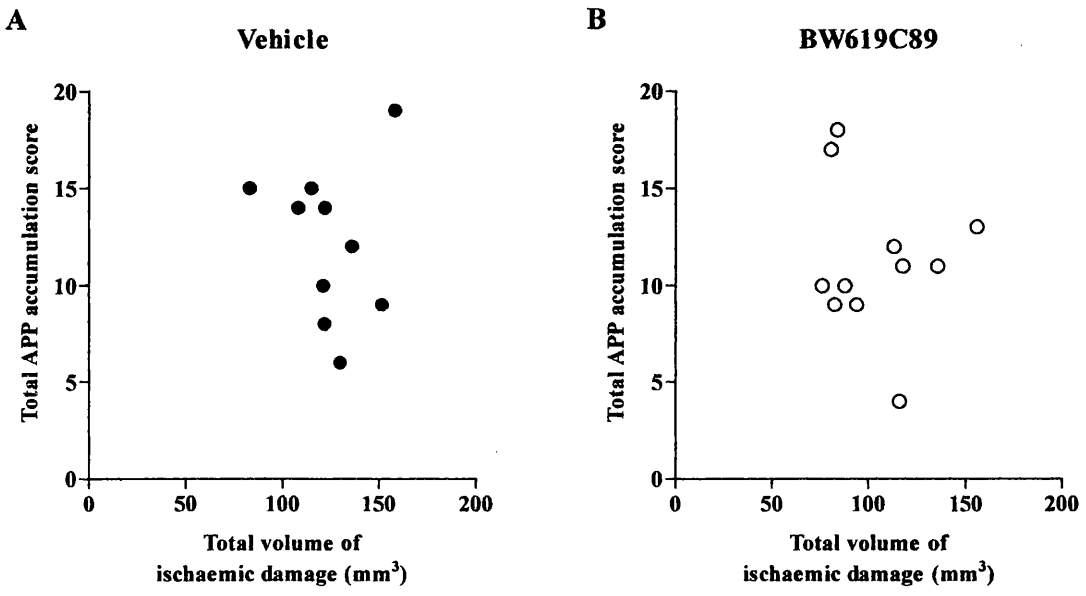

The volume of ischaemic damage in the cerebral hemisphere was compared to total accumulation of APP for each animal in A) vehicle treated control animals and B) BW619C89 treated animals. The total APP accumulation was the score sum for the eight coronal levels. Each point represents data from a single animal.

Figure 5.10 APP accumulation score in BW619C89 treated animals: subgroup analysis

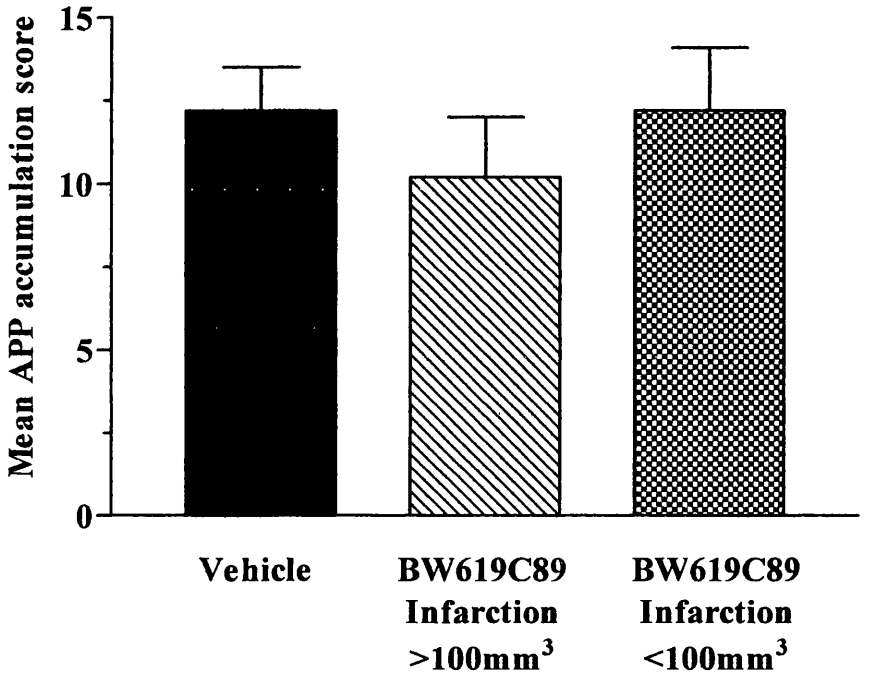

The mean APP score for the vehicle treated group and for the BW619C89 treated animals was compared. The drug treated group was further broken down into those animals that had hemispheric infarction greater than $100mm^3$ and those with less than $100mm^3$. The drug treated animals with the smallest volumes of infarction did not have a significant decrease in mean APP accumulation score. Data are presented as mean $\pm$ SEM. Vehicle (n = 10); BW619C89 with infarction > $100mm^3$ (n = 5) and BW619C89 with hemispheric infarction < $100mm^3$ (n = 6).

5.5 DISCUSSION

The demonstration of axonal injury requires special staining techniques. APP has previously been shown to be a good marker of axonal injury and in Chapter 4, a method of semi-quantitative analysis of APP was described. This technique was utilised to determine whether MK-801 or BW619C89 attenuates the axonal alteration previously described following MCA occlusion.

In the MK-801 study the reduction in cerebral infarction in the drug treated group was not as large as has been previously reported. Unilateral, permanent occlusion of the MCA in rats has gained increasing acceptance in recent years as a model of ischaemic stroke and has been widely used to assess the efficacy and potency of various drugs. Several groups have found neuroprotection with MK-801 (Gill et al. 1991; Park et al. 1988b), but others have failed to do so (Dirnagl et al. 1990). Although there may be experimental differences between laboratories, the discrepant findings of non-competitive NMDA antagonists may relate to variability in the extent of cerebral infarction after MCA occlusion in different strains of rat (Duverger and MacKenzie, 1988) or from slight differences in individual surgical techniques. In this regard, even in untreated control rats, the extent and variability of infarct size depends on the rat strain (Duverger and MacKenzie, 1988). Furthermore, the extent of total infarct volume reduction elicited by three drugs, including MK-801 is significantly varied among rat strains (Sauter and Rudin, 1995). A plausible reason for the strain-dependant infarct size in untreated control rats has been traced to the vascular anatomy, as the varying arterial branching, number of anastomoses and collaterals in different rat strains seems to correlate with the final size of infarction (Coyle and Heistad, 1991) and this is supported by cerebral blood flow studies (Carswell et al., in press). Previous studies investigating

the effect of MK-801 upon the amount of ischaemic brain damage following MCA occlusion have tended to use Sprague Dawley rats. However, due to the smaller and more variable lesions of this rat species, Fischer 344 rats were used in the present study. The possibility that Fischer rats have less salvageable tissue following MCA occlusion i.e. more core than penumbra, thus resulting in only a small amount of tissue salvage following MK-801 treatment, cannot be discounted. It must also be considered whether the dose of MK-801 was adequate. The dose selected for this study has previously shown to give a highly significant reduction in volume of ischaemic brain damage in the cerebral cortex and hemisphere (Gill et al. 1991). Despite this, it is not possible to say with certainty that a steady state plasma level of MK-801, previously shown to be neuroprotective, was achieved since plasma samples were not collected for measurement of MK-801.

MK-801 failed to significantly reduce the APP score. Since the reduction in infarct volume was less than might have been expected, the MK-801 treated animals were divided into two groups for further subgroup analysis of APP accumulation; those with volumes of infarction greater than $100mm^3$ and those with less than $100mm^3$. Even in the group of animals with volumes of infarction less than $100mm^3$, significantly lower than that of the vehicle group, there was only a marginal reduction in APP accumulation score. This would suggest that the NMDA antagonist, MK-801, fails to protect axons following focal cerebral ischaemia in the rat. Perhaps this is not a surprising finding. Since NMDA receptors are thought to be active mainly in the grey matter (Jones and Baughman, 1991), is it likely to exert its protective effect on axons following cerebral ischaemia?

In contrast, the contribution of sodium and calcium ion channels to the mechanisms leading to anoxic white matter injury have been well characterised by

Waxman and co-workers in the optic nerve (see section 1.5.3). BW619C89, which acts at such sites, resulted in a significant reduction in neuronal necrosis. Despite this, the drug did not appear to cause significant protection of axons as assessed by the difference in APP accumulation score between the drug treated and vehicle group. However, some difficulties in allocating an APP score to the sections were encountered. The reasons for this were twofold. Firstly, the sections had marked oedema, and although this is a consistent feature of the MCA occlusion stroke model (Sydserff et al. 1996), it was quite pronounced in this particular rat material. The oedema may be an explanation for the relatively small amount of APP immunoreactivity present, even in the vehicle treated animals, compared to other sections analysed throughout this thesis. The oedema may also have been attributed to the fact that the rats in this study survived for 24 hours rather than 4 hours as in the MK-801 study. This survival time was selected because the relationship of volume of infarction to APP score at 4 hours in the MK-801 study (for both the vehicle and drug treated animals), was poor compared to that seen following 24 hours as described in Chapter 4 (Fig. 4.7). Despite this survival time, there was not a clear relationship between volume of ischaemia and APP accumulation, thus further compounding the difficulties in assessing the putative protection of axons in the BW619C89 treated group. Perhaps this latter problem could also have been attributed to the oedema. The possibility that BW619C89 protects axons following MCA occlusion in the rat cannot be discounted. However, from this study no firm conclusions can be drawn.

Although a method of semi-quantitative analysis of APP accumulation had been developed, there were some difficulties in the practical application of the method for the assessment of axonal injury and protection following drug intervention. Although not all of the problems encountered in the studies described were directly related to the method

of quantification, some were. One concern was that the semi-quantitative analysis was not sensitive enough to measure small changes in axonal injury following therapy. This may in part be due to the small variance in lesion size between the two groups making separation of APP scores between vehicle and drug treated animals more difficult. Furthermore, the lesion sizes within groups was within a narrow range making it more difficult to assess the association of APP score with infarction size (Fig. 5.4 and Fig. 5.9).

Perhaps a more refined method for quantification of APP may be required which is more robust and, at the same time, more sensitive to small changes in APP accumulation. Methods by which the sensitivity could be increased may be achieved by assessing a greater number of coronal levels rather than just the eight that were used in these studies. Alternatively, the experiment could be undertaken in a species in which there is more white matter relative to that of grey matter such that protection of axons can be more easily visualised. To look at the association of APP score with infarction, a wide range of infarction values would also be desirable. To this effect, experiments in the following chapter describe analysis of axonal injury in the cat using modified methods of quantification to overcome the limitations encountered in these rat studies.

CHAPTER 6

QUANTITATIVE ANALYSIS OF APP FOLLOWING DRUG INTERVENTION IN THE CAT

6.1 INTRODUCTION

APP was demonstrated to be a viable marker of axonal injury in the rat (Chapter 4). However, when used to assess the effects of drug intervention, it proved difficult to see either a shift in the topography of increased APP immunoreactivity in relation to the boundary of infarction, or a significant change in the APP score. Indeed, this may simply be because the neuroprotective drugs, MK-801 and BW619C89, are not saving white matter following an ischaemic injury. In the rat brain the volume of white matter is relatively small compared to the volume of grey matter, therefore the possibility that neuroprotective drugs such as MK-801, are saving white matter but this protection is unable to be detected in the rat brain, must be considered. The cat brain is more comparable to that in man in that it is gyrencephalic and the volume of white matter is relatively large. Unlike in the rat, the boundary between viable and necrotic neurones after focal ischaemia in the cat can be shifted several centimetres across the cortical surface (Fig. 6.1). Since there is also a larger amount of underlying white matter within the salvaged zone compared to that in the rat, this theoretically should allow easier evaluation of white matter protection. Furthermore, by assessing a larger number of coronal levels, and by refining the method of APP quantification, limitations encountered in the rat tissue could potentially be overcome. It is feasible that with such refinements there would be increased sensitivity of APP as marker of axonal injury

following MCA occlusion. Conceivably, a shift in the boundary and a change in the quantity of APP accumulation could be more readily appreciated following neuroprotection in the cat than the rat.

The experiment undertaken in the cat had three inter-related purposes. Firstly, it was necessary to establish whether increased APP immunoreactivity was a consistent outcome following focal cerebral ischaemia; secondly, to establish if there is a relationship between the quantity of APP immunoreactivity and volume of infarction. And finally, once the first two questions have been established, to use APP as a marker of axonal injury to ascertain whether the classic NMDA antagonist, MK-801, protects white matter as well as grey matter following focal cerebral ischaemia in the cat.

Figure 6.1 Tissue salvage following NMDA receptor blockade in the cat and rat

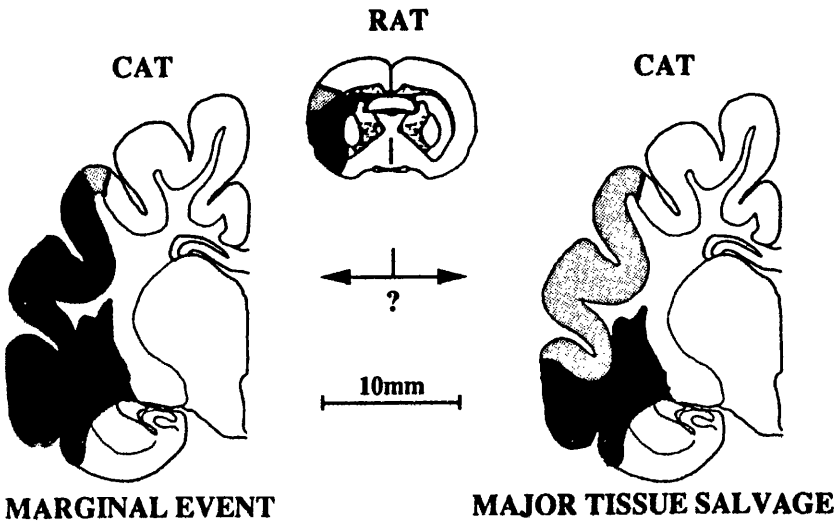

Neuronal protection with NMDA receptor blockade after MCA occlusion has been investigated in both rats and cats. Following MK-801 administration, the stippled area is the salvaged zone derived from median animals and the solid area is never salvaged (Modified from Ozyurt et al, 1988). Because of the physical size, mechanisms in the salvaged cortex and underlying white matter can be more readily evaluated in the cat than the rat.

6.2 METHOD

6.2.1 Anaesthesia, MCA occlusion and tissue processing

Anaesthesia was induced in 16 cats (section 2.2.2) and MCA occlusion performed as previously described (section 2.2.3). MCA occlusion was performed by Mr. Laurence Dunn, Consultant Neurosurgeon, Southern General Hospital. The cats were randomly divided into a vehicle treated control group (n=10) and a drug treated group (n=6). The vehicle treated control group of cats received a one ml intravenous injection of saline 15 minutes prior to MCA occlsion and then an intravenous saline infusion at a rate of 0.15ml/min for the duration of the experiment. The drug treated group received a bolus of MK-801 (0.5 mg/kg) which was administered by intravenous injection 15 minutes before MCA occlusion and then infused at 0.14 mg/kg/hour after completion of the bolus injection (0.15ml/min). Although there has been no implicit investigation of neuroprotection with this dose, the bolus and infusion concentrations were selected to achieve a steady state target plasma concentration of 300nM. This dosing regime was based on previous experiments which have provided the information on the plasma half life of MK-801 (see below) , knowledge of loading dose requirements (Mayer et al. 1975) and previous experiments stating plasma concentrations of MK-801 that have resulted in neuroprotection (Gill et al. 1991). The half life of plasma MK-801 was calculated from assays taken in 9 separate experiments where intravenous MK-801 had been administered at a concentration of 5mg/kg (Table 6.1 and Fig. 6.2) (Ozyurt et al. 1988). MK-801 was prepared as described below.

Drug preparation

Bolus: Weigh (cat weight divided by 2) mg of MK-801

Dissolve in 5 ml saline

Inject over 2 mins

Infusion: Weigh (1.94 x cat weight) mg

Dissolve in 125 ml saline

Infuse at 0.15 ml/min

Basis of calculation:

$T_{1/2}$ cat of 2.5 hours (Ozyurt et al. 1988)

Loading dose = 1.4 x $T_{1/2}$ x maintenance dose (Mayer et al. 1975)

Following MCA occlusion, anaesthesia was maintained for 6 h and physiological parameters were monitored as previously described (section 2.2.2) (Table 6.2). The animals were killed by transcardiac perfusion with FAM and brain processed (section 2.2.3). The sections were stained by haematoxylin and eosin and a method combining cresyl violet and Luxol fast blue and areas of infarction transcribed onto scale diagrams at 16 predetermined coronal planes (Fig. 2.6) and volume of ischaemic damage subsequently calculated (section 2.5.2).

Sections adjacent to those used for mapping areas of infarction were prepared for immunocytochemistry so that the topography of increased APP immunoreactivity could be compared to that of infarction (section 2.3.1). The tissue sections were microwaved to enhance antigenicity (section 2.3.3) and APP antibody used at a concentration of 1:300.

Table 6.1 Plasma MK-801 concentration analysis

MK-801 cat studies: dosing at 5mg/kg. Samples were assayed from 9 separate experiments (Ozyurt et al. 1988).

	Time after MK-801 administration (hours)					
	1	2	3	4	5	6
Experiment no.	Plasma MK-801 concentration (μm)					
1	2.2	1.5	1.0	0.9	0.8	0.5
2	2.6	2.0	1.6	1.3	1.2	0.9
3	2.1	1.2	1.0	0.9	0.8	0.6
4	2.1	1.4	1.2	0.9	2.6	0.8
5	2.5	2.1	1.6	1.8	1.3	1.1
6	4.5	1.8	1.8	1.3	1.0	1.0
7	3.5	2.2	1.4	1.1	1.0	0.9
8	3.5	4.0	1.8		1.4	1.3
9	2.0	1.3	1.3	1.0	0.9	0.7
Average	2.78	1.94	1.40	1.13	1.22	0.86
Std dev	0.86	0.85	0.32	0.32	0.57	0.25
SEM	0.29	0.28	0.11	0.11	0.19	0.08

Figure 6.2 Plasma MK-801 concentration analysis

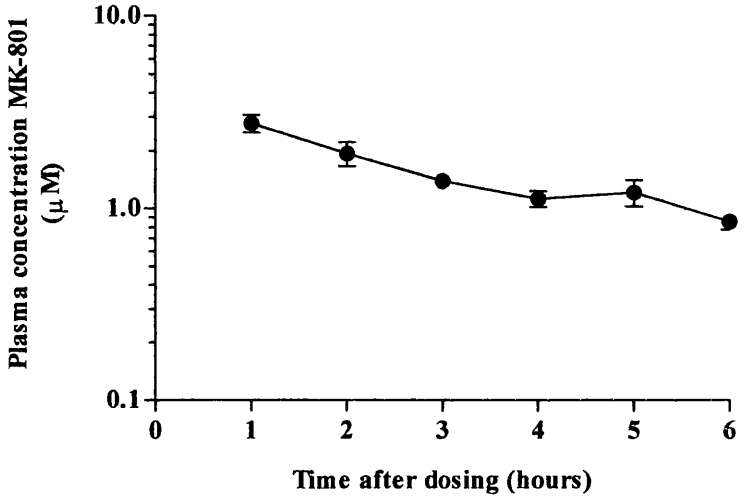

Mean plasma MK-801 concentration following intravenous administration at 5mg/kg, 30 minutes prior to MCA occlusion (Ozyurt et al, 1988). Data are presented as mean ± SEM on a log scale. n = 9 at all time points except at 5 hours, where n = 8. The plasma half life of MK-801 is approximately 2.5 hours.

Table 6.2 Physiological variables prior to and following MCA occlusion in the cat

	MABP (mmHg)	pH	$PaCO_2$ (mmHg)	PaO_2 (mmHg)	Rectal Temp. (°C)
Vehicle					
pre-MCAO	97 ± 4	7.46 ± 0.01	27.7 ± 2.0	203 ± 11	36.2 ± 0.2
MCAO	102 ± 3	7.46 ± 0.01	27.7 ± 1.4	204 ± 10	36.9 ± 0.2
15 min	97 ± 3	7.45 ± 0.02	26.4 ± 7.7	197 ± 10	36.5 ± 0.1
30 min	98 ± 3	7.44 ± 0.01	28.7 ± 1.3	194 ± 10	36.5 ± 0.2
1 h	102 ± 4	7.44 ± 0.01	28.3 ± 1.0	192 ± 7	36.6 ± 0.1
2 h	96 ± 3	7.44 ± 0.01	30.2 ± 1.0	204 ± 7	36.9 ± 0.1
3 h	98 ± 4	7.43 ± 0.02	32.2 ± 0.8	202 ± 9	36.8 ± 0.1
4 h	100 ± 3	7.42 ± 0.02	30.7 ± 0.8	195 ± 8	36.9 ± 0.1
5 h	99 ± 3	7.41 ± 0.02	29.8 ± 1.0	182 ± 12	36.7 ± 0.1
6h	95 ± 4	7.42 ± 0.03	30.6 ± 1.4	190 ± 10	36.6 ± 0.1
MK-801					
pre-MCAO	111 ± 11	7.43 ± 0.03	32.4 ± 1.5	191 ± 3	36.4 ± 0.2
MCAO	103 ± 7	7.45 ± 0.02	31.6 ± 1.0	194 ± 1	36.7 ± 0.1
15 min	97 ± 8	7.47 ± 0.03	31.7 ± 1.0	189 ± 2	36.8 ± 0.1
30 min	100 ± 4	7.47 ± 0.02	29.2 ± 0.6	181 ± 12	36.8 ± 0.1
1 h	107 ± 6	7.47 ± 0.02	28.9 ± 0.8	189 ± 4	36.8 ± 0.2
2 h	107 ± 4	7.48 ± 0.02	28.3 ± 1.3	184 ± 8	36.7 ± 0.0
3 h	111 ± 1	7.47 ± 0.02	27.8 ± 1.4	190 ± 5	36.7 ± 0.1
4 h	102 ± 2	7.46 ± 0.01	28.8 ± 1.0	181 ± 9	36.8 ± 0.1
5 h	101 ± 3	7.46 ± 0.01	29.6 ± 1.4	186 ± 6	36.7 ± 0.0
6 h	96 ± 2	7.45 ± 0.01	28.0 ± 1.1	191 ± 2	36.7 ± 0.1

MABP: mean arterial blood pressure; Rectal temp.: rectal temperature. Data are presented as mean ± S.E.M. Vehicle, n = 10; MK-801, n = 6.

6.2.2 Topographical analysis of APP immunoreactivity

Since diaminobenzidine was used as the chromagen in the immunocytochemistry, the increase in APP immunoreactivity within the white matter was brown (Fig. 6.3). An accurate determination of the topography in increased APP immunoreactivity for the two groups of cats was established using the method previously described for the rat (see section 4.2.4). In brief, images from 16 equivalent coronal sections from each animal, at defined coronal planes, were viewed on a monitor, digitised and printed. The images produced showed the increased APP immunoreactivity. The sections were also viewed using a conventional light microscope at x 2.5 magnification. Any increased APP immunoreactivity visible on the slides but which was not visible on the scanned images was manually drawn onto the image. This procedure was repeated for each animal at each coronal level. In this way, an accurate determination of the overall topography of increased APP immunoreactivity for the two groups of animals could be established by tracing and superimposing the increased APP immunoreactivity at each coronal level for the two groups of animals onto a single line diagram which was drawn on an acetate sheet. The superimposition of increased APP immunoreactivity for the animals was repeated at each of the 16 coronal levels (Fig. 6.4).

Figure 6.3 APP immunoreactivity in the cat

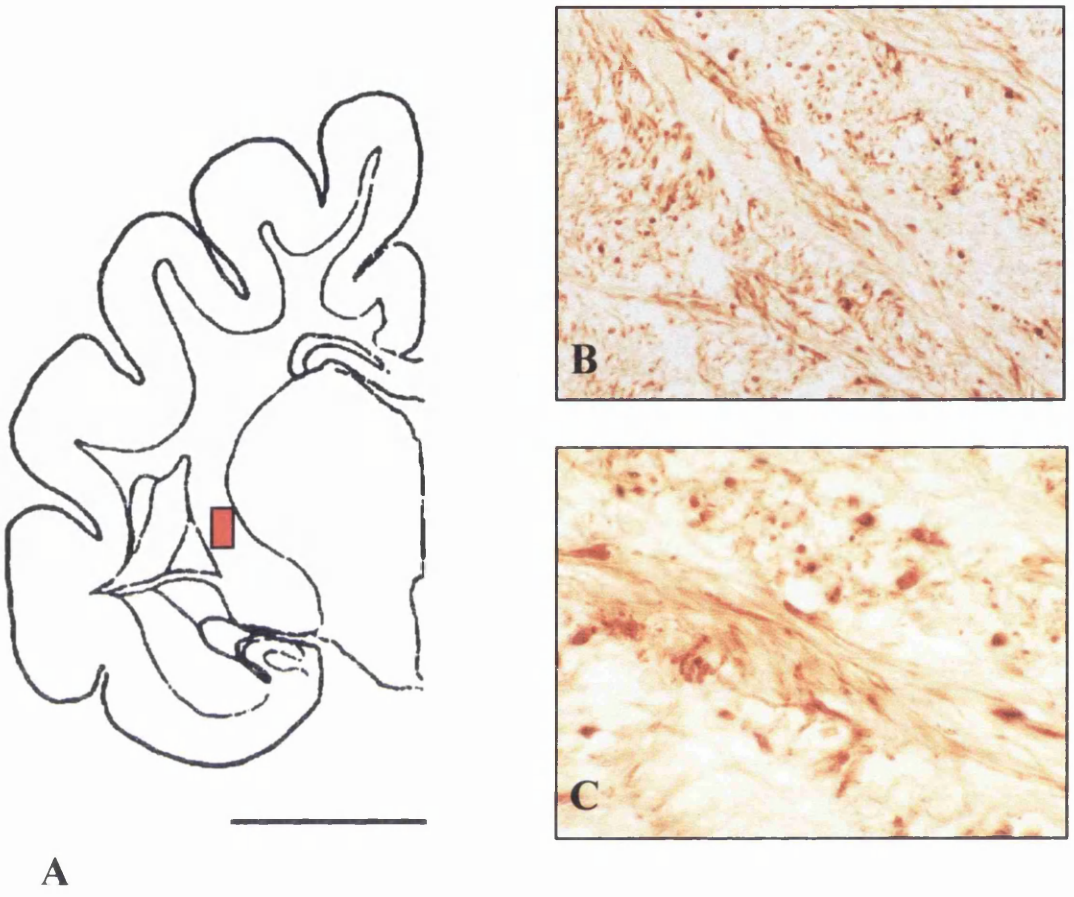

Typical example of increased APP immunoreactivity in the cat following MCA occlusion. A) Line diagram of coronal level 6 showing the location of the following micrographs, (scale bar approximately 0.5cm). B) Increase in APP immunoreactivity in white matter tracts x400 and C) x1,000.

Figure 6.4 Topography of APP immunoreactivity: vehicle group

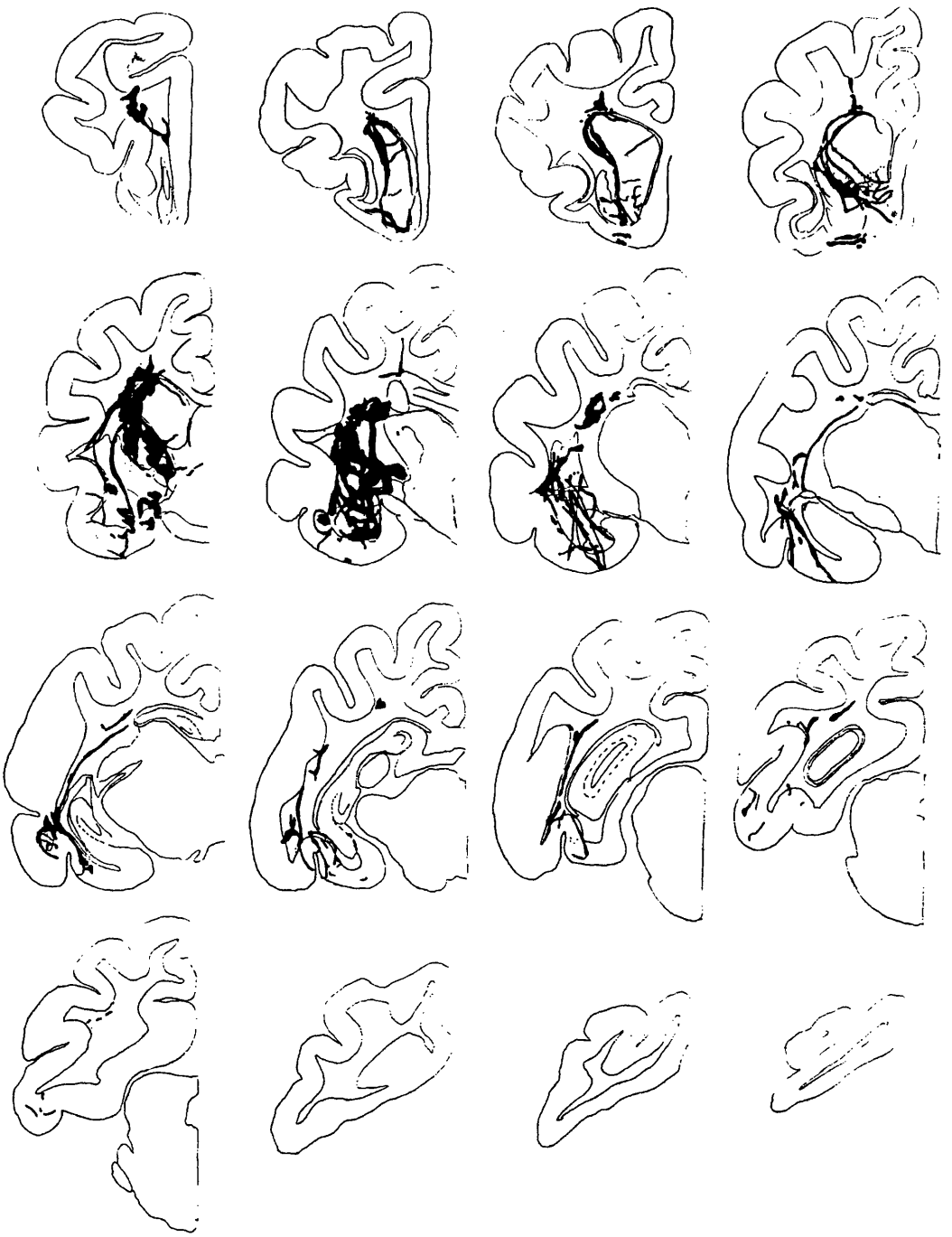

Topography of the APP immunoreactivity for the 16 preselected coronal levels in the cats after MCA occlusion (vehicle, n = 10; MK-801, n = 6). To gain an overall impression of distribution of increased APP immunoreactivity for the two groups of cats, the APP was mapped onto line diagrams which were subsequently superimposed (represented as dots).

Figure 6.4 cont... Topography of APP immunoreactivity: MK-801 group

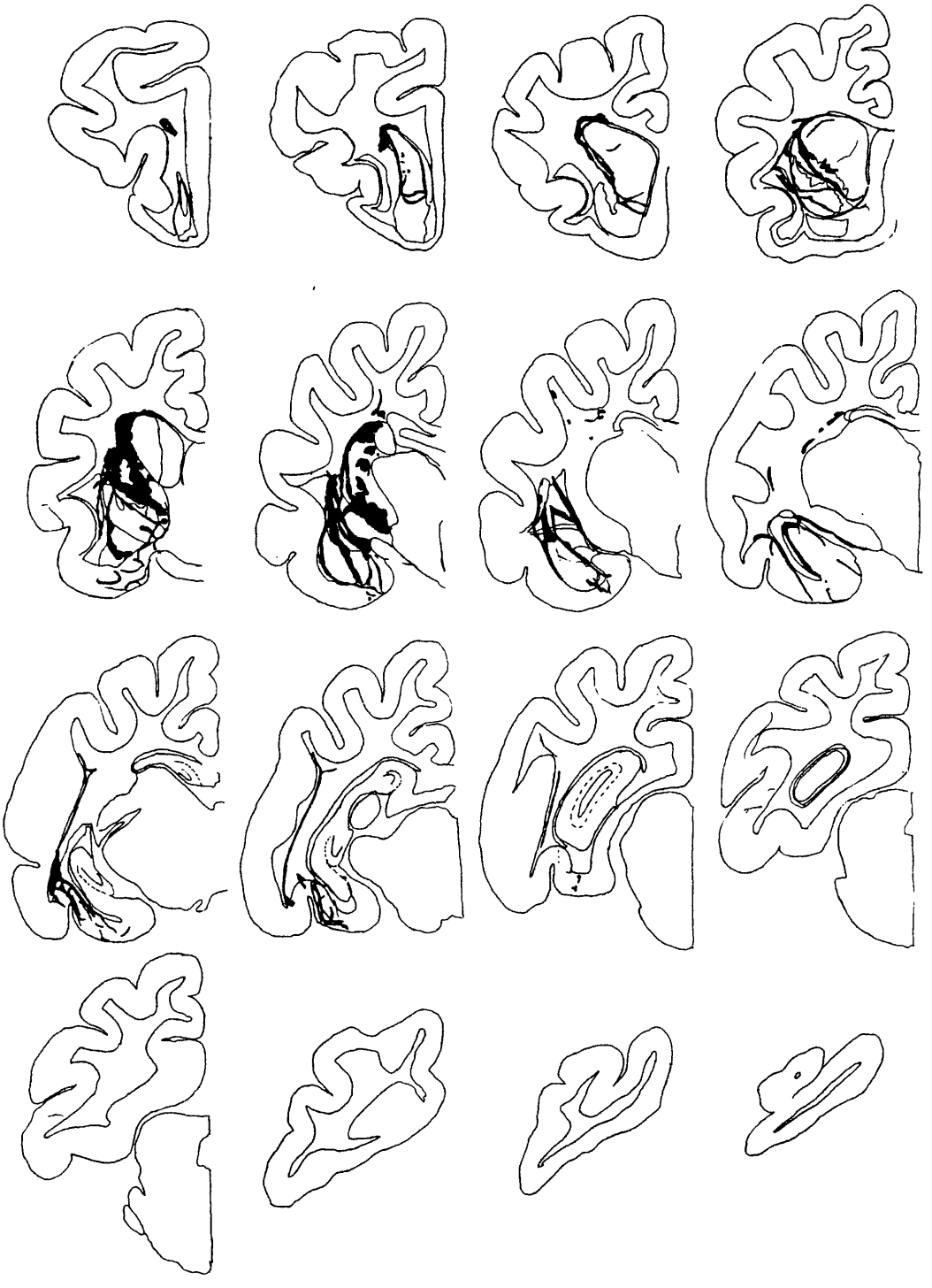

6.2.3 Quantification of APP immunoreactivity

Semi-quantitative analysis

In order to assess the relationship of APP immunoreactivity and volume of infarction, each coronal section was analysed for APP by light microscopy and a semi-quantitative rating allocated, viz. O for no APP, 1 for some APP, 2 for a moderate amount of APP and 3 for large amounts of APP, the method previously described for the rat (section 4.2.5) (Fig. 6.5). Sections from a single coronal level from all animals were assessed simultaneously in order to keep the scoring system consistent for each animal within and between groups. The total APP immunoreactivity score for each animal in both the vehicle and drug treated groups, out of a maximum of 48, was the sum of the scores for the 16 coronal levels (Table 6.3). To assess the reproducibility of semi-quantitative analysis of APP immunoreactivity in the cat, the scoring system was repeated for two of the coronal levels three weeks after the initial assessment by the same scorer (for intra-rater variability) and by a different scorer (for inter-rater variability) (Fig. 6.6).

Quantitative analysis

For quantitative analysis, the images from 16 equivalent coronal sections, from each animal, showing the increased APP immunoreactivity, obtained as described in section 6.2.2., were analysed. A transparent counting grid, arranged in a regular square array, was randomly placed over each image and the number of points overlying the area of increased APP immunoreactivity was counted (Fig 6.7). This was performed on all sixteen levels for both the drug and vehicle treated animals. The total APP score for each animal was the sum of the points on target for all sixteen levels (Table 6.4). The intra-rater variability was tested by repeating the count

for a randomly selected sample from the two cat populations and comparing the two sets of results (Fig. 6.8A). To assess the inter-rater reliability of this technique, a novice was asked to use the grid system and count the number of 'hits' in a randomly selected sample of images from the two cat groups (Fig. 6.8B).

Figure 6.5 Scoring of APP by semi-quantitative and quantitative methods

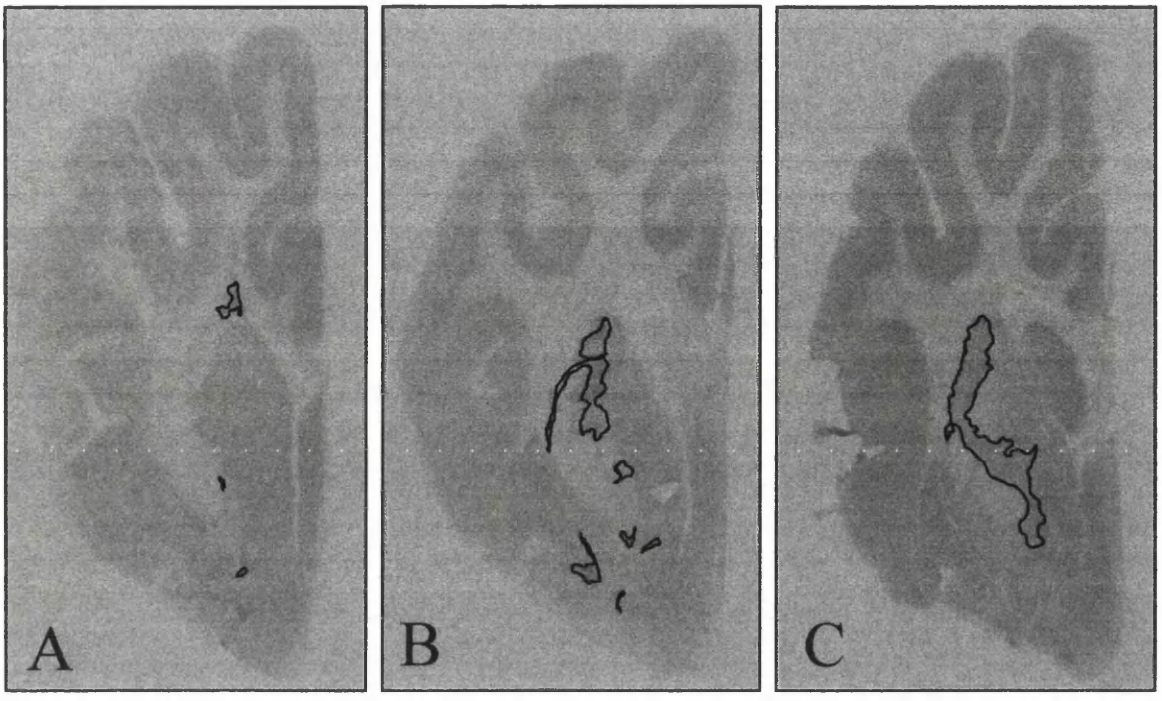

	A	B	C
Semi-quantitative APP score	1	2	3
Quantitative APP score	16	74	117

Scanned cat images at a single coronal level to show the area of increased APP immunoreactivity (outline in black) following MCA occlusion. Table shows the semi-quantitative score for each section allocated; 0 for no APP, 1 for some APP (A), 2 for a moderate amount of APP (B) and 3 for large amounts of APP (C). Scores allocated using quantitative analysis by point-counting grid; 16 for (A), 74 for (B) and 117 for (C).

Table 6.3 Semi-quantitative APP score for vehicle and MK-801 treated cats

An APP score of 0, 1, 2, or 3 was allocated to each of the 16 sections for each cat in the vehicle and drug treated group.

Vehicle	Level 1	Level 2	Level 3	Level 4	Level 5	Level 6	Level 7	Level 8	Level 9	Level 10	Level 11	Level 12	Level 13	Level 14	Level 15	Level 16	Total
LSD2	0	2	2	3	2	3	1	2	1	1	1	0	0	0	0	0	18
LSD 3	0	1	2	3	3	2	1	2	2	1	1	1	0	0	0	0	19
LSD 7	0	2	2	3	3	3	3	3	3	2	1	1	0	0	0	0	26
LSD 8	0	2	2	2	2	3	3	1	2	1	1	1	1	0	0	0	21
LSD 10	0	1	3	3	3	2	1	1	2	0	0	0	0	0	0	0	16
LSD 15	0	2	2	3	3	3	2	3	1	1	1	1	0	0	0	0	21
LSD 17	0	2	3	3	2	2	1	1	2	2	1	1	0	0	0	0	20
LSD 20	2	3	3	1	1	3	3	3	3	2	2	1	1	1	0	0	29
LSD 23	0	2	3	3	2	3	2	2	3	2	1	0	0	0	0	0	23
LSD 26	0	2	3	3	2	1	2	1	1	1	1	0	0	0	0	0	16
Average	0.2	1.9	2.5	2.7	2.3	2.5	1.9	1.9	2	1.3	1	0.6	0.2	0.1	0	0	20.9
Std dev	0.6	0.6	0.5	0.7	0.7	0.7	0.9	0.9	0.8	0.7	0.5	0.4	0.3	0.0	0.0	0.0	4.2
SEM	0.2	0.2	0.2	0.2	0.2	0.2	0.3	0.3	0.3	0.2	0.1	0.2	0.1	0.1	0.0	0.0	1.3
MK-801	Level 1	Level 2	Level 3	Level 4	Level 5	Level 6	Level 7	Level 8	Level 9	Level 10	Level 11	Level 12	Level 13	Level 14	Level 15	Level 16	Total
LSD 4	0	1	3	3	3	3	1	2	2	1	0	0	0	0	0	0	19
LSD 5	0	1	2	3	2	3	3	2	2	2	1	0	0	0	0	0	21
LSD 6	0	2	2	3	1	3	2	2	2	2	2	1	0	0	0	0	22
LSD 9	0	0	1	2	3	3	3	2	1	1	1	0	0	0	0	0	17
LSD 14	0	2	2	3	3	3	1	1	2	2	1	1	1	0	0	0	22
LSD 16	0	3	2	3	3	3	3	3	2	1	0	0	0	0	0	0	23
Average	0.0	1.5	2.0	2.8	2.5	3.0	2.2	2.0	1.8	1.5	0.8	0.3	0.2	0.0	0.0	0.0	20.7
Std dev	0.0	1.0	0.6	0.4	0.8	0.0	1.0	0.6	0.4	0.5	0.8	0.5	0.4	0.0	0.0	0.0	2.3
SEM	0.0	0.4	0.3	0.2	0.3	0.0	0.4	0.3	0.2	0.2	0.3	0.2	0.2	0.0	0.0	0.0	0.9

Figure 6.6 Reproducibility of the semi-quantitative APP analysis

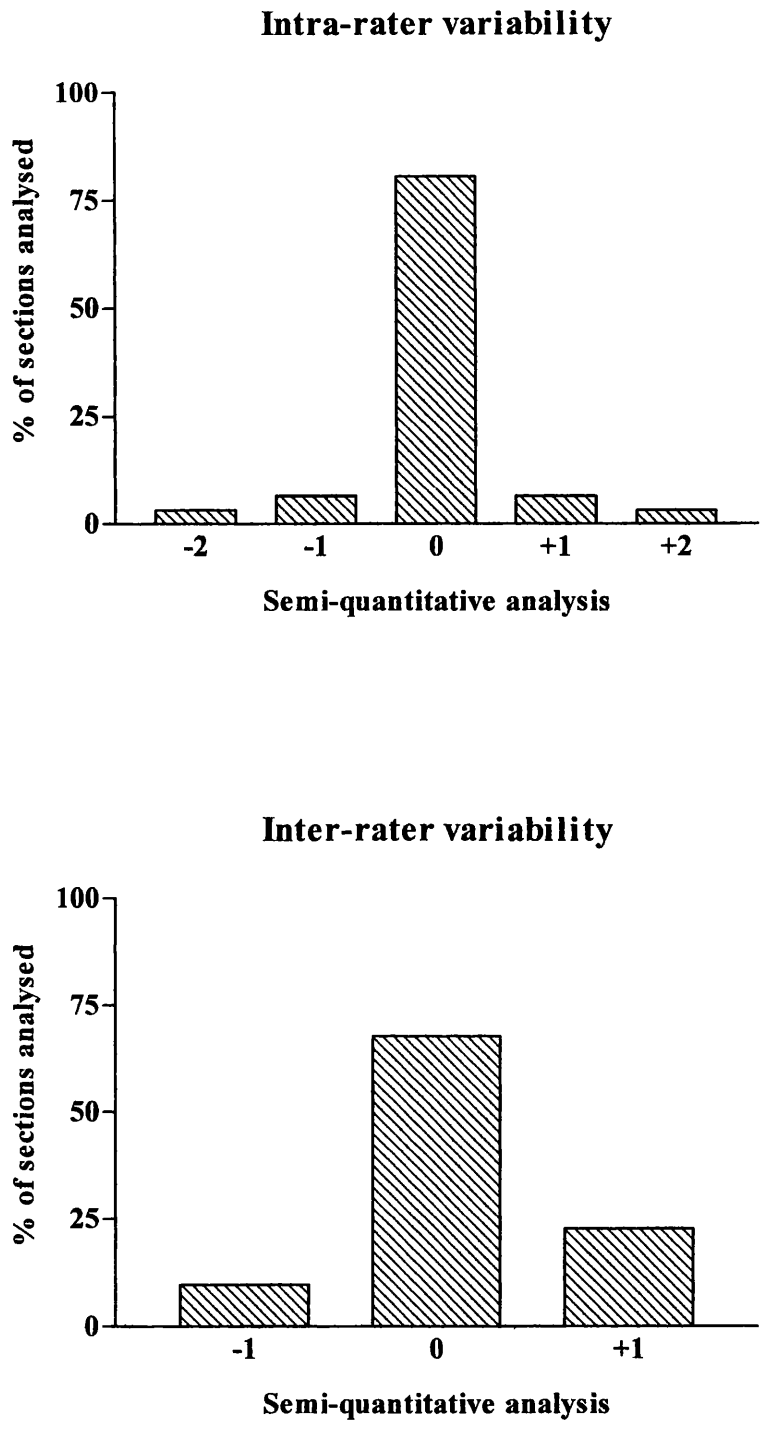

A random selection of cat sections were analysed to assess intra-scorer variability and inter-scorer variability. An APP score of 0, 1, 2 or 3 was given on each occasion as previously described. The value allocated on the second occasion was deducted from that on the first occasion to give a final result ranging from -2 to +2. Therefore, where a section was given the same score on both occasions the value allocated was 0.

Figure 6.7 Method of quantitative APP analysis in the cat

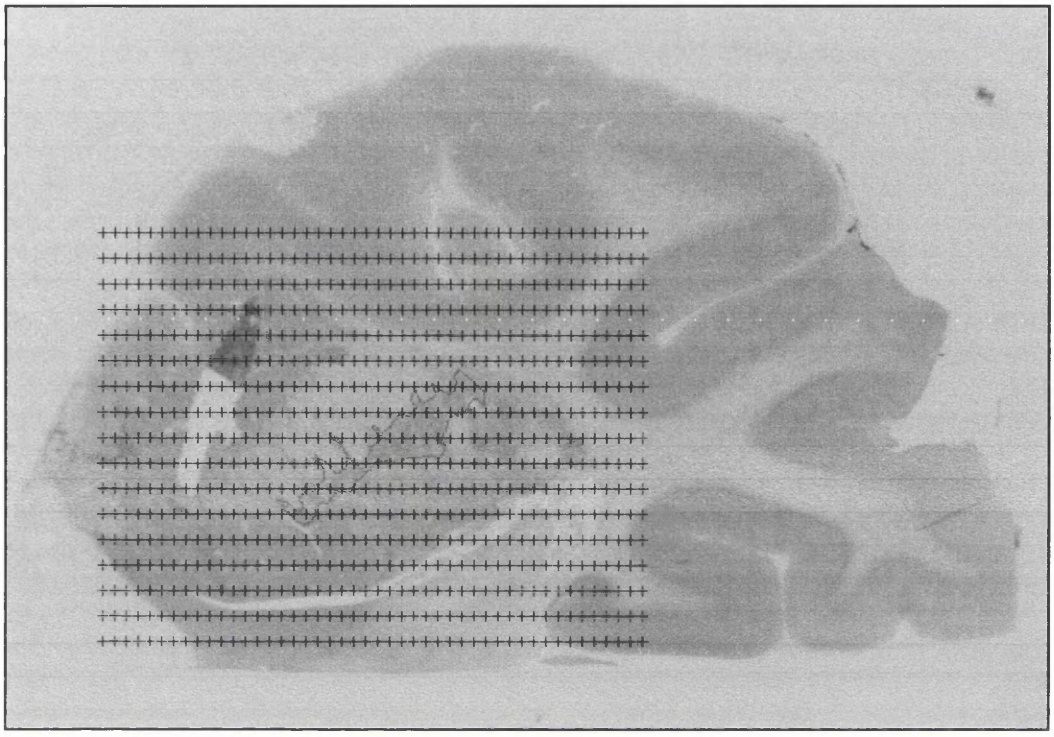

Coronal slice of cat brain overlaid with a point-counting grid. The image from a defined coronal plane, is viewed on a monitor, digitised and printed. The image produced shows the increased APP immunoreactivity (outline in red). A transparent counting grid, arranged in a regular square array, is randomly placed over the image and the number of points overlying the area of increased APP immunoreactivity are counted.

Table 6.4 Quantitative APP score for vehicle and MK-801 treated cats

Vehicle	Level 1	Level 2	Level 3	Level 4	Level 5	Level 6	Level 7	Level 8	Level 9	Level 10	Level 11	Level 12	Level 13	Level 14	Level 15	Level 16	Total
LSD2	0	20	32	41	77	57	15	30	2	0	0	0	0	0	0	0	274
LSD 3	0	0	9	24	28	38	14	17	23	6	2	3	0	0	0	0	164
LSD 7	0	0	14	24	71	34	27	31	24	16	18	1	0	0	0	0	260
LSD 8	0	20	30	25	46	61	45	14	15	9	4	6	0	0	0	0	275
LSD 10	0	0	18	26	30	82	30	12	14	0	0	0	6	0	0	0	218
LSD 15	0	13	20	34	55	46	22	15	20	4	1	0	0	0	0	0	230
LSD 17	0	11	16	25	74	19	10	17	25	7	4	0	0	0	0	0	208
LSD 20	33	38	35	31	16	75	48	26	18	13	19	12	8	0	0	0	372
LSD 23	0	15	24	42	67	90	22	27	17	8	1	0	0	0	0	0	313
LSD 26	0	14	16	28	33	74	14	14	15	9	0	0	0	0	0	0	217
Average	3	13	21	30	50	58	25	20	17	7	5	2	1	0	0	0	253
Std dev	10	12	9	7	22	23	13	7	7	5	7	4	3	0	0	0	59
SEM	3	4	3	2	7	7	4	2	2	2	2	1	1	0	0	0	19
MK-801	Level 1	Level 2	Level 3	Level 4	Level 5	Level 6	Level 7	Level 8	Level 9	Level 10	Level 11	Level 12	Level 13	Level 14	Level 15	Level 16	Total
LSD 4	21	0	31	44	111	90	24	24	28	10	0	0	0	0	0	0	383
LSD 5	0	6	29	32	67	77	46	61	18	17	3	0	0	0	0	0	356
LSD 6	0	19	18	34	36	111	26	14	20	14	12	6	0	0	0	0	310
LSD 9	0	0	4	19	117	74	40	21	6	1	2	0	0	0	0	0	284
LSD 14	0	13	13	42	67	65	12	4	15	9	2	0	1	0	0	0	243
LSD 16	0	30	29	36	115	42	39	33	25	6	0	0	0	0	0	0	355
Ave	4	11	21	35	86	77	31	26	19	10	3	1	0	0	0	0	322
Std dev	9	12	11	9	34	23	13	20	8	6	4	2	0	0	0	0	53
SEM	3	5	4	4	14	9	5	8	3	2	2	1	0	0	0	0	21

Figure 6.8 Reproducibility of quantitative APP analysis

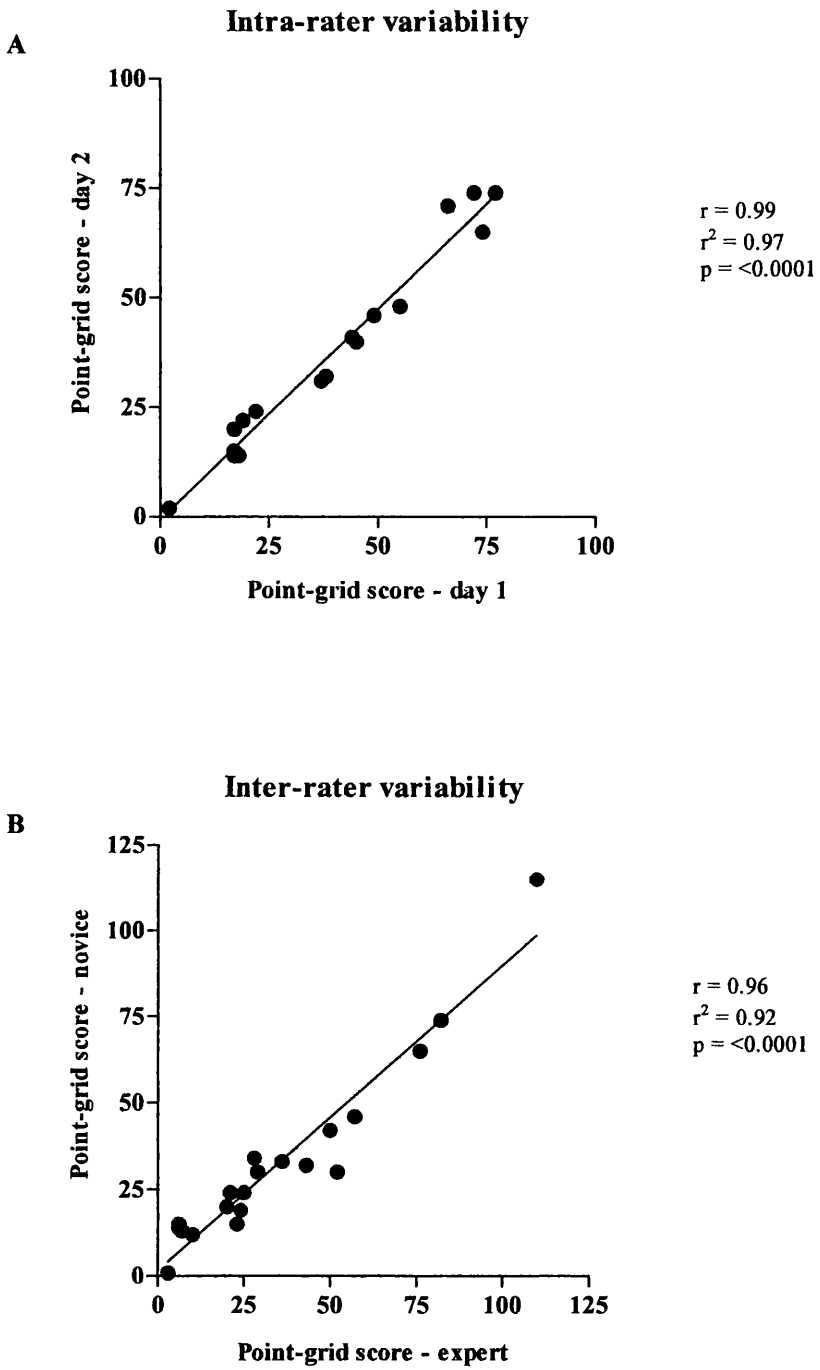

Assessment of the APP accumulation score by point-grid analysis resulted in both the intra-scorer variability (i.e. when the same images were scored on repeated occasions by the same person) (A), and inter-scorer variability (i.e. when the same images were scored by different people) (B), being minimal.

6.3 RESULTS

6.3.1 APP immunocytochemistry after MCA occlusion

In the ipsilateral ischaemic hemisphere, all animals in both the vehicle and MK-801 treated groups had increased APP immunoreactivity in subcortical white matter. The increased axonal immunoreactivity was 'bulbous' in appearance (Fig. 6.3), as previously seen in the rat subcortical white matter and myelinated tracts permeating the striatum (Fig. 4.5), and thought to be an early indication of axotomy (Povlishock, 1992).

6.3.2 Relationship between ischaemia and APP accumulation

The administration of MK-801 reduced the volume of ischaemic damage in the cerebral hemisphere by 30% compared to untreated cats and by 44% in the cortex compared to untreated cats following MCA occlusion (Table 6.5 and Table 6.6 and Fig. 6.9). The volume of ischaemic damage in the caudate nucleus was affected minimally by treatment with MK-801. In the cerebral hemisphere and cortex, MK-801 reduced the area of ischaemic damage in every coronal plane studied (Fig. 6.10A).

In the vehicle treated animals, there was an association between the volume of ischaemic damage and the amount of increased APP immunoreactivity as assessed by both semi-quantitative and quantitative analysis (Fig. 6.11A and 6.12A), the increase in APP immunoreactivity being greatest in cats with the largest volumes of neuronal necrosis.

6.3.3 Effect of MK-801 on APP accumulation

In the MK-801 treated cats, with increasing volume of ischaemic damage there was a general increase in APP accumulation as assessed by semi-quantitative and quantitative

analysis (Fig. 6.11B and 6.12B). The primary hypothesis being tested was that if MK-801 protects axons, the APP score should be reduced. However, despite there being a reduction in the volume of infarction in the MK-801 treated animals, MK-801 failed to significantly reduce the APP score. Using semi-quantitative analysis the mean total APP score for the vehicle treated group was 21 $\pm$ 1 and the mean total APP score for the MK-801 treated group was 21 $\pm$ 1. Using quantitative analysis the mean total APP score for the vehicle treated group was 253 $\pm$ 19 and the mean total APP score for the MK-801 treated group was 322 $\pm$ 22 (Fig. 6.9 B and 6.9C) (Table 6.6). Overall, the quantitative mean APP score in the MK-801 treated group was significantly higher ($P<0.05$, two-tailed t-test) than the APP score in the vehicle treated group. The amount of axonal injury, as assessed by the quantitative APP score, was corrected for the size of ischaemic damage thus allowing the effect of MK-801 on the ratio of white matter:grey matter injury to be established (Table 6.7 and Fig. 6.13). The difference in the ratios between the vehicle treated animals and drug treated animals was significantly different using the one tailed Welch's t-test ($P < 0.05$). For a given volume of infarction, the total APP accumulation score was the same or higher in the drug treated animals as compared to the vehicle treated animals (Fig. 6.11B and 6.12B).

In addition to looking at the total APP score, the relationship of the APP score and area of ischaemia at different coronal planes was assessed (Fig. 6.10). Despite a reduction in the area of ischaemic damage at each coronal plane following MK-801 administration, there was not a similar reduction in APP score as assessed by either semi-quantitative or quantitative analysis.

6.3.4 Semi-quantitative analysis versus point-counting technique of APP

The intra and inter-rater variability for both techniques are illustrated in Fig. 6.5 and Fig. 6.7. Using the semi-quantitative method the intra-rater correlation, r = 0.73 and inter - rater correlation, r = 0.69 (Spearman rank correlation, assuming nonparametric correlation). Using the quantitative method of APP analysis, the intra-rater correlation, r = 0.99 and the inter-rater correlation, r = 0.96 (Pearson correlation assuming Gaussian distribution)

Table 6.5 Ischaemic damage following MCA occlusion in the cat: vehicle group

Hemisphere	Level 1	Level 2	Level 3	Level 4	Level 5	Level 6	Level 7	Level 8	Level 9	Level 10	Level 11	Level 12	Level 13	Level 14	Level 15	Level 16	Total (mm3)
LSD2	12.1	43	74.8	69.1	106.8	123.4	80.7	19.3	14	14.7	9.5	0	0	0	0	0	1165
LSD3	0	21	44.1	59.7	64.7	72.2	106.2	86.6	62.9	45.8	36.3	25.4	10	0	0	0	1270
LSD7	46	104.8	113.4	150	163.1	170.8	166.3	118.1	132.1	98.6	98.9	73.3	27.7	9.8	6.7	0	3074
LSD8	48.4	87.4	107.9	152	120.6	111.8	121.6	71.4	67.9	45.9	43.5	38.5	26.6	12.9	15.2	6.9	2282
LSD10	3.6	28.2	42.9	72.4	82.2	56.7	64.3	21.3	14.7	6.8	0	0	0	0	0	0	759
LSD 15	0	32.9	48.1	84.2	109.1	115.7	121.3	52.3	46	6.2	0	0	0	0	0	0	1232
LSD 17	0	32.2	61.9	90.9	123.9	145.4	145.3	89.1	72.5	50.7	48.2	29.1	8.5	0	0	0	1795
LSD 20	82.5	129.1	147.3	168.4	175.6	171.5	194.7	136	122.5	95.4	100.8	67.3	59.2	35.8	22.8	14.1	3659
LSD 23	0	32.3	64.8	82.9	111.4	106.4	112.2	84.8	69.1	72.7	44.9	41.8	14.6	5.6	0	0	1687
LSD26	0	15.1	40.3	56.1	58.2	50.1	76.7	81.5	67.6	59.3	27.3	12.1	0	0	0	0	1089
Mean	19.26	52.6	74.55	98.57	111.56	112.4	118.93	76.04	66.93	49.61	40.94	28.75	14.66	6.41	4.47	2.1	1801.2
Std Dev	29.28	39.58	36.47	41.84	37.90	43.15	41.00	37.35	38.52	33.48	35.85	26.88	18.90	11.38	8.14	4.74	938.08
SEM	9.27	12.52	11.54	13.24	11.99	13.66	12.98	11.82	12.19	10.60	11.34	8.51	5.98	3.60	2.58	1.50	296.86
Cortex	Level 1	Level 2	Level 3	Level 4	Level 5	Level 6	Level 7	Level 8	Level 9	Level 10	Level 11	Level 12	Level 13	Level 14	Level 15	Level 16	
LSD2	12.1	18.2	46.6	37.3	53.5	85.9	47.5	19.3	14	14.7	9.6	0	0	0	0	0	747
LSD3	0	0	0	0	7.2	32.8	81.2	86.5	62.9	45.8	36.3	25.4	10	0	0	0	776
LSD7	46	76.6	75	96.8	102.7	127.6	138.2	118.1	132.1	98.6	98.9	73.3	27.7	9.7	6.7	0	2571
LSD8	48.4	69.8	74.8	92.5	64	69.5	91.4	71.4	67.9	45.9	43.5	38.5	26.6	12.9	15.2	6.9	1802
LSD10	3.6	0	0	13.1	17.1	15	34.9	21.8	14.7	6.8	0	0	0	0	0	0	263
LSD 15	0	2.4	8.3	56.9	49	71.4	91.7	52.3	46	6.2	0	0	0	0	0	0	768
LSD 17	0	2.7	8.8	31	59.9	102.1	112.3	89.1	72.5	50.7	48.2	29.1	8.5	0	0	0	1230
LSD 20	82.5	98.6	96	104.6	108.6	127.8	155	136	122.5	95.4	100.8	67.3	59.2	35.8	22.8	14.1	3067
LSD 23	0	2.8	23.2	25.8	41.4	63.7	79.9	84.8	69.1	72.7	44.9	41.8	14.6	5.6	0	0	1141
LSD26	0	0	0	0	0	8.2	47	81.5	67.6	59.3	27.3	12.1	0	0	0	0	607
Mean	19.26	27.11	33.27	45.8	50.34	70.4	87.91	76.08	66.93	49.61	40.95	28.75	14.66	6.4	4.47	2.1	1297.2
Std Dev	29.28	38.68	36.85	39.89	36.52	42.44	39.27	37.26	38.52	33.48	35.84	26.88	18.90	11.37	8.14	4.74	909.14
SEM	9.27	12.24	11.66	12.62	11.56	13.43	12.43	11.79	12.19	10.60	11.34	8.51	5.98	3.60	2.58	1.50	287.70

Table 6.5 cont... Ischaemic damage following MCA occlusion in the cat: vehicle group

Caudate	Level 1	Level 2	Level 3	Level 4	Level 5	Level 6	Level 7	Level 8	Level 9	Level 10	Level 11	Level 12	Level 13	Level 14	Level 15	Level 16	Total (mm3)
LSD2	0	20.6	23.7	28.4	13.7	0	0	0	0	0	0	0	0	0	0	0	163
LSD3	0	16.8	39.2	42.3	17.8	1.8	0	0	0	0	0	0	0	0	0	0	227
LSD7	0	23.6	33.8	35.2	21.8	6.1	0	0	0	0	0	0	0	0	0	0	229
LSD8	0	13.5	28.5	39.2	18.6	5.8	0	0	0	0	0	0	0	0	0	0	205
LSD10	0	23.2	37.6	42.8	24.5	5.4	0	0	0	0	0	0	0	0	0	0	255
LSD 15	0	24.4	34.6	11.7	23	6	0	0	0	0	0	0	0	0	0	0	187
LSD 17	0	23.9	47.3	39.8	24.6	5.2	0	0	0	0	0	0	0	0	0	0	270
LSD 20	0	25.1	46.8	44.6	25	6	0	0	0	0	0	0	0	0	0	0	283
LSD 23	0	24.5	36.4	40.2	21.5	6.1	0	0	0	0	0	0	0	0	0	0	245
LSD26	0	10.3	35.8	39.5	19.6	3.3	0	0	0	0	0	0	0	0	0	0	212
Mean	0	20.59	36.37	36.37	21.01	4.57	0	0	0	0	0	0	0	0	0	0	227.6
Std Dev	0.00	5.24	7.23	9.79	3.61	2.15	0.00	0.00	0.00	0.00	0.00	0.00	0.00	0.00	0.00	0.00	37.27
SEM	0.00	1.66	2.29	3.10	1.14	0.68	0.00	0.00	0.00	0.00	0.00	0.00	0.00	0.00	0.00	0.00	11.79

Table 6.5 cont... Ischaemic damage following MCA occlusion in the cat: MK-801 group

Hemisphere	Level 1	Level 2	Level 3	Level 4	Level 5	Level 6	Level 7	Level 8	Level 9	Level 10	Level 11	Level 12	Level 13	Level 14	Level 15	Level 16	Total (mm3)
LSD4	0	30.5	49.7	71.1	104.3	100.2	96.9	30.4	14.1	11.4	0	0	0	0	0	0	1017
LSD5	0	30.1	51.6	49.8	50.1	46.4	33.8	14.6	12.5	12	11.2	0	0	0	0	0	624
LSD6	28.4	74	67.5	214.9	146.2	145.9	126.9	90.8	78	52.8	65.2	47.2	39.7	7	0	0	2440
LSD9	0	7.1	27.3	54	70.1	83.1	69.7	27	12.1	13.4	0	0	0	0	0	0	728
LSD 14	0	29.6	45.3	56.4	60.8	93.3	85.4	18.5	13	14.6	12	13.5	11.2	4.7	3.5	0	923
LSD 16	5.6	106	99.2	120.1	115.7	115.6	103.5	81.6	39.1	30.4	43.2	33.3	16.6	10.3	0	0	1855
Mean	5.67	46.22	56.77	94.38	91.20	97.42	86.03	43.82	28.13	22.43	21.93	15.67	11.25	3.67	0.58	0.00	1264.50
Std Dev	11.36	36.49	24.46	64.48	37.03	33.21	31.90	33.44	26.59	16.49	26.46	20.23	15.61	4.39	1.43	0.00	722.00
SEM	4.64	14.90	9.98	26.32	15.11	13.55	13.02	13.65	10.85	6.73	10.80	8.26	6.37	1.79	0.58	0.00	294.70
Cortex	Level 1	Level 2	Level 3	Level 4	Level 5	Level 6	Level 7	Level 8	Level 9	Level 10	Level 11	Level 12	Level 13	Level 14	Level 15	Level 16	
LSD4	0	0	0	9	40.1	58.1	66.7	30.4	14.1	11.4	0	0	0	0	0	0	460
LSD5	0	0	0	0	0	5.9	5.8	14.6	12.5	12	11.2	0	0	0	0	0	124
LSD6	28.4	43.7	22.2	75.2	82.4	102	99.6	90.8	78	52.8	65.2	47.2	39.7	7	0	0	1740
LSD9	0	0	0	0	12.7	41.5	43.2	27	12	13.4	0	0	0	0	0	0	300
LSD 14	0	0	0	0	7.6	50.8	52.7	18.5	13	14.6	12	13.5	11.1	4.7	3.5	0	404
LSD 16	5.6	77.9	56.7	46.3	50.2	74.9	72.4	81.6	39.1	30.4	43.2	33.3	16.6	10.3	0	0	1291
Mean	5.67	20.27	13.15	21.75	32.17	55.53	56.73	43.82	28.12	22.43	21.93	15.67	11.23	3.67	0.58	0.00	719.83
Std Dev	11.36	33.21	23.11	31.75	31.40	32.32	31.55	33.44	26.60	16.49	26.46	20.23	15.61	4.39	1.43	0.00	642.73
SEM	4.64	13.55	9.43	12.96	12.81	13.19	12.88	13.65	10.86	6.73	10.80	8.26	6.37	1.79	0.58	0.00	262.34

Table 6.5 cont... Ischaemic damage following MCA occlusion in the cat: MK-801 group

Caudate	Level 1	Level 2	Level 3	Level 4	Level 5	Level 6	Level 7	Level 8	Level 9	Level 10	Level 11	Level 12	Level 13	Level 14	Level 15	Level 16	Total (mm3)
LSD4	0	25.8	45.3	45.5	25.5	5.8	0	0	0	0	0	0	0	0	0	0	283
LSD5	0	25.8	46.6	31.3	12.1	2	0	0	0	0	0	0	0	0	0	0	223
LSD6	0	25.5	40.3	33.6	25.2	5.4	0	0	0	0	0	0	0	0	0	0	247
LSD9	0	7.1	22.1	38	18.6	5.3	0	0	0	0	0	0	0	0	0	0	179
LSD 14	0	24.1	40.5	39.9	14.9	6.2	0	0	0	0	0	0	0	0	0	0	239
LSD 16	0	23	38.3	44.2	24.8	4.9	0	0	0	0	0	0	0	0	0	0	259
Mean	0.00	21.88	38.85	38.75	20.18	4.93	0.00	0.00	0.00	0.00	0.00	0.00	0.00	0.00	0.00	0.00	238.33
Std dev	0.00	7.33	8.80	5.64	5.84	1.50	0.00	0.00	0.00	0.00	0.00	0.00	0.00	0.00	0.00	0.00	35.36
SEM	0.00	2.99	3.59	2.30	2.38	0.61	0.00	0.00	0.00	0.00	0.00	0.00	0.00	0.00	0.00	0.00	14.43

Table 6.6 Influence of MK-801 upon the volume of ischaemic damage and APP score in the cat after MCA occlusion

	Volume of ischaemic damage (mm^3)	
	Vehicle	MK-801
Cerebral hemisphere	1801 ± 297	1265 ± 295
Cerebral cortex	1297 ± 288	720 ± 262
Caudate nucleus	228 ± 12	238 ±14
APP score (semi-quantitative)	21 ± 1	21 ± 1
APP score (quantitative)	253 ± 19	322 ± 21
n	10	6

Data are presented as mean ± SEM.

Figure 6.9 Effect of MK-801 on total volume of ischaemic damage and total APP score following MCA occlusion

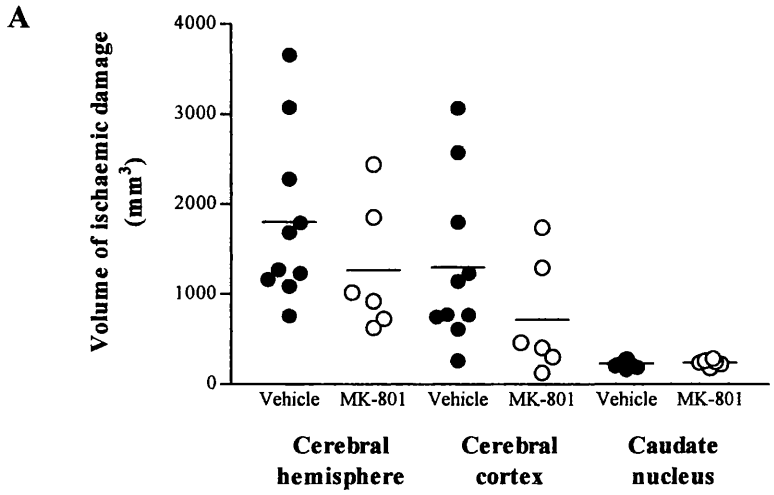

Volume of ischaemic brain damage in cerebral hemisphere, cerebral cortex, and caudate nucleus in vehicle treated control cats and in cats treated with MK-801. Each point represents data from a single animal. The mean value for the group is indicated by a solid horizontal line.

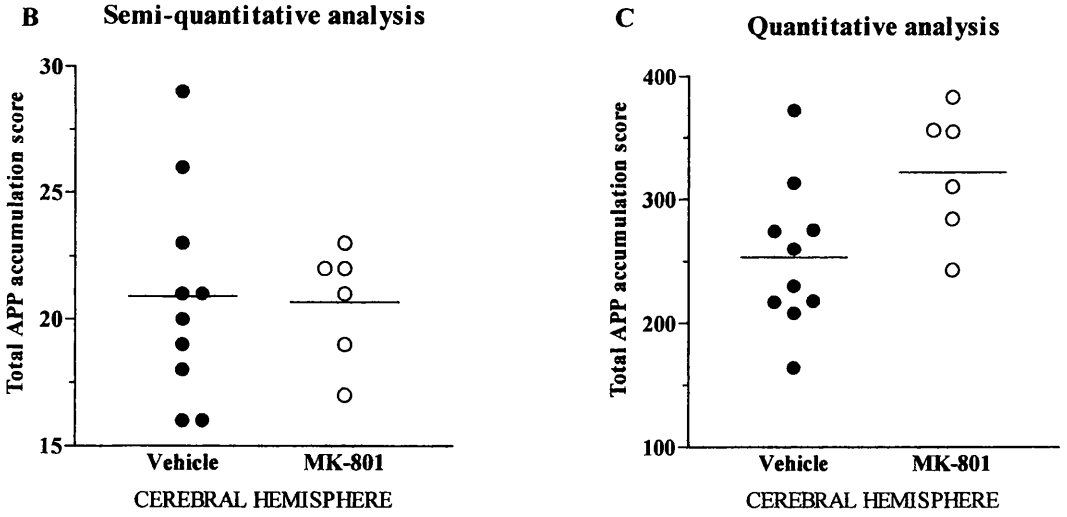

Total APP accumulation score as assessed by semi-quantitative (B) and quantitative (C) analysis in the cerebral hemisphere in vehicle treated control cats and in cats treated with MK-801 after MCA occlusion. Each point represents data from a single animal. The mean value for the group is indicated by a solid horizontal line.

Figure 6.10 Effect of MK-801 on area of ischaemic damage and mean APP score at eight defined coronal levels following MCA occlusion in the cat

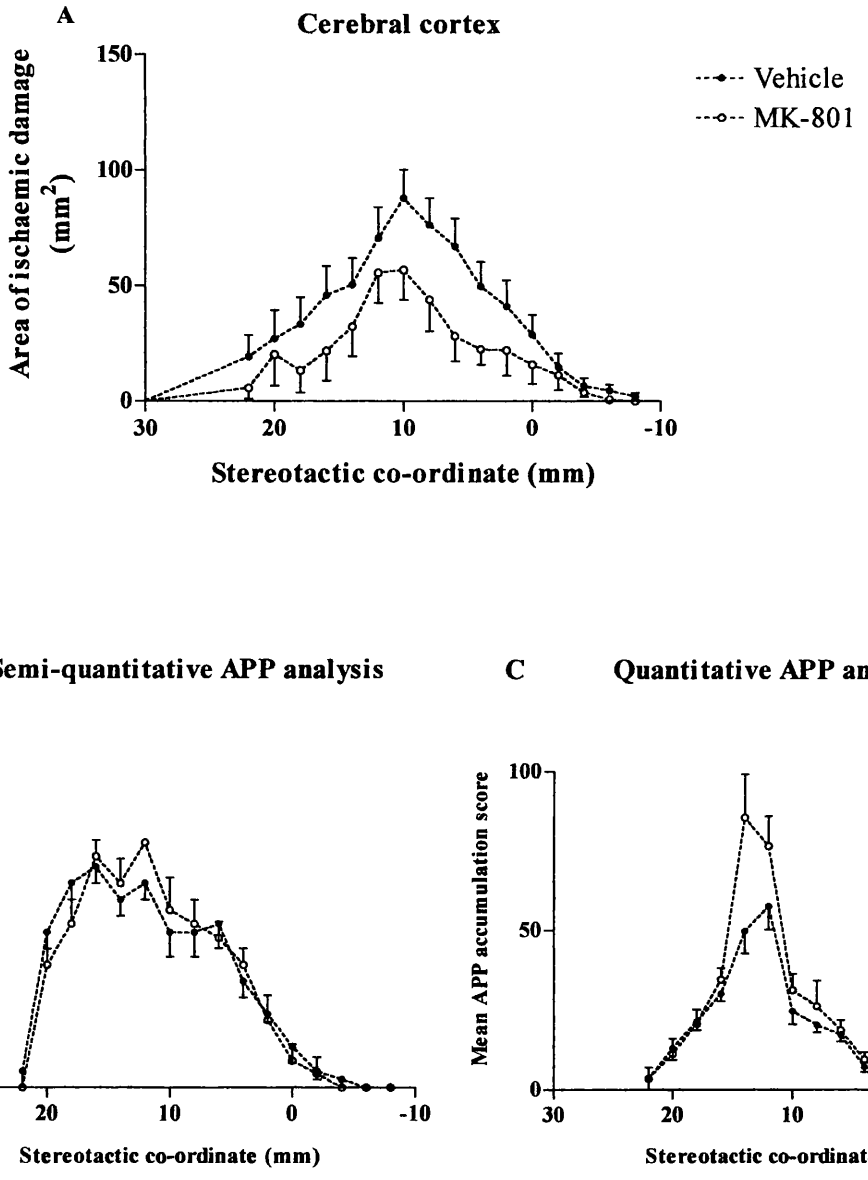

(A) The effect of MK-801 upon the area of ischaemic damage in the cerebral cortex at 16 defined coronal planes. (B) Mean APP accumulation score as assessed by semi-quantitative analysis and (C) quantitative analysis at each coronal level. Despite the MK-801 treated animals having a smaller area of ischaemic damage at each of the coronal levels (A), there was no reduction in the APP score compared to the vehicle treated animals when assessed by either method of analysis (B and C). Data are presented as mean ± SEM. Vehicle (n = 10); MK-801 (n = 6).

Figure 6.11 Volume of ischaemic damage and semi-quantitative APP accumulation score

A

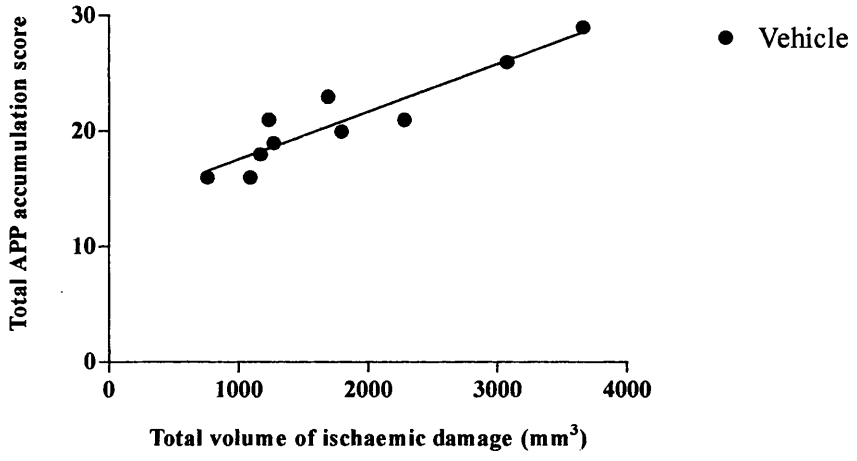

B

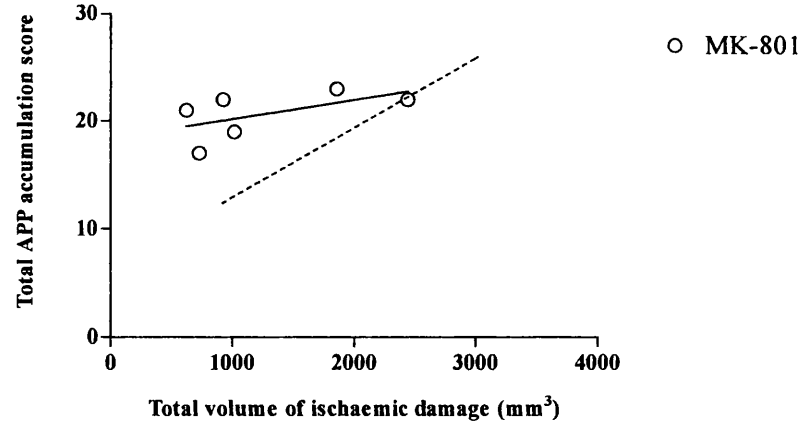

The volume of ischaemic damage was compared to total accumulation of APP for each animal in A) Vehicle treated animals and B) MK-801 treated animals. The total APP accumulation was the score sum for the 16 coronal levels. Total APP accumulation score increased with increasing volume of infarction. Each point represents data from single animal. The dotted line in B represents best fit line for vehicle animals.

Figure 6.12 Volume of ischaemic damage and quantitative APP accumulation score

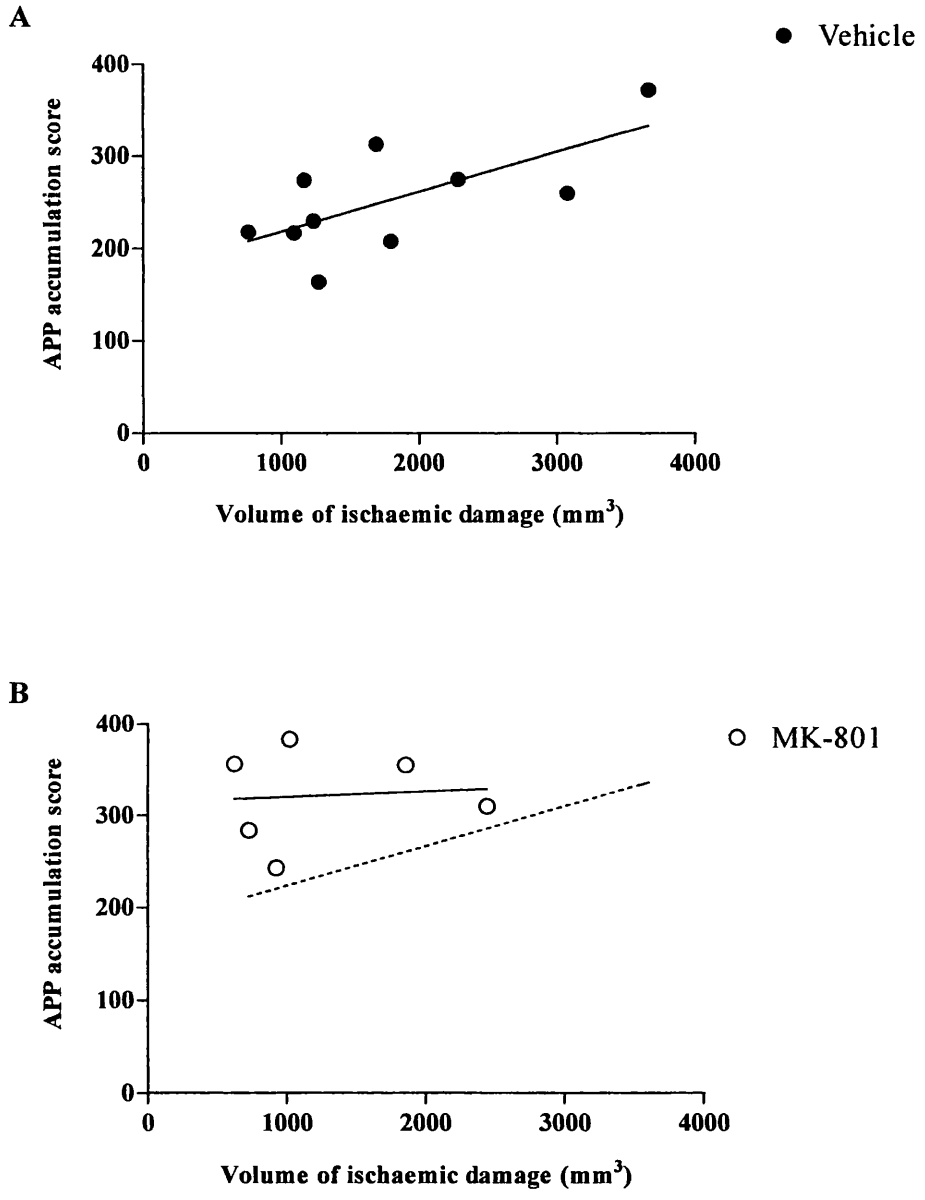

The volume of ischaemic damage was compared to total accumulation of APP for each animal in the vehicle and MK-801 treated groups. The total APP accumulation score was the score sum for the 16 coronal levels obtained using the point grid system. (A) In the vehicle group, total APP accumulation score increased with increasing volume of infarction. (B) For a given volume of infarction, the drug treated animals had a higher total APP accumulation score (solid line) as compared to vehicle animals (dotted line)

Table 6.7 White matter injury:grey matter injury ratio following MCA occlusion

	Volume of infarction (mm3)	Quantitative APP score	APP score : infarct volume
Vehicle	1165	274	0.24
	1270	164	0.13
	3074	260	0.08
	2282	275	0.12
	759	218	0.29
	1232	230	0.19
	1795	208	0.12
	3659	372	0.10
	1687	313	0.19
	1089	217	0.20
MK-801	1017	383	0.38
	624	356	0.57
	2440	310	0.13
	728	284	0.39
	923	243	0.26
	1855	355	0.19

The amount of axonal injury was corrected for the size of ischaemic damage by generating a ratio of APP score:infarct volume for the vehicle treated and MK-801 treated animals.

Figure 6.13 White matter injury:grey matter injury ratio following MCA occlusion

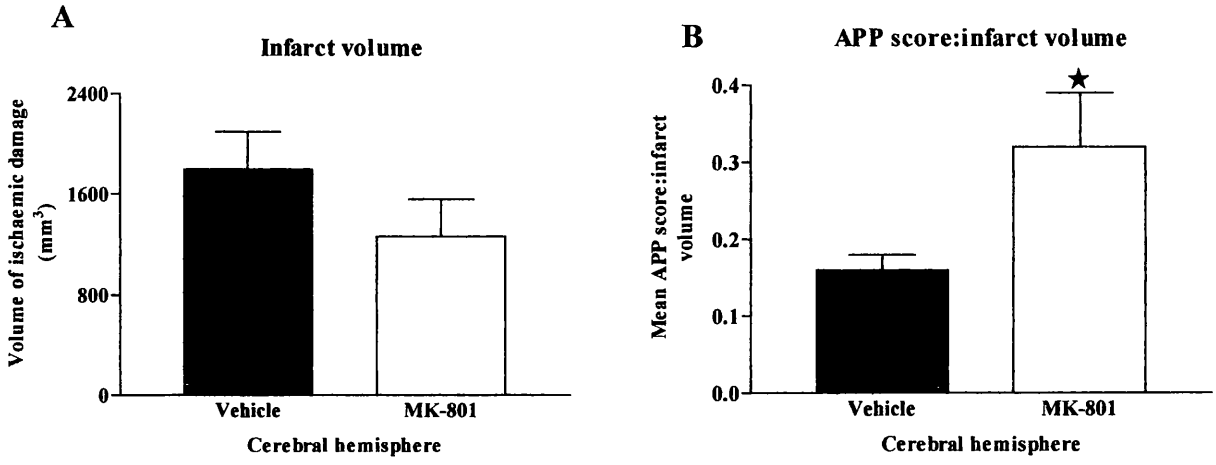

(A) Volume of ischaemic brain damage in the cerebral hemisphere in vehicle treated control cats and in cats treated with MK-801. (B) Ratio of APP score, as assessed by quantitative analysis, and infarct volume. The APP score:infarct volume ratio is significantly higher in the drug treated animals compared to the vehicle treated animals ($P < 0.05$, Welch's one sided t-test) despite a reduction in infarction volume in the drug treated group. Data are presented as mean $\pm$ SEM. Vehicle (n = 10); MK-801 (n = 6).

6.4 DISCUSSION

6.4.1 The species issue

Many advantages have accrued from the use of rodent models for neuroscience research. The extensive normotensive data, their relatively small size and modest cost has allowed the conduction of a large battery of structural and functional studies to be undertaken in rats which would not be possible in higher order animals because of the technical as well as financial limitations (Povlishock et al. 1994). The lissencephalic nature of the rodent cortex, however, is recognised as a deficiency in that it does not allow the complete modelling of all changes occurring in the complex gyri and sulci of the gyrencephalic brain. The experiments described in previous chapters using the rat model, although suggestive that axons are not salvaged following the administration of MK-801, were not conclusive. This was due firstly to the small shifts of neuronal necrosis following drug administration in the rat brain, secondly, due to the difficulty of assessing the protective effects of MK-801 in such a small volume of white matter, and thirdly, due to the small variance in lesion size within the groups making separation of APP scores between the two groups difficult. The potential implications of the failure of the classic neuroprotective drug, MK-801, to save white matter following ischaemia are huge. The use of higher order animals, such as the cat, which more closely reflects the cerebral anatomy of man, was considered necessary to characterise better the pathology of white matter injury following therapeutic intervention.

6.4.2 Semi-quantitative versus quantitative analysis of APP

Before a new methodology can be accepted it is important to establish the reliability of the technique. Although the semi-quantitative method of analysis of APP has already

been described for the rat in chapter 4, this had not previously been applied to the cat. One could predict that the major limitation of semi-quantitative analysis is that it is purely subjective and hence liable to error. However, the results show that the intra-rater reproducibility is quite good with the same score being allocated to approximately 80% of sections. The weakness of the semi-quantitative system is revealed when a different scorer is asked to assess the sections. In this case only 67% of sections were allocated the same score by the two assessors. The use of the point-grid technique was developed to overcome the subjectivity associated with the semi-quantitative analysis.

Quantification of APP using a fine, regular square array point-grid system was found to be a relatively rapid technique. The count of points is always an integer value and therefore an approximation. In general, the more points superimposed on any given outline, the more accurate the estimate of area. When used for quantification of APP in the cat, it was found to be a relatively sensitive scoring method since the scores between coronal levels ranged from 1-177 as compared to 1-3 for semi-quantitative analysis. Furthermore, it is a more reliable, robust and user friendly method as compared to the semi-quantitative analysis. This is highlighted by the fact that there were no significant differences between the results obtained by myself and the novice, who had had only a few minutes of tuition about the technique (Fig. 6.8B). Using this quantitative methodology, it was possible to confidently evaluate the effect of MK-801 treatment on the extent of APP accumulation in the white matter tracts of the cat brain following MCA occlusion.

6.4.3 MK-801 and the protection of axons

The experiment was designed to answer three questions. In answer to the first, the study demonstrated that increased APP immunoreactivity is a consistent outcome in white

matter after focal cerebral ischaemia in the cat. Secondly, using two different scoring systems for APP, it was found that the larger the volume of the ischaemic lesion, the greater the extent of increased APP immunoreactivity. Once these two facts had been established, it was possible to investigate whether the classic neuroprotective drug, MK-801, protects axons following MCA occlusion. The results obtained strongly suggest that MK-801 fails to protect axons, as judged by the APP accumulation score, despite MK-801 reducing the volume of ischaemic injury of grey matter by 30%. Following MK-801 administration the axonal injury was not decreasing with infarct volume at the same rate as vehicle treated animals. This was established by assessing the axonal injury:infarct volume ratios for the drug treated and vehicle animals. The increased ratio in the drug treated group suggests that MK-801 results in more axonal injury relative to that of grey matter injury following MCA occlusion (Fig. 6.13). Even at each coronal level, where the MK-801 resulted in reduced neuronal necrosis, the mean APP score was approximately the same or higher than that in the vehicle treated animals. It appeared that the APP score in the MK-801 treated animals was a value similar to that that would be expected if they had not received any treatment at all; the neuroprotective drug saved neurons but not axons. This finding has tremendous implications in the design and development of drugs for the treatment of stroke. The use of agents targeted towards the protection of grey matter alone may be inimical to the function of the brain as a whole. The failure of many recent drug trials, and the findings of the present study, suggest that the success of future strategies will be dependant on the protection of the brain as a whole; that is, the development of either single agents or combination therapy targeted at the protection of both grey and white matter. The findings and implications of this study will be discussed in more depth in the following chapter.

CHAPTER 7

DISCUSSION

7.1 INTRODUCTION

The functional integrity of the CNS as a whole depends not only on the normal operation of neurons and their synaptic connections, but also on the axons that interconnect neurons with each other and carry input and output to and from the CNS. Classically white matter has been considered less vulnerable than grey matter to ischaemic injury (Marcoux et al. 1982), however recent evidence would suggest otherwise (Dewar and Dawson, 1997; Pantoni et al. 1996). Until recently, much less was known about the mechanisms of injury in white matter compared to grey matter. Since white matter does not contain neuronal cell bodies or synapses, it was considered likely that the mechanisms of injury and strategies for its protection were different from those in grey matter. Waxman and colleagues, using an in vitro model of isolated optic nerves (Waxman et al. 1991; Waxman et al. 1992), have confirmed that myelinated axons are susceptible to anoxia in the absence of their perikarya and that functional and structural impairment occurs within the axon itself, and not only as a consequence of impaired perikaryal function. Using this model, the excitability of CNS axons has shown to be critically dependent on an adequate supply of energy and that irreversible axonal injury depends on energy failure and the presence of extracellular Ca^{2+} (Section 1.5.3) (Stys et al. 1990). Although Stys has claimed that at least qualitatively, the mechanisms described using the in vitro optic nerve model are operative in an in vivo situation (Stys, 1996), very little work has been published on axonal injury in vivo following focal cerebral ischaemia to substantiate this claim. In fact most of the literature pertaining to axonal injury in vivo is related to traumatic brain injury.

Studies of traumatic brain injury in a non-human primate model alerted Neuroscientists to the importance of white matter injury; Gennarelli and colleagues in 1982 suggested a direct link between the extent of diffuse axonal injury and the ensuing patient morbidity (Gennarelli et al. 1982). This experimental finding has been corroborated by evidence of diffuse axonal injury in man in which the most severe grades had the commonest association with the vegetative state and severe disability (Adams et al. 1989) (section 1.7.2).

Despite these findings, over the last decade the major mechanistic advances in the therapy of stroke have been targeted towards the protection of the neuronal cell body, with protection of white matter being largely neglected. Following ischaemia, the extracellular concentration of the excitatory neurotransmitter glutamate has been show to increase to levels that are toxic to neurones, and consequently, drug development has been targeted at the blockade of glutamate release or prevention of its action at the postsynaptic receptors (Wahlgren, 1997). Since the predominant pathway for calcium ion entry into nerve cells in ischaemic CNS tissue is via the glutamate activated NMDA receptor channel complex (section 1.5.2), much effort has been focused on the discovery and development of molecules that can inhibit the ion fluxes induced by activation of this receptor-channel complex. Many studies using NMDA antagonists, including MK-801, have been demonstrated in the experimental setting to reduce the volume of neuronal necrosis following an ischaemic insult (Fig. 1.8) (Park et al. 1988a and 1988b; Ozyurt et al. 1988) (see section 1.6.2). The reported success of these NMDA antagonists in the experimental setting, has permitted the progression of drugs to clinical trials in man (Bullock, 1998; Small and Buchan, 1997). The results of the phase III trials have generally been disappointing. Some of the trials have been stopped prematurely when interim analysis has raised concerns about the risk-benefit ratio, and others have been

stopped when there has been no difference between active treatment and placebo (Muir and Lees, 1995). Even in those trials that have been completed, the results have not necessarily proven the clinical efficacy of the drugs concerned. The reasons for these drug failures are almost certainly multifactorial. However, it cannot be ignored that NMDA antagonists are targeted towards the salvation of grey matter and therefore will not be effective in cell components such as white matter which are devoid of NMDA receptors.

In order that the effect of therapeutic intervention on the protection of white matter can be assessed, a method by which white matter injury can be visualised and quantified is required. The work described in this thesis set out to investigate different markers of axonal injury, develop a suitable method for quantification of axonal injury, and finally, using this information, to investigate whether classic neuroprotective drugs, such as MK-801, protect axons following an ischaemic insult. In the following sections, the results described in the preceding chapters, and the implications for future drug development in stroke research, are discussed .

7.2 THE SEARCH FOR A MARKER OF AXONAL INJURY

7.2.1 MAP5, SNAP25, NF68kD and APP

In the era of silver impregnation techniques, axonal bulbs were thought to develop over a 12-18 h period (Adams et al. 1989). With the advent of a variety of markers used to define the responses of axons to injury, the time scale of axonal bulb visualisation seems to have speeded considerably with positive axonal swellings being demonstrated using APP at only 1.75 h after head injury (Blumbergs et al. 1995)! APP has attracted particular interest as a marker of axonal damage in blunt head injury since it

accumulates at the location of disruption in axonal transport (McKenzie et al. 1996; Gentleman et al. 1995; Sherriff et al. 1994a and 1994c; Blumbergs et al. 1994). Furthermore, local neurofilament (NF) changes following blunt head injury in human post-mortem and experimental studies have been described using antibodies targeted against the 68kDa subunit. Alterations in the staining of these antibodies following head injury are sensitive in detecting early changes in the axon which correlate with the genesis of impaired axoplasmic transport (Yaghmai and Povlishock, 1992; Grady et al. 1993; Erb and Povlishock, 1988; Povlishock et al. 1983).

Various markers of axonal injury have been investigated after cerebral ischaemic challenges, including APP (Yam et al. 1997; Stephenson et al. 1992; Kalaria et al. 1993). As in response to traumatic brain injury (Sherriff et al. 1994c; Gentleman et al. 1993; Blumbergs et al. 1994), the increase in APP immunoreactivity in axons which occurs in response to cerebral ischaemia is bulb like in appearance and has been suggested to be indicative of dysfunction of axonal transport (Shigematsu and McGeer, 1992). The dependence of axonal transport on the integrity of the cytoskeleton would therefore suggest that accumulation of transported proteins may be preceded by evidence of changes in cytoskeletal proteins. In this respect, alterations in immunostaining of proteins associated with axonal microtubules at 2 and 6 h after induction of focal cerebral ischaemia in the rat has been reported (Dewar and Dawson, 1997). Although axonal damage can be detected in head-injured patients who survive only a few hours (Sherriff et al. 1994c; McKenzie et al. 1996; Gentleman et al. 1995), demonstration of increased APP immunoreactivity in the rat had been demonstrated, prior to this thesis, following at least 24 h of focal cerebral ischaemia (Stephenson et al. 1992; Yam et al. 1997).

The work described in Chapter 3 was undertaken to determine the time course of changes induced by focal cerebral ischaemia in axonal transport and proteins associated with the microtubular and neurofilament components of the cytoskeleton. Alterations in immunoreactivity of antibodies directed at an axonally transported protein, a microtubule associated protein and a neurofilament protein were investigated at different times following permanent MCA occlusion in rats. SNAP25 which plays a role in synaptic exocytosis and like APP, undergoes fast anterograde transport (Sollner et al. 1993; Oyler et al. 1989), the NF68kD subunit of neurofilament protein, which has been extensively studied in diffuse axonal injury after traumatic brain injury (Yaghmai and Povlishock, 1992; Grady et al. 1993; Erb and Povlishock, 1988; Povlishock et al. 1983), and MAP5 which is a component of the microtubular system (Ochs, 1972) and has been shown to be sensitive to cerebral ischaemia (Dewar and Dawson, 1997), were all examined.

The study demonstrated that ischaemia results in abnormalities of axonal neurofilament and microtubule proteins as well as disruption of axonal transport. Importantly, these changes occur early in the evolution of ischaemic brain damage with both cytoskeletal structural abnormalities and disruption of axonal transport being detected within 1 h of MCA occlusion (Table 3.1). SNAP25 immunoreactivity was increased in a circumscribed zone in the subcortical white matter (Fig. 3.5) and in the white matter tracts permeating the striatum, bordering the area of infarction (Fig. 3.4). SNAP25 undergoes fast anterograde transport to the synapse (Hess et al. 1992) and therefore its presence within axons at the site of injury may be due to its accumulation following inhibition of axoplasmic flow. This hypothesis is supported by the fact that the site of its accumulation was found to be very similar to that of APP which also undergoes fast anterograde axonal transport (Koo et al. 1990) along microtubules by

kinesin (Amaratunga et al. 1995), and has been previously shown to accumulate in similar regions after inhibition of axoplasmic flow (Yam et al. 1997; Nakamura et al. 1992; Kawarabayashi et al. 1991; Shigematsu et al. 1992; Otsuka et al. 1991) (see below). In addition, the increased immunostaining with SNAP25 after focal ischaemia was 'bulbous' in appearance, reminiscent of axonal swellings which occur following traumatic brain injury and which have been suggested to be an early indicator of axotomy (Povlishock, 1992) (Fig. 7.1). Where microtubules remain in the intact axoplasm, fast axonal transport, both anterograde and retrograde, continues resulting in accumulation of proteins and organelles at the point or points of damage along the length of the axon. SNAP25 appears to be a sensitive marker of axonal injury in this model of focal ischaemia. Changes in the immunostaining were evident from 1 h and marked by 4 h post MCA occlusion.

The early onset of altered SNAP25 immunoreactivity was consistent with the change in NF68kD immunostaining in axons after ischaemia. NFs are composed from three subunit polypeptides, the so-called 'neurofilament triplet' (for review see Schlaepfer, 1987 and section 1.3). Antibodies to the 68kD subunit have proved to be the most useful for detecting reactive axonal change following traumatic brain injury in both man and animals (Yaghmai and Povlishock, 1992; Grady et al. 1993). NFs play a critical role in determining axonal calibre (Hoffman et al. 1984) and it was interesting that by 2 h following MCA occlusion, NF68kD immunostaining was rough and disorganised in appearance compared to the contralateral hemisphere and to sham operated animals (Fig. 3.7). Also, by 4 h, as with SNAP25, this change of pattern was more accentuated (Fig. 3.6 and Fig. 3.7). Furthermore, the electron microscope findings described in Chapter 3 support the light microscopic findings, also indicating disruption of axonal cytoskeletal structure following MCA occlusion. In the ipsilateral caudate

nucleus within the core of the infarct, NF spacing in individual myelinated fibre tracts was more dispersed and disorganised compared to that in the contralateral hemisphere (Fig. 3.10). Misalignment of NFs and accumulation of organelles has previously been described to occur in a model of traumatic brain injury at similar time points to that found in this study of ischaemic brain injury (Yaghmai and Povlishock, 1992). However, it is the microtubular component of the cytoskeleton, rather than the NFs, which provide the tracks for axonal transport. Microtubules are composed of a core cylinder of α and β-tubulin, the stability and assembly of which is dependent on a variety of microtubule associated proteins including MAP1a and MAP5 (Ludin and Matus, 1993). Therefore it was significant to find that within 2 h of MCA occlusion, altered immunoreactivity was also seen with MAP5 staining. The pattern in the myelinated fibre tracts permeating the striatum had a clumped, globular appearance (Fig. 3.8). Changes in MAP5 immunoreactivity were also evident in the subcortical white matter, where the staining was granular in appearance, as has been previously reported (Dewar and Dawson, 1997). Early microtubule disruption is supported by ultrastructural studies at 2 h after focal ischaemia in the rat (Pantoni et al. 1996) and at even earlier time points following axonal stretch injury in the guinea-pig (Maxwell and Graham, 1997). Loss of microtubules in the axons may provide an explanation for the focal perturbation of axonal transport that results in the formation of axonal swellings characterised by increased SNAP25 and APP immunoreactivity and aggregates of axonal organelles as seen by electron microscopy (Fig. 3.13).

Figure 7.1

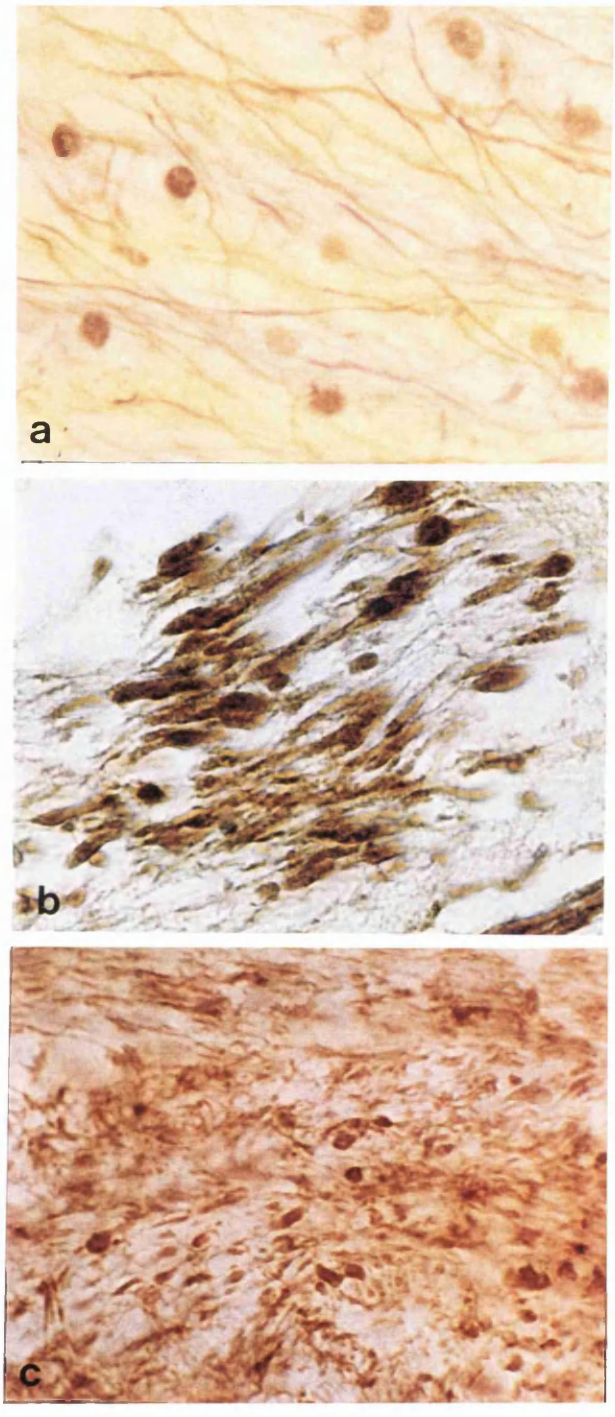

Axonal bulb formation following head injury and ischaemia. APP bulbs following diffuse axonal injury in man (a) and focal ischaemia in the rat (b). The presence of axonal bulbs are also evident following focal ischaemia in the rat using antibodies to SNAP25 (c).

Amyloid precursor protein immunoreactivity following focal cerebral ischaemia was assessed in the rat and cat (Chapter 4 and Chapter 6 respectively). APP immunoreactivity was assessed at a single time point but in greater detail than that described for MAP5, SNAP25 and NF68kD as described above, with a view to possible quantification. APP is considered to be a sensitive marker of axonal injury following human head injury and ischaemic insults in man and animals (Yam et al. 1997; Suenaga et al. 1994; Stephenson et al. 1992; Kalaria et al. 1993; McKenzie et al. 1996; Gentleman et al. 1995; Sherriff et al. 1994c; Blumbergs et al. 1994). The studies using APP as a marker of axonal injury described in this thesis demonstrated that increased APP immunoreactivity is a consistent outcome in white matter after focal cerebral ischaemia in both the rat and cat. As with SNAP25, increased APP immunoreactivity is likely to reflect APP accumulation (Shigematsu and McGeer, 1992) due to disruption of axonal microtubules (McKenzie et al. 1996). The topographical increase in immunoreactivity of APP in white matter tracts is correlated with the distribution of infarction (Fig 4.1). In the rat, the APP accumulations were generally found in the corpus callosum immediately ventral to the anterior cingulate cortex, a region in which pallor in haematoxylin and eosin stained sections was not present after MCA occlusion. In addition increased APP staining was also present in white matter tracts permeating the caudate nucleus but only at the margin of the zones of neuronal necrosis (Fig. 4.9). This is similar to immunocytochemical studies in the human brain where APP immunoreactivity was not observed in the core of the infarct (Ohgami et al. 1992).These findings lend credence to the possibility that focal ischaemia results in accumulation of APP at the periphery of the infarct due to disturbances in axoplasmic flow. Several experiments in the rat support this theory; axonal APP accumulation has been reported to occur after cytoskeletal disruption incurred after needle stab injury (Otsuka et al.

1991) and injections of excitotoxins such as kainic acid (Kawarabayashi et al. 1991; Shigematsu et al. 1992) or ibotenic acid (Nakamura et al. 1992). The possibility that there is increased synthesis following such insults could also account for increased APP immunoreactivity following such insults. In situ hybridisation techniques have shown an increase in APP gene expression in a transectomised facial nucleus (Palacios et al. 1992) and ischaemic brain injuries have been shown previously to induce accumulations of APP in neuronal perikarya of the rat (Stephenson et al. 1992; Kalaria et al. 1993).

In the studies undertaken in the cat and rat described in this thesis, the interpretation that axonal APP immunoreactivity represents damage to axons is supported by the fact that it was found within swollen axons (Fig. 4.8 and Fig. 6.3) and it occurred in the areas bordering the area of infarction where axonal disruption is likely to have taken place (Fig. 4.1). Since APP is transported by fast anterograde axonal transport (Koo et al. 1990), 6 hours in the cat and 24 hours in the rat following MCA occlusion appeared to be adequate time for the protein, which is synthesised in the cell bodies, to be delivered to and accumulate at the site of axonal injury in sufficient quantities for it to be detected. Electron microscope findings would support this view since there was evidence of axotomy with accumulation of APP and organelles suggestive of disrupted axonal transport (Fig. 3.13). The axons in which APP accumulation occurs may thus have viable cell bodies in regions not located within boundaries of the ischaemic lesion. The absence of APP staining within the zone of ischaemic necrosis reflects the intense ischaemia affecting both axons and cell bodies; transport and subsequent accumulation of APP does not occur due to total energy failure.

Until recently it was widely thought that white matter showed greater resistance to ischaemia-induced damage compared to grey matter. However, the results described

above using a variety of markers targeting different structures within axons, contribute to the growing evidence demonstrating the acute vulnerability of axons to cerebral ischaemia in vivo (Dewar and Dawson, 1997; Pantoni et al. 1996). Furthermore, the studies described in both rat and cat models of MCA occlusion indicate that APP may be a useful marker of axonal injury, and, provided that a suitable method of APP quantification could be devised, potentially suitable for the assessment of therapeutic intervention in the protection of white matter following an ischaemic insult.

7.2.2 Does APP accumulation reflect irreversible injury to axons?

One could speculate that within the first few hours of MCA occlusion there exists a 'therapeutic window' during which axons can be saved, however no consensus of opinion on this matter has yet been reached. APP 'swellings', where continuity of the axon is still maintained, may reflect a temporary disturbance in axoplasmic flow which has the potential for recovery. However, the development of APP positive axonal bulbs, whereby secondary axotomy has occurred, may indicate the evolution of irreversible brain damage (Maxwell et al. 1997). The time course of axonal bulb formation in the ischaemic rat model has yet to be established although increased SNAP25 immunoreactivity was demonstrated following 1h of MCA occlusion (Chapter 3). In human head injury, there appears to be a potential for recovery which is time-dependent, in that within the first 10 hours recovery may be possible in just under 35% of the axons whereas from 10 hours onwards, there is potential for recovery in less than 10% of the axons (McKenzie et al. 1996).

7.2.3 Axonal injury: Common mechanisms following head injury and focal cerebral ischaemia

The similarities between the pathobiology of blunt head injury and cerebral ischaemia are increasingly recognised. As previously mentioned, axonal damage, which constitutes a significant feature of brain pathology resulting from blunt head injury, also occurs in response to cerebral ischaemia. The mechanisms underlying axonal damage after blunt head injury are thought to involve cytoskeletal abnormalities and disruption of axonal transport (Bartus, 1997). The susceptibility of axons to blunt head injury is well established and diffuse axonal injury makes a significant contribution to post-injury coma and persistent disability (Gennarelli et al. 1982; Adams et al. 1989). The mechanisms underlying axonal damage after blunt head injury are thought to involve disruption of both neurofilaments and microtubule components of the cytoskeleton leading to disruption of axonal transport (Maxwell et al. 1997). The study described in Chapter 3 using different markers of axonal injury, indicates that events described following head injury may also be features of axonal damage resulting from cerebral ischaemia. Certain details pertaining to axonal anoxic/ischaemic injury overlap with head trauma. Nondisruptive axonal injury causes perturbation of the axolemma, disruption of ionic homeostasis, and Ca^{2+} overload with activation of Ca^{2+} dependent enzymes such as calpains and kinases (Maxwell et al. 1997). Although the primary insults of stroke and head injury may differ, downstream events may be funnelled into a common progression, culminating in irreversible cellular injury (Fig. 7.2). Ischaemic brain damage is by far the most common secondary insult following traumatic brain injury in man and is still found in more than 80% of fatal head injury cases despite modern intensive management (Graham et al. 1989). Although the pathogenesis of ischaemic brain damage is not yet fully understood, it is thought to occur due to the

impairment of the normal regulation of the cerebral vasculature following brain trauma. This then raises the possibility that axonal damage present after blunt head injury may be a consequence not only of the primary insult but also of secondary white matter ischaemia.

Figure 7.2 **Mechanisms of axonal injury following traumatic brain injury and ischaemia**

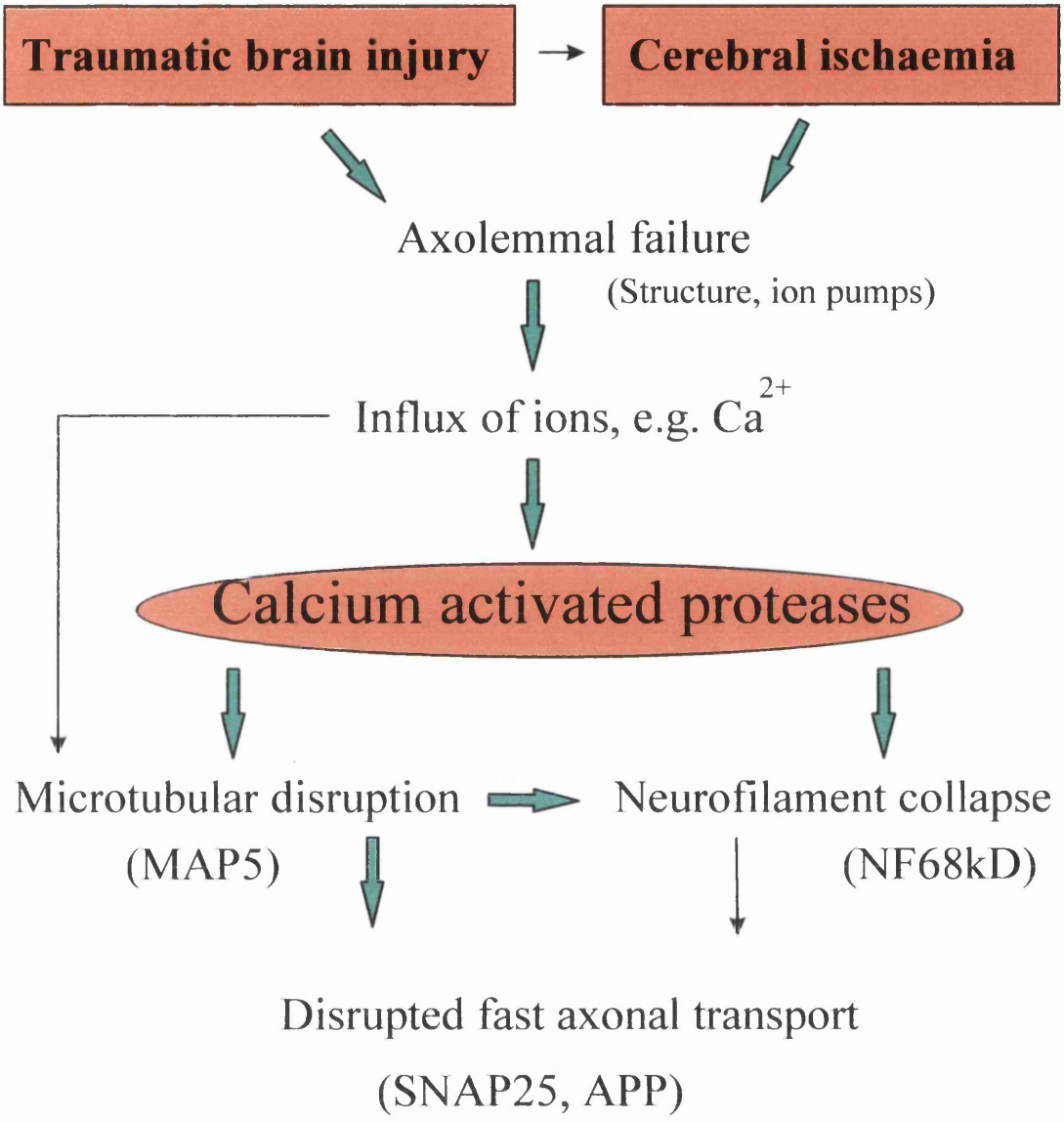

7.3 QUANTIFICATION OF AXONAL INJURY

Changes in the immunostaining of a variety of proteins associated with the neuronal cytoskeleton following cerebral ischaemia have been described in the preceding chapters. The quantitative assessment of acute axonal pathology would be an extremely important tool in studies of axonal injury following cerebral ischaemia, particularly for the assessment of therapeutic intervention. Of the antibodies investigated, APP seemed to be the most promising for this purpose for several reasons. Firstly, APP has previously been established as a marker of axonal injury (Gentleman et al. 1993) and methods for its quantification have been investigated following head trauma (section 1.7.2). Secondly, on a more practical level, APP immunostaining was found to be superior in FAM fixed paraffin embedded material compared to PAM fixed material, the former also being compatible with the accurate delineation of neuronal necrosis. Thirdly, APP could be used successfully in both rat and cat material at concentrations that were economically viable. A variety of methods were investigated for the quantification of APP and are described in detail in Chapter 4, Chapter 6 and Appendix 4. Desired criteria for a method of quantification include ease of use, reliability and robustness. Methods of quantification were initially developed in rat tissue and later refined in the cat tissue. In essence, three methods were assessed; firstly a semi-quantitative method in which sections were visualised by light microscopy and a score ranging from 0-3 allocated based on the quantity and extent of increased APP immunoreactivity; secondly a more complex method of quantification was developed using the image analyser system which measured the area of APP immunoreactivity, distinguishing it from background staining by differences in optical density. Finally, a stereotactic method for measuring area of increased APP immunoreactivity was

developed for use in the cat material. Each method had both advantages and disadvantages.

The semi-quantitative analysis was relatively quick and easy to perform. Some of the shortfalls of this method could be related to the inherent subjectivity associated with it. To minimise subjectivity, all sections had to be assessed in the course of one day to maximise scoring consistency. When a selection of slides were re-scored on a second occasion the correlation was found to be poor in the rat. However, in the cat, semi-quantitative analysis resulted in acceptable intra and inter-rater variability. An explanation for this discrepancy could be that the increased APP immunoreactivity in the cat sections could be visualised with the naked eye rather than having to use the light microscope, thus allowing simultaneous assessment of sections at each coronal level.

The sensitivity of the quantification method is restricted when it is based on a score ranging from only 1-3. This was of particular relevance in the rat in which only 8 coronal levels were assessed, compared to the 16 levels in the cat. The total APP score for each rat was dominated by the number of levels with a score of three. However in the cat, this effect was diluted by the increased number of levels and lower scores over extended distances. This may indicate that increased sensitivity in the rat material could be achieved by increasing the number of coronal levels assessed. The eight levels used in this study had simply been extrapolated from the work of Osborne et al (1987), describing the appropriate levels for calculating volume of infarction following MCA occlusion. Sensitivity of the APP score in the rat tissue could perhaps have been enhanced by assessing sixteen coronal levels, as was the case in the cat, rather than just eight. The other potential pitfall of the semi-quantitative analysis, especially in the rat tissue, was the danger of allocating a similar APP score for dense APP immunoreactivity in a restricted area as for pale APP immunoreactivity with a more

widespread distribution, i.e. inadvertently the method failed to set clear criteria for differentiation of intensity and extent of immunoreactivity. Despite these factors, this semi-quantitative method in both the cat and the rat, demonstrated that the larger the volume of neuronal necrosis, the greater the extent of increased APP immunoreactivity (Fig. 4.3, Fig. 4.10 and Fig. 6.11).

A quantitative method of APP analysis was investigated in rat tissue using the MCID image analyser system (Appendix 4). This was developed to measure the area of increased APP immunoreactivity, differentiating it from background staining by differences in optical density. The theoretical advantage of this technique is that of a more accurate and reliable quantification of APP. However, in practice there were two main sources of errors which reduced this expected accuracy. Firstly, threshold settings had to be manually set by the operator to minimise the inclusion of background staining. As with semi-quantitative analysis, this introduced subjectivity into the technique and consequently correlation of repeated measures was poor. Secondly, the method was very time consuming, requiring multiple steps including visualisation of APP immunoreactivity by light microscopy, image capture, threshold setting for each section and data analysis. Despite investigating a variety of analytical procedures, the methods remained flawed for the reasons just described. This was disappointing since previous reports of quantitative analysis using similar systems have been encouraging (Sutherland et al. 1996; McKenzie et al. 1995). However, the main difference in one of these reports was that the number of positive pre-α cells in cases of Alzheimer's disease in the entorhinal cortex were counted rather than having their area measured as described in Appendix 4. The pre-α cells were of a uniform size and shape, a fact not true for APP swellings or bulbs as seen following focal ischaemia. In another paper describing the quantification of features of Creutzfeldt-Jakob disease (Sutherland et al. 1996), a

completely automated microscope and motorised stage was available which doubtless speeded up proceedings. An algorithm was set for spongiform change recognition which assumed that each site of vacuolation would have a minimum specified diameter. The diameter represented a compromise between the false inclusion of small areas of artifactual tissue separation which can occur in human post mortem tissue and the rejection of genuine areas of fine vacuolation (Sutherland et al. 1996). Unfortunately it would have been difficult to set such criteria for increased APP immunoreactivity since the size was variable and often similar to that of tissue artefacts. However, prion protein analysis was measured by manual setting of image intensity criteria, the authors reporting confidence in the accuracy of the system but failed to verify this statistically (Sutherland et al. 1996).

Following 6h MCA occlusion in the cat, increased APP immunoreactivity was dense and widespread within the white matter. In recent years stereological techniques have been developed to obtain quantitative biological data. This technique could be readily adapted for use in the cat material to assess the area within which there was increased APP immunoreactivity (Fig. 6.6). Images of sections could be captured and printed using the MCID, and using a point square array grid, the number of points superimposed on the area of increased APP immunoreactivity counted. The advantages of this technique were that it was relatively rapid and robust. The correlation between both inter and intra-scorers was very high. Furthermore, the confounding effect of difference in intensity of immunoreactivity was removed, with results reflecting purely the extent of immunoreactivity. The technique was simple and could be readily implemented without the need for high levels of operator skills. Compared to the semi-quantitative methods, the potential usefulness of this method could be attributed to its considerable statistical power, allowing a higher probability of detecting changes in APP

immunoreactivity following putative treatments. In the future it would be interesting to develop a stereologic means of assessing increased APP immunoreactivity in rat sections; this would inevitably be required to be undertaken at the light microscope level.

The other novel technique developed was the topographical mapping of increased APP immunoreactivity and relating this to the region and extent of infarction (Fig. 4.1). This confirmed that APP in white matter tracts is correlated with the distribution of infarction. The main weakness in the technique was that the presence of APP was represented as an 'all or none event', consequently no overall indication of incidence of APP immunoreactivity was captured on the diagrams. This is in contrast to those diagrams showing ischaemic damage where the incidence of damage had been successfully achieved by using a colour scale (Fig. 4.1). Nevertheless, the pictures obtained were very interesting, providing information which had never previously been captured. The development of these techniques were fundamental for the subsequent use of APP as a marker of axonal injury to assess therapeutic interventions in the protection of white matter after an ischaemic insult.

7.4 NEUROPROTECTION: BRAIN PROTECTION?

Until recently virtually no information was available on the mechanisms of anoxic/ischaemic damage in central white matter tracts. Given the drastically different structure and function of grey matter and white matter regions of the mammalian CNS, it is reasonable to expect that these mechanisms may be different. This has important implications for the development of therapeutic intervention in diseases such as stroke and other conditions, such as traumatic brain injury, in which white matter is a prominent target of anoxia/ischaemia.

7.4.1 Glutamate antagonists in clinical trials

The rationale for glutamate antagonists in the treatment of stroke is due to converging lines of evidence from several animal studies which suggest that glutamate plays a pivotal role in the pathogenesis of neuronal cell death following acute focal or global ischaemia of the CNS (Muir and Lees, 1995) (see section 1.5.2). Perhaps the most powerful evidence in support of glutamate-induced neurotoxicity in focal ischaemia comes from many animal studies, performed with a variety of NMDA and non-NMDA glutamate antagonists, and glutamate release inhibitors, in which neuroprotective efficacy has been shown (see section 1.6). The reason that such a variety of different strategies for the development of neuroprotective drugs have been developed is because the cascade of events leading from the onset of stroke to cell damage and infarction is extremely complex. This has resulted in therapeutic intervention being targeted at different points along the injury cascade.

In the early 1990's a wave of clinical trials testing the efficacy of NMDA antagonists in the treatment of cerebral ischaemia was launched (Table 7.1). The results

have generally been disappointing with many trials being suspended. The clinical development of MK-801 was discontinued as a consequence of safety concerns including effects on the cardiovascular system and the finding of vacuolation in the rat brain following MK-801 administration (Wahlgren, 1997). In 1995, patient recruitment in all phase III clinical trials for CGS 19755, Selfotel (a competitive glutamate site NMDA antagonist) was terminated based on a report suggesting that the 'benefit-to-risk' was not significant to warrant continuation of the trial. An acute stroke study of another competitive NMDA antagonist, eliprodil (a polyamine site NMDA glutamate antagonist), was also recently stopped as an interim analysis revealed that, although there were no safety problems, the drug failed to demonstrate a statistically significant difference between active treatment and placebo groups. The latest drug trial to have been discontinued is that using the non-competitive NMDA antagonist, Aptiganel, due to concerns raised over the benefit to risk ratio of the drug treatment.

Two major factors are probably at least partly responsible for the chronicle of failed projects; firstly, the complexity of the clinical situation, and secondly, the lack of animal models of acute CNS injury which can predict the clinical effectiveness of the therapeutic intervention. Some people believe that clinical trials for NMDA antagonists in stroke may have been launched prematurely with less than perfect compounds (Small and Buchan, 1997); others believe that patient selection and imprecise physiological monitoring and control may be partly responsible for the lack of success of clinical trials (J. McCulloch, personal communication). Clearly, it is complex. Undoubtedly, the reasons for drug trial failure are multifactorial. The issue that has not yet been addressed is whether these drugs protect white matter following ischaemia. Perhaps one reason for drug failure is that many drugs have been designed to specifically target grey matter with little attention being paid to white matter.

Table 7.1 Glutamate antagonists and clinical trials

Drug	Mode of Action	Phase	Result	Comments
PRESYNAPTIC				
BW619C89 (Wellcome)	Sodium channel blocker	II	Ongoing	
POSTSYNAPTIC				
Dizocilpine (MK-801) (Merck)	NMDA receptor antagonist Non-competitive, high affinity	II	Suspended	Vacuolar changes within cingulate gyrus neurones Cardiovascular effects, depression of level of consciousness
Aptiganel HCl (Cambridge Neuroscience)	NMDA receptor antagonist Non-competitive, high affinity	III	Suspended	Lack of evidence for clinical efficacy
Dextrorphan (Hoffman-LaRoche)	Channel blocker Non-competitive, Intermediate affinity	II	Suspended	Hypotension
Remacemide (Astra)	Channel blocker Non-competitive, Low affinity	II	Suspended	
Eliprodil (SyntheLabo Lorex)	NMDA receptor antagonist Competitive, Polyamine site	III		No beneficial effect Lack of specificity, Cardiovascular side effects
Selfotel (Ciba-Geigy)	NMDA receptor antagonist Competitive	III		No change in benefit-to-risk

7.4.2 Cerebral white matter is highly vulnerable to ischaemia

White matter has classically been considered less vulnerable than grey matter to ischaemic injury initiated by a large artery occlusion (Marcoux et al. 1982). However, a recent spate of papers, in addition to the results reported in the preceding chapters of this thesis, suggest that cerebral white matter is in fact highly vulnerable to an ischaemic insult (Pantoni et al. 1996; Dewar and Dawson, 1997; Yam et al. 1997). White matter is critical to motor, sensory, visual and higher cerebral function (Filley, 1998). As an indispensable component of the neural networks, cerebral white matter contributes to the functional architecture of the brain. Structural or metabolic disturbances of white matter may result in functional impairments of the numerous networks within the brain, even if neurons are intact. Following most cases of stroke in man, there is infarction which, by definition, means pannecrosis of all cellular elements including those in both grey and white matter. Because of the essential role of white matter for brain function, the necessity for treatments to protect the brain as a whole is paramount.

7.4.3 NMDA antagonists: preservation of white matter?

In the case of ischaemic injury, one approach to treatment is to attenuate secondary damage propagation by blocking the NMDA receptors using suitable antagonists (for review see Muir and Lees, 1995). These receptor-operated channels are widely distributed on cell bodies of CNS neurons (section 1.5.2). Their apparent absence in white matter (Jones and Baughman, 1991) raises the question as to whether NMDA-receptor channels play a role in acute injury of CNS white matter.

In a recent study, partial crush lesion was inflicted on the optic nerve of adult rats and was followed immediately by an injection of MK-801 (Yoles et al. 1997). Protection of neurons from secondary degeneration was assessed by retrograde labelling

of the ganglion cells and by measurement of the visual evoked potential response to light. Two weeks after injury, the mean number of neurons that were still intact was about three times higher in the MK-801 treated group than in the saline treated group, indicating a treatment induced protection of neurons that had escaped primary injury. A positive visual evoked potential was obtained in 90% of the MK-801 treated animals but in only 50% of injured controls. These results indicate that treatment with MK-801 following partial crush injury of the optic nerve results in the protection of initially spared neurons from secondary degeneration. It is most likely that the primary site of action of MK-801 is at the retinal ganglion cells rather than at the lesion site itself as the former express high levels of NMDA receptors. It cannot be ruled out that the site of the MK-801 was directly on either the optic nerve fibres or on their associated astrocytes.

In the study just described, the protection of cell bodies from secondary degeneration following a primary lesion of the optic nerve was assessed. The question remains as to whether MK-801 protects both neuronal cell bodies and axonal fibres following a primary insult such as ischaemia. To address this question, experiments were undertaken in both the rat and cat and are described in this thesis. APP has been found to be a suitable marker of axonal injury (section 7.2.1) and a method for APP quantification has been developed (section 7.3). The primary hypothesis being tested was that if MK-801 protects axons, the APP score should be reduced. Rats were subjected to MCA occlusion and the axonal injury in the two groups of animals, a vehicle group and an MK-801 group, were compared. MK-801 resulted in a 15% reduction of neuronal necrosis but there was little difference in the APP score between the groups. Furthermore, subgroup analysis which was performed to tease out trends within the data, revealed no evidence of a reduced APP score following MK-801 treatment. The cat offered a number of advantages over the rat for assessment of axonal

injury allowing the limitations encountered in the rat study to be overcome (section 7.3). Following 6h of focal cerebral ischaemia in the cat, the MK-801 treated group had a reduction in cerebral hemisphere neuronal necrosis of about 30%. A highly reproducible method of APP quantification revealed that there was no such reduction in APP accumulation score in the MK-801 group of animals. Overall, the quantitative mean APP score in the MK-801 treated group was significantly higher than the APP score in the vehicle treated group. In addition, the amount of axonal injury, as assessed by the quantitative APP score, was corrected for the size of ischaemic damage thus allowing the effect of MK-801 on the ratio of white matter:grey matter injury to be established (Table 6.7 and Fig. 6.13). The difference in the ratios between the vehicle treated animals and drug treated animals was significantly different. The finding that the APP score was not reduced following MK-801 administration suggests that MK-801 fails to protect axons following focal cerebral ischaemia.

Given that MK-801 has progressed to clinical trials, it is of great significance that MK-801 failed to reduce the APP score at any of the 16 coronal levels studied in the cat and failed to cause a reduction in the total APP score in drug treated animals compared to vehicle treated animals following MCA occlusion. The possibility that the drug effects were insufficient to reveal a protective effect on axonal injury as assessed by the APP score cannot be disregarded. Additionally it is possible that the method of quantification of APP was inadequate. This may be more pertinent to the studies undertaken in the rat tissue in which the semi-quantitative scoring method was less reproducible and subject to more error than that developed for the cats. Nevertheless, the findings described provide no evidence to suggest that MK-801 protects axons. Other approaches to support and verify these findings are now required.

As had been the aim, a method was developed to mark and quantify axonal injury and was then applied in both the cat and rat following drug intervention. The utility of this method in the rat will remain unclear until a positive control can be demonstrated whereby the APP score is reduced following MCA occlusion; in this regard, a drug that is markedly protective of white matter is eagerly awaited. The application of the technique using negative controls, is much more difficult to evaluate. Despite similar drawbacks in the cat experiments to that in the rat, the cat, due to its greater volume of white matter, provided greater value to the investigation. MK-801 showed no evidence of axonal protection following an ischaemic insult. Based on these findings, it is not unreasonable to hypothesise that clinical trial failure using glutamate antagonists, which have been specifically tailored to exert effects on neuronal cell bodies, may in part be due to the lack of protection of functionally essential white matter tracts. With this in mind, therapeutic strategies should be aimed at the protection of both grey and white matter. 'Brain protection', rather than neuroprotection, is perhaps the key to future success.

7.5 THE FUTURE

Historically, the study of structural changes affecting the cerebral white matter after a single artery occlusion has been neglected in favour of experiments that evaluate volume of neuronal necrosis (Osborne et al. 1987). This outcome measure has been chosen so that it may be measured precisely and comparisons can then be made between studies. Such is the case for proximal MCA occlusion where the striatum is always infarcted and irreversibly damaged. However, the relationship of the outcome measure of this model (the reduction in volume of cortical infarct) has little correlation to functional

outcome (Rogers et al. 1992). Damage to the striatum would leave a human subject paralysed. Only rarely have the histological changes of white matter components during the first few hours after occlusion of a large cerebral artery been reported (Pantoni et al. 1996). As yet, there is no clear consensus on the best measures of outcome but clearly functional recovery is the end-point most relevant to the patients. Therefore, if the outcome measure is the reduction in the volume of brain damage, it is also necessary to ascertain whether it is accompanied by improved functional outcome. Ideally the outcome measures after experimental stroke in animals should be multiple, and include morphological, biochemical, functional and behavioural assays with more emphasis being placed on assessing improvement in functional deficits, such as impaired cognition or motor co-ordination, in relation to the cerebroprotective properties of a drug. An alternative approach to immunocytochemistry for the assessment of axonal injury would be the use of the deoxyglucose method. Since glucose is almost the sole substrate for cerebral oxidative function, and its utilisation is stoichiometrically related to oxygen consumption, the analogue 2-deoxy-D-(^{14}C) glucose, allows glucose metabolism to be traced and the measure of local cerebral glucose utilisation to be measured by the autoradiographic technique (for review see Kennedy et al. 1992). In addition, the development of improved imaging techniques which can be used for man and animals, may result in more power to pick up a drug effect in white matter than would various rating scales of neurological impairment of functions of daily living activities.

The current findings looking at axonal pathology emphasise the need for future drug therapies for cerebral ischaemia to target, or at least to operate so as to include white matter injury. With this in mind, experimental protocols which are necessary when evaluating potential neuroprotective drugs in order to be able to claim that the

compound is worthy of serious evaluation as a candidate drug, must include the evaluation of white matter. With a greater understanding of the details of pathophysiology of white matter injury, we will be in a better position to design combinations of interventions specifically tailored to each tissue type. For example, glutamate antagonists for grey matter with Na^{+}-Ca^{2+} exchange blockers for white matter, or to select common events for inhibition, such as sodium channel blockade. As William Holt so eloquently said, 'Neurons are transmogrified by necrotic vicissitude or apoptotic predisposition into noisome nebulae that are aesthetically pleasing to only the nappiest of neuronecrophiliacs' (Holt, 1997). Drug development to prevent a similar outcome for axons following ischaemia would be ideal.

APPENDIX 1

SOURCES OF COMMONLY USED MATERIALS

Monoclonal Anti-MAP1b (MAP5)	Sigma	Product no. M-4528
Monoclonal anti-β-Tubulin	Sigma	Product no. T-4026
Monoclonal Anti-Neurofilament 68	Sigma	Product no. N-5139
Monoclonal Anti-Alzheimer Precursor Protein (clone 22C11)	Boehringer Mannheim	
Normal Horse Serum	Vector	S-2000
Biotinylated Anti-Mouse IgG (H + L) (Rat adsorbed) Made in horse	Vector	BA-2001
Vectastain® *Elite* ABC Kit (Mouse IgG)	Vector	PK-6102
Vectastain® Standard Peroxidase Kit	Vector	PK-4000
DAB Substrate Kit for Peroxidase	Vector	SK-4100
Poly-L-Lysine solution	Sigma	P 8920

APPENDIX 2

STOCK SOLUTIONS AND BUFFERS

Tris Buffer

Dissolve 24.4 g Tris in 200 ml of distilled water

Add 148 ml of 1 N HCl

Dilute to 4 l with distilled water

pH to 7.6 $\pm$ 0.2

Tris buffered saline

1 part tris buffer to 9 parts saline

Citrate Buffer for microwaving

Citric acid 8.4 g

4 l of distilled water

pH to 6.0 using 1 M NaOH

Store in fridge

Preparation of PAM fixative

Require 200 ml per animal

Shelf life is 1 week at 4°C

Make up appropriate volume of phosphate buffer

Weigh out PAM in fume cupboard (4 g/100 ml PB)

Add PAM to buffer and heat to 60-65°C on heated stirrer in fume hood.

Once dissolved completely leave to cool

Preparation of Poly-L-Lysine slides

Clean racks in 1 % acid alcohol to remove any residual dye

Wash well in running tap water

Load racks with slides and place in poly-L-Lysine solution.0.1 % solution diluted with distilled water for 5 minutes at room temperature

Drain well and dry at room temperature covering to prevent dust

MATERIALS FOR ELECTRON MICROSCOPY

Resin

A)	Durcupan A/M Epoxy Resin	10g
Sigma (D-0291 Lot 74H2526)		
B)	Dodecenyl Succinic Anhydride (DDSA)	10g
Agar Scientific Ltd R1053		
C)	2,4,6-Tri (dimethylaminomethyl) phenol (DMP-30)	0.3g
Agar Scientific Ltd R1065		
D)	Dibutyl Phthalate	0.3g
Agar Scientific Ltd R1071		

For resin, the components A:B:C:D were mixed in a disposable plastic beaker.

Uranyl acetate

Use a saturated solution of uranyl acetate in 50% methanol.

Filter before use.

Lead Citrate

Dissolve 1.3g lead nitrate in 30 ml distilled water and add 1.76g sodium citrate.

Shake in a 50 ml volumetric flask. Let stand for 30 minutes with intermittent shaking.

Add 8 ml 1M NaOH to clear and dilute to 50 ml with distilled water.

Mix by inversion.

Store in well filled, tightly stoppered bottles.

APPENDIX 3

HAEMATOXYLIN AND EOSIN STAINING FOR PARAFFIN SECTIONS

- Histoclear 10 min
- 100% alcohol 2 min
- 95% alcohol 2 min
- Wash in water
- Haematoxylin 2-3 min
- Wash in water
- Acid alcohol seconds
- Wash in water
- Scot's tap water until sections turn blue
- Eosin 3 min
- Wash in water
- 95% alcohol 2 min
- 100% alcohol 2 min
- Histoclear
- Mount in DPX

LUXOL FAST BLUE STAINING FOR PARAFFIN SECTIONS

- Histoclear 10 min
- 100% alcohol 2 min
- 95% alcohol 2 min
- Luxol fast blue 3-4 h
- Methylated spirit 5-10 min
- Wash in water 10 min
- Lithium carbonate few seconds
- 70% methylated spirits until background clear and myelin blue
- Wash in water
- Cresyl violet 5-10 min
- Wash in water
- Acid alcohol (acetic acid in methylated spirit)
- 95% alcohol 2 min
- 100% alcohol 2 min
- Histoclear
- Mount in DPX

APPENDIX 4

DENSITOMETRIC ANALYSIS OF APP IN THE RAT

A4.1 METHOD

In order to investigate a quantitative assessment of the relationship between increased APP immunoreactivity and infarction, a standard section from each animal was selected for evaluation. This corresponded to coronal level 3, the level of the septal nuclei, as previously described (Osborne et al. 1987) from the atlas of Konig and Klippel (1963). In total 13 sections, one from each animal, was analysed.

For the purpose of quantitative analysis of APP, the 'Microcomputer Imaging Device' (MCID), an image analysis package, proprietary to 'Imaging Research Inc.', was used. Since the images are a mosaic of pixels, and measurements based on pixel counts are completely dependent upon magnification, it was necessary to calibrate the system. Pixels were therefore calibrated to a scale using microns. A standard distance was captured on the computer screen with the x 2.5 objective by using a reticule which was provided with the MCID system. A horizontal line was drawn and the number of pixels for the distance counted (Fig. A4.1). The procedure was repeated for the vertical axis. System resolution could be increased either by increasing the number of pixels in an image, or by increasing the image magnification so that a smaller area fills a fixed number of pixels.

The simplest criterion for APP detection was optical density since APP was visualised as a brown precipitate. A blue filter was used when capturing images to enhance the contrast between the positive stain and the counterstain which had been used on the tissue. Increased APP immunoreactivity was recognised by the computer in

terms of image intensity. This process involved setting an image intensity threshold so that increased APP immunoreactivity was defined such that all pixels darker or lighter than the threshold values were ignored. Pixels lying within the threshold density range were valid targets and the area of pixels in this threshold range measured. These thresholds were chosen to optimise selection of increased APP immunoreactivity whilst minimising inclusion of artifactual tissue. This interactive thresholding for each section, rather than automated image thresholding, was necessary due to the variability in staining of the sections.

The region of interest i.e. the scan area, was selected by the operator and the area of increased APP immunoreactivity (within the scan area and threshold range) was subsequently measured. In order to quantify the area of increased APP immunoreactivity in a repeatable manner, it was necessary to develop a method of analysis whereby the maximum area of increased APP immunoreactivity was measured whilst minimising tissue artefact inclusion which lay within the image intensity threshold range. Two different methods for achieving this were investigated and are described below.

Method 1: Contralateral and ipsilateral artefact considerations

The system was calibrated using the x 2.5 objective. Each section was viewed by light microscopy and digitised so that the image was seen on the monitor. An image intensity threshold was chosen to define the increased APP immunoreactivity on the ipsilateral hemisphere. In order to compensate for the inclusion of artefact within the threshold range in the ipsilateral hemisphere, it was assumed that there was a similar area of artefact within the threshold range in the contralateral hemisphere. The area of artefacts within the threshold range in the contralateral regions were therefore measured and deducted from the equivalent ipsilateral regions of interest. Consequently, in total four

regions were analysed, namely; ipsilateral corpus callosum, contralateral corpus callosum, ipsilateral caudate and contralateral caudate. Since the total areas of interest could not be visualised on the monitor at the x 2.5 magnification, images were captured and 'patched together' so that the complete area of interest was analysed. Figure A4.2A and A4.2B illustrates this method of analysis for the caudate. All measurements were repeated on two consecutive days, the operator unaware of the prior threshold settings, to assess method reproducibility.

Method 2: Exclusion of artefacts in ipsilateral hemisphere

The calibration and image intensity range were set as described above. In order to minimise inclusion of tissue artefact, rather than selecting the whole corpus callosum and caudate as previously described in method 1, the scan area was selected to only include (as far as possible) the increased APP immunoreactivity within these regions of interest. Animals which did not have any increased APP immunoreactivity in the ipsilateral hemisphere in the coronal level 3 were not included. Since there were minimal tissue artefact included in the scan areas, assessment of the contralateral hemisphere was not required. Figure A4.2C and 2D illustrates this method of analysis.

The same procedure was repeated using the x 5 objective rather than the x 2.5 objective to magnify the image. Each method was assessed for reproducibility by comparing the results obtained on two consecutive days. Graphs were plotted for each method and linear regression analysis performed (Fig. A4.3).

Figure A4.1 Spatial - Distance Calibration

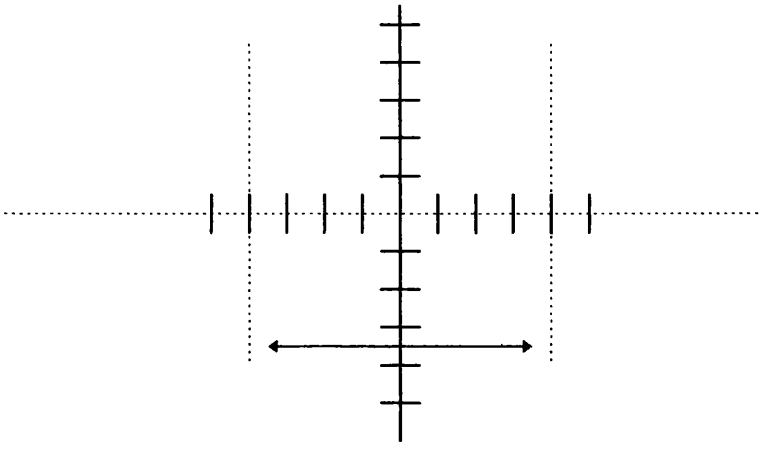

The spatial-distance calibration procedure allows the conversion of pixels to real distances. With distance calibrated, the MCID can provide fully quantitative values for area.

For the x 2.5 magnification:

	Pixels	μm	
Horizontal	601	3,000	pixels/μm : 0.200
Vertical	432	2,000	pixels/μm : 0.226

For the x 5 magnification:

	Pixels	μm	
Horizontal	556	1,400	pixels/μm : 0.397
Vertical	405	900	pixels/μm : 0.450

Figure A4.2 Quantification of APP

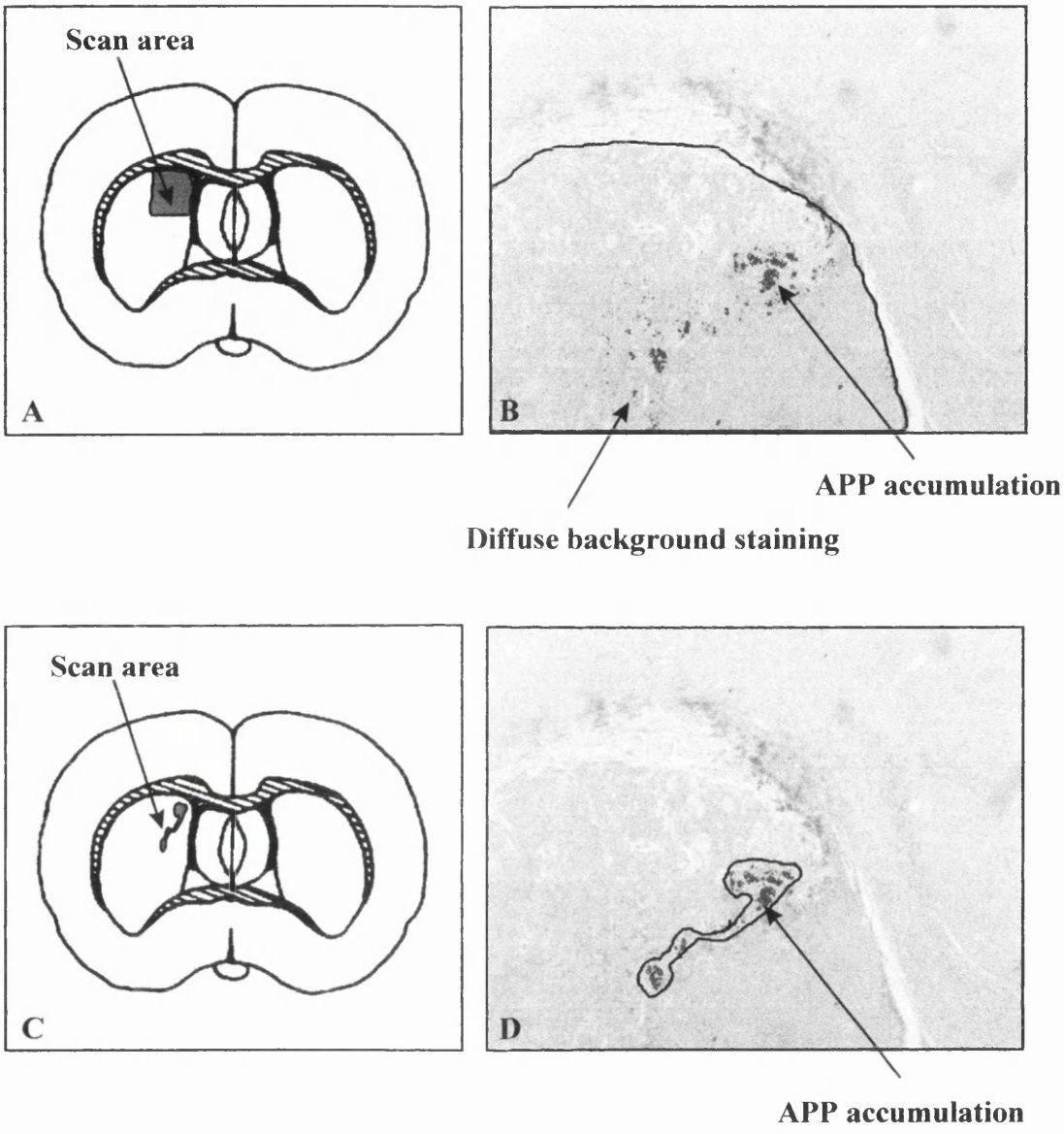

Representation of the two methods of quantification of APP accumulation. Method 1: A, the entire ipsilateral caudate is scanned and threshold range selected. Target area in the contralateral caudate, at the same threshold, is deducted from ipsilateral target area. B, computer output showing scan area as seen in A with recognition of artefacts and APP accumulation within the target range. Method 2: C, scan area in method 2 selected to include only APP accumulations. D, computer output showing scan area as seen in C. There is minimal inclusion of tissue artefacts within the threshold range.

Figure A4.3 Assessment of reproducibility for quantitative APP analysis

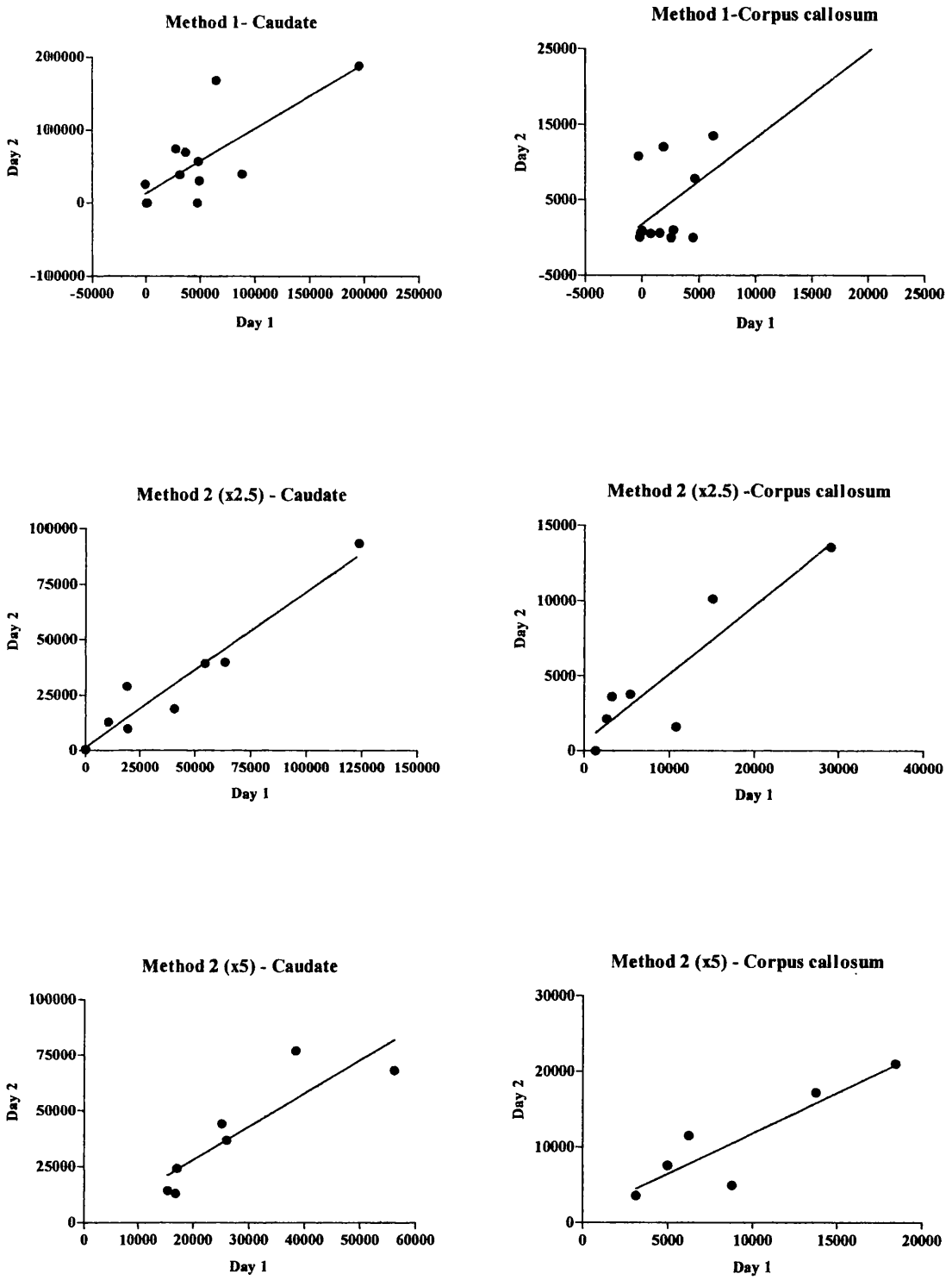

Relationship of APP area in the caudate nucleus and corpus callosum on day 1 and day 2. The quantity of APP was assessed at coronal level 3 for each animal using different methods as described above. This analysis was repeated for each animal and the correlation co-efficient calculated. The line of linear regression is shown for each graph.

A4.2 RESULTS

A4.2.1 Reproducibility of quantitative analysis

For the quantitative analysis using the MCID system, repeated measures for each method were drawn on scatter plots to assess reproducibility. The equation for each line was derived by a least-squares regression method. A summary of the gradient (m), correlation co-efficient (r) and (r^2) for each line is summarised in the Table A4.1. Using method 1 (in which the entire ipsilateral hemisphere is analysed), the r^2 values, 0.59 for the caudate nucleus and 0.64 for the corpus callosum, suggest a lack of linearity of the response i.e. a high accumulation score on one day may be low the next and vice versa. However, in method 2 (in which the scan area is selected to include only APP accumulations) at the lower system resolution, the m value for the corpus callosum indicates that the values obtained on day 1 (0.46) are approximately half the values obtained on day 2 (0.70). However, the r^2 values of 0.82 and 0.93 indicate that by using this method, APP accumulation measurements remain consistent relative to each other (i.e. a good linearity of response). With increased system resolution, the r^2 value for each line is 0.80 and 0.77, again suggesting that the relationship of APP accumulation between sections is consistent on a day to day basis. The consistency of values (as indicated by the slope of the line) was also good, particularly for the corpus callosum where m was 1.07. In conclusion, method 2 could potentially be a useful method of quantitative analysis of APP provided that all comparative analysis is performed in one sitting to ensure consistency of results.

Table A4.1 Linear regression analysis of repeated measures

	Method 1		Method 2 (x 2.5)		Method 2 (x 5)	
	Corpus callosum	Caudate nucleus	Corpus callosum	Caudate nucleus	Corpus callosum	Caudate nucleus
Slope	1.15	0.89	0.46	0.70	1.07	1.50
Correlation co-efficient, r	0.80	0.77	0.90	0.96	0.89	0.88
r^2	0.64	0.59	0.82	0.93	0.80	0.77
p	0.001	0.002	0.005	0.0001	0.02	0.009
n	13	13	13	13	13	13

The slope, correlation co-efficient, r and r^2 values for the repeated measures using the different methods of densitometric analysis of APP accumulation. Method 1; the entire ipsilateral caudate is scanned and threshold range selected. The target area in the contralateral caudate, at the same threshold, is deducted from the ipsilateral target area. Method 2; the scan area is selected to only include increased APP immunoreactivity so that there is minimal inclusion of tissue artefact within the threshold range.

Figure A4.4 Relationship of area of APP immunoreactivity to volume of infarction

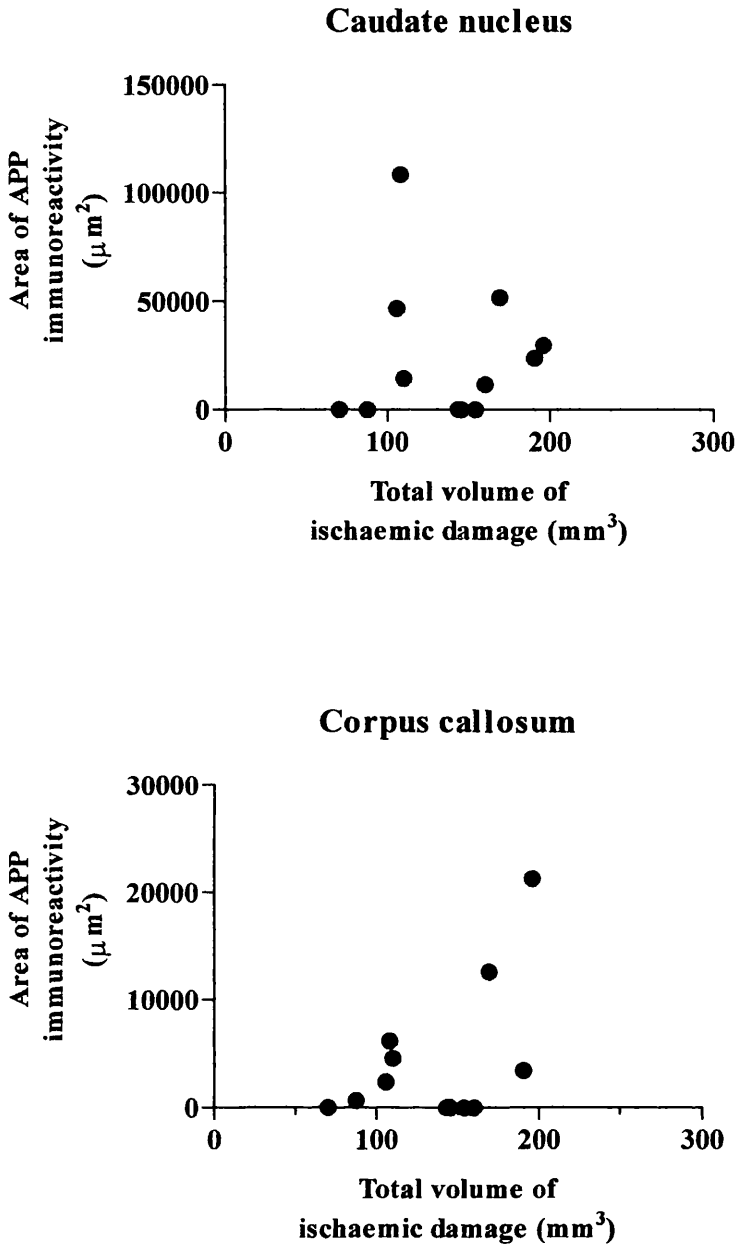

The volume of ischaemic damage was compared to area of APP immunoreactivity at coronal level 3 in the caudate nucleus and corpus callosum as assessed by quantitative analysis using method 2 (in which the scan area was selected to only include increased APP immunoreactivity). Each point represents data from a single animal.

A4.2.2 Relationship between ischaemia and APP accumulation

For the quantitative analysis, based on the reproducibility findings, it was decided to analysis further the results obtained using method 2 (exclusion of artefacts in ipsilateral hemisphere) at the low system resolution. The mean area of APP immunoreactivity in the caudate nucleus and mean area of APP immunoreactivity in the corpus callosum (from measurements on day 1 and day 2) at coronal level 3 were compared to volume of neuronal necrosis for each rat (Fig. A4.4). In the caudate nucleus there did not appear to be a direct relationship between area of APP accumulation and total volume of ischaemic damage. However, in the corpus callosum there is a more obvious relationship although this does not quite reach significance. Since the values represent only those for coronal level 3, no firm conclusions can be drawn.

A4.3 DISCUSSION

In order to use APP as a quantitative marker of axonal injury, and to assess the potential beneficial effects of therapeutic intervention, a reliable method of quantifying the increased APP immunoreactivity is required. It is now also feasible to consider using quantitative image analysis techniques as a substantial part of the assessment process; however, as with the semi-quantitative analysis, it is necessary to test and validate these approaches before they are used for investigative purposes. An inherent problem with immunocytochemistry is that of diffuse background staining. Since APP immunoreactivity was defined by optical density, inclusion of artefacts and diffuse background staining, which were of similar optical density to the APP immunoreactivity, were considered to be a likely source of error. It is for this reason that different methods of analysis of APP immunoreactivity were developed and

investigated. In the first method, it was assumed that the area of artefact in both ipsilateral and contralateral hemispheres would be comparable. Therefore, at the same threshold setting, the contralateral target area was deducted from the ipsilateral target area, in order to negate the artifactual effects. In the second method the scan area was drawn as closely round the target areas as possible to minimise the inclusion of background staining and artefacts. The repeatability using this method was superior to that used in method 1, particularly at the higher system resolution.

Precautions were taken to try to maintain constancy throughout the experiments, including using the same calibration, microscope filter and light intensity. However, using either method, two obvious areas that required operator intervention in the measurement of increased APP immunoreactivity were the field selection and image thresholding stages. To quantify APP within the corpus callosum and caudate in a repeatable manner it was necessary that the delineation of anatomic boundaries was accurately selected from each section prior to analysis. This function was performed manually. This is particularly pertinent to method 1, in which the scan area was much larger than that used in method 2. The greater the variation in scan area, the greater the variation in background staining and artefacts included. Secondly, operator intervention in the image thresholding stage was considered a source of error since it represented a compromise between the false inclusion of small areas of artifactual tissue and the rejection of genuine areas of increased APP immunoreactivity. The two methods of analysis were designed in order to minimise this error. Ideally, target criteria other than optical density would be included, such as that of target size, to ensure that targets are more clearly discriminable from the background. However, this was extremely difficult to apply to APP staining since often the accumulations were of similar size to the artefacts. Furthermore, due to the differences in staining and counterstaining between

sections, it was necessary to reset the threshold range for each section. This problem could potentially be overcome by staining and counterstaining all of the sections in one batch.

The images for both quantitative methods were captured using a monochrome system, each pixel being allocated a grey level value based on the brightness and intensity of the image. Although not undertaken, another option would have been to capture images using a colour system; the advantages being that the colour system is more sophisticated operating using red, green and blue channels. Ultimately, information capacity is increased and the system is better equipped for detecting subtle changes of the image as compared to monochrome systems (McKenzie et al. 1995).

Overall, the quantitative method of analysis was quite time consuming and automation of the technique would be necessary to make it more suitable for routine use. Method 2 appeared to be the quantitative method of choice, probably using the lower system resolution for speedier results. The results discussed only focus on coronal level 3 and it would be interesting in the future to assess the other 7 coronal levels using this method to give a more precise measure of APP immunoreactivity for each animal. Because of the ease with which semi-quantitative analysis could be performed, and the fact that it showed that APP accumulation is determined by lesion size, the semi-quantitative method was chosen for the quantification of APP following therapeutic intervention in the rat (Chapter 5).

REFERENCES

Adams, J.H., Mitchell, D.E., Graham, D.I. and Doyle, D. (1977) Diffuse brain damage of immediate impact type: Its relationship to 'primary brainstem damage' in head injury. *Brain* 100, 487-502.

Adams, J.H., Graham, D.I., Scott, G., Parker, L. and Doyle, D. (1980) Brain damage in fatal non-missile head injury. *J. Clin. Pathol.* 33, 1132-1145.

Adams, J.H., Graham, D.I., Murray, L.S. and Scott, G. (1982) Diffuse axonal injury due to non-missile head injury in humans: An analysis of 45 cases. *Ann. Neurol.* 12, 557-563.

Adams, J.H., Graham, D.I. and Gennarelli, T.A. (1983) Head injury in man and animals. *Acta Neurochir.* 32, 15-30.

Adams, J.H., Doyle, D., Ford, I., Graham, D.I. and McLellan, D. (1989) Diffuse axonal injury in head injury;Definition, diagnosis and grading. *Histopath.* 15, 49-59.

Allinquant, B., Moya, K.L., Bouillot, C. and Prochiantz, A. (1994) Amyloid precursor protein in cortical neurons: coexistence of two pools differentially distributed in axons and dendrites and association with cytoskeleton. *J. Neurosci.* 14, 6842-6854.

Amaratunga, A., Leeman, S.E., Kosik, K.S. and Fine, R.E. (1995) Inhibition of kinesin synthesis in vivo inhibits the rapid transport of representative proteins for three transport vesicle classes into the axon. *J. Neurochem.* 64, 2374-2376.

Arvin, B., Neville, L.F., Barone, F.C. and Feuerstein, G.Z. (1996) The role of inflammation and cytokines in brain injury. *Neuroscience and Biobehavioural Reviews* 20, 445-452.

Baird, A.E. and Warach, S. (1998) Magnetic resonance imaging of acute stroke. *J. Cereb. Blood Flow Metab.* 18, 583-609.

Bamford, J., Sandercock, P., Jones, L. and Warlow, C. (1987) The natural history of lacunar infarction: the Oxfordshire community stroke project. *Stroke* 18, 545-551.

Bartus, R.T., Hayward, N.J., Elliott, P.J., Sawyer, S.D., Baker, K.L., Dean, R.L., Akiyama, A., Straub, J.A., Harbeson, S.L., Li, Z., Powers, J. and Kontos, H.A. (1994) Calpain inhibitor AK295 protects neurons from focal brain ischemia: Effects of postocclusion intra-arterial administration. *Stroke* 25, 2265-2270.

Bartus, R.T. (1997) Calpain inhibition: A common therapeutic rationale for treating multiple neurodegenerative conditions? In: Bar, P.B. and Beal, F.M. (Eds.) *Neuroprotection in CNS diseases*, pp. 71-86. New York: Marcel Dekker

Bennett, V. (1985) The membrane skeleton of human erythrocytes and its implications for more complex cells. *Annu. Rev. Biochem.* 54, 273-304.

Blumbergs, P.C., Scott, G., Manavis, J., Wainwright, H., Simpson, D.A. and McLean, A.J. (1994) Staining of amyloid precursor protein to study axonal damage in mild head injury. *Lancet* 344, 1055-1056.

Blumbergs, P.C., Scott, G., Manavis, J., Wainwright, H., Simpson, D.A. and McLean, A.J. (1995) Topography of axonal injury as defined by amyloid precursor protein and the sector scoring method in mild and severe closed head injury. *J. Neurotrauma* 12, 565-572.

Bonita, R. (1992) Epidemiology of stroke. *Lancet* 339, 342-344.

Bostock, H. and Grafe, P. (1985) Activity-dependent excitability changes in normal and demyelinated rat spinal root axons. *J. Physiol. (Lond)* 365, 239-257.

Brierley, J.B. and Graham, D.I. (1984) Hypoxia and vascular disorders of the central nervous system. In: Adams, J.H., Corsellis, J.A.N. and Duchen, L.W. (Eds.) *Greenfield's Neuropathology*, 4th edn. pp. 125-207. London: Edward Arnold

Brown, A.M., Fern, R., Jarvinen, J.P., Kaila, K. and Ransom, B.R. (1998) Changes in $[Ca2+]_0$ during anoxia in CNS white matter. *NeuroReport* 9, 1997-2000.

Bullock, R. (1998) Strategies for neuroprotection with glutamate antagonists. In: Boland, B., Cullinan, J. and Kimball, C. (Eds.) *Neuroprotective agents. Clinical and experimental aspects*, pp. 272-278. New York: New York Academy of Sciences

Butcher, S.P., Bullock, R., Graham, D.I. and McCulloch, J. (1990) Correlation between amino acid release and neuropathological outcome in rat striatum and cortex following middle cerebral artery occlusion. *Stroke* 21, 1727-1733.

Card, J.P., Meade, R.P. and Davis, L.G. (1988) Immunoctyochemical localization of the precursor protein for b-amyloid in the rat central nervous system. *Neuron* 835-846.

Carswell, H.V.O., McCulloch, J., Dominiczak, A.F. and Macrae, I.M. Genetics of stroke: the search for phenotypes in the stroke-prone spontaneously hypertensive rat (SHRSP). *In press* (Abstract)

Chiu, S.Y. and Ritchie, J.M. (1982) Evidence for the presence of potassium channels in the internode of frog myelinated nerve fibres. *J. Physiol. (Lond)* 322, 485-501.

Chiu, S.Y. and Ritchie, J.M. (1984) On the physiological role of internodal potassium channels and the security of conduction in myelinated nerve fibers. *Proc. R. Soc. Lond* 220, 415-422.

Choi, D.W. (1990) Cerebral hypoxia:Some new approaches and unanswered questions. *J. Neurosci* 10, 2493-2501.

Christman, C.W., Grady, M.S., Walker, S.A., Holloway, K.L. and Povlishock, J.T. (1994) Ultrastructural studies of diffuse axonal injury in humans. *J. Neurotrauma.* 11, 173-186.

Cleveland, D.W., Monteiro, M.J., Wong, P.C., Gill, S.R., Gearhart, J.D. and Hoffman, P.N. (1991) Involvement of neurofilaments in the radial growth of axons. *J. Cell. Sci.* Suppl 15, 85-95.

Conn, P.J. and Pin, J. (1997) Pharmacology and functions of metabotropic glutamate receptors. *Ann. Rev. Pharmacol. Toxicol.* 37, 205-237.

Coria, F., Moreno, A., Torres, A., Ahmad, I. and Ghiso, J. (1992) Distribution of Alzheimer's disease amyloid protein precursor in normal human and rat nervous system. *Neuropathol. Appl. Neurobiol.* 18, 27-35.

Coyle, P. and Heistad, D.D. (1991) Development of collaterals in the cerebral circulation. *Blood Vessels* 28, 183-189.

Dawson, D.A. and Hallenbeck, J.M. (1996) Acute focal ischemia-induced alterations in MAP2 immunostaining: description of temporal changes and utilization as a marker for volumetric assessment of acute brain injury. *J. Cereb. Blood Flow Metab.* 16, 170-174.

Dewar, D. and Dawson, D.A. (1997) Changes of cytoskeletal protein immunostaining in myelinated fibre tracts after focal cerebral ischaemia in the rat. *Acta. Neuropathol.* 93, 71-77.

Dirnagl, U., Tanabe, J. and Pulsinelli, W. (1990) Pre- and post-treatment with MK-801 but not pretreatment alone reduces neocortical damage after focal cerebral ischemia in the rat. *Brain Res.* 527, 62-68.

Duc, C. and Catsicas, S. (1995) Ultrastructural localization of SNAP-25 within the rat spinal cord and peripheral nervous system. *J. Comp. Neurol.* 356, 152-163.

Duverger, D. and MacKenzie, E.T. (1988) The quantification of cerebral infarction following focal ischemia in the rat: influence of strain, arterial pressure, blood glucose concentration, and age. *J. Cereb. Blood Flow Metab.* 8, 449-461.

Erb, D.E. and Povlishock, J.T. (1988) Axonal damage in severe traumatic brain injury: an experimental study in cat. *Acta Neuropathol. Berl.* 76, 347-358.

Fern, R., Waxman, S.G. and Ransom, B.R. (1994) Modulation of anoxic injury in CNS white matter by adenosine and interaction between adenosine and GABA. *J. Neurophysiol.* 72, 2609-2616.

Fern, R., Ransom, B.R. and Waxman, S.G. (1995a) Voltage-gated calcium channels in CNS white matter: Role in anoxic injury. *Journal of Neurophysiology* 74, 369-377.

Fern, R., Waxman, S.G. and Ransom, B.R. (1995b) Endogenous GABA attenuates CNS white matter dysfunction following anoxia. *J. Neurosci.* 15, 699-708.

Fern, R., Ransom, B.R. and Waxman, S.G. (1996a) Autoprotective mechanisms in the CNS. Some new lessons from white matter. *Molecular and Chemical Neuropathology* 27, 107-129.

Fern, R., Ransom, B.R. and Waxman, S.G. (1996b) White matter stroke: Autoprotective mechanisms with therapeutic implications. *Cerebrovascular Diseases* 6, 59-65.

Filley, C.M. (1998) The behavioural neurology of cerebral white matter. *Neurology* 50, 1535-1540.

Fisher, C.M. (1982) Lacunes; small deep cerebral infarcts. *Neurology* 15, 777-784.

Follis, F., Scremin, O.U., Blisard, K.S., Scremin, A.M.E., Pett, S.B., Scott, W.J., Kessler, R.M. and Wernly, J.A. (1993) Selective vulnerability of white matter during spinal cord ischemia. *J. Cereb. Blood Flow Metab.* 13, 170-178.

Friede, R.L. and Samorajski, T. (1970) Axon caliber related to neurofilaments and microtubules in sciatic nerve fibres of rats and mice. *Anat. Rec.* 379-388.

Gennarelli, T.A., Thibault, L.E., Adams, J.H., Graham, D.I., Thompson, C.J. and Marcincin, R.P. (1982) Diffuse axonal injury and traumatic coma in the primate. *Ann. Neurol.* 12, 564-574.

Gentleman, S.M., Nash, M.J., Sweeting, C.J., Graham, D.I. and Roberts, G.W. (1993) Beta-amyloid precursor protein (beta APP) as a marker for axonal injury after head injury. *Neurosci. Lett.* 160, 139-144.

Gentleman, S.M., Roberts, G.W., Gennarelli, T.A., Maxwell, W.L., Adams, J.H., Kerr, S. and Graham, D.I. (1995) Axonal injury: a universal consequence of fatal closed head injury. *Acta. Neuropathol.* 89, 537-543.

Gill, R., Brazell, C., Woodruff, G.N. and Kemp, J.A. (1991) The neuroprotective action of dizocilpine (MK-801) in the rat middle cerebral artery occlusion model of focal ischaemia. *Br. J. Pharmacol.* 103, 2030-2036.

Gillespi, M.J. and Stein, R.B. (1983) The relationship between axon diameter, myelin thickness and conduction velocity during the atrophy of mammalian peripheral nerves. *Brain Res.* 259, 41-56.

Glenner, G.G. and Wong, C.W. (1984) Alzheimer's disease and Down's syndrome: sharing of a unique cerebrovascular amyloid fibril protein. *Biochem. Biophys. Res. Commun.* 122, 1131-1135.

Goldin, S.M., Subbarao, K., Sharma, R., Knapp, A.G., Fischer, J.B., Daly, D., Durant, G.J., Reddy, N.L., Hu, L., Maga, S., Perlman, M.E., Chen, J., Graham, S.H., Holt, W.F., Berlove, D. and Margolin, L.D. (1995) Neuroprotective use-dependent blockers of Na^+ and Ca^+ channels controlling presynaptic release of glutamate. *Ann. N. Y. Acad. Sci.* 765, 210-229.

Goldstein, M.E., Sternberger, N.H. and Sternberger, L.A. (1987) Phosphorylation protects neurofilaments against proteolysis. *J. Neuroimmunol* 14, 149-160.

Grady, M.S., McLaughlin, M.R., Christman, C.W., Valadka, A.B., Fligner, C.L. and Povlishock, J.T. (1993) The use of antibodies targeted against the neurofilament subunits for the detection of diffuse axonal injury in humans. *J. Neuropathol. Exp. Neurol.* 52, 143-152.

Graf, R., Kataoka, K., Rosner, G. and Heiss, W.D. (1990a) Focal cerebral ischemia in cats: Disturbance of neuronal activity in cortical areas with different degrees of CBF reduction. *J. Cereb. Blood Flow Metab.* 21, 923-928.

Graf, R., Kataoka, K., Wakayama, A., Rosner, G., Hayakawa, T. and Heiss, W.-D. (1990b) Functional impairment due to white matter ischemia after middle cerebral artery occlusion in cats. *Stroke* 21, 923-928.

Graham, D.I. (1977) Pathology of hypoxic brain damage in man. *J. Clin. Path* 30, Suppl. 170-180.

Graham, D.I., Ford, I., Adams, J.H., Doyle, D., Teasdale, G.M., Lawrence, A.E. and McLellan, D.R. (1989) Ischaemic brain damage is still common in fatal non-missile head injury. *J. Neurol. Neurosurg. Psychiatry* 52, 346-350.

Graham, D.I., Gentleman, S.M., Lynch, A. and Roberts, G.W. (1995) Distribution of b-amyloid protein in the brain following severe head injury. *Neuropathology and Applied Neurobiology* 21, 27-34.

Graham, D.I. (1996) Blunt head injury: prospects for improved outcome. *Neuropathol. Appl. Neurobiol.* 22, 505-509.

Graham, S.H., Chen, J., Lan, J.Q., Leach, M.J. and Simon, R.P. (1994) Neuroprotective effects of a use-dependant blocker of voltage-dependant sodium channels, BW619C89, in rat middle cerebral artery occlusion. *Journal of Pharmacology and Experimental Therapeutics* 269, 854-859.

Gultekin, S.H. and Smith, T.W. (1994) Diffuse axonal injury in craniocerebral trauma. A comparative histologic and immunohistochemical study. *Arch. Pathol. Lab. Med.* 118, 168-171.

Haddad, G.G. and Jiang, C. (1993) Oxygen deprivation in the central nervous system: on mechanisms of neuronal response, differential sensitivity and injury. *Prog. Neurobiol.* 40, 277-318.

Hall, G.F. and Lee, V.M.-Y. (1995) Neurofilament sidearm proteolysis is a prominent early effect of axotomy in lamprey giant central neurons. *J. Comp. Neurol.* 353, 38-49.

Hallenbeck, J.M. (1996) Inflammatory reactions at the blood-endothelial interface in acute stroke. In: Siesjo, B.K. and Wieloch, T. (Eds.) *Advances in Neurology: Cellular and molecular mechanisms of ischemic brain damage*, pp. 281-297. Philadelphia: Lippincott-Raven

Hamakubo, T., Kannagi, R., Murachi, T. and Matus, A. (1986) Distribution of calpains 1 and 2 in rat brain. *J. Neurosci.* 6, 3103-3111.

Hammerschlag, R., Cyr, J.L. and Brady, S.T. (1994) Axonal transport and the neuronal cytoskeleton. In: Siegel, G.J., Agranoff, B.W., Albers, R.W. and Molinoff, P.B. (Eds.) *Basic Neurochemistry*, 5th edn. pp. 545-571. New York, NY: Raven Press

Hess, D.T., Slater, T.M., Wilson, M.C. and Pate Skene, J.H. (1992) The 25 kDa synaptosomal-associated protein SNAP-25 is the major methionine-rich polypeptide in rapid axonal transport and a major substrate for palmitoylation in adult CNS. *J. Neurosci.* 12, 4634-4641.

Hirano, A. and Llena, J.F. (1995) Morphology of central nervous system axons. In: Waxman, S.G., Kocsis, J.D. and Stys, P.K. (Eds.) *The axon. Structure, function and pathophysiology*, pp. 49-67. New York: Oxford University Press

Hirokawa, N., Glicksman, M.A. and Willard, M.B. (1984) Organization of mammalian neurofilament polypeptides within the neuronal cytoskeleton. *J. Cell Biol.* 98, 1523-1536.

Hisanaga, S., Gonda, Y., Inagaki, M., Ikai, A. and Hirokawa, N. (1990) Effects of phosphorylation of the neurofilament L protein on filamentous structures. *Cell Regul.* 1, 237-248.

Hoffman, P.N., Griffin, J.W. and Price, D.L. (1984) Control of axonal caliber by neurofilament transport. *J. Cell Biol.* 99, 705-714.

Hoffman, P.N., Thompson, G.W., Griffin, J.W. and Price, D.L. (1985) Changes in neurofilament transport coincide temporally with alterations in the caliber of axons in regenerting motor fibers. *J. Cell. Biol.* 101, 1332-1340.

Hoffman, P.N. and Lasek, R.J. (1975) The slow component of axonal transport: identification of the major structural polypeptides of the axon and their generality among mammalian neurons. *J. Cell. Biol.* 66, 351-366.

Holt, W.F. (1997) Glutamate in health and disease: the role of inhibitors. In: Bar, P.B. and Beal, F.M. (Eds.) *Neuroprotection in CNS diseases*, pp. 87-119. New York: Marcel Dekker

Hong, S.C., Goto, Y., Lanzino, G., Soleau, S., Kassell, N.F., Lee, K.S. and Chan, P.H. (1994) Neuroprotection with a calpain inhibitor in a model of focal cerebral ischemia. *Stroke* 25, 663-669.

Isard, P.A. and Forbes, J.F. (1992) The cost of stroke to the National Health Service in Scotland. *Cerebrovascular Diseases* 2, 47-50.

Jackson, P. and Blythe, D. (1993) Immunolabelling techniques for light microscopy. In: Beesley, J.B. (Ed.) *Immunocytochemistry. A practical approach*, pp. 15-41. New York: Oxford University Press

Jafari, S.S., Nielson, M., Graham, D.I. and Maxwell, W. (1998) Axonal cytoskeletal changes after non-disruptive axonal injury. II Intermediate sized axons. *J. Neurotrauma*

Jones, K.A. and Baughman, R.W. (1991) Both NMDA and non-NMDA subtypes of glutamate receptors are concentrated at synapses on cerebral cortical neurons in culture. *Neuron* 7, 593-603.

Kalaria, R.N., Bhatti, S.U., Palatinsky, E.A., Pennington, D.H., Shelton, E.R., Chan, H.W., Perry, G. and Lust, W.D. (1993) Accumulation of the beta amyloid precursor protein at sites of ischemic injury in rat brain. *Neuroreport.* 4, 211-214.

Kampfl, A., Posmantur, R.M., Zhao, X., Schmutzhard, E., Clifton, G.L. and Hayes, R.L. (1997) Mechanisms of calpain proteolysis following traumatic brain injury: implications for pathology and therapy: a review and update. *J. Neurotrauma* 14, 121-134.

Karnovsky, M.J. (1965) A formaldehyde-gluteraldehyde fixative of high osmolality for use in electron microscopy. *J. Cell Biol* 27, 137A

Kawaguchi, K. and Graham, S.H. (1997) Neuroprotective effects of the glutamate release inhibitor 619C89 in temporary middle cerebral artery occlusion. *Brain Research* 749, 131-134.

Kawarabayashi, T., Shoji, M., Harigaya, Y., Yamaguchi, H. and Hirai, S. (1991) Expression of APP in the early stage of brain damage. *Brain Res.* 563, 334-338.

Kemp, J.A., Foster, A.C. and Wong, E.H.F. (1987) Non-competitive antagonists of excitatory amino acid receptors. *Trends neurol. Sci.* 10, 294-298.

Kennedy, C., Smith, C.B. and Sokoloff, L. (1992) Metabolic mapping of local neuronal activity. In: Stamford, J.A. (Ed.) *Monitoring neuronal activity. A practical approach*, pp. 203-229. New York: Oxford University Press

Kitagawa, K., Matsumoto, M., Niinobe, M., Mikoshiba, K., Hata, R., Ueda, H., Handa, N., Fukunaga, R., Isaka, Y., Kimura, K. and Kamada, T. (1989) Microtubule-associated protein 2 as a sensitive marker for cerebral ischemic damage - Immunohistochemical investigation of dendritic damage. *Neuroscience* 31, 401-411.

Konig, J.F.R. and Klippel, R.A. (1963) *The Rat Brain: a Stereotaxic Atlas of the Forebrain and Lower Parts of the Brain Stem*, New York: Krieger.

Koo, E.H., Sisodia, S.S., Archer, D.R., Martin, L.J., Weidemann, A., Beyreuther, K., Fischer, P., Masters, C.L. and Price, D.L. (1990) Precursor of amyloid protein in Alzheimer disease undergoes fast anterograde axonal transport. *Proc. Natl. Acad. Sci. U. S. A.* 87, 1561-1565.

Lam, A.G.M., Soriano, M.A., Monn, J.A., Schoepp, D.D., Lodge, D. and McCulloch, J. (1998) Effects of the selective metabotropic glutamate agonist LY354740 in a rat model of permanent ischaemia. *Neurosci. Lett.* 254, 1-3.

Leach, M.J., Swan, J.H., Eisenthal, D., Dopson, M. and Nobbs, M. (1993) BW619C89, a glutamate release inhibitor, protects against focal cerebral ischemic damage. *Stroke* 24, 1063-1067.

Lee, M.K. and Cleveland, D.W. (1996) Neuronal intermediate filaments. *Annu. Rev. Neurosci.* 19, 187-217.

Lewen, A., Li, G.L., Olsson, Y. and Hillered, L. (1996) Changes in microtubule-associated protein 2 and amyloid precursor protein immunoreactivity following traumatic brain injury in rat: influence of MK-801 treatment. *Brain Research* 719, 161-171.

Lewis, S.B., Finnie, J.W., Blumbergs, P.C., Scott, G., Manavis, J., Brown, C., Reilly, P.L., Jones, N.R. and McLean, A.J. (1996) A head impact model of early axonal injury in the sheep. *J. Neurotrauma* 13, 505-514.

Li, Z. and Banik, N.L. (1995) The localization of mcalpain in myelin: immunocytochemical evidence in different areas of rat brain and nerves. *Brain Res.* 697, 112-121.

Lucas, D.R. and Newhouse, J.P. (1957) The toxic effect of sodium L-glutamate on the inner layers of the retina. *Archives of Ophthalmology* 193-201.

Ludin, B. and Matus, A. (1993) The neuronal cytoskeleton and its role in axonal and dendritic plasticity. *Hippocampus* 3, 61-71.

Makris, N., Worth, A.J., Sorensen, A.G., Papadimitriou, G.M., Wu, O., Reese, T.G., Wedeen, V.J. and Davis, T.L. (1997) Morphometry of In Vivo human white matter association pathways with diffusion-weighted magnetic resonance imaging. *Ann. Neurol.* 42, 951-962.

Marcoux, F.W., Morawetz, R.B., Crowell, R.M., DeGirolami, U. and Halsey, J.R. (1982) Differential regional vulnerability in transient focal cerebral ischemia. *Stroke* 13, 339-346.

Marmot, M.G. and Poulter, N.R. (1992) Primary prevention of stroke. *Lancet* 339, 344-347.

Maxwell, W., Kosanlavit, R., McCreath, B.J., Reid, O. and Graham, D.I. (1998) Freeze-fracture and cytochemical evidence for structural and functional alteration in the axolemma and myelin sheath of adult guinea-pig optic nerve fibres after stretch-injury. *In preparation*

Maxwell, W.L. (1995) Microtubular changes in axons after stretch injury. *J. Neurotrauma* 12, 363 (Abstract)

Maxwell, W.L., McCreath, B.J., Graham, D.I. and Gennarelli, T.A. (1995) Cytochemical evidence for the redistribution of membrane pump calcium-ATPase and ecto-Ca-ATPase activity, and calcium influx in myelinated nerve fibres of the optic nerve after stretch injury. *Journal of Neurocytology* 24, 925-942.

Maxwell, W.L. (1996) Histopathological changes at central nodes of ranvier after stretch-injury. *Microscopy Research and Technique* 34, 522-535.

Maxwell, W.L., Povlishock, J.T. and Graham, D.I. (1997a) A mechanistic analysis of non-disruptive axonal injury: a review. *J. Neurotrauma* 419-440.

Maxwell, W.L. and Graham, D.I. (1997b) Loss of axonal microtubules and neurofilaments after stretch-injury to guinea-pig optic nerve fibers. *J. Neurotrauma* 14, 603-614.

Mayer, S.E., Melmon, K.L. and Gilman, A.G. (1975) Introduction; the dynamics of drug absorption, distribution, and elimination. In: Gilman, A.G. (Ed.) *The pharmacological basis of therapeutics*, 6th edn. pp. 1-21. New York: MacMillan publishing co.

McAuley, M.A. (1995) Rodent models of focal ischemia. *Cerebrovascular and Brain Metabolism Reviews* 7, 153-180.

McCulloch, J. (1992) Excitatory amino acid antagonists and their potential for the treatment of ischaemic brain damage in man. *Br. J. Clin. Pharmacol.* 34, 106-114.

McKenzie, J.E., Gentleman, S.M., Roberts, G.W., Graham, D.I. and Royston, M.C. (1995) Quantification of beta APP immunoreactive pre-alpha cells in the entorhinal cortex using image analysis. *Neurodegeneration.* 4, 299-306.

McKenzie, K.J., McLellan, D.R., Gentleman, S.M., Maxwell, W.L., Gennarelli, T.A. and Graham, D.I. (1996) Is b-APP a marker of axonal damage in short-surviving head injury? *Acta. Neuropathol.*

McNaughton, N.C.L., Leach, M.J., Hainsworth, A.H. and Randall, A.D. (1997) Inhibition of human N-type voltage-gated Ca2+ channels by the neuroprotective agent BW619C89. *Neuropharmacology* 36, 1795-1798.

Muir, K.W. and Lees, K.R. (1995) Clinical experience with excitatory amino acid antagonist drugs. *Stroke* 26, 503-513.

Nakahara, I., Kikuchi, H., Taki, W., Nishi, S., Kito, M., Yonekawa, Y., Goto, Y. and Ogata, N. (1991) Degradation of mitochondrial phospholipids during experimental cerebral ischemia in rats. *J. Neurochem.* 57, 839-844.

Nakamura, Y., Takeda, M., Niigawa, H., Hariguchi, S. and Nishimura, T. (1992) Amyloid beta-protein precursor deposition in rat hippocampus lesioned by ibotenic acid injection. *Neurosci. Lett.* 136, 95-98.

Nakanishi, S. (1992) Molecular diversity of glutamate receptors and implications for brain function. *Science* 258, 597-603.

Ng, H.K., Mahaliyana, R.D. and Poon, W.S. (1994) The pathological spectrum of diffuse axonal injury in blunt head trauma: assessment with axon and myelin stains. *Clin. Neurol. Neurosurg.* 96, 24-31.

Ochs, S. (1972) Rate of fast axoplasmic transport in mammalian nerve fibers. *J. Physiol.* 227, 627-645.

Ohgami, T., Kitamoto, T. and Tateishi, J. (1992) Alzheimer's amyloid precursor protein accumulates within axonal swellings in human brain lesions. *Neurosci. Lett.* 136, 75-78.

Okabe, S., Miyasaka, H. and Hirokawa, N. (1993) Dynamics of the neuronal intermediate filaments. *J. Cell Biol.* 121, 375-386.

Olney, J.W. (1978) Kainic acid as a tool in neurobiology. In: McGeer, E.G., Olney, J.W. and McGeer, P.L. (Eds.) *Neurotoxicity of excitatory amino acids*, pp. 95-121. New York: Raven Press

Olney, J.W., Price, M.T., Salles, K.S., Labruyere, J. and Friedrich, G. (1987) MK-801 powerfully protects against N-methyl aspartate neurotoxicity. *Eur. J. Pharmacol.* 141, 357-361.

Orrenius, S., Ankarcrona, M. and Nicotera, P. (1996) Mechanisms of calcium-related cell death. In: Siesjo, B.K. and Wieloch, T. (Eds.) *Cellular and molecular mechanisms of ischemic brain damage*, pp. 137-151. Philadelphia: Lippincott-Raven Publishers

Orrison, W.W. (1989) Computed tomography and magnetic resonance imaging. In: Orrison, W.W. (Ed.) *Introduction to neuroimaging*, pp. 65-174. Boston: Little, Brown and Company

Osborne, K.A., Shigeno, T., Balarsky, A.M., Ford, I., McCulloch, J., Teasdale, G.M. and Graham, D.I. (1987) Quantitative assessment of early brain damage in a rat model of focal cerebral ischaemia. *J. Neurol. Neurosurg. Psychiatry* 402-410.

Otsuka, N., Tomonaga, M. and Ikeda, K. (1991) Rapid appearance of beta-amyloid precursor protein immunoreactivity in damaged axons and reactive glial cells in rat brain following needle stab injury. *Brain Res.* 568, 335-338.

Ouimet, C.C., Baerwald, K.D., Gandy, S.E. and Greengard, P. (1994) Immunocytochemical localization of amyloid precursor protein in rat brain. *J. Comp. Neurol.* 348, 244-260.

Oyler, G.A., Higgins, G.A., Hart, R.A., Battenberg, E., Billingsley, M., Bloom, F.E. and Wilson, M.C. (1989) The identification of a novel synaptosomal-associated protein, SNAP-25, differentially expressed by neuronal subpopulations. *J. Cell Biol.* 109, 3039-3052.

Oyler, G.A., Polli, J.W., Higgins, G.A., Wilson, M.C. and Billingsley, M.L. (1992) Distribution and expression of SNAP-25 immunoreactivity in rat brain, rat PC-12 cells and human SMS-KCNR neuroblastoma cells. *Brain Res. Dev. Brain Res.* 65, 133-146.

Ozyurt, E., Graham, D.I., Woodruff, G.N. and McCulloch, J. (1988) Protective effect of the glutamate antagonist, MK-801 in focal cerebral ischemia in the cat. *J. Cereb. Blood Flow Metab.* 8, 138-143.

Palacios, G., Palacios, J.M., Mengod, G. and Frey, P. (1992) Beta-amyloid precursor protein localization in the Golgi apparatus in neurons and oligodendrocytes. An immunocytochemical structural and ultrastructural study in normal and axotomized neurons. *Brain Res. Mol. Brain Res.* 15, 195-206.

Pantoni, L., Garcia, J.H. and Gutierrez, J.A. (1996) Cerebral white matter is highly vulnerable to ischemia. *Stroke* 27, 1641-1647.

Park, C.K., Nehls, D.G., Graham, D.I., Teasdale, G. and McCulloch, J. (1988a) Focal cerebral ischaemia in the cat: treatment with the glutamate antagonist MK-801 after induction of ischaemia. *J. Cereb. Blood Flow Metab.* 8, 757-762.

Park, C.K., Nehls, D.G., Graham, D.I., Teasdale, G.M. and McCulloch, J. (1988b) The glutamate antagonist MK-801 reduces focal ischemic brain damage in the rat. *Ann. Neurol.* 24, 543-551.

Pedrotti, B., Francolini, M., Cotelli, F. and Islam, K. (1996) Modulation of microtubule shape in vitro by high molecular weight microtubule associated proteins MAP1A, MAP1B, AND MAP2. *FEBS Letters* 384, 147-150.

Pettus, E.H., Christman, C.W., Giebel, M.L. and Povlishock, J.T. (1994) Traumatically induced altered membrane permeability: its relationship to traumatically induced reactive axonal change. *J. Neurotrauma.* 11, 507-522.

Pettus, E.H. and Povlishock, J.T. (1996) Characterization of a distinct set of intra-axonal ultrastructural changes associated with traumatically induced alteration in axolemmal permeability. *Brain Res.* 722, 1-11.

Posmantur, R., Kampfl, A., Siman, R., Liu, S.J., Zhao, X., Clifton, G.L. and Hayes, R.L. (1997) A calpain inhibitor attenuates cortical cytoskeletal protein loss after experimental traumatic brain injury in the rat. *Neuroscience* 77, 875-888.

Povlishock, J.T., Becker, D.P., Cheng, C.L.Y. and Vaughan, G.W. (1983) Axonal change in minor head trauma. *J. Neuropathol. Exp. Neurol.* 42, 225-242.

Povlishock, J.T. (1992) Traumatically induced axonal injury: pathogenesis and pathobiological implications. *Brain Pathol.* 2, 1-12.

Povlishock, J.T., Hayes, R.L., Michel, M.E. and McIntosh, T.K. (1994) Workshop on animal models of traumatic brain injury. *J. Neurotrauma.* 11, 723-732.

Povlishock, J.T., Marmarou, A., McIntosh, T., Trojanowski, J.Q. and Moroi, J. (1997) Impact acceleration injury in the rat: evidence for focal axolemmal change and related neurofilament sidearm alteration. *J. Neuropathol. Exp. Neurol.* 56, 347-359.

Povlishock, J.T. and Christman, C.W. (1995) The pathobiology of traumatically induced axonal injury in animals and humans: a review of current thoughts. *J. Neurotrauma* 12, 555-564.

Povlishock, J.T. and Pettus, E.H. (1996) Traumatically induced axonal damage: evidence for enduring changes in axolemmal permeability with associated cytoskeletal change. *Acta Neurochir. Suppl. Wien.* 66, 81-86.

Prichard, J.W. and Cummings, J.L. (1997) The insistent call from functional MRI. *Neurology* 797-800.

Ransom, B.R., Stys, P.K. and Waxman, S.G. (1990a) The pathophysiology of anoxic injury in central nervous system white matter. *Stroke* 21, 52-57.

Ransom, B.R., Waxman, S.G. and Davis, P.K. (1990b) Anoxic injury of CNS white matter: Protective effect of ketamine. *Neurology* 40, 1399-1403.

Refolo, L.M., Wittenberg, I.S., Friedrich, V.L., Jr. and Robakis, N.K. (1991) The Alzheimer amyloid precursor is associated with the detergent-insoluble cytoskeleton. *J. Neurosci.* 11, 3888-3897.

Reinoso-Suarez, F. (1961) *Topograpischer hirnatlas der katze, fur experimental-physiologische undersuchungen*, Darmstadt.

Roberts, G.W., Gentleman, S.M., Lynch, A. and Graham, D.I. (1991) bA4 amyloid protein deposition in brain after head trauma. *Lancet* 338, 1422-1423.

Roberts-Lewis, J.M., Savage, J.M., Marcy, V.R., Pinsker, L.R. and Siman, R. (1994) Immunolocalization of calpain I-mediated spectrin degradation to vulnerable neurons in the ischemic gerbil brain. *Journal of Neuroscience* 14, 3934-3944.

Rogers, D.C., Wright, P.W., Roberts, J.C., Reavill, C., Rothaul, A.L. and Hunter, A.J. (1992) Photothrombotic lesions in frontal cortex impair the performance of the delayed non-matching to position task by rats. *Behav. Brain Res.* 49, 231-235.

Rothman, S. and Olney, J.W. (1986) Glutamate and the pathophysiology of hypoxic-ischemic brain damage. *Ann. Neurol.* 19, 105-111.

Saatman, K.E., BozyczkoCoyne, D., Marcy, V., Siman, R. and McIntosh, T.K. (1996a) Prolonged calpain-mediated spectrin breakdown occurs regionally following experimental brain injury in the rat. *Journal of Neuropathology and Experimental Neurology* 55, 850-860.

Saatman, K.E., Murai, H., Bartus, R.T., Smith, D.H., Hayward, N.J., Perri, B.R. and McIntosh, T.K. (1996b) Calpain inhibitor AK295 attenuates motor and cognitive deficits following experimental brain injury in the rat. *Proceedings of the National Academy of Sciences of the United States of America* 93, 3428-3433.

Salzer, J.L. (1997) Clustering of sodium channels at the node of Ranvier: close encounters of the axon-glia kind. *Neuron* 18, 843-846.

Sauter, A. and Rudin, M. (1995) Strain-dependent drug effects in rat middle cerebral artery occlusion model of stroke. *Journal of Pharmacology and Experimental Therapeutics* 274, 1008-1013.

Schlaepfer, W.W. (1987) Neurofilaments: structure, metabolism and implications in disease. *J. Neuropathol. Exp. Neurol.* 46, 117-129.

Sciamanna, M.A., Zinkel, J., Fabi, A.Y. and Lee, C.P. (1992) Ischemic injury to rat forebrain mitochondria and cellular calcium homeostasis. *Biochim. Biophys. Acta.* 1134, 223-232.

Sharkey, J., Kelly, J.S. and Butcher, S.P. Inflammatory responses to cerebral ischemia. Implications for stroke treatment. In: Ter Horst, G.J. and Korf, J. (Eds.) *Clinical pharmacology of cerebral ischemia*, Totowa,NJ: Humana Press Inc.

Sherriff, F.E., Bridges, L.R., Gentleman, S.M., Sivaloganathan, S. and Wilson, S. (1994a) Markers of axonal injury in post mortem human brain. *Acta Neuropathol. Berl.* 88, 433-439.

Sherriff, F.E., Bridges, L.R. and Jackson, P. (1994b) Microwave antigen retrieval of beta-amyloid precursor protein immunoreactivity. *NeuroReport* 5, 1085-1088.

Sherriff, F.E., Bridges, L.R. and Sivaloganathan, S. (1994c) Early detection of axonal injury after human head trauma using immunocytochemistry for beta-amyloid precursor protein. *Acta Neuropathol. Berl.* 87, 55-62.

Shigematsu, K., McGeer, P.L., Walker, D.G., Ishii, T. and McGeer, E.G. (1992) Reactive microglia/macrophages phagocytose amyloid precursor protein produced by neurons following neural damage. *J. Neurosci. Res.* 31, 443-453.

Shigematsu, K. and McGeer, P.L. (1992) Accumulation of amyloid precursor protein in neurons after intraventricular injection of colchicine. *Am. J. Pathol.* 140, 787-794.

Shigeno, T., McCulloch, J., Graham, D.I., Mendelow, A.D. and Teasdale, G. (1985) Pure cortical ischemia versus striatal ischemia. *Surg. Neurol.* 24, 47-51.

Siesjo, B.K. (1986) Calcium and ischemic brain damage. *Eur. Neurol.* 25, 45-56.

Siman, R., Bozyczko-Coyne, D., Savage, M.J. and Roberts-Lewis, J.M. (1996) The calcium-activated protease calpain I and ischemia-induced neurodegeneration. *Advances in Neurology* 71, 167-175.

Small, D.L. and Buchan, A.M. (1997) NMDA antagonists: their role in neuroprotection. In: *Neuroprotective agents and cerebral ischaemia*, pp. 137-171. Acadamic Press Ltd

Smith, S.E., Lekieffre, D., Sowinski, P. and Meldrum, B.S. (1993) Cerebroprotective effect of BW619C89 after focal or global cerebral ischemia in the rat. *NeuroReport* 4, 1339-1342.

Smith, S.E., Hodges, H., Sowinski, P., Man, C.M., Leach, M.J., Sinden, J.D., Gray, J.A. and Meldrum, B.S. (1997) Long-term beneficial effects of BW619C89 on neurological deficit, cognitive deficit and brain damage after middle cerebral artery occlusion in the rat. *Neuroscience* 77, 1123-1135.

Sollner, T., Whiteheart, S.W., Brunner, M., Erdjument-Bromage, H., Geromanos, S., Tempst, P. and Rothman, J.E. (1993) SNAP receptors implicated in vesicle targeting and fusion. *Nature* 362, 318-324.

Steffensen, I. and Stys, P.K. (1996) The NA+-CA2+ exchanger in neurons and glial cells. *Neuroscientist* 2, 162-171.

Stephenson, D.T., Rash, K. and Clemens, J.A. (1992) Amyloid precursor protein accumulates in regions of neurodegeneration following focal cerebral ischemia in the rat. *Brain Res.* 593, 128-135.

Stys, P.K., Ransom, B.R., Waxman, S.G. and Davis, P.K. (1990) Role of extracellular calcium in anoxic injury of mammalian central white matter. *Proceedings of the National Academy of Sciences of the United States of America* 87, 4212-4216.

Stys, P.K., Waxman, S.G. and Ransom, B.R. (1991a) Na+-Ca2+ exchanger mediates Ca2+ influx during anoxia in mammalian central nervous system white matter. *Ann. Neurol.* 30, 375-380.

Stys, P.K., Waxman, S.G. and Ransom, B.R. (1991b) Reverse operation of the Na+-Ca2+ exchanger mediates Ca2+ influx during anoxia in mammalian CNS white matter. *Annals of the New York Academy of Sciences* 639, 328-332.

Stys, P.K., Ransom, B.R. and Waxman, S.G. (1992a) Tertiary and quaternary local anesthetics protect CNS white matter from anoxic injury at concentrations that do not block excitability. *J. Neurophysiol.* 67, 236-240.

Stys, P.K., Waxman, S.G. and Ransom, B.R. (1992b) Ionic mechanisms of anoxic injury in mammalian CNS white matter: Role of Na+ channels and Na+-Ca2+ exchanger. *Journal of Neuroscience* 12, 430-439.

Stys, P.K., Sontheimer, H., Ransom, B.R. and Waxman, S.G. (1993) Noninactivating, tetrodotoxin-sensitive Na+ conductance in rat optic nerve axons. *Proc. Natl. Acad. Sci. U. S. A.* 90, 6976-6980.

Stys, P.K., Ransom, B.R., Black, J.A. and Waxman, S.G. (1995) Anoxic/ischemic injury in axons. In: Waxman, S.G., Kocsis, J.D. and Stys, P.K. (Eds.) *The axon: structure, function and pathophysiology*, pp. 462-479. New York: Oxford University Press

Stys, P.K. (1996) Ions, channels, and transporters involved in anoxic injury of central nervous system white matter. *Advances in Neurology* 71, 153-166.

Stys, P.K., Lehning, E.J., Sauberman, A.J. and LoPachin, R.M. (1997) Intracellular concentrations of major ions in rat myelinated axons and glia: calculations based on electron probe X-ray microanalyses. *J. Neurochem.* 1920-1928.

Stys, P.K. (1998) Anoxic and ischemic injury of myelinated axons in CNS white matter: from mechanistic concepts to therapeutics. *J. Cereb. Blood Flow Metab.* 18, 2-25.

Stys, P.K., Hubatsch, D.A. and Leppanen, L.L. (1998) Effects of K^+ channel blockers on the anoxic response of CNS myelinated axons. *NeuroReport* 9, 447-453.

Suenaga, T., Ohnishi, K., Nishimura, M., Nakamura, S., Akiguchi, I. and Kimura, J. (1994) Bundles of amyloid precursor protein-immunoreactive axons in human cerebrovascular white matter lesions. *Acta Neuropathol. Berl.* 87, 450-455.

Sutherland, K., MacDonald, S.T. and Ironside, J.W. (1996) Quantification and analysis of the neuropathological features of Creutzfeldt-Jakob disease. *J. Neurosci. Methods* 64, 123-132.

Sydserff, S.G., Green, A.R. and Cross, A.J. (1996) The effect of oedema and tissue swelling on the measurement of neuroprotection: a study using chlormethiazole and permanent middle cerebral artery occlusion in rats. *Neurodegeneration* 5, 81-85.

Tamura, A., Graham, D.I., McCulloch, J. and Teasdale, G.M. (1981) Focal cerebral ischaemia in the rat. I. Description of technique and early neuropathological consequences following middle cerebral artery occlusion. *J. Cereb. Blood Flow Metab.* 1, 53-60.

Teasdale, G.M. (1995) Head injury. *J. Neurol. Neurosurg. Psychiatry* 58, 526-539.

Viossat, I., Duverger, D., Chapelat, M., Pirotzky, E., Chabrier, P.E. and Braquet, P. (1993) Elevated tissue endothelin content during focal cerebral ischemia in the rat. *J. Cerebrovasc. Pharmacol.* 22, S306-S308.

Wahlgren, N.G. (1997) A review of earlier clinical studies on neuroprotective agents and current approaches. In: Anonymous *Neuroprotective agents and cerebral ischaemia*, pp. 337-363. Academic Press Ltd

Wallace, M.C., Teasdale, G.M. and McCulloch, J. (1992) Autoradiographic analysis of ^{3}H-MK-801 in vivo uptake, and in vitro binding, after focal cerebral ischemia in the rat. *J. Neurosurg.* 76, 127-134.

Warach, S., Gaa, J., Siewert, B., Wielopolski, P. and Edelman, R.R. (1995) Acute human stroke studied by whole brain echo planar diffusion-weighted magnetic resonance imaging. *Ann. Neurol.* 37, 231-241.

Warlow, C. (1993) Disorders of cerebral circulation. In: Walton, J. (Ed.) *Brain's diseases of the nervous system*, 10th edn. pp. 197-268. New York: Oxford University Press

Waxman, S.G., Ransom, B.R. and Stys, P.K. (1991) Non-synaptic mechanisms of Ca(2+)-mediated injury in CNS white matter. *Trends. Neurosci.* 14, 461-468.

Waxman, S.G., Black, J.A., Stys, P.K. and Ransom, B.R. (1992) Ultrastructural concomitants of anoxic injury and early post-anoxic recovery in rat optic nerve. *Brain Res.* 574, 105-119.

Waxman, S.G., Black, J.A., Ransom, B.R. and Stys, P.K. (1993) Protection of the axonal cytoskeleton in anoxic optic nerve by decreased extracellular calcium. *Brain Res.* 614, 137-145.

Waxman, S.G., Black, J.A., Ransom, B.R. and Stys, P.K. (1994) Anoxic injury of rat optic nerve: ultrastructural evidence for coupling between Na+ influx and Ca(2+)-mediated injury in myelinated CNS axons. *Brain Res.* 644, 197-204.

Waxman, S.G. (1995) Voltage-gated ion channels in axons: Localisation, function, and development. In: Waxman, S.G., Kocsis, J.D. and Stys, P.K. (Eds.) *The Axon: Structure, Function and Pathophysiology*, pp. 218-243. New York: Oxford University Press

Waxman, S.G. and Ritchie, J.M. (1993) Molecular dissection of the myelinated axon. *Ann. Neurol.* 33, 121-136.

Wong, E.H.F., Kemp, J.A., Priestley, T., Knight, A.R., Woodruff, G.N. and Iversen, L.L. (1986) The anticonvulsant MK-801 is a potent N-methyl-D-aspartate antagonist. *Proc. Natl. Acad. Sci. U. S. A.* 83, 7104-7108.

Xiong, Y., Gu, Q., Peterson, P.L., Muizelaar, J.P. and Lee, C.P. (1997) Mitochondrial dysfunction and calcium perturbation induced by traumatic brain injury. *J. Neurotrauma* 14, 23-34.

Yaghmai, A. and Povlishock, J. (1992) Traumatically induced reactive change as visualized through the use of monoclonal antibodies targeted to neurofilament subunits. *J. Neuropathol. Exp. Neurol.* 51, 158-176.

Yam, P.S., Takasago, T., Dewar, D., Graham, D.I. and McCulloch, J. (1997) Amyloid precursor protein accumulates in white matter at the margin of a focal ischaemic lesion. *Brain Res.* 760, 150-157.

Yamori, Y., Horie, R., Handa, H., Sato, M. and Fukase, M. (1976) Pathogenetic similarity of strokes in stroke-prone spontaneously hypertensive rats and humans. *Stroke* 7, 46-53.

Yanagihara, T., Brengman, J.M. and Mushynski, W.E. (1990) Differential vulnerability of microtubule components in cerebral ischemia. *Acta. Neuropathol.* 80, 499-505.

Yoles, E., Muller, S. and Schwartz, M. (1997) NMDA-receptor antagonist protects neurons from secondary degeneration after partial optic nerve crush. *J. Neurotrauma* 14, 665-675.

Zea Longa, E., Weinstein, P.R., Carlson, S. and Cummins, R. (1989) Reversible middle cerebral artery occlusion without craniectomy in rats. *Stroke* 20, 84-91.

ABSTRACTS AND PAPERS

Yam, P. S., Patterson, J., Graham, D. I., Takasago, T., Dewar, D. and McCulloch, J. (1998) Topographical and quantitative assessment of white matter injury following a focal ischaemic lesion in rat brain. Brain Research; Brain Research Protocols, **2** (4) 315-322

Yam, P. S., Dewar, D. and McCulloch, J. (1998) Axonal injury in the rat following a focal ischaemic lesion. Journal of Neurotrauma, **15** (6) 441-450

Yam, P. S., McCulloch, J. and Graham, D. I. (1998) Amyloid precursor protein immunoreactivity following focal cerebral ischaemia in the rat: influence of MK-801 treatment. Neuropathology and Applied Neurobiology, **24**,145

Yam, P. S., Dewar, D. and McCulloch, J. (1997) Axonal injury: common pathways following traumatic and ischaemic insults? Journal of Neurotrauma, **14** (10) 788

Yam, P. S., Takasago, T., Dewar, D., Graham, D. I. and McCulloch, J. (1997) Amyloid precursor protein: a marker of white matter injury after focal cerebral ischaemia in the rat. Journal of Cerebral Blood Flow and Metabolism, **17** (1) S613

Yam, P. S., Takasago, T., Dewar, D., Graham, D. I. and McCulloch, J. (1997) Amyloid precursor protein accumulates in white matter at the margin of a focal ischaemic lesion. Brain Research **760**, 150-157

Yam, P. S., Takasago, T., Dewar, D., Graham, D. I. and McCulloch, J. (1997) Amyloid precursor protein as a marker of axonal injury after a focal ischaemic lesion in the rat. Association of Veterinary Teachers and Research Workers 51st Scientific Meeting, pp39